Inertia Decrease and Frequency Performance

Assessment Study to Analyse the Impact of System Inertia Reduction on the Frequency Performance of the Dutch Power System Caused by the High Penetration of Renewables

A.A.Z. SATTAM

TECHNOLOGY UNIVERSITY OF DELFT

DNV·GL

TU Delft

Challenge the Future

Inertia Decrease and Frequency Performance

Assessment Study to Analyse the Impact of System Inertia Reduction on the Frequency Performance of the Dutch Power System Caused by the High Penetration of Renewables

By

Ala'a Sattam

in partial fulfilment of the requirements for the degree of

Master of Science
in Electrical Engineering - Electrical Sustainable Energy

at the Delft University of Technology,
to be defended publicly on November 30, 2018 at 09:00 AM.

Student Number:	4583876	
Project Duration:	February 5, 2018 – November 30, 2018	
Supervisor:	Prof. ir. P. (Peter) Vaessen	TU Delft
	Dr.ir. J.L. (Jose) Rueda Torres	TU Delft
	Dr.ir. L.A. (Luis) Hurtado	DNVGL
Thesis committee:	Prof. ir. P. (Peter) Vaessen	TU Delft
	Dr. ir. J.L. (Jose) Rueda Torres	TU Delft
	Dr. ir. Mohamad Ghaffarian Niasar	TU Delft

ABSTRACT

In the last decades, concerns of the energy expenditure and environmental sustainability have resulted in the need for national as well as international agreements to tackle such topics. From this perspective, the main aim of the European countries, including that of the Netherlands, is the shifting towards an electricity production dominated by renewable energy sources (nearly 70%) by mid-century as such sources provide energy in a (much) cheaper and better environmental manner.

Possibly, this energy transition would have a significant impact on grid stability as renewables behave differently than the conventional synchronous power generation units. Besides their intermittent nature, they are also unable to contribute to system inertia. This inability to produce inertia would have considerable consequences for the frequency performance of a power system. Since the level of grid inertia affects both the initial Rate of Change of Frequency (RoCoF) and maximum frequency deviation (Nadir-Point) following power contingencies.

Due to these developments, the overall goal of this assessment study is to analyse the future frequency performance of the Dutch power system as part of the Synchronous Grid of Continental Europe. The paper will focus on the decrease in grid inertia caused by the high penetration of renewables, and their relative share in the total electricity production.

The conclusions of this work are based on a dynamic model of a power system developed using DNVGL tool KERMIT. This model consists of one primary node (NL) that represents the Dutch power system, connected to two synchronous nodes (ESNL & SONL) through AC transmission lines. Both nodes (ESNL and SONL) contain the aggregated generation and load profiles of the countries covering the Regional Group (RG)-Continental Europe and RG-Baltic as defined by ENTSO-e.

Moreover, two scenarios have been created with different simulation purposes; the first scenario (the so-called pre-scenario) has been developed to study the current frequency performance of the studied area with the present level of grid inertia. The latter was estimated using the synchronous Net Generation Capacities of the year (2017). The second scenario (main-scenario) has been used to assess the impact of inertia reduction on frequency stability in a future situation. The data of both the demand and production annual growth used in this analysis have been gathered from the Energy Transition Outlooks of DNVGL and ENTSO-e.

According to the simulation results of both scenarios, it has been found that the developed model of the Dutch grid as part of Continental Europe is sufficient to predict the possible frequency stability issues foreseen to occur in the future. Furthermore, these results have shown that the Dutch grid might be subjected to real problems with respect to inertia decrease as both values of the Nadir-Point and RoCoF would reach the operating limits at the end of the analysed period (2017-2050).

However, the rapid development of control system technologies allows us to argue that such problems would be mitigated in the near future. Given that the current main focus of TSOs and researchers is to find suitable ways to produce synthetic or virtual inertia from renewables.

The thesis work’s primary objective was fulfilled by developing a dynamic power system model that can be used to examine the frequency performance of the Dutch power system as part of Continental Europe. Despite the limited accuracy of the simulation results, this project can be considered as a first step towards the development of a DNVGL position regarding inertia reduction issues, not only in the Netherlands but also in other regions.

Finally, it is highly recommended to modify both the developed power system model and KERMIT tool, in such a way that they would be capable of sharing the active power produced by renewables in the control actions. Such a modification can provide an insight into the (possible) future role of renewables to mitigate frequency stability issues.

ACKNOWLEDGEMENTS

First, special thanks to TU Delft for the guidance throughout the programme of master Electrical Engineering, and to the Dutch location of DNVGL for the opportunity to conduct this thesis work at Arnhem. This assignment was a part of projects related to the analysis of future development and changes in dynamic networks supported by the power system planning department.

Next, I am grateful to my supervisors: Prof. Ir. Peter Vaessen (TU Delft/DNVGL), Dr. Ir. Jose Rueda Torres (TU Delft), and Dr.ir. Luis Hurtado (DNVGL) for their expertise and guidance, which lead me on the right path during this project and throughout the compilation of the thesis report.

Finally, I would like to express my gratitude and appreciation to all my friends, colleagues, classmates, family, girlfriend, and parents for their help and support during my study.

CONTENTS

ABBREVIATIONS

Abbreviation	Description
ACE	Area Control Error
AGC	Automatic Generation Control
CCGT	Combined Cycle Gas Turbine
CCT	Critical Clearing Time
CE	Continental Europe
CGSs	Conventional Synchronous Generators
CHP	Combined Heat and Power
COI	Centre of Inertia
DG	Decentralized Generation
DSOs	Distribution System Operators
ENTSO-e	European Network Transmission System Operators for Electricity
ESNL	East Area of the Netherlands
FCT	Fault Clearing Time
FD	Frequency Deviation
FD	Frequency Deviation
FR	Frequency Response
IR	Inertial Response
LFC	Load Frequency Control
MPP	Maximum Power Point
NGC	Net Generation Capacity
NSF	Nominal System Frequency
PQS	Power Quality Service
PrC	Primary Control
PVs	Photovoltaics
RES-e	Renewable Energy Sources for Electricity
RG	Regional-Groups
RoCoF	Rate of Change of Frequency
SACE	Smoothed Area Control Error
SCADA	Supervisory Control and Data Acquisition
SeC	Secondary Control
SONL	South Area of the Netherlands
TeC	Tertiary Control
TiC	Time Control
TSOs	Transmission System Operators
WTGs	Wind Turbine Generators

LIST OF FIGURES

LIST OF TABLES

1. INTRODUCTION

This chapter contextualizes the project background, motivation, goal and research questions, overall objectives, the scope of work, and the organization of this document.

1.1. Research Background

The traditional structure of the European power system, including that of the Netherlands, has been subjected over the last decades to an extensive change mainly with the increased amount of renewable energy sources (RES) and cross-border market coupling for the trade of energy. The expectation for the near future is that the existing power systems may face enormous challenges due, mostly, to the ageing infrastructures, the increase of electricity demand, and the massive deployment of renewables.

Moreover, the development of renewable sources and their power electronics has led to a fast transition of the traditional electrical power system into the current hybrid power system. The inverter-connected RES components, i.e. Solar photovoltaics (PVs) and wind turbine generators (WTGs), are currently displacing the conventional power generators since their generated electricity becomes cheaper than electricity produced from burning fossil fuels as stated in [1].

From a power system perspective, the generated power from renewable sources behaves differently than that from conventional synchronous generators (CSGs). Besides the intermittent nature of such sources, they do not contribute to the system inertia. In general, WTGs have almost no contribution to the frequency response. As, WTGs are equipped with back-to-back converters that electrically decouple the wind generators from the power grid, although, there is stored kinetic energy in the turbine rotor. On the other hand, PVs are not capable of delivering any inertia to electric grids.

However, system inertia is typically considered as an essential parameter for the synchronised operation of a power system. Such a parameter represents the capability of synchronous power generation units to inject/absorb the kinetic energy into/from the grid to arrest the frequency deviation during power contingencies. This reaction is often known as the inertial response.

More deployment of RES-e to replace CSGs means a lower level of grid inertia, which in turn, leads the system frequency to react continually on the change of generation and load patterns. This makes existing frequency control and system operation more complicated and less stable. Traditionally, the synchronized operation of power systems is based on the assumption that inertia is sufficiently high to keep the system stable. Given in [2] that this assumption might not be valid in the future with the highly increased penetration of renewable sources.

1.2. Motivation

Typically, the acceptable frequency operating ranges and the stability requirements of a given power system are maintained by the stored kinetic energy of the rotating synchronous generators, which provides the power grid with the required inertia. In turn, this inertia provides sufficient support to system control actions to limit frequency deviations following disturbances, making frequency dynamics slower and increasing the proper response for any fault. In general, system inertia justifies the conventional assumption of a fully controllable operation of a power system.

However, the large-scale deployment of renewable sources and their relative share will repeal the assumption mentioned above. The consequences of this energy transition bring up the question regarding the time when the grid frequency performance becomes compromised, as a result of the reduction in the system inertia (caused by replacing the conventional power generators with inverter-connected wind turbines and solar photovoltaics).

1.3. Goal and Research Questions

This assessment study has been conducted to support developing a position for DNVGL regarding the consequences of system inertia reduction in a specific region. The overall goal of this thesis is to assess the frequency performance of the **Dutch power system as part of the Synchronous Grid of Continental Europe** (CE) by considering the decrease in system inertia caused by a massive deployment of renewable sources. For this purpose, the so-called Kermit Tool developed by DNVGL has been used to achieve the overall project objectives.

The research questions that will be answered in this thesis report are:

- **Q1:** How accurate can a model be implemented in Kermit to allow reliable assessment of the frequency performance of the Dutch power system?

- **Q2:** Which metrics can be applied to indicate the impact of inertia reduction on system frequency deviation and frequency control actions during disturbances?

- **Q3:** Under which circumstances will the decrease in system inertia be a real issue for system frequency performance?

- **Q4:** Which measures can be used to mitigate the influence of system inertia reduction regarding the massive deployment of renewable sources in the future power system?

1.4. Scope of Work

The scope of work needed to answer the research questions consists of the following tasks:

a. Perform a literature study that covers the following topics:
   - Review the current stability criteria
   - Define the impacts of RES on the frequency stability criteria
   - Study the currently used metrics to analyse frequency deviation
   - Examine the influences of renewable sources on the current level of grid inertia
   - Assess the future gird inertia regarding the massive deployment of renewable sources

b. Develop a high-level dynamic model in Kermit that represents **the Dutch power system as part of the Synchronous Grid of Continental Europe.** This model should have the ability to analyse the present system frequency performance with the current inertia level. (**Q1** & **Q2**)

c. Create simulation scenarios based on the annual changes in both the demand and production as forecasted in the **Energy Transition Outlook of DNVGL**. Such scenarios give the possibility of assessing the future frequency performance by considering the possible decrease in inertia. (**Q3**)

d. Develop a so-called Graph Indicator that predicts the time it takes until inertia reduction becomes a real stability issue as well the possible contribution of renewables to mitigate the potential problems of such a decrease. An example of this graph is illustrated in figure **1-1**. (**Q4**)

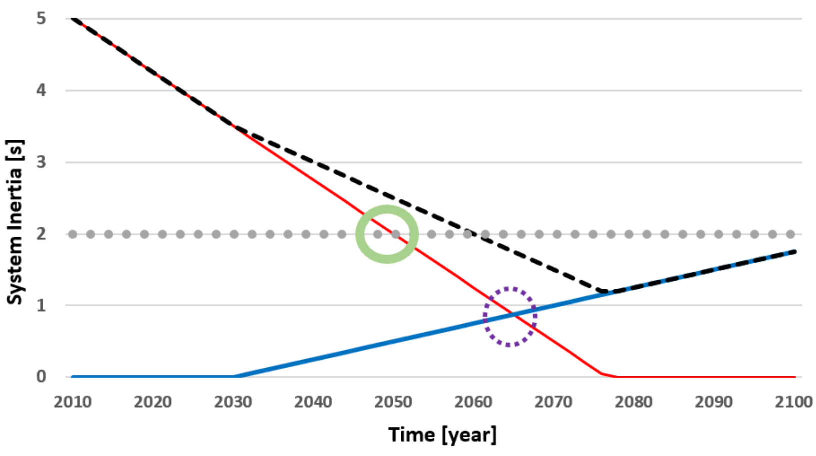

Figure 1-1: Graph Indicator; Example of a Possible Outcome

Where:

- The red line represents the annual inertia reduction due to the high penetration of renewables.
- The dashed grey line defines a specific frequency operating limit that the inertia decrease should not cross it.
- The green circle indicates the time it takes until inertia reduction would be a stability issue.
- The blue line shows the inertia produced by the inverters of renewables, which is possible to be available in the future.
- The dashed purple circle gives an example when the inertia produced by renewables would mitigate the potential problems caused by the decrease of conventional inertia.
- The dashed black line indicates the total grid inertia which is the sum of inertia generated by non-renewables (typical case) and inertia produced by renewables (optimistic case).

1.5. Overall Objectives

The overall objectives of this thesis project are illustrated in the flowchart below:

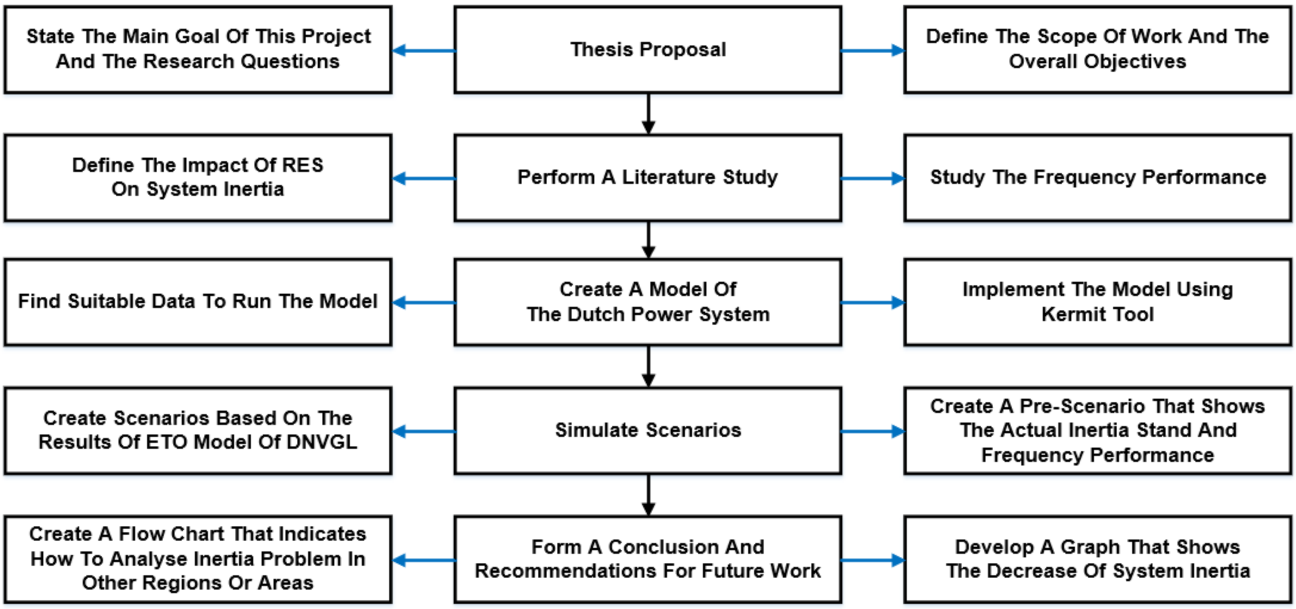

Figure 1-2: Thesis Overall Objectives

1.6. Document Outline

This section gives an overview of this document:

- **Chapter 1**: introduces the thesis background, motivation, goal, research questions, the scope of work, and the project overall objectives.

- **Chapter 2**: elaborates on the work performed during the period of literature survey. It describes the topics related to the area of this thesis based on published papers.

- **Chapter 3**: describes how the model of the Dutch power system as part of the synchronous grid of **Continental Europe** has been implemented using DNVGL tool Kermit.

- **Chapter 4**: shows the simulation results of the created scenarios with an analysis of the obtained findings.

- **Chapter 5**: gives an overall conclusion of the work done throughout this thesis project with the possible directions for future research.

2. LITERATURE REVIEW

This chapter summarizes the performed research during the literature review period. It consists of five primary topics: a stability analysis of traditional power systems, integration of renewables in Continental Europe, the impact of renewables on stability criteria, the influence of RE-e on grid inertia, and finally the system inertia in a future situation. These topics will give a sufficient knowledge to develop a suitable way of analysing the frequency performance and frequency stability of a given power system if a future situation.

2.1. Stability Analysis of Power Systems

Power system stability has often been considered as one of the most critical issues for reliable and secure system operation. In modern (hybrid) power system, different parameters often result in many forms of instability, e.g. frequency deviations, voltage collapse, and inter-area oscillations. Examples of such parameters are the increasing number of interconnections, the deployment of renewable sources, the rapid development of new control strategies, the ageing infrastructures, and the highly stressed operation (e.g. large number of generators and bus voltages with significant power flows over weak transmission lines).

In general, any power system is considered as an example of a constrained dynamical system due to its feasible operating regions. Such regions ensure safe operation and a satisfactory system structure. Appendix (A) gives a brief description of this concept.

Stated in [4] that the operation of a power system is based on three essential concepts:

a. **Reliability:** the ability of a power system to provide sufficient services continually, with allowable limits of interruptions.

b. **Security:** the ability of a power system to survive during contingencies without interruption of the agreed services

c. **Stability**: the ability of a power system to return to a steady-state condition following disturbances. The criteria of this concept are classified based on the following considerations:

   - The physical nature of an instability mode.
   - The size of a disturbance
   - The time span, devices, and process
   - The most suitable method applied to calculate and predict the resulting instability.

Figure 2-2 shows the traditional classification of stability criteria:

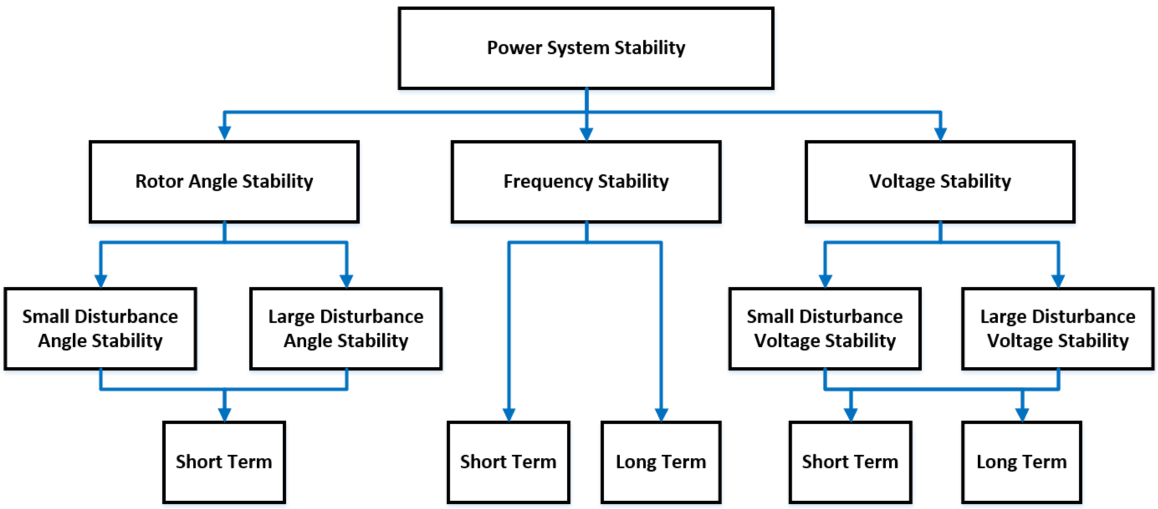

Figure 2-1: Traditional Classification of Stability Criteria [4]

2.1.1. Rotor Angle Stability

This criterion is defined in [4] as the ability of synchronous power generation units to maintain synchronism following disturbances. In general, rotor angle stability depends on the ability of a power system to keep the balance between mechanical and electrical torques of each synchronous generator within the interconnected system.

Instability often occurs in the form of expanded angular swings of some synchronous generators, resulting in loss of their synchronism with other generators. A fundamental factor of such issues is related to the output power variations of generators. In case that a power system is being subjected to disturbances, the equilibrium between both torques is upset, and generator speeds are not constant anymore, which in turn, causes a (de)acceleration of the rotor's speed.

Described further in [4] that the difference between the angular position of two generators occurs when one generator rotates faster than the other. This difference often results in load transfer from the slower generators towards, the faster machine, depending on the non-linear power-angle relationship. Beyond a specific limit, a further increase in angular separation, and hence, speed difference, is followed by a reduction in power transfer, resulting in the inability of the system to absorb the kinetic energy as results of a speed difference, which in turn, leads to rotor angle instability.

This criterion can be further classified into:

a. **Small-disturbance** (or small-signal) rotor angle stability: indicates the ability of the power system to maintain synchronism under so-called small disturbances at given initial operating conditions. Instability of small disturbances often occurs in two forms:

    - **Non-periodic instability** due to the loss of synchronising torque that results in increasing in rotor angle.

    - **Periodic instability** due to the lack of damping torque that increases the amplitude of rotor oscillations.

b. **Large-disturbance** (or transient stability) rotor angle stability: indicates the ability of a power system to maintain synchronism following (severe) disturbance, e.g., a short circuit on a transmission line. The resulting system response contains large rotor oscillations of increasing amplitude.

    In general, this sub-criterion depends on both the initial operating conditions of the system and the size of disturbances. Instability often results in a non-periodic angular separation form due to the loss of synchronising torque.

The time frame needed to study small signal stability is on the order of (10-20s), while the time required to study transient stability is in range of (3-5s) and might be extended to (10-20s). Therefore, both modes of angle rotor stabilities can be categorized as short-term phenomena. Measurement of rotor angles against local bus voltage is one of the most known methods applied to examine the transient stability as described in Appendix (B).

2.1.2. Frequency Stability

This criterion is defined in [4] as the ability of a power system to restore its nominal frequency following (severe) disturbances. In general, frequency stability depends on the ability of a system to maintain the balance between generation and load sides with a minimum loss of load.

Instability often occurs in the form of sustained frequency oscillations that results in loss of load/generation units. During Such oscillations, the time span of an activated process can vary between a fraction of seconds to several minutes. Therefore, frequency stability can be considered as a short/long-term phenomenon.

Traditionally, the operation of a power system assumes that synchronous generators maintain the scheduled grid frequency due to their electro-mechanical coupling. During frequency oscillations, for instance, such coupling allows the rotating mass of these generators to supply the grid with the required amount of kinetic energy, which in turns, provides the so-called moment of inertia.

This inertia is typically known as the system resistance to any change, and it is directly proportional to the amount of rotating mass of the synchronous generators in the system. This quantity prevents thus sudden frequency deviation, and hence, nominal frequency is maintained. The relation between system frequency and inertia constant is further described in Appendix (B).

2.1.3. Voltage Stability

This criterion is defined in [4] as the ability of a power system to restore constant voltages at all system buses following some perturbations at a given equilibrium set. In general, this criterion depends mainly on the ability of a power system to keep the balance between the supply and demand sides.

Instability often occurs in the form of a progressive fall/rise of voltages at some buses in the system, which results in cascading outages or major blackouts due to the tripping of some transmission lines by protective equipment, or the loss of load in specific areas. Mechanisms of analysing voltage instability and their indicators are given in Appendix (B). Voltage stability can further be characterized into:

a. **Small-disturbance**: represents the ability of a power system to restore constant voltages following small perturbations, e.g. gradual variations in the load of the system.

b. **Large-disturbance**: represents the ability of a power system to maintain steady voltages following large disturbances, e.g. switching events.

The time frame of voltage instability is in range of a few seconds to tens of minutes. Therefore, voltage stability may be either a short or long-term phenomenon. **Short-term phenomenon** represents the dynamics of fast active components, while **Long-term** phenomenon indicates the dynamics of slow active components.

From an engineering perspective, it is possible to argue that the high penetration of renewables will cause radical changes in the way how the traditional stability criteria are defined. These changes are shown in figure 2-1, and will be elaborated in the throughout the following sections of this chapter:

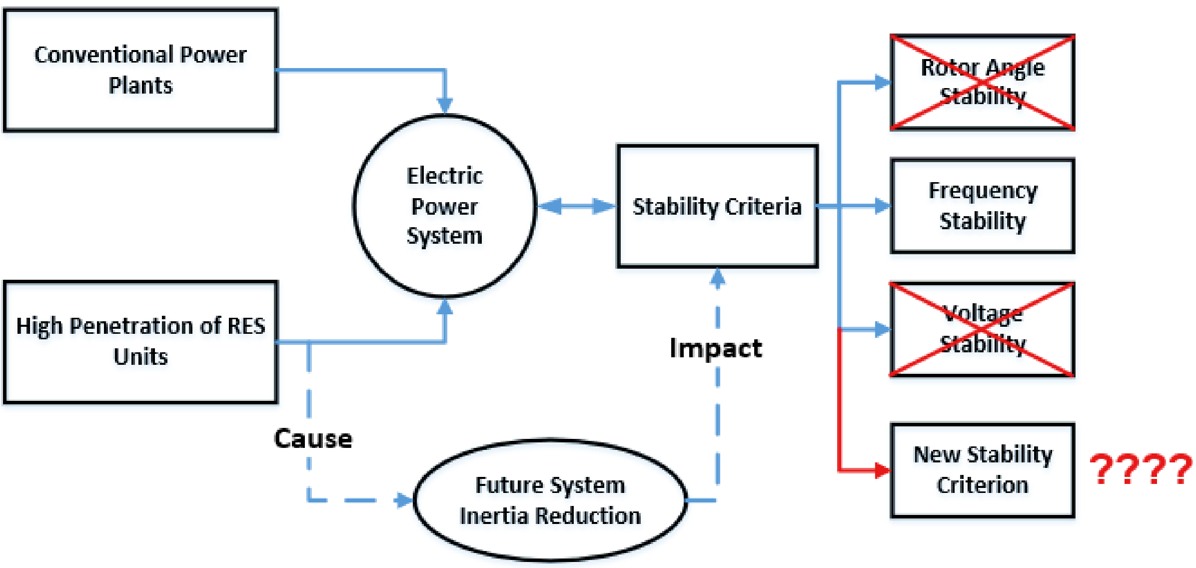

Figure 2-2: Possible Changes foreseen to Occur in the Traditional Stability Criteria

2.2. Integration of Renewable Sources

Different factors related to the global warming environmental impacts and fossil-fuel depletion have raised the need to guide the current power system on more cost-effective and sustainable paths. Such an energy transition leads to different power generation scenarios based on the level of renewable sources penetration. For instance, the model analysis of **Continental Europe** described in [5] focuses on the expansion of RES share between 2020 and 2030, and it considers three main scenarios:

a. **Optimistic Scenario (1):** corresponding to the 'High-RES share scenario' with a 68% share of RES around 2030, characterised by a fast expansion of RES share-based generation.

   Furthermore, two sub-scenarios have been created in this model analysis to investigate the impacts of RES share on systems with different levels of energy consumption. These sub-scenarios were recognized as variations of scenario one:

   - **Sensitivity optimistic sub-scenario with high load (1a)**
   - **Sensitivity optimistic sub-scenario with high energy efficiency (1b)**

b. **Middle Scenario (2):** corresponding to the 'Diversified Supply Technology' scenario' with a 59% share of RES around 2030.

c. **Pessimistic Scenario (3)**: corresponding to the 'Current Policy Initiatives' scenario, with a Low-RES share expansion trajectory of 51% around 2030.

The study performed in [5] has also demonstrated that different scenarios may require a different structure of power generation capacity. The need for conventional generation capacity is primarily driven by the evolution of electricity demand, whereas the choice of different variable RES technologies appears to be of secondary importance. For example, the study shows that the optimistic scenario might lead to a notable decrease of conventional power generation capacity as illustrated in figure 2-3 below:

Scenario 1	2020	2025	2030
Nuclear	125	107	91
Coal conv.	119	69	44
Gas conv.	155	138	92
Oil	33	11	6
Back up	63	89	157
Hydro	115	117	120
Biomass	61	70	78
Wind (on)	186	223	313
Wind (off)	64	92	157
Solar	54	88	188
Other RES-E	2	2	5
Total	976	1,008	1,250

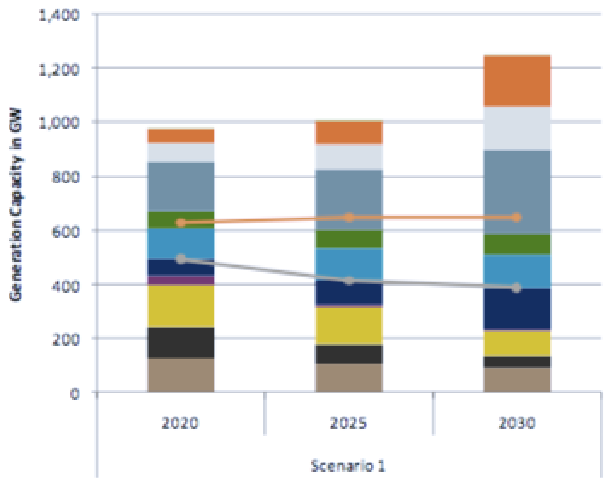

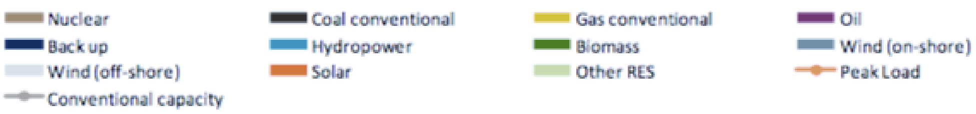

Figure 2-3: Expected Installed Capacity Within Continental Europe Based on The Optimistic Scenario [5]

2.3. Stability Criteria in Future Power System

The energy transition mentioned in section (2.2) is expected to have a significant impact on the way how power systems operate. More integration of renewable sources means less synchronous generators, which in turn, results in a reduction of system inertia.

It is quite essential to specify which types of stability criteria would possibly be affected if system inertia is reduced. Mentioned in [6] that system inertia has a crucial role in changing the dynamic behaviour of a particular power system. The dynamic interactions in current power systems and the corresponding control actions are often characterized by different timescales as shown in figure 2-4. Such dynamic interactions can be classified into four groups:

- Wave
- Electromagnetic
- Electromechanical
- Non-electrical Dynamics

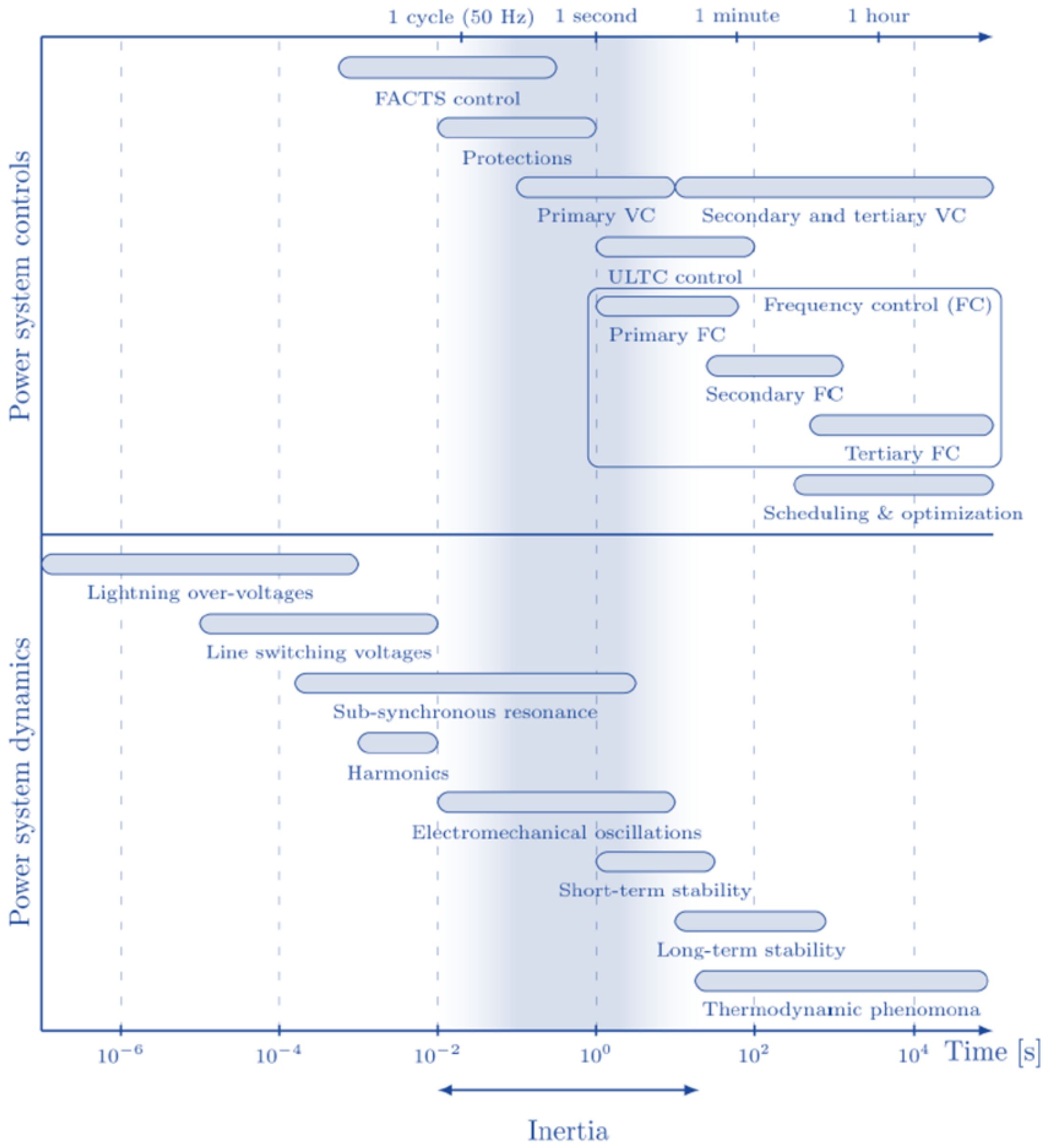

Figure 2-4: Different Timescales of Power System Dynamical Interactions and The Accompanied Controls [6]

As mentioned before, frequency stability is directly related to system inertia. From this perspective and by considering the system dynamic behaviour described above, it can be concluded that the electromechanical interactions and the corresponding control actions, i.e. primary and secondary controllers, would be possibly influenced by the decrease of inertia in a future power system. The time frame of interest of such interactions is on the order of several milliseconds to a couple of seconds as highlighted with blue colour in figure 2-4.

Within this timescale, different control actions are activated to ensure system stability following a disturbance. Depending on the size and origin of a specific disturbance, short or long-term oscillations are initiated, resulting in different modes of instabilities. Typically, system stability can be defined as its capability to damp such oscillations to ensure a proper system operation.

From the perspective of low inertia system, the stability criteria can be further categorized depending on the time frame of interest and the driving forces of instabilities modes, which can be either load or generator driven:

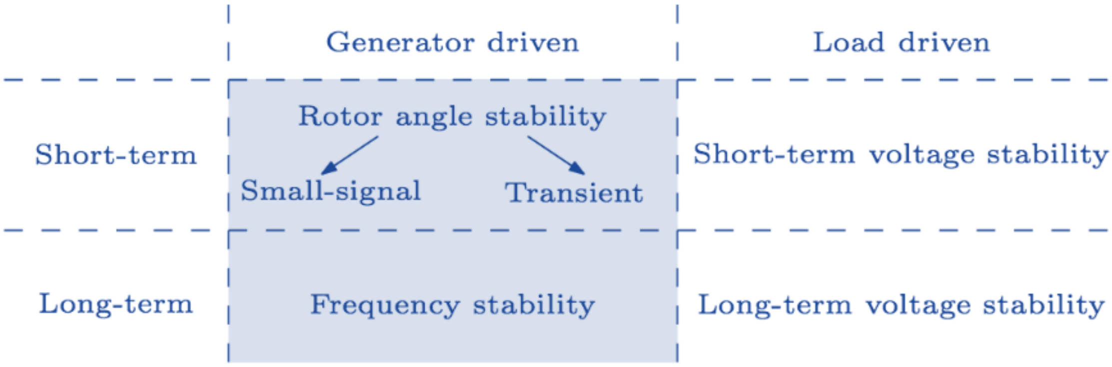

Figure 2-5: Classification of Stability Criteria of The Current Power System [6]

Given in [10] that voltage stability is often recognised as a local phenomenon due to the direct relationship between system voltage and load. This relationship explains the reason why the load driven category is not considered to be a critical factor for the studies of system inertia reduction. In contrast to the load driven category, generator driven stabilities could be affected by low inertia level. This impact can be described by the swing equation as the system inertia directly affects the frequency and angles of power generation units.

Mentioned further in [10] that inertia reduction may influence the rotor angle stability. This impact often relies on different parameters, e.g. the displacement of conventional generators by RES units, and the change of power flow patterns in response to the shift in generation location. However, this criterion will be excluded from the future studies when the share of renewable sources would reach 100%.

From the perspective of power system operation, the expected reduction of system inertia would have a significant impact on the stability of system frequency. Such an impact has to do with the contribution of system inertia to frequency deviation following disturbances. For this reason, **the long-term generator driven category will only be considered in this thesis project**, since, the focus is on the deterioration of frequency oscillations concerning inertia reduction.

2.3.1. Inertia and Frequency Stability

In general, the frequency of an AC power system is related to the rotational synchronous speed of the conventional generators. During the steady-state situation, system frequency should always be in a satisfactory range nearly to **50Hz in the synchronous grid of Continental Europe** (CE). Deviation in system frequency occurs due to different parameters, e.g., a power imbalance event. Such deviations might cause:

- A flow of undesirable magnetisation currents in the induction motors and transformers
- A deterioration of the performance of specific conventional power plant.

In [6] is stated that the critical frequency operating range for a satisfactory operation differs from one power system to other; therefore, different control mechanisms are applied in power systems to restore the desired frequency range following disturbances. Appendix (F) gives a detailed explanation of Frequency-Load-Control and Performance.

The restoration process from the moment of a specific disturbance to the moment of the restoration of the nominal frequency can be divided into the following stages:

- **Primary Control (PrC):** initiates within seconds and it is a property of synchronous generation units. During a power imbalance between supply and demand sides, the synchronous speeds of rotating masses in all conventional power generators either slow down (if there is an excess at the demand side) or speed up (if there is an excess at the supply side) to return the system to its steady-state condition to stop speed change. This distribution of power change among all existing synchronous generators results in a relatively small frequency deviation within the allowable frequency operating ranges.

- **Secondary Control (SeC):** replaces PrC over minutes and is being activated only by Transmission System Operators (TSOs). This controller maintains the minute-to-minute balance of cross-border power exchange throughout the whole day and returns the system frequency to the standard nominal value.

- **Tertiary Control (TeC):** partially complements and finally replaces SeC by re-scheduling generation plans and is being activated only by (responsible) TSOs. This controller

- **Time Control (TiC):** corrects the global time deviations of all performed actions.

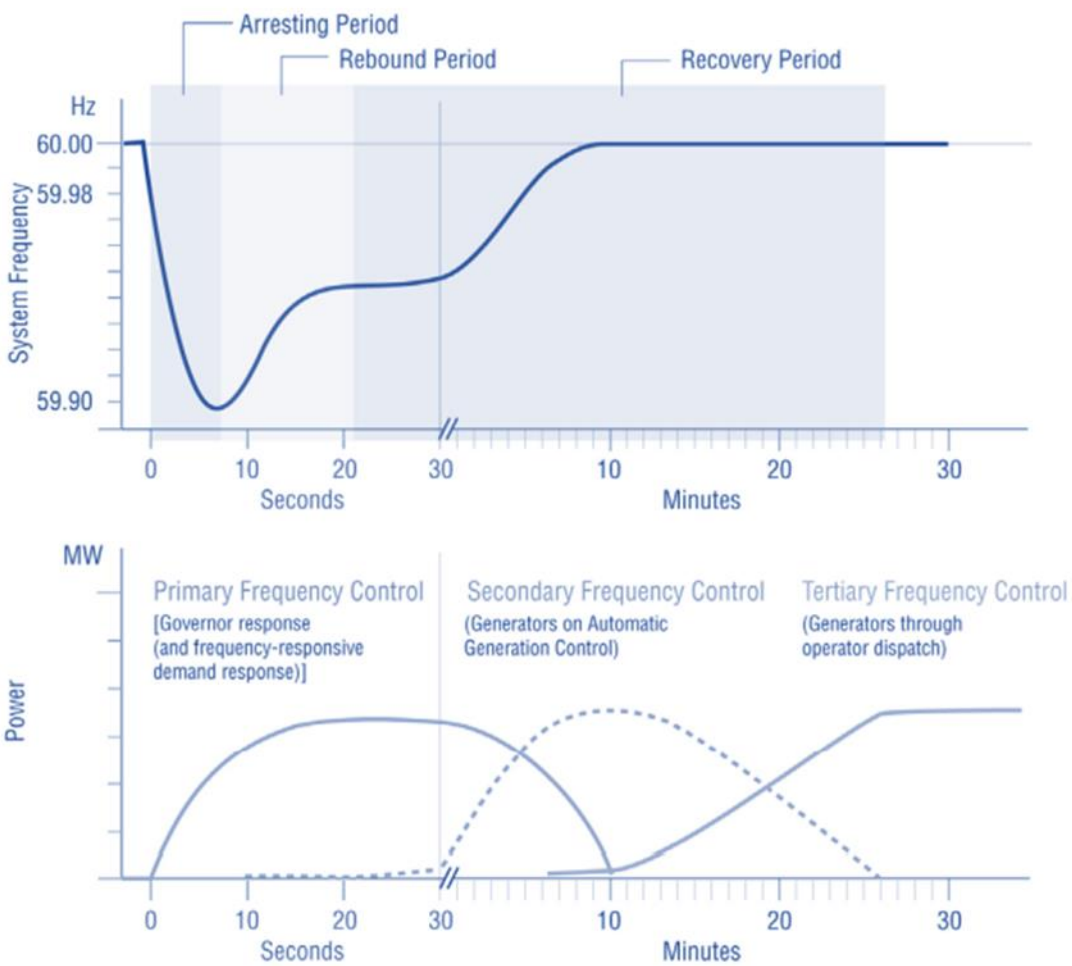

Figure 2-6: Frequency Control Actions with Their Relevant Timescales [7]

An example of such a process is given in figure 2-7 below. In this example, the synchronous generation units supply the grid with the required amount of kinetic energy to oppose frequency oscillations. This release of kinetic energy immediately occurs after a significant power difference between the supply (P_G) and the demand (P_L) sides. The restoration process of system frequency is typically performed by three controllers: Primary Control, Secondary Control, and Tertiary Control.

The **Primary Control** Consists of two phases: Inertial Response and Governor Response. Within the first phase, the impact of power change is distributed by the Inertial Response among all synchronous generators to counteract the frequency oscillations. Once these frequency deviations are smoothed out, a typical system frequency decline is reached as shown in figure 2-7. The end-point of this decline is known as **NADIR point**. The timescale of this stage (Inertial Response stage) is on the order of (0-10s), and it is often called the **Arresting Period** see figure 2-6.

The next phase is called the Governor Response. Typically, all synchronous generators are provided with speed controllers (or the so-called governors). Such controllers start acting when frequency deviation exceeds a specified dead-band. For instance, the frequency dead-band of the 50Hz synchronous grid of CE is specified by **European Network of Transmission System Operators** (ENTSO-E) in the range of (49.98 and 50.02Hz). When frequency oscillations exceed this range, governors react by increasing the amount of power output of the generator's prime-mover proportional to the speed change of the generator's rotor. Such a reaction limits frequency deviation, which in turn, results in restoration of power balance between supply and demand sides. The timescale of the whole primary stage is in the range of (10-30s), and it is often called the **Rebound Period**.

Within the Primary stage, system frequency is stabilized because of the proportional actions. However, there is still a small frequency deviation (f_{ss}) as illustrated in figure 2-7. This small offset from the nominal frequency value is fully damped out during the **Secondary Control** stage. This controller is much slower than the primary control, and it is typically on the order of (10-30mins) and known as the **Recovery Period**.

Given in [6] that the implementation process of secondary control different from one system to another. For instance, the secondary control of the 50Hz synchronous grid of CE is fully automated, and it is a part of the so-called **Automatic Generation Control** (AGC). This automatic control often returns the frequency to its nominal rated values by further adjusting the power setpoints of prime-mover to keep the power exchange between control zones within their scheduled values.

The final stage is called **Tertiary Control** that is provided to restore the reserves of the secondary control. Such reserves are standardised by the Transmission System Operators (TSOs), which have the responsibility to guarantee the stability of system frequency at both supply and demand sides.

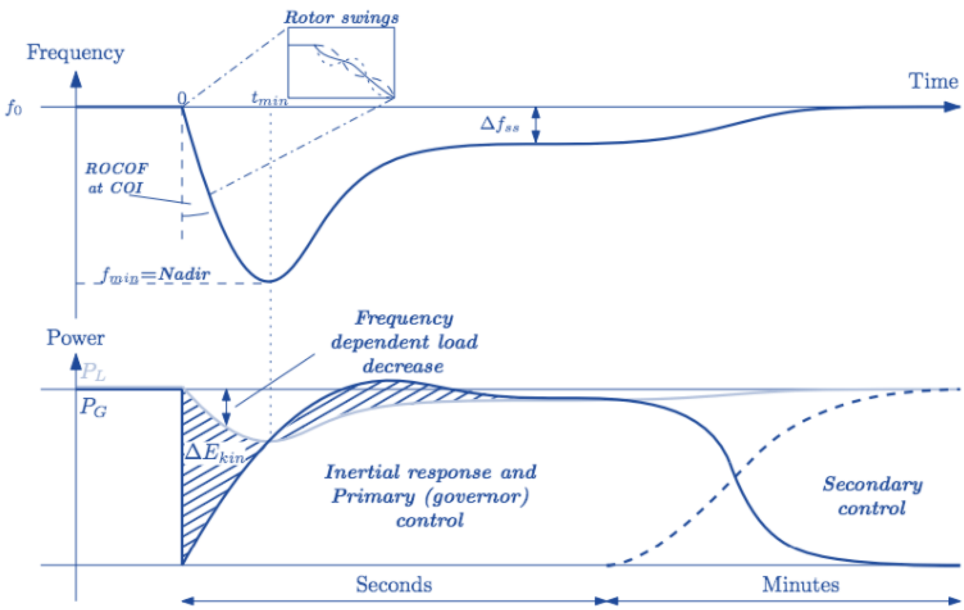

Figure 2-7: Frequency Response Following a Power Imbalance Event [6]

2.3.2. Frequency Stability Indicators

In general, stability indicators provide the possibility of detecting the abnormal behaviour of a power system and its orientation towards significant voltage collapses. These indicators provide the possibility of covering the whole electric system within a short time. Meanwhile, they supply the Transmission System Operators (TSOs) with the required grid information, i.e. system frequency and generator outputs to make quick decisions.

In [7], the so-called Key Performance Indicators (KPIs) have been studied. Such indicators make possible to predict and avoid unstable operating conditions, and hence, preventing intermittent generation behaviour or significant blackouts.

From the perspective of future power system with a high share of renewable sources and low inertial response caused by inertia reduction, KPIs are handy to predict the deterioration of frequency deviation within the arresting period that is typically in a range of (0-10s) see figure 2-6.

a. NADIR Metric

This metric indicates the lowest frequency point immediately after a power imbalance event. Examples of such points are highlighted with dots in figures 2-8 and 2-9. There are two ways to compute this point; analytically and mathematically as described in [7]. Analytically, the first local minimal point should be obtained after a specific disturbance, e.g. at ($t > t_1$), while the way of computing this point mathematically is by using the automatic function **Find-peak in MATLAB**. This Function performs the computation process as follows:

- **a.** Finding a derivative of the system frequency
- **b.** Setting this derivative to zero
- **c.** Getting the instants when the slopes are zero; this makes possible to find the local maxima and minima of the system frequency
- **d.** Evaluating the frequency functions at these instants; the minimum value is the NADIR metric

This metric plays a crucial role in frequency stability monitoring processes, and stability is satisfied when:

$$\mathrm{f_{NADIR}} \geq \mathrm{f_{min}} \tag{2.1}$$

Within the 50Hz synchronous grid of Continental Europe, the minimum allowable frequency point following a disturbance is set to (f_{min} = 49.2Hz) by ENTSO-E. For instance, if the minimum frequency point (NADIR) at a specific moment following disturbances is lower than that value, frequency deviation might be dangerous, and they could then break the security limits, resulting in system collapses.

b. Rate of Change of Frequency (RoCoF)

Stated in [7] that this metric is intended to indicate the change of system frequency following a massive power imbalance between supply and demand sides. Frequency deviation occurs in an electric power system immediately following a power generation loss. Moreover, the oscillations of system frequency have been analysed with focusing on the arresting period using different values of system inertia (1s, 5s, and 10s). The results of this analysis are highlighted in figure 2-8.

Typically, the rate of change of frequency (ROCOF) is given in [Hz/s] and defined analytically using frequency deviation as shown in equation (2.2):

$$\mathrm{ROCOF} = \frac{\mathrm{df}}{\mathrm{dt}} \tag{2.2}$$

However, the definition of RoCoF metric requires a mathematical way of computation because this metric is intended to show the frequency gradient following a power imbalance event. For this purpose, a mathematical way of computing RoCoF for the synchronous grid of CE is given in [7] based on the standards of ENTSO-E. This computation process is given as follows:

a. Calculate the centre of inertia (COI) frequency:

$$f_{COI}(t) = \frac{\sum_{i=1}^{n} H_i * S_{base} * f_i(t)}{\sum_{i=1}^{n} H_i * S_{base}} \qquad (2.3)$$

Where:
- $f_{COI}(t)$ = frequency centre of inertia in [Hz]
- H_i = inertia constant in [s]
- S_{base} = nominal apparent power in [MVA]
- $f_i(t)$ = frequency in [Hz]
- i^{th} = number of generators in [-]

b. Use the instant of the event (t_1) as shown in figure 2-9 below
c. Use the NADIR instant (t_2)
d. Determine the index of a specific intermediate period: ($t_3 = t_1 + 0.5s$)
e. Find a linear fitting point to the computed $f_{COI}(t)$, where: ***(t) in range of [t_1, t_3] with ($t_1 < t_3$)***
f. Compute the frequency decline slope following a disturbance.

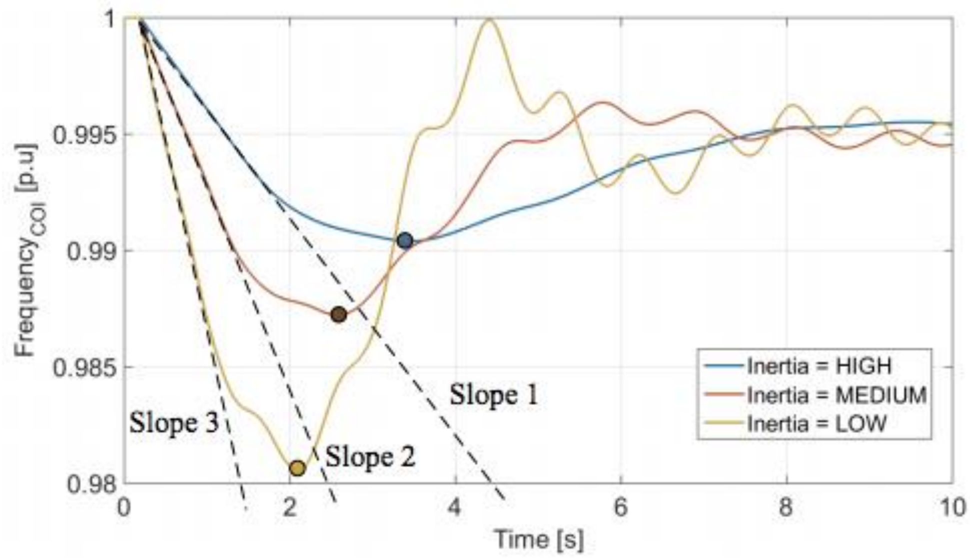

Figure 2-8: Visual Representation of Frequency Slopes When Different Inertia Values Are Applied to a System [7]

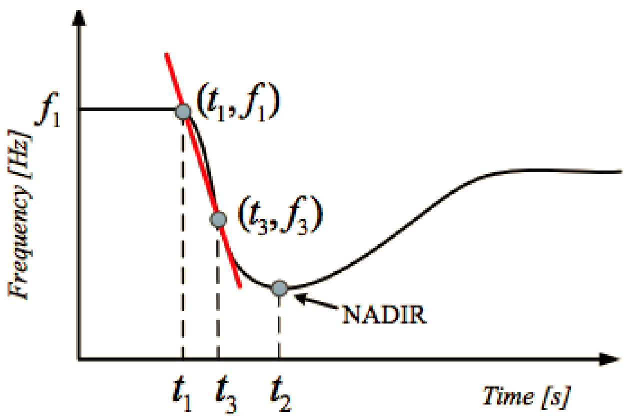

Figure 2-9: Required Points to Execute the Mathematical Way of RoCoF Computation [7]

2.4. Impact of Renewable Sources on Inertia

The energy transition towards an electricity generation based on a combination between CSGs and RES units will have substantial impacts on the traditional structure of power systems. In general, renewable sources behave differently than conventional generation units. Besides their intermittent behaviour, they do not contribute to system inertia because these sources are connected to grids through electronic devices that electrically decouples them from the power grid.

Figure 2-10 below shows the difference between the traditional and hybrid power systems. This difference is often represented by the amount of system inertia constant (H_{system}). This constant could be significantly reduced in the future due to the displacement of conventional generators by RES units.

Based on the traditional **swing equation** of Rotational Inertia see Appendix (C), the total inertia in a certain power system that combines both synchronous generators (characterised by H) and RES control converters (characterised by Hv), can be expressed as follows:

$$H_{system} = \frac{\text{sum of } (H_i * S_i) + \text{sum of } (H_{V,i} * S_i)}{S_{system}} = \frac{\text{sum of } \left(E_{kin,i}\right) + \text{sum of } (E_{V,i})}{S_{system}}, \qquad i = 1, \dots, n \qquad (2.4)$$

Where:

- H_i = inertia constant of an individual power generation unit in [s]
- H_v = inertia constant of an individual inverted connected unit [s]
- S_i = individual synchronous capacity connected to a conventional generator in [MVA]
- S_{system} = common system base in [MVA]
- H_{system} = equivalent inertia constant of the overall system in [s]
- E_i = individual kinetic energy of an individual power generation unit in [MWs]
- E_v = individual kinetic energy of an individual inverted connected unit [MWs]

Equation (2.4) indicates the importance of RES control converters in the future power system. The contribution of such converters to the power system control might avoid the expected inertia decline as they manage the energy exchange with the grid using their measured frequency as described in [6]. The control action of such converters is based on the Virtual Inertia Response approach, which is further explained in Appendix (D).

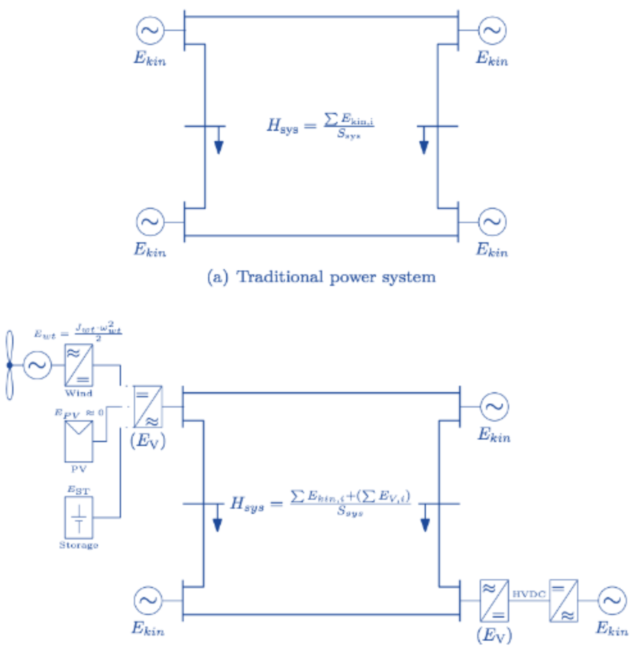

(b) Future power system

Figure 2-10: kinetic energy storage and inertia in different power systems [6]

Furthermore, figure 2-11 below shows the difference in energy exchange between the traditional and future power systems. The block area in the figure 5a represents the amount of kinetic energy available within the relevant system because:

- The **width** of a block is directly proportional to the sum of the moment of inertia (J) over a square of the number of poles pairs.
- The **height** of a block is directly proportional to the square of rated synchronous rotational speed (ω_e) divided by 2.

The blue shaded area indicates the amount of stored kinetic energy at a rated frequency ($\omega_{e,0}$). This energy always varies between ($\omega_{e,min}$) and ($\omega_{e,max}$) because any power system is developed to operate within a specified bandwidth.

For instance, the occurrences of a power imbalance event within the system (A) at (t_0) will lead to power compensation by synchronous generators in the form of kinetic energy (see the hatched area illustrated in the figure 2-11a), resulting in a decline of system frequency at (t_1) as shown in the figure 2-11b.

Stated in [6] that the decline of system frequency requires, in general, specific control actions with increasing the set-points of power generation units; otherwise, there will be a depletion of the stored kinetic energy that results in system voltage collapses, leading in some rare situations to cascading contingencies. An example of such a scenario is given in Appendix (E).

Systems (B) and (C) provide the possibility to observe the influences of renewable sources on the future power systems regarding the system inertia reduction. These influences can be seen from the decreased amount of kinetic energy within the relevant block-areas.

Finally, the rate of change of frequency (ROCOF) during a power imbalance event will be, for instance, more significant in the system (C) than in system (A), but lesser than system (B). In other words, the frequency deviation is higher within the system (C) than system (A) but lower than system (B), which reflects the positive contribution of virtual kinetic energy in the future power system.

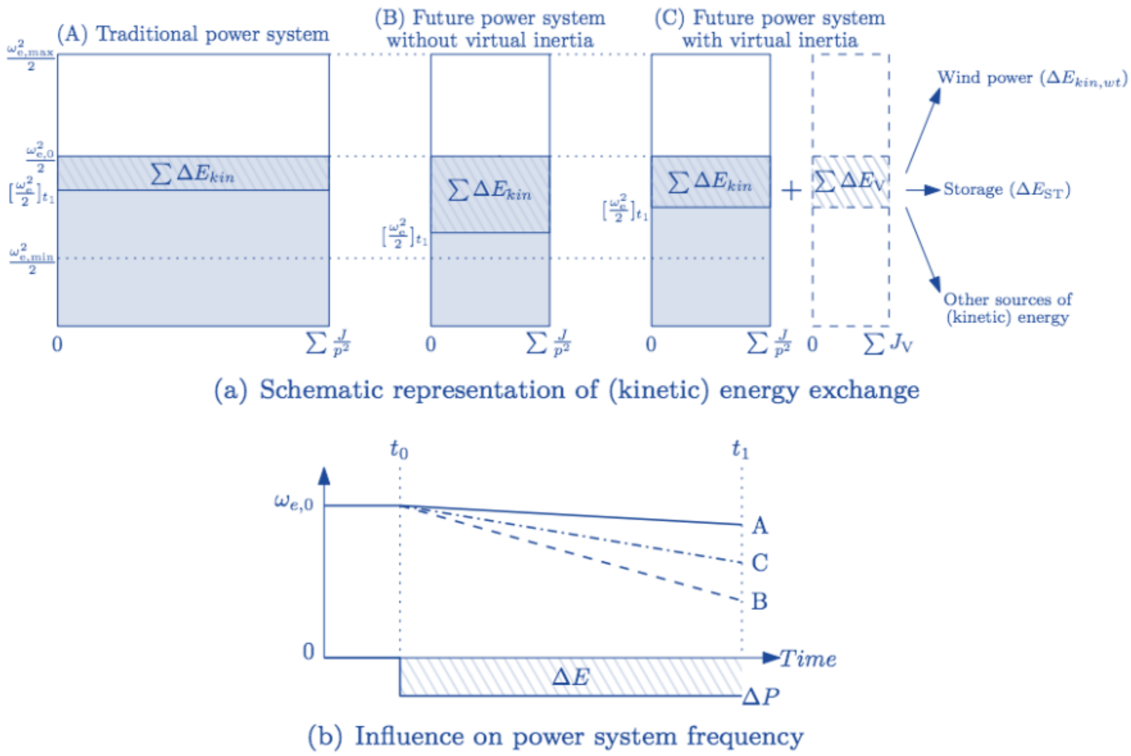

Figure 2-11: the difference between conventional and future power systems concerning energy exchange [6]

2.5. Inertia and Share of Renewable Sources

In general, it is quite complicated to obtain the minimum required inertia in the grid as inertia depends on several system parameters. Appendix (G) describes the current methods that are being used to estimate the exact amount of available inertia in a particular power system.

Depicted in [6] two different scenarios where the future reduction of system inertia might be situated between them. These two scenarios are illustrated in figure 2-12:

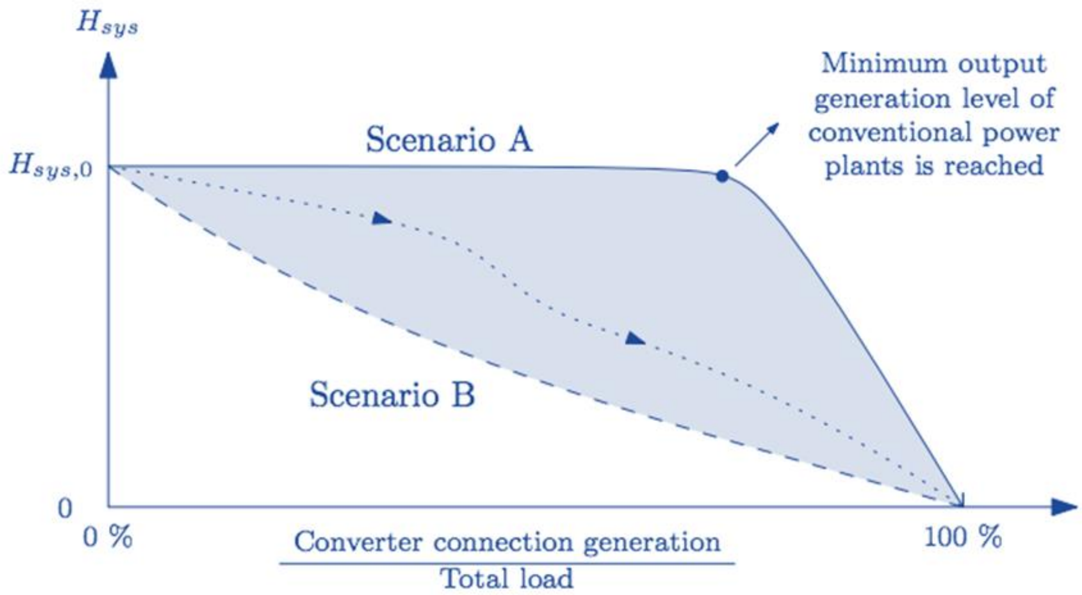

Figure 2-12: Two Depicted Scenarios Where Future Inertia Decline Could Be Situated Between Them [6]

In **scenario (A)**, the number of RES units is continuously increased while the system inertia provided by CSGs is maintained constant or slightly decreased, while in **scenario (B)** the conventional generation units are gradually being replaced with renewable sources, resulting in a significant reduction in system inertia. This scenario is based on two assumptions:

- RES units and their storage devices could provide the Required reserve of primary control
- Spinning power generators might operate at the maximum power output level.

Moreover, different approaches corresponding to these extreme scenarios should be applied to ensure a stable operation of a power system with high penetration of renewable sources and low inertia level provided by synchronous generators.

The **first approach (1)** is corresponding to scenario (A) till the knee point of the curve in figure 2-12. This approach could be possibly reached by decreasing the minimum generation level of synchronous generation units and increasing the control margins to provide more frequency control. In other words, system inertia could be kept up to a specific level of renewable sources by dispatching the conventional plants to lower power output levels instead of removing CSGs from power plants.

Also, system inertia can be maintained at a desired level by modifying the existing synchronous compensation condensers. Typically, such condensers are installed in a borderline condition between a power generation unit and a motor without prime-mover and load. They are mostly used to compensate the power factor of a particular network by injecting/absorbing reactive power to the line in order to support grid voltage. An example of such a compensator is installed in Denmark with a capacity value of 270MVA. This compensator consists of a flange connected to the rotor shaft of a generator, making possible to connect an additional flywheel in the future to further increase the level of system inertia if it is needed.

The **second approach (2)** deals with scenario (B). This approach can be achieved by adapting the current power system devices, protective equipment, and generator grid code. Such an adaption might provide the possibility of managing the expected high ROCOF values and frequency oscillations. Further studies are also needed to find out the maximum admissible levels that ROCOF and frequency limits could reach without endangering the stability of a particular power system.

ENTSO-E has defined in [8] the impact of reduced inertia on the operation of the 50Hz synchronous grid of **Continental Europe**. It has been shown that the primary parameter to be considered for the studies of system inertia reduction is the allowable operating ranges of ROCOF. Based on the analysis of the last power imbalance events performed in ENTSO-E report, the acceptable ROCOF ranges of the 50Hz grid of CE is on the order of (500mHz/s-1Hz/s).

The **third approach (3)** is corresponding to scenario (B). This scenario can be achieved by reducing both the probability and size of contingencies. Such a reduction could be figured out by limiting the amount of power injected into a single point (node) in the system or by designing special protective equipment that is able to prevent network splitting and cascading outages.

The **final approach (4)** also deals with scenario (B). This approach tries to enforce the renewable sources and their control converters to provide the future power system with more virtual inertia and frequency control margins. Within the area of this approach, different solutions might be possible, e.g. the emulation of the behaviour of conventional power plants to supply the grid with the required amount of power after the frequency decline has reached a specific threshold.

Figure 2-13 below gives a summarization of these approaches:

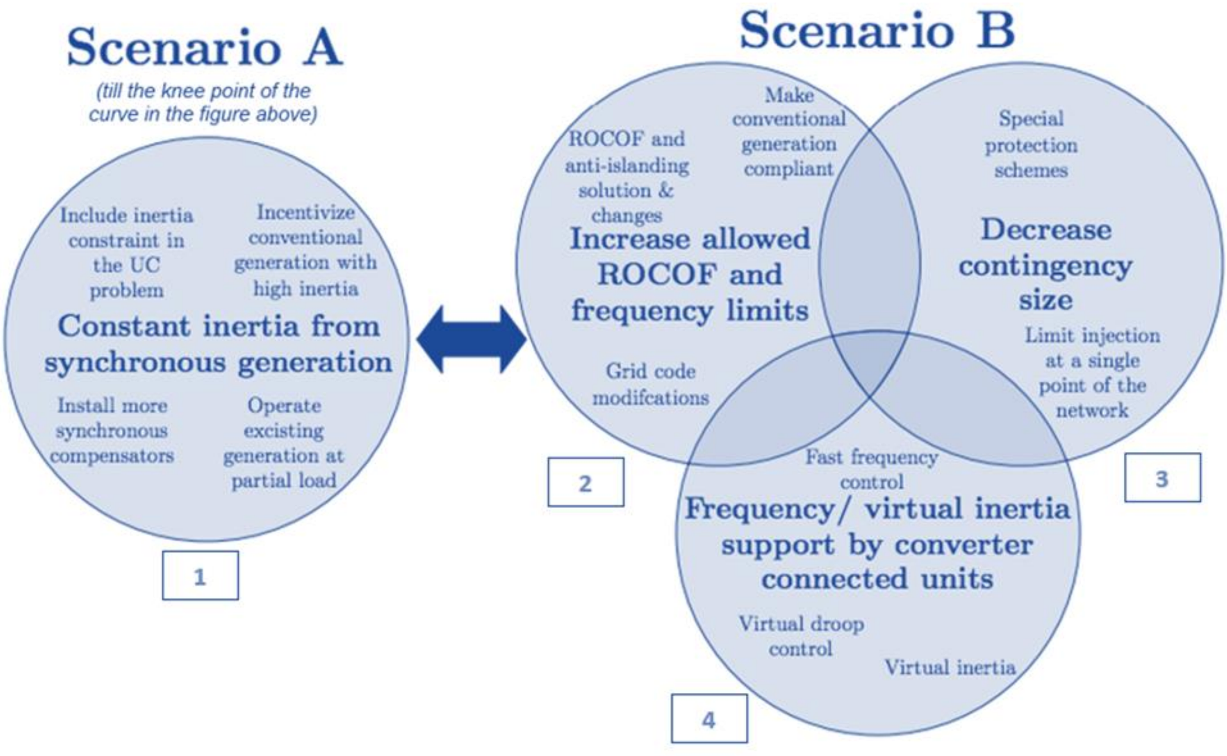

Figure 2-13: Different Approaches to Ensure a Stable Operation of a Power System with Low Inertia Level [6]

In short, the massive penetration of renewable sources described by these two extreme scenarios would influence not only the system inertia but also the operation and control actions of an electric network. Therefore, combinations of both the current practice and future developed technologies are required to cope with these challenges and to ensure optimal operation.

2.6. Reflection on Literature Study

In general, a stable and reliable operation of power systems is maintained through the traditional stability criteria. Such criteria ensure that generator rotor angles, system frequency, and bus voltages will be returned to the balance states after (severe) disturbances, e.g. power imbalance events.

However, the increased complexity of power systems, the more dependency on control actions, and the energy transition towards an electricity production dominated by renewable energy generation will pose many challenges, which might cause radical changes in the operation of a power system and its frequency performance.

Moreover, the high penetration of renewables and their relative share will cause a reduction in grid inertia. This decrease would, in turn, affect the overall frequency performance of a given electric network; resulting in significant frequency deviation as both values of the RoCoF and Nadir-Point are directly related to the current level of grid inertia. Based on the work done in the published papers regarding the main problem of this thesis, it has been found that future inertia will have two possible figures, which requires innovative solutions to tackle their consequences.

The impacts of high renewable energy generation share in the total electricity production followed by a reduction in system inertia can are summarized in the figure below:

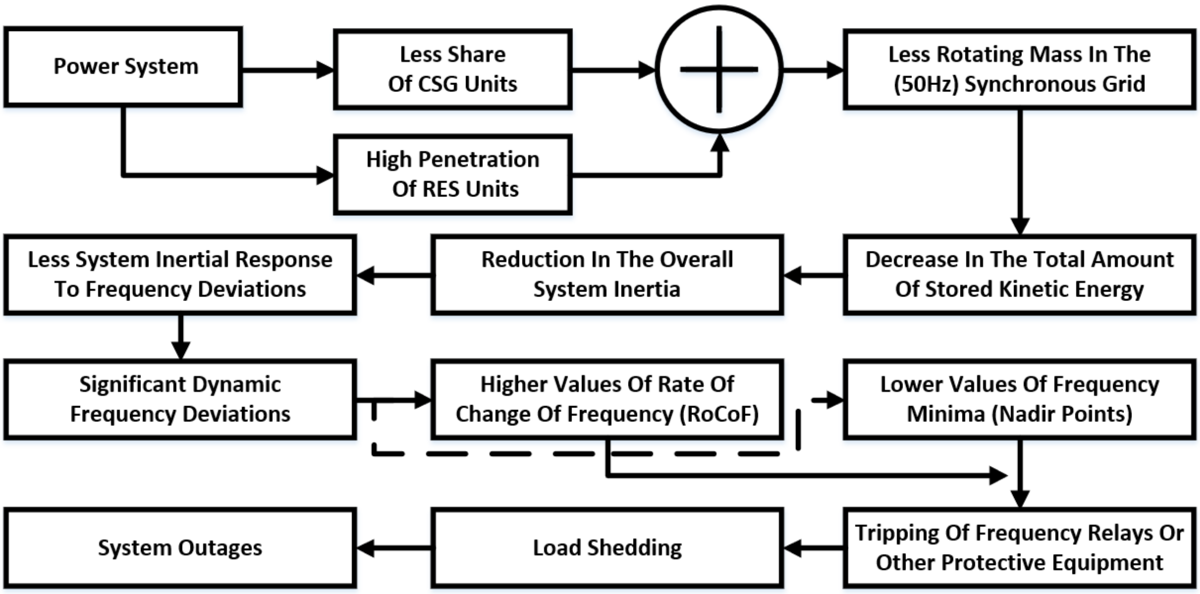

Figure 2-14: An Overview of the Impact of High Penetration of Renewable on Power System Operation

2.7. Boundaries of The Thesis Scope

In the future power system of **Continental Europe, including that of the Netherlands**, it is expected that the embedded systems and micro-grids will also influence the traditional transient stability in different ways. However, the deployment of such systems is still limited; therefore, this thesis project does not consider their impacts on the traditional stability criteria, especially the frequency stability criterion of the European grid.

On the other hand, the increased number of renewable energy sources followed by a reduction in system inertia will have considerable impacts on the frequency performance of the future power systems as described in the previous section. However, the boundaries of such impacts exclude both rotor angle and voltage criteria from stability studies as a decrease in system inertia will only affect the system frequency behaviour during disturbances as mentioned in section (**2.3**).

Therefore, this thesis will only examine the impact of renewable sources on the frequency deviation and frequency control action of the Dutch power system as a part of the Synchronous Grid of Continental Europe.

3. APPROACH IMPLEMENTATION

This chapter elaborates on the work performed during the implementation phase of the dynamic model that represents **the Dutch power system as part of the Synchronous Grid of Continental Europe** using DNVGL tool Kermit. Throughout this chapter, several tasks have been carried out to get the desired model; starting from developing a detailed approach for the involved model towards a simplified approach that can be used to assess the frequency performance not only for the Netherlands but also for other regions.

3.1. Block Diagram of the Proposed Approaches

According to [9], the **European power grid** is divided into five regional groups (RG). These groups are based on the synchronous interconnections as shown in figure 3-1 below. The primary purpose of this division is to maintain a secure and reliable operation of the power grid to ensure a sustainable balance between the supply and demand sides.

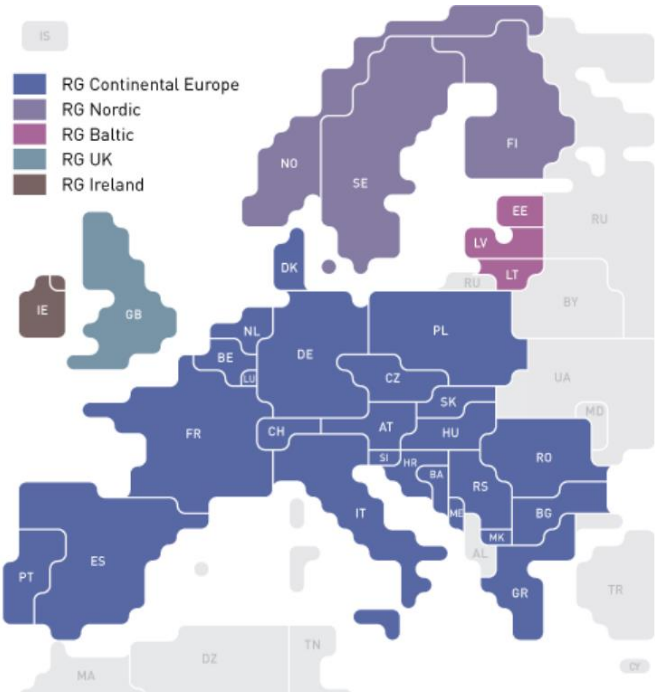

Figure 3-1: Countries and Interconnections of CE Under the ENTSO-E [9]

Concerning the problem of this thesis project, the following countries are considered in the design of the Dutch power system model as part of the European power grid using Kermit:

- All countries of **RG-CE,** including the Netherlands, because they are synchronously connected through AC interconnection lines. Thus, they share the same frequency (50Hz).
- All countries of **RG-Baltic,** because they are synchronously connected to **RG-CE** through the AC interconnection line between LT-PL. Thus, they also share the same frequency (50Hz) as the countries of **RG-CE**.
- The UK, as it is connected to the Dutch power system through an HVDC cable. It is worth mentioning that the UK-NL interconnection does not affect the frequency of the 50Hz regional groups. This HVDC interconnection is only needed for load and generation balance.
- Norway has a similar situation as the UK.
- The western part of Denmark as it is synchronously connected to **RG-CE** through the AC interconnection between **DK-DE**.

For simplification, every country has been represented by one node (**can also be called as a zone**) based on the model given in [5]. Besides, each of these nodes contains different power generation plants both dispatchable and non-dispatchable. The inner transmission lines between these plants have not been considered in this approach. Figure 3-2 shows the block diagram of this model which consists of 25 nodes. The total number of power transmission lines are 60 (14 DC and 46 AC).

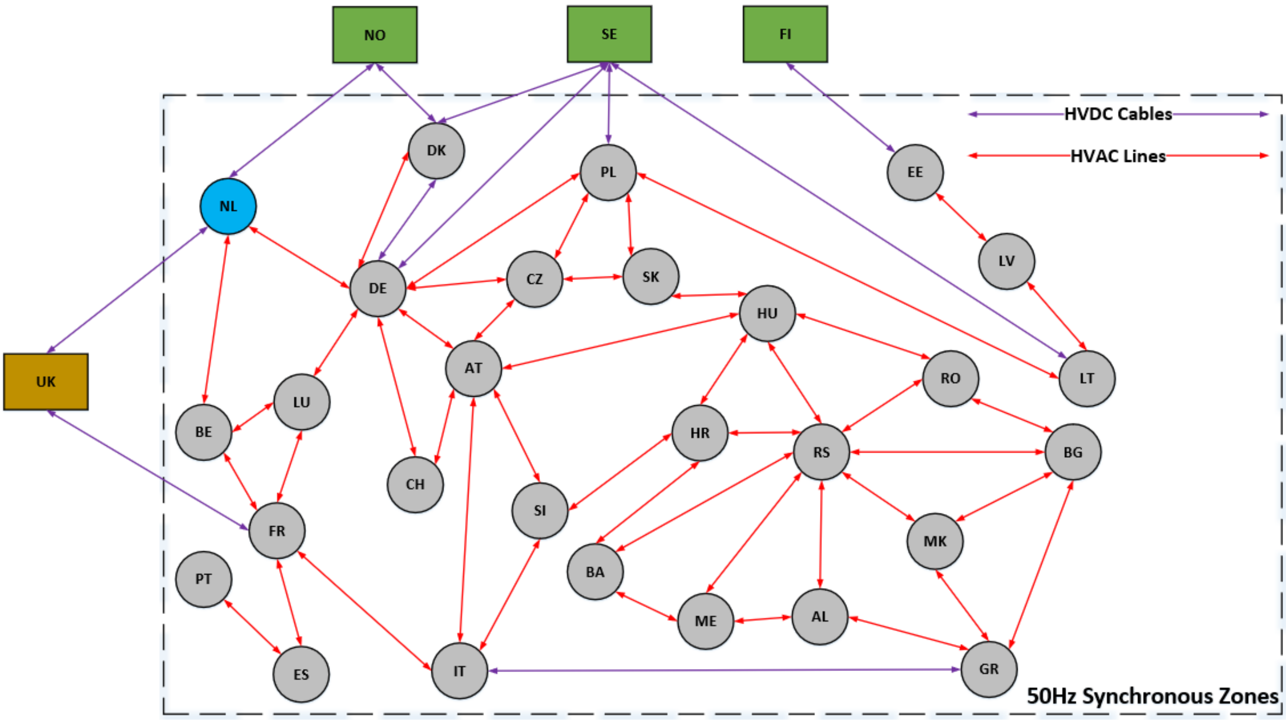

Figure 3-2: Block Diagram of the First Approach

The analysis of frequency performance using this approach has several advantages and disadvantages as listed below:

- <u>**Advantages**</u>: this model provides the possibility of analysing the frequency performance of each node within the studied regional groups. In other words, this approach provides the possibility of analysing the frequency performance of the whole synchronous grid of CE including that of the Netherlands.

- <u>**Disadvantages:**</u> to implement the current condition of the Dutch power system using this model might be complicated because of the following difficulties:

  - The need for a day-ahead generation schedule for every node
  - The need for a day-ahead load schedule for every node
  - The need for the day-ahead power exchange data between every two nodes
  - The need for technical and mechanical data of every power generation plant
  - The need for technical data of every transmission line within the proposed model
  - The need for power exchange data between the 50Hz areas and other areas, e.g., between nodes (''EE, LV, LI, PO, RO, HU, and SK'' and ''Russia, Ukraine, Moldova, and Bulgaria'', (''Italy'' and ''Malta''), (''Spain'' and ''Morocco''), and (''Greece'' and ''Turkey''). Collecting such data is quite hard because ENTSO-E does not publish it.

Due to these difficulties and time considerations, the decision was, **after a discussion with DNVGL**, to propose another approach which provides a more straightforward way to study the impact of system inertia decrease on frequency oscillations and frequency control actions. However, the first model shown above can still be implemented if all data is available.

Figures 3-3 and 3-4 below show the **second proposed approach**:

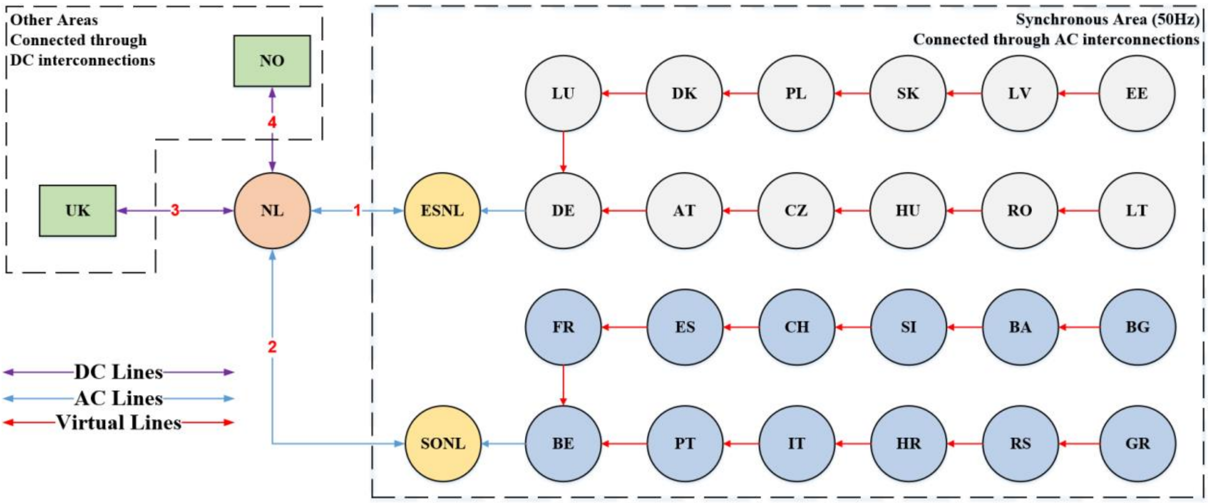

Figure 3-3: Second Approach as A Detailed Model

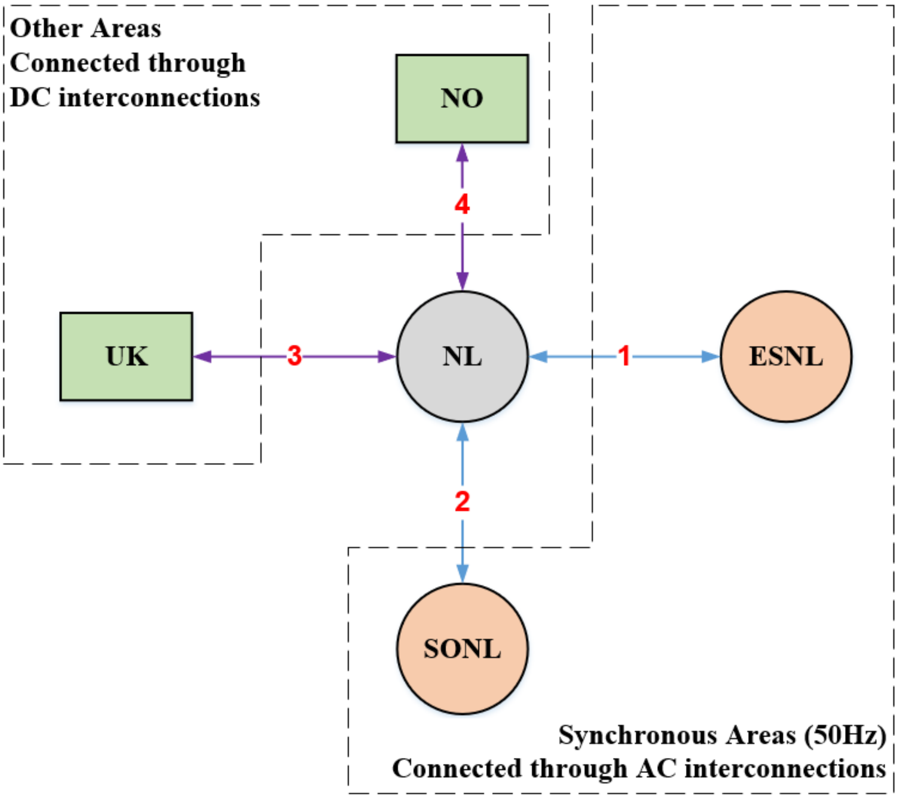

Figure 3-4: Second Approach as An Aggregated Model

The idea of the second approach is to study the frequency performance of **the Dutch power system as part of the Synchronous Grid of Continental Europe** that includes the regional-groups mentioned before. Through this approach, it is possible to analyse the consequence of the increased number of renewables on the frequency performance in the Dutch grid regarding the decrease in system inertia. This model consists of five nodes and four transmission lines. A detailed explanation of these components is given as follows:

- **Node NL (1): it is a part of the 50Hz synchronous grid of CE and** represents the Dutch power system, and it consists of one aggregated dispatchable plants and one aggregated non-dispatchable plants. This node is connected to the 50Hz Synchronous areas (ESNL and SONL) through 2 AC transmission lines (no. 1 and 2) and to the other non-synchronous areas (the UK and NO) through DC transmission lines (no.3 and 4). It contains one aggregated dispatchable plant and one aggregated non-dispatchable plant.

- **Node ESNL (2): it is a part of the 50Hz synchronous grid of CE** and consists of 12 countries as shown in figure 3-3; therefore, it can be considered as a virtual aggregated node. This node is connected to NL through an AC transmission line (no.1). It contains one aggregated dispatchable plant and one aggregated non-dispatchable plant.

- **Node SONL (3): it is a part of the 50Hz synchronous grid of CE** and consists of 12 countries as shown in figure 3-3; therefore, it can be considered as a virtual aggregated node. This node is connected to NL through an AC transmission line (no.2). It contains one aggregated dispatchable plant and one aggregated non-dispatchable plant.

- **Node UK (4):** represents the British power system, and it is connected to the Netherlands through a DC transmission link (no.3); therefore, its generation and load profiles are not considered.

- **Node NO (5):** represents the Norwegian power system, and it is connected to the Netherlands through a DC transmission link (no.4); therefore, its generation and load profiles are not considered.

- **Transmission Line (1):** it is an aggregated HVAC line, which represents the AC power flow between the Dutch power system and the German power system. It covers four inner regions with six transmission circuits in total as shown in table 3-1:

Table 3-1:DE AC Transmission Line no.1 A\as Published by TenneT [10]

Inner Regions	No. of Transmission Circuits	Voltage [KV]	Capacity [MW]
Hengelo-Gronau	2	380-400 AC	1700
Maasbracht-Rommerskirchen	1	380-400 AC	1700
Maasbracht-Siersdorf	1	380-400 AC	1700
Meeden-Diele	2	380-400 AC	1700

- **Transmission Line (2):** it is an aggregated HVAC line, which represents the AC power flow between the Dutch power system and the Belgian power system. It covers three inner regions with four transmission circuits in total as shown in table 3-2:

Table 3-2: NL-BE AC Transmission Line no.2 as Published by TenneT [10]

Regions	No. of Transmission Circuits	Voltage [KV]	Capacity [MW]
Maasbracht-Van Eyck	2	380-400 AC	1645
Borsele-Zandvliet	1	380-400 AC	1645
Geertruidenberg-Zandvliet	1	380-400 AC	1645

- **Transmission Line (3):** called BritNed and represents the HVDC submarine power cable between the Dutch power system and the British power system.

Table 3-3: BritNed HVDC Cable no.3 as Published by TenneT [18]

Inner Region	No. of Transmission Circuits	Voltage [KV]	Capacity [MW]
Maasvlakte-Isle of Grain	2	450 DC	1000

- **Transmission Line (4):** called NorNed and represents the HVDC submarine power cable between the Dutch power system and the Norwegian power system.

Table 3-4: NorNed HVAC Cable no.4 as Published by TenneT [18]

Inner Region	No. of Transmission Circuits	Voltage [KV]	Capacity [MW]
Eemshaven-Feda	One 12-pulse converter	450 DC	700

Similar to the first approach, the second model also has its advantages and disadvantages:

- **<u>Advantages:</u>** in this model, there are only four power transmission lines/cables instead of 67 compared to the first model. This significant difference in the number of lines/cables limits the need for technical specification and power exchange data. Moreover, the analysis of the frequency deviation within the 50Hz synchronous area is more feasible in this approach compared to the first approach because there are only three nodes instead of 25. This difference, in turn, makes the design of the system frequency control actions (primary and secondary controls) a bit easier.

- **<u>Disadvantages</u>**: the first approach analyses the frequency behaviour of the whole synchronous area of CE, while the second approach examines the frequency performance of the Dutch power system as a part of the synchronous grid. In other words, the second model focuses on the inertia decrease of node NL interconnected with the synchronous area through two virtual nodes. However, if the second model works well, it can be used for other regions after scaling up.

Figure 3-5 below gives the technical diagram of the second model. It is worth mentioning that each node represents a separate area; thus, the model shown in figure 3-4 has in total five areas; 3 synchronous and two non-synchronous areas. Besides, this approach consists of three areas; 2 synchronous areas and one non-synchronous area.

For **frequency performance** and **load-frequency control** (LFC) studies, each control area can be represented by one synchronous generator and one non-synchronous generator that exhibit the overall performance of that area. This fair assumption was given in [12] since such studies consider the so-called collective performance of all generators within a particular area and not the transmission system performance or intermachine oscillations. This assumption allows thus the representation of the Dutch power system with one dispatchable power plant and one non-dispatchable plant. Alongside, it gives the possibility of estimating equivalent inertia for each area that is equal to the sum of inertia of all generators within that area as described in paragraph (3.3.1).

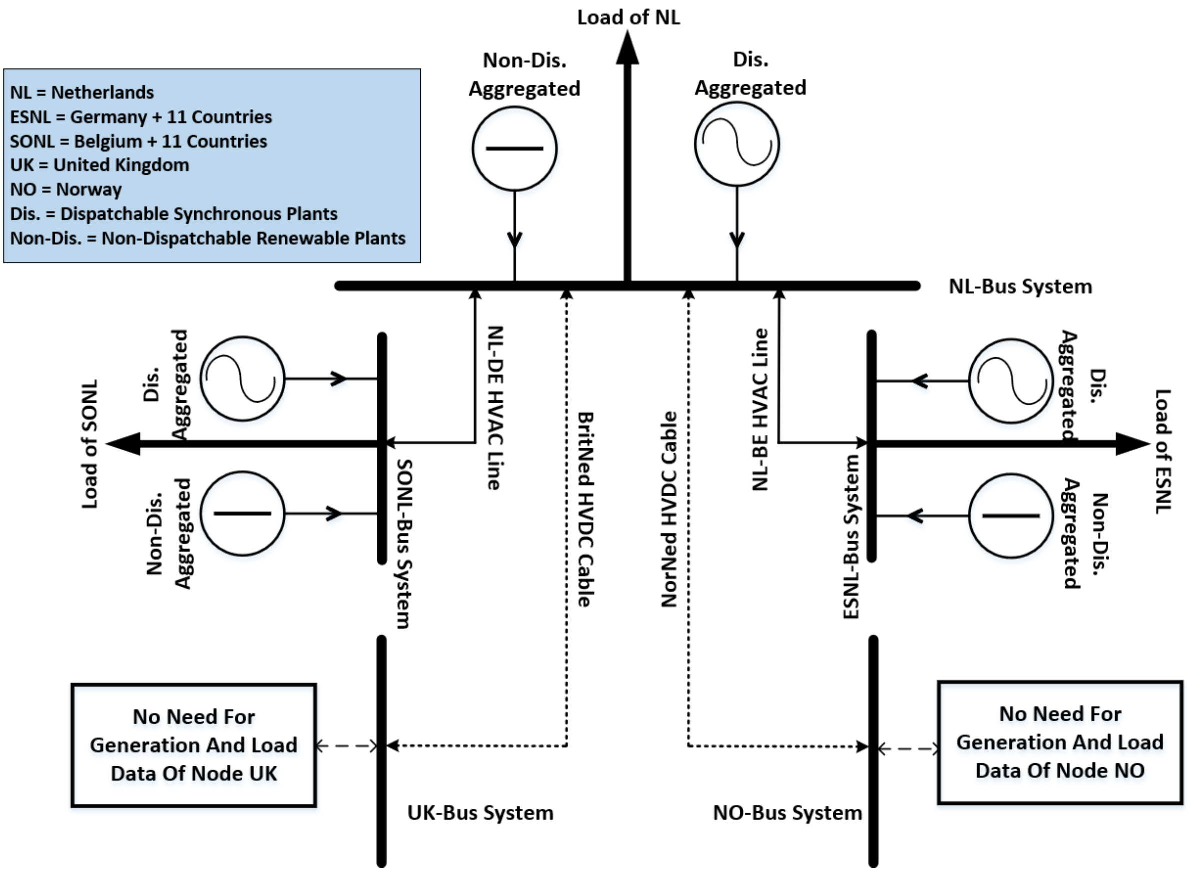

Figure 3-5: Technical diagram of the second approach

3.2. Kermit Tool

In general, any power system can be implemented using different software's, i.e., MATLAB, Power Factory, PSCAD, and Vision Network Analysis. For the objectives of this thesis, the so-called **Kermit tool** has been made available by DNVGL, which is suited for designing as well as simulating the second approach proposed in section (3.1).

Kermit is intended to investigate studies for regulation, dispatch, and frequency dynamics of an electric network. The analysis of power system using Kermit typically focuses on the time range of 1 second to one day. Based on this time domain, this tool is suitable to study the frequency balance states associated with Automatic Generation Control (AGC) of the secondary control.

This control, in turn, maintains the minute-to-minute balance throughout the whole day and returns the system frequency to the standard scheduled value by adjusting the power set-points of the generator's prime mover, resulting in a regulation of the system frequency. Moreover, AGC adapts the power reference set-points of the generators to keep the power exchange within the scheduled values.

Kermit requires the following software's to be installed:

- **MATLAB**
- **Simulink**
- **Microsoft Excel**

Figure 3-6 shows how these programs work when a particular power system model is simulated using Kermit:

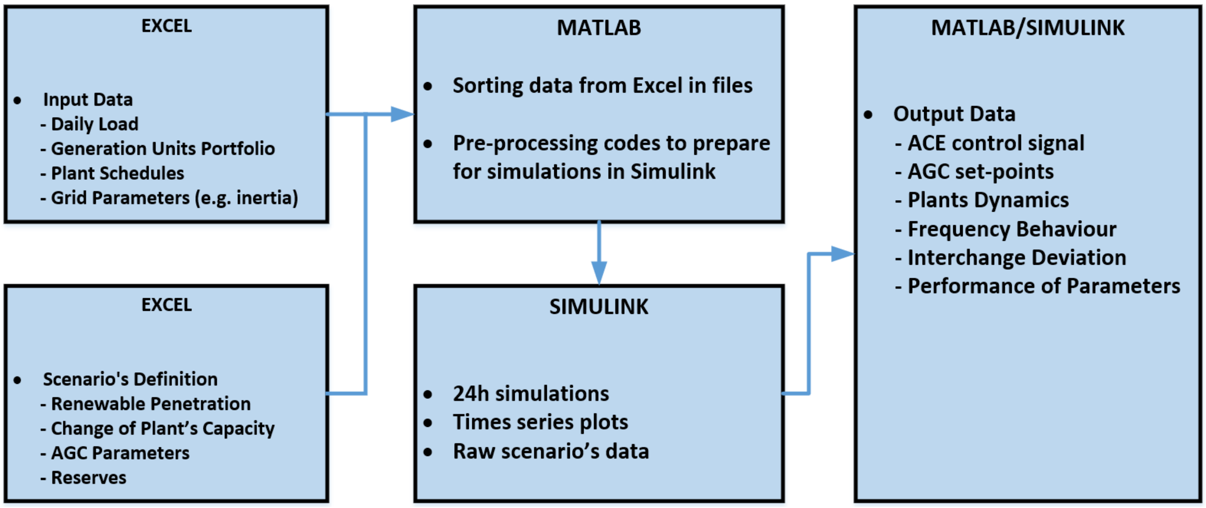

Figure 3-6: Kermit's main structure and data flow

The implementation of the second approach requires the following input data: power plants portfolio, wind production, solar production, daily load, generation schedules, interchange schedules, system inertias and interconnection model. These inputs are provided through an Excel-based interface (or **control panel**) to allow a proper data management.

Initializing and running the model is prepared in MATLAB and performed in Simulink. During the simulation phase, there is minimal user interaction needed because data managing is almost automatically done by Kermit tool.

The outputs of the proposed model include Area Control Error (AC), AGC set points, Frequency Deviations, Area Interchange Deviations, and outputs of power plants either dispatchable or non-dispatchable plants. These outputs are made available in customised Simulink plots as well as in **raw. mat** data format to allow for post-processing and analysis.

3.3. Kermit Power System Model

It needs to be noted that understanding how the Kermit-Simulink power system model including the MATLAB Codes works was quite hard as there has been very little information documented about the Kermit tool. For this purpose, it has been decided to create a so-called technical manual throughout this section to elaborate on the operation of Kermit-Simulink to make it more usable and accessible for both the future academic and advisory projects.

Figure 3-7 below shows the power system model used in Simulink that uses the model parameters and information it gets from the control panel, runs the simulation and outputs the results into a specific folder. This model consists of four main parts that are responsible for running the Kermit tool. These parts are:

- **Schedules and time-series data**
- **Inter-zonal AC load flow and system inertial model**
- **Automatic Generation Control (AGC)**
- **Power plants**

In general, Kermit makes a difference between time-series data and model parameters. Time-series data (e.g. 24-hour schedule for a specific generator) are typically different for each simulation day, while model parameters (e.g. generation capacity) are typically constant.

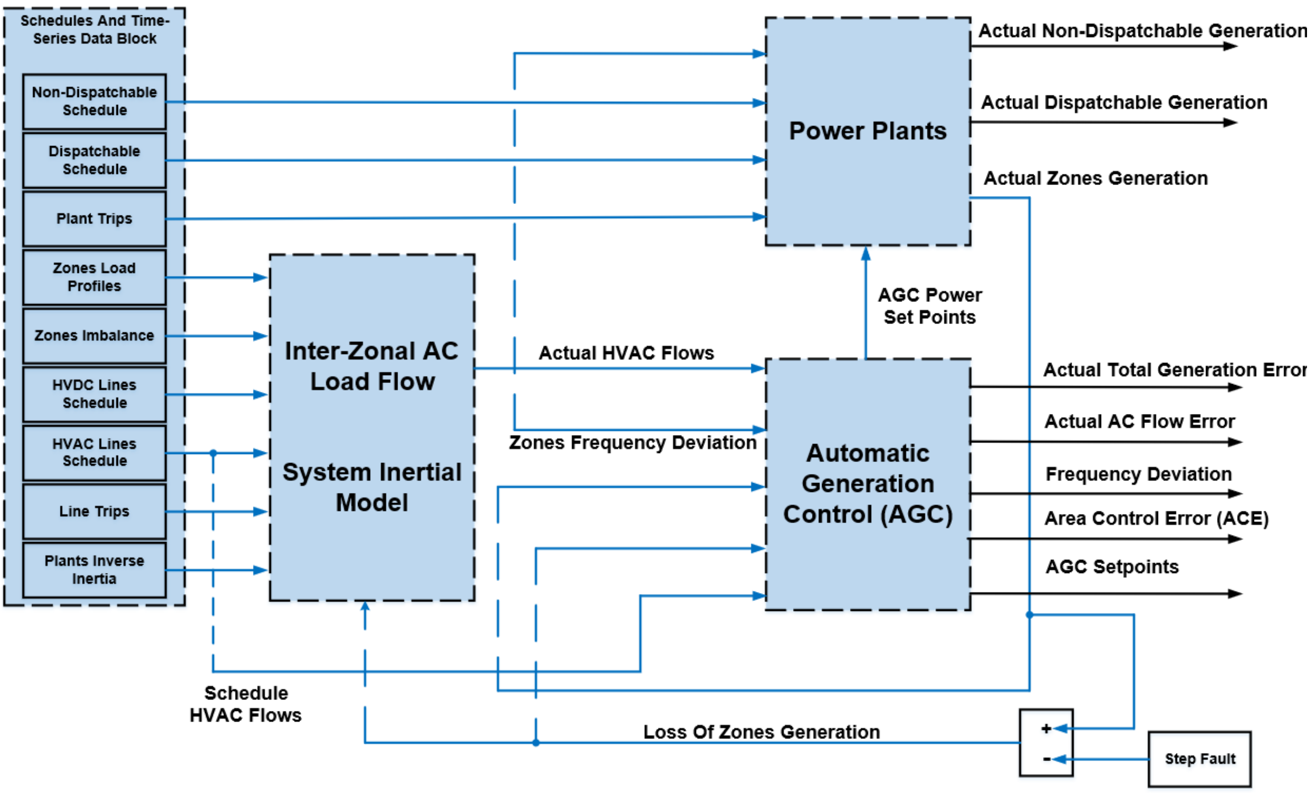

Figure 3-7: Simulink Power System Model of Kermit Tool

3.3.1. Schedules and Time-series Data

This part requires schedule time-series data for a specific day as Kermit operation is based on 24-hour simulations with a high time resolution. For this purpose, the choice was to analysis the power system shown in the figure above with the focus on a time domain of one day that is **January 18, 2017**. This 24-hour simulation is further performed with a time resolution of **15 minutes**. The use of this schedule time-series data and date is due to:

- The highest ENTSO-E load values per each country were on this day

- The start date of this thesis was in February 2018 where no electricity data was announced.
- The results of DNVGL-ETO model was published in 2017
- The time resolution of every 900s is needed because this thesis deals with analysing the system frequency and its controllers. These controllers have time response in the range of (0-30min or 0-1800s).

The scheduling part consists further of eight blocks, which each represents the relevant sheet in Excel control panel. The time-series data needed for each of these blocks are listed below:

- **Dispatchable Schedule:**
  - Aggregated Synchronous Plant Generation NL
  - Aggregated Synchronous Plant Generation ESNL
  - Aggregated Synchronous Plant Generation SONL

  - Aggregated synchronous generation is assumed to be the sum of all **conventional** generation units of the studied regions based on the published generation data by [11]. For example, the aggregated synchronous plant of NL contains the sum of Coal generation, Combined Cycle Gas Turbine (CCGT) generation, and Nuclear Generation.

- **Non-Dispatchable Schedule:**
  - Aggregated RES Plant Generation NL
  - Aggregated RES Plant Generation ESNL
  - Aggregated RES Plant Generation SONL

  - Aggregated synchronous generation is assumed to be the sum of all **renewable** generation units of the studied regions based on the published generation data by [11]. For example, the aggregated RES plant of NL contains the sum of wind generation, PV-solar generation, and the generation of other RES units.

- **Plant Trips:** this sheet in Excel gives the possibility of creating disturbances for specific plants at a particular time. Plant disturbances are in per unit [pu]. 1pu means a full power generation of a specific plant, while 0pu means the power output of the plant is forced to zero.

- **Line Trips:** are also in pu, similar to plant trips sub-block

- **Zones Load:** ***(in Kermit nodes are defined as zones)***
  - Load Profile of node NL
  - Load Profile of node ESNL
  - Load Profile of node SONL

- **Zones Imbalance:** this sheet can be only used if there are specific disturbances occurred on a simulated day. For this project, it is assumed that no disturbances occurred on January 18, 2017.

- **HVDC Schedule:**

  - Power Flow Profile of NL-UK (BritNed) HVDC Link
  - Power Flow Profile of NL-NO (NorNed) HVDC Link

- **HVAC Schedule:** there are only schedules for AC transmission lines between the synchronous zones:

  - Power Flow Profile of ESNL-NL HVAC Line
  - Power Flow Profile of SONL-NL HVAC Line

- **Plants Inverse Inertia:** the computation process of the inertia within any region is quite complicated. Such a process requires information of the load and generation profiles of every country, technical specifications of the online power generators, and power exchange data between the different nodes within the studied regional groups.

For this purpose, a list of assumptions has been formed to provide a suitable way to calculate the available inertia roughly. Mentioned in [11] that the formation of such assumptions is based on the determination of the total inertia constant of every country by using the following equation:

$$H_{sys} = \frac{\sum_{i=1}^{n} H_n * S_{bn}}{S_{b,sys}} \quad (3.1)$$

Where:

- Base apparent power of system is defined as:

$$S_{b,sys} = \sum_{n=1}^{N} S_{bn} \quad (3.2)$$

- Variable (H_n) indicates the inertia constants of synchronous power generation units given in [s] and is equal to the values shown in the table below:

Table 3-5: Assumed Inertia Constant Values of Synchronous Generation Units [11]

Generation Type	Inertia Constant in [s]
Nuclear	6.3
Thermal	4
Hydro Conventional	3
Small Hydro	1
Wind/PV	0

- Variable (n) indicates the types of power generation plants:
  - (n = 1) indicates power generation plant of type nuclear
  - (n = 2) indicates power generation plant of type thermal
  - (n = 3) indicates power generation plant of type conventional hydro
  - (n = 4) indicates power generation plant of types (small hydro + other types)

- Variable (S_{bn}) indicates the rated apparent power of each power plant given in [VA]. However, it is quite complicated to determine this value for every generation plant. One of the possible ways to estimate this variable is through the following equation:

$$S_{bn} = \frac{P_n}{pf} \quad (3.3)$$

With:

- n = active power of each generation plant given in [W], which is assumed to be equal to the Net Generation Capacity in [MW] provided by ENTSO-E Statistical Factsheet 2017 [13].
- pf = power factor, which is assumed to be (0.9) as has been used in [13].

The example below explains a simple way to estimate the inertia constant of the **Dutch power system** based on the previous assumptions:

1. **Nuclear:** $S_{b1} = \frac{P_1}{pf} = \frac{486\ \text{MW}}{0.9} = 540\ [\text{MVA}]$
2. **Thermal:** $S_{b2} = \frac{P_2}{pf} = \frac{23068\ \text{MW}}{0.9} = 25627\ [\text{MVA}]$
3. **Hydro:** $S_{b3} = \frac{P_3}{pf} = \frac{0\text{MW}}{0.9} = 0\ [\text{MVA}]$

4. Small Hydro + Other types: $S_{b4} = \frac{P_4}{pf} = \frac{0MW}{0.9} = 0\ [MVA]$

5. Total Apparent Power: $S_{b,sys} = S_{b1} + S_{b2} + S_{b3} + S_{b4} = 26167\ [MVA]$

6. Total Inertia Constant:

$$H_{NL} = \frac{\sum_{n=1}^{N} H_n * S_{bn}}{S_{b,sys}} = \frac{6.3s*540MVA+4s*25627+3s*0MVA+1s*0MVA}{26167\ MVA} = 4.05\ [s]$$

Similarly, the inertia constants of the other countries involved in this study have been estimated. These values are further shown in figure 3-8 below, which gives the possibility of assuming that the average inertia constant for each country is approximately 4.2s with a 39% average share of renewables in total Net Generation Capacity (NGC). It is worth to be noted that these figures of inertia constant have been obtained using the values of synchronous net generation capacity published by ENTSO-e in [14] for the year 2017.

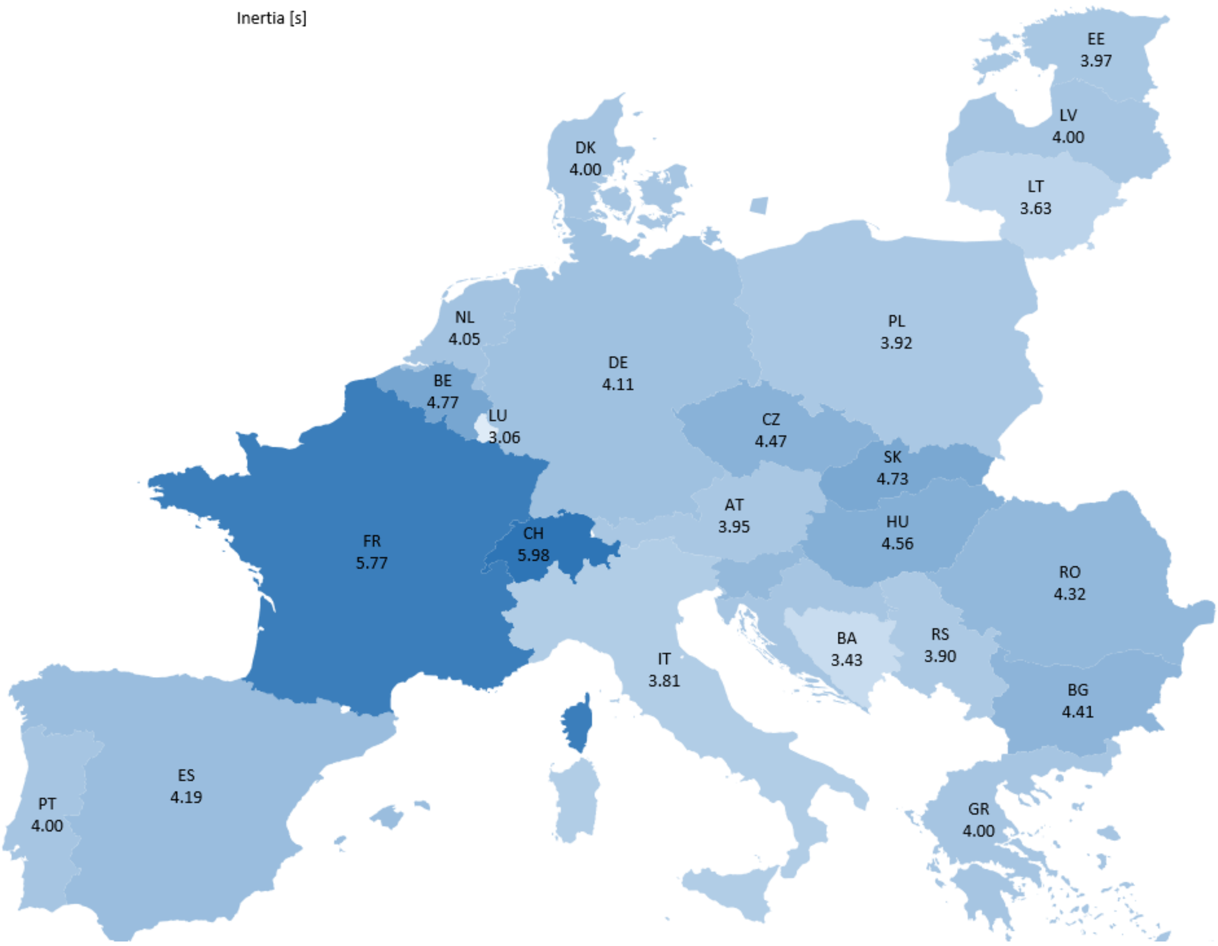

Figure 3-8: Estimated Inertia Constants of Continental Europe Countries

Next, these values are given to Excel as a time-series data, and then exported to MATLAB in which they will be converted to inverse inertia values using the method given in [12]. The conversion process is based on the following equation:

$$II_n = \frac{f_{sys}}{2 * H_n * S_n} \tag{3.4}$$

Where:

- II_n = Inverse Inertia of node (n) in [Hz/MWs]

- H_n = Inertia Constant of node (n) in [s], equals to those values shown above.
- f_{sys} = System Frequency in [Hz], equals to (50Hz)
- S_n = Rated Power in [MW], equals to the maximum capacity of the aggregated synchronous power plant of node (n)

Preparing the time-series input data is an essential step towards the approach implementation. However, gathering such data is quite complicated due to the ETSOE **Code of Conduct** that restricts the TSOs to treat electricity data as confidential and the non-ability of DNVGL to make this data available for this project. Therefore, this step took a very long time to gather all the needed data that gives the ability to perform the desired simulations.

Possible ways to find the time series data are the Transparency Platform of ETSOE [14] and the Data Store of TSOs, i.e. TenneT [15], Amprion [16], and Elia [17]. These stores provide the required data in aggregated time-series datasets of every 15 minutes or every 1 hour.

The computed power flows data between two nodes are usually indicative values, and provided by individual TSOs; thus, they cannot be considered as approved values. For this purpose, a comparison has been performed between the data published by ENTSO-E and the data stored on the websites of TSOs in order to provide the control panel with the most realistic data.

Moreover, specific nodes of the synchronous grid of Continental Europe could have more than one inner region, e.g. node Italy has entirely ten inner regions. In order to provide the generation and load data for this node, the single generation and load profiles of each region should be added to those of the other regions. This way gives the possibility of providing Excel with a complete generation/load dataset of the whole of Italy.

Finally, some of the time-series data published by ENTSO-E or the other Data Stores are not provided for every **15 minutes.** For this purpose, a simple linear interpolation method has been used as described below:

- **Case 1:** data for every hour, with different values between two certain hours.

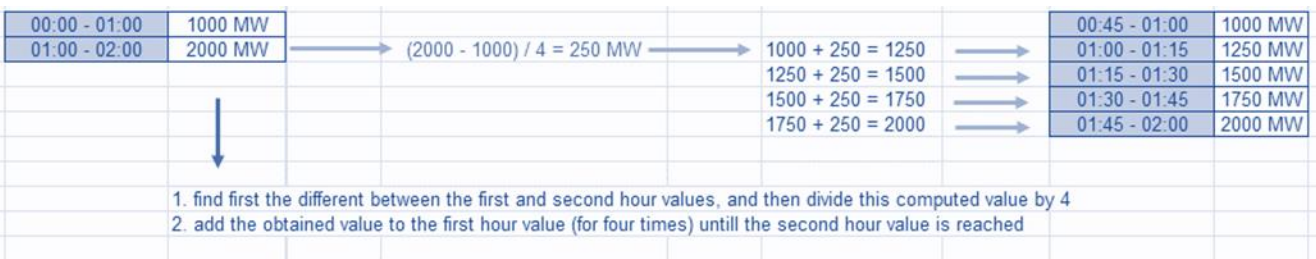

Figure 3-9: Data interpolation case 1

- **Case 2:** data for every hour, with same values between two certain hours.

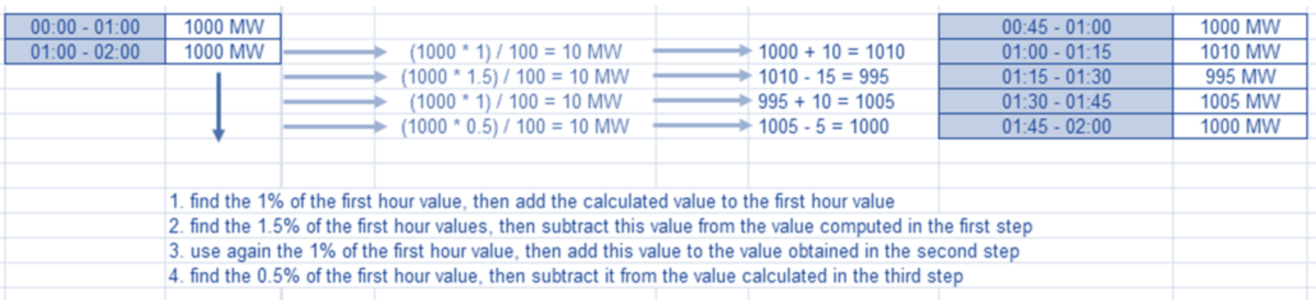

Figure 3-10: Data interpolation case 2

It is worth mentioning that the analysis of system frequency performance requires (at least) quarterly hour change in the generation, load, and power flow in order to examine the frequency response to these deviations. For this reason, the small perturbations of (0.5-1%) have been used in the table above.

3.3.2. Inter-Zonal AC Load Flow & System Inertial Model

Within this part, several tasks are being performed in order to provide the following outputs:

- **Actual HVDC Flow**
- **Actual Zones Load Dynamic**
- **Actual Zones Surpluses**
- **Actual HVAC Flow**
- **Actual Zones Angles**
- **Actual Zones Frequency Deviation**

The main structure of this part is illustrated in figure 3-11:

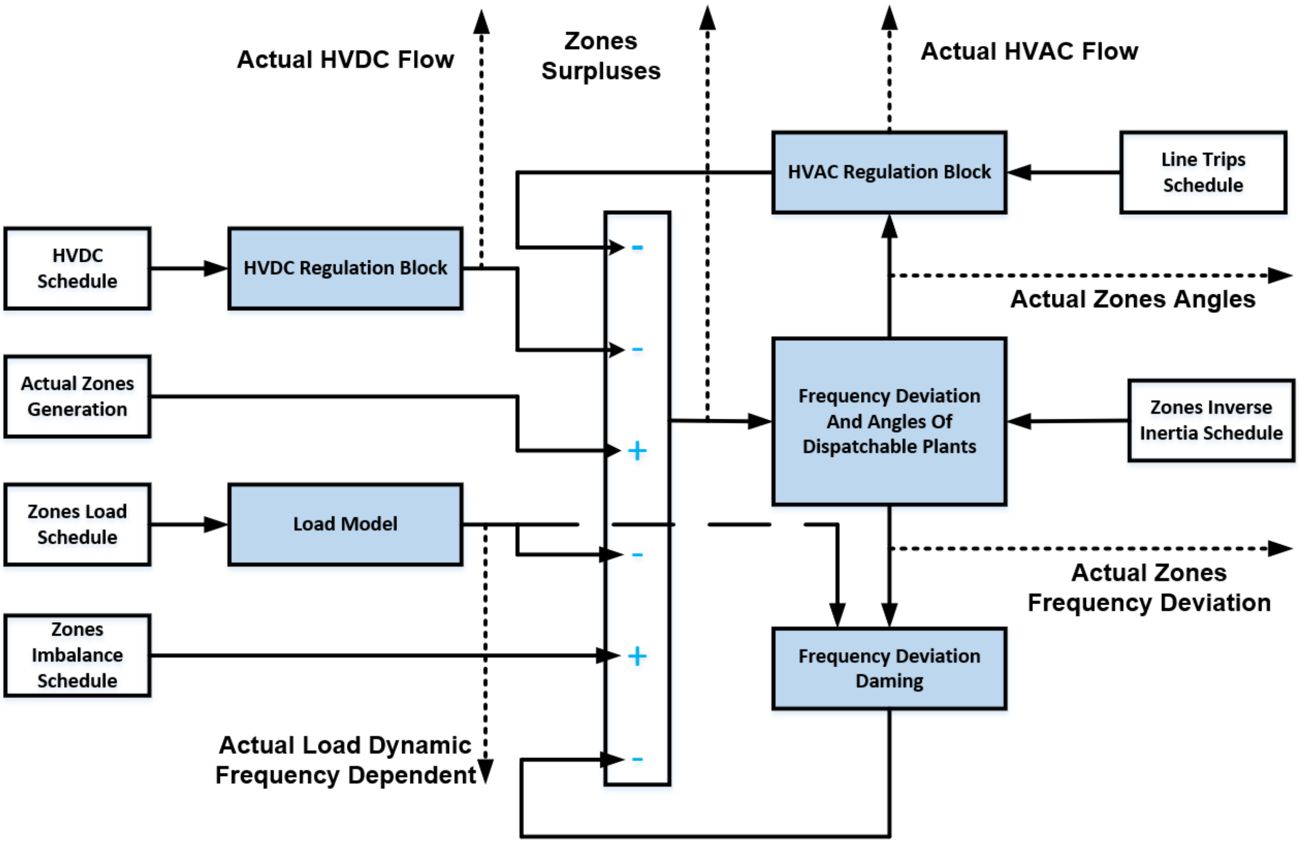

Figure 3-11: Main Structure of Inter-Zonal AC Load Flow Block

The white blocks shown above represent the input ports, which provide the required times-series data to the blue blocks. Each of the blue blocks has its function that all together are responsible for determining the outputs of this part. Below follows a functional explanation of the blue blocks:

- **HVDC Regulation Block:** gets its input from the HVDC Schedule port and determines the actual power flow through the HVDC links as an output. This block needs the following technical information of each HVDC links mentioned in section (3.3):

Table 3-6: HVDC Parameters Required for HVDC Regulation Block

Name of HVDC Link	From Zone	To Zone	Ramp Rate Limit [%/min]	Pmax [MW]
NorNed	NL	NO	4.29	929
BritNed	NL	UK	3	1203

Where:

- The direction of each HVDC link has been selected based on the second model shown in figure 3-4. The choice for both links has set NL to be the origin of the direction, while both the UK and NO are the destination zones. Therefore, both UK and NO can be considered as loads to zone/node NL.

- The TSOs apply the Ramp Rate Limits when their hourly power generation plan changes more than 200MW as for the HVDC links between CE and RG-Nordic or 100MW as HVDC links between CE and RG-UK as given in [19] and [20] respectively.

  Mentioned further in [19] that ENTSO-E and the relevant TSOs restrict the maximum gradient for change in power flow to 30[MW/min]. Concerning the capacity values of both the HVDC links used in this model:

  - **Ramp Rate Limit of NorNed:**

  $$\mathrm{RR_{NorNed}} = \frac{\text{Restriction Value}}{\text{Capacity Value}} = \frac{30\,\left[\frac{\mathrm{MW}}{\mathrm{min}}\right]}{700\ \mathrm{MW}} * 100 = 4.29\,\left[\frac{\%}{\mathrm{min}}\right] \quad (3.4)$$

  - **Ramp Rate Limit of BritNed:**

  $$\mathrm{RR_{BritNed}} = \frac{\text{Restriction Value}}{\text{Capacity Value}} = \frac{30\,\left[\frac{\mathrm{MW}}{\mathrm{min}}\right]}{1000\ \mathrm{MW}} * 100 = 3\,\left[\frac{\%}{\mathrm{min}}\right] \quad (3.5)$$

- Based on the scheduled time-series data of the HVDC links, the maximum power transfer has been computed as follow:

  - **Maximum power of NorNed:**

  $$\mathrm{P_{max,\ NorNed}} = \mathrm{Max\ P_{schedule,\ Excel}} + \mathrm{P_{change,\ NorNed}} = 729 + 200 = 929\ [\mathrm{MW}] \quad (3.6)$$

  - **Maximum power of BritNed:**

  $$\mathrm{P_{max,\ BritNed}} = \mathrm{Max\ P_{schedule,\ Excel}} + \mathrm{P_{change,\ BritNed}} = 1103 + 100 = 1203\ [\mathrm{MW}] \quad (3.7)$$

  Where ($\mathrm{P_{max}}$) is the maximum power needed to cover the maximum scheduled power flow at a certain moment throughout the simulated day ($\mathrm{Max\ P_{schedule,\ Excel}}$) plus the amount of power change as defined by ENTSO-E ($\mathrm{P_{change}}$).

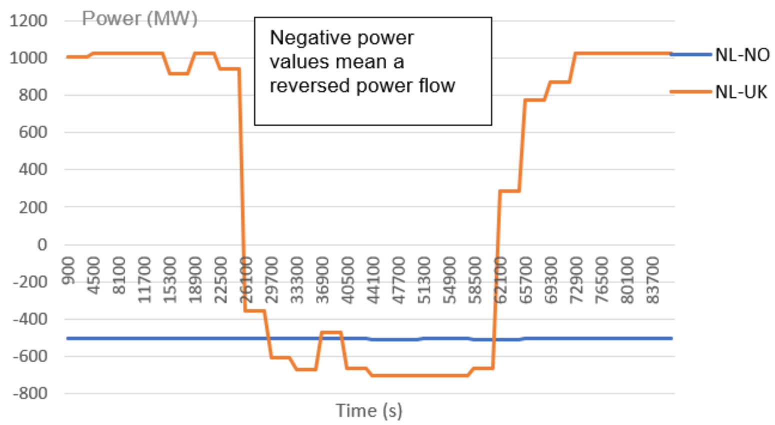

Figure 3-12: Scheduled Time-Series Power Flow Through HVDC Links on 18/01/2017

In general, this block gets the scheduled time-series data shown in figure 3-12 as input, checks if the power flow through both HVDC links are within the limits mentioned above, and finally provides the actual power flow through the HVDC interconnections between the studied nodes.

- ○ **Load Model Block:** gets the load scheduled time-series and the frequency deviation of each synchronous zone as input and determines the dynamic load output of these zones through the block diagram shown in figure 3-13:

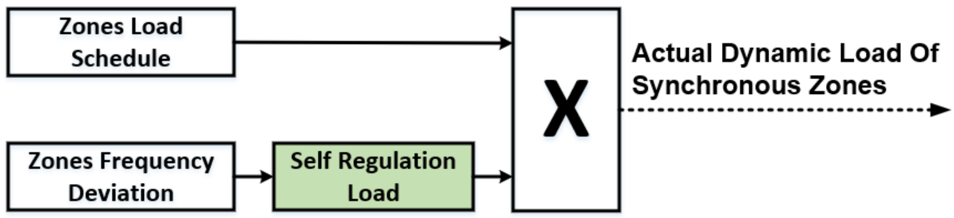

Figure 3-13: Block Diagram to Obtain the Dynamic Load of Synchronous Zones

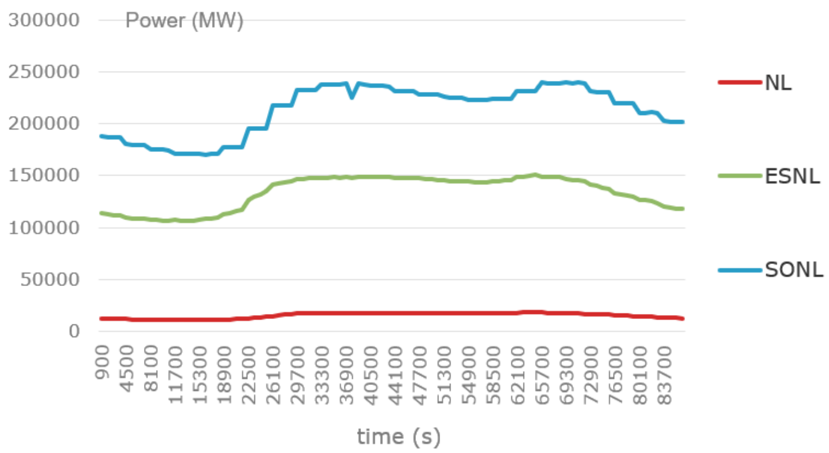

Figure 3-14: Scheduled Time-Series Load Data of Synchronous Zones on 18/01/2017

In figure 3-13 above, the **Self-Regulation Load** sub-block is inserted into the Load Model block to create the so-called self-regulating effect of synchronous zones, which is directly related to the synchronous generators of these zones. This effect represents the required energy that the system load exchange with power grid due to frequency oscillations. Thus, any change in system frequency results in a proportional change in the power consumed by the system load to stabilize the frequency of that system.

Stated in [8] that the limits for the scope of frequency stability analysis are the acceptable frequency operating ranges, the maximum RoCoF, and the frequency NADIR. The main factors within this scope are covered by the definition of maximum RoCoF that occurs at the first instants after a specific disturbance:

$$\mathrm{RoCoF_{Max}} = \frac{\mathrm{df}}{\mathrm{dt_{Max}}} = \frac{\Delta \mathrm{P_{Imbalance}}}{\mathrm{P_{dispatchable}}} * \frac{\mathrm{f_0}}{\mathrm{H_{system}}} \quad \mathrm{in} \left[\frac{\mathrm{Hz}}{\mathrm{s}}\right] \tag{3.8}$$

Where:

- df = change in frequency following incidents in [Hz]
- $\mathrm{dt_{Max}}$ = maximum change in time during the first instants in [s]
- $\mathrm{P_{dispatchable}}$ = active power produced by dispatchable power plant in [MW]
- $\Delta\ \mathrm{P_{Imbalance}}$ = power imbalance due to disturbances, related to system load in [MW]
- $\mathrm{f_0}$ = nominal frequency of system [50Hz]
- $\mathrm{H_{system}}$ = system inertia in [s]

In case that both system inertia and power imbalance are known, the maximum ROCOF can then be computed from equation 3.8. As system frequency is load dependent, the self-regulating effect and primary control are thus both able to reduce the higher values of ROCOF during severe disturbances.

Assumed in [21] that the load self-regulation of the synchronous grid of CE is **1%/Hz**. This value allows the system to keep frequency with the acceptable ranges at the instant of an incident and to stabilize the frequency decline without the need for additional control actions. Once the inertial response and self-regulation effect arrest this decline, governors and AGC start responding to recover the nominal value of system frequency.

In Kermit, the actual dynamic load of synchronous zones is obtained as follows:

$$\text{Load Dynamic} = P_{\text{Load}} * [1 + (\text{df} * \text{self regulation})] \quad \text{in [MW]} \tag{3.9}$$

- **Zones Frequency Deviation and Angels Block:** computes the frequency deviation per each synchronous zone. The computation process depends in fact on two impacting factors:

  - **Zones Surpluses:** or zones power imbalance in [MW]. This mismatch between the generation and load profiles of each zone is being calculated inside Kermit using the following equation:

    $$\text{Zones Surpluses} = P_{\text{Load}} + P_{\text{AC}} + P_{\text{DC}} + P_{\text{damping}} + P_{\text{sch. Imb.}} \quad \text{in [MW]} \tag{3.10}$$

    Where:
    - P_{Load} = Actual Load Dynamic [MW]
    - P_{AC} = Actual Power Flow through AC Lines [MW]
    - P_{DC} = Actual Power Flow through HVDC links [MW
    - P_{damping} = Actual Damping Power related [MW]
    - $P_{\text{sch.}\ Imb.}$ = Scheduled Power Imbalance [MW]

  - **Synchronous Zones Inverse Inertia:** this depends on the inertia constant of each country within the studied synchronous zones as explained in section (3.3.1). An example of estimating the average inertia constant over the entire simulated day is shown below in which the relevant values indicated in figure 3-8 are divided by the number of countries involved:

    - $$\text{H}_{\text{NL}} = \mathbf{4.05}\ [s] \tag{3.11}$$
    - $$\text{H}_{\text{ESNL}} = 4.11_{\text{DE}} + 4_{\text{DK}} + 4.47_{\text{CZ}} + 4.73_{\text{SK}} + 3.92_{\text{PL}} + 3.97_{\text{EE}} + 4_{\text{LV}} + 3.63_{\text{LT}} + 4.56_{\text{HU}} + 4.32_{\text{RO}} + 3.95_{\text{AT}} + 3.06_{\text{LU}} = \frac{48.73}{12} = \mathbf{4.06}\ [s] \tag{3.12}$$
    - $$\text{H}_{\text{SONL}} = 5.77_{\text{FR}} + 4.77_{\text{BE}} + 4_{PT} + 3.81_{\text{IT}} + 4_{\text{GR}} + 4.19_{\text{ES}} + 5.98_{\text{CH}} + 3.43_{\text{BA}} + 4_{\text{HR}} + 4.3_{\text{SI}} + 4.41_{\text{BG}} + 3.9_{\text{RS}} = \frac{52.39}{12} = \mathbf{4.37}\ [s] \tag{3.13}$$

    It should be noted that these values are corresponding to the following percentage of both the renewable and non-renewable capacities as given by ENTOSE:

    - **NL:** the total net generation capacity is 32GW; 23.55GW non-renewable and 8.43GW renewable. These values mean that synchronous generation has a share in total generation equals to 74%, while that of RES is 26%.

    - **ESNL:** the relevant values of this zone have been calculated as the sum of all relevant capacities divided by the number of countries involved. The total net generation capacity is 355GWMW; 238GW non-renewable and 117GW renewable. The share of synchronous generation in the total generation equals to 67%, while RES is 33%.

    - **SONL:** similar to ESNL zone. The total net generation capacity is 477GW; 270GW non-renewable and 207GW renewable. These values mean that share of synchronous is 57%, while RES is 43%.

Furthermore, the frequency deviation is obtained within Kermit using the traditional swing equation. This method is illustrated in figure 3-16 below:

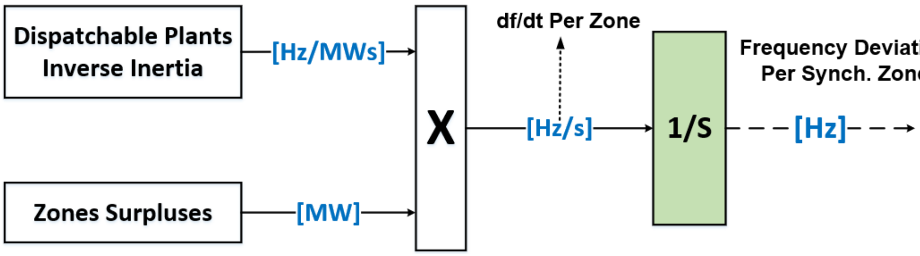

Figure 3-15: Implementation of Swing Equation to Obtain Frequency Deviation per Synchronous Zone

Figure 3-16 below depicts the inertia constant values that are exported from Excel to MATLAB for the entire simulated day. These values have been estimated as shown in the previous example. Furthermore, it was assumed that these values do not change over the entire day for simplification purposes.

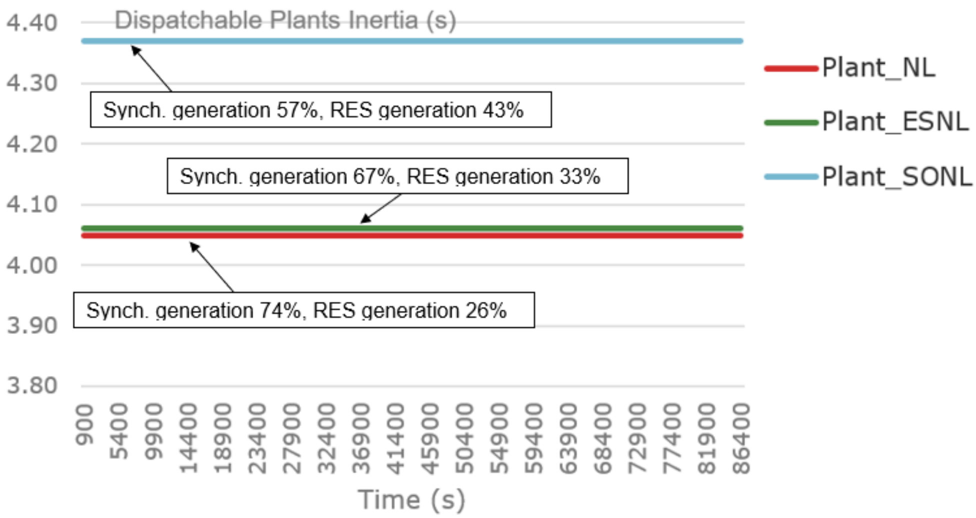

Figure 3-16: Inertia Constant of the Synchronous Dispatchable Plants throughout the Simulated day 18/01/2017

- **Damping Block:** This block contains the load damping constant, which represents the overall frequency-dependent characteristic in response to any change in system load. The damping constant (D) is commonly expressed as the percentage of load change for 1% change in system frequency. Mentioned in [12] that the typical values for this constant are in the range of [1-2]. For example, a value of D=1 means that 1% change in the nominal frequency will lead to a 1% change in system load.

  The Implementation of the load damping constant is performed in Kermit as illustrated in figure 3-17 below:

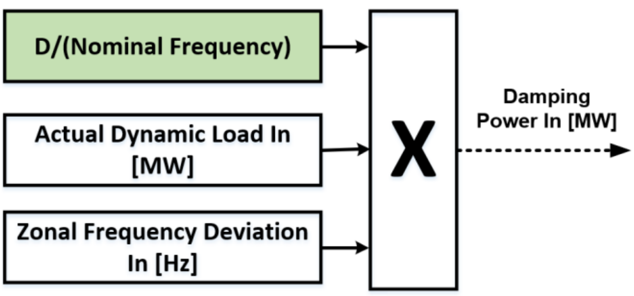

Figure 3-17:Implementation of Damping Block inside Kermit

- **HVAC Regulation Block:** contains the main parameters of AC transmission lines. It is responsible for determining the actual power flow through these interconnections and the amount of active power export per each synchronous zone. The implementation of this block within Kermit is illustrated in the figure below:

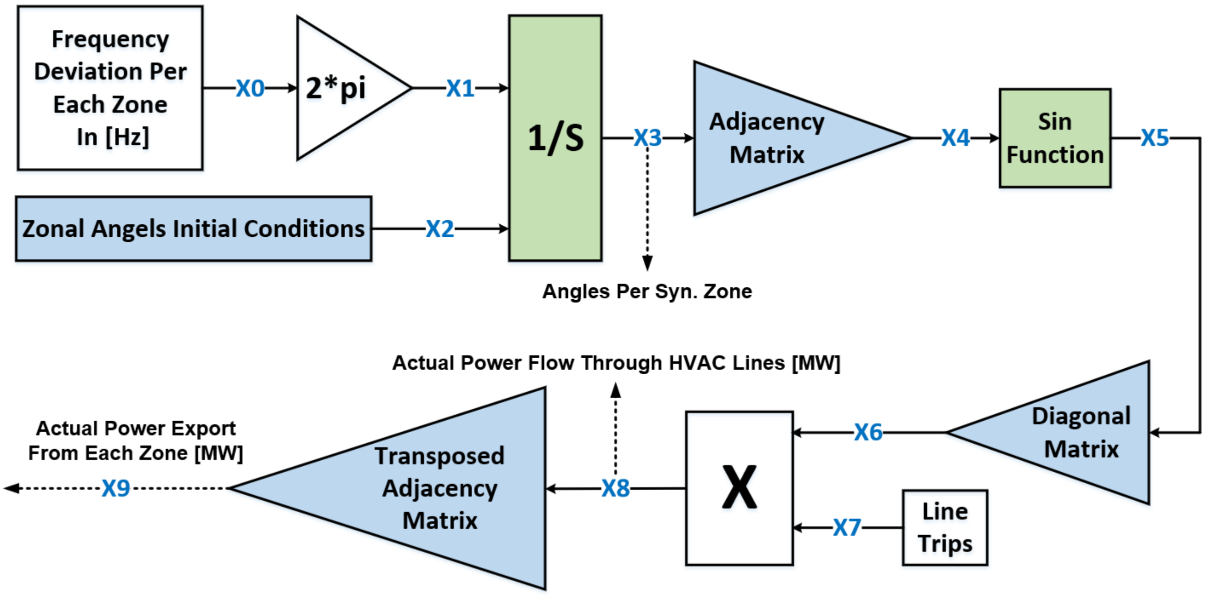

Figure 3-18: HVAC Regulation Block inside Kermit

Where:

- The first input to this block is the Zonal Frequency Deviation (X0) elaborated earlier in this section. This input gives the possibility of obtaining the change in synchronous speed using the following equation:

$$d\omega = 2\pi * df \rightarrow X1 = 2\pi * X0 \text{ in } [\frac{\text{rad}}{\text{s}}] \quad (3.14)$$

- The second input is the Zonal Angles Initial Conditions (X2). Such conditions are computed in MATLAB through the equation mentioned below:

$$X2 = \frac{(\text{Diagonal Matrix} * \text{Adjacency Matrix})^{-1} * \text{Adjacency Matrix}}{\text{Full Zonal Generation} - \text{Full Zonal Load}} \quad (3.15)$$

Solving equation 3.15 requires the formation of two matrices:

- **Adjacency Matrix (ADJ):** the main task of this matrix is the conversion from Zones to Lines dependent on the technical data of lines that are given in table 3-7 below. Based on both the power flow monitoring and direction of AC lines, it is possible to create the adjacency matrix:

$$\text{ADJ} = \begin{pmatrix} -1 & 1 & 0 \\ -1 & 0 & 1 \end{pmatrix} \quad (3.16)$$

Table 3-7: HVAC Interconnection Lines Technical Data

Name of HVAC Line	From Zone	To Zone	Power Flow Monitoring (0=no; 1=forward; -1=reversed)	Capacity [MW] [A]	NO. of lines [B]	Pij [MW] assumed: [A] * [B]
ESNL-NL	ESNL	NL	1	1700	4	6800
BritNed	SONL	NL	1	1645	3	4935

- **Diagonal Matrix (Diag):** contains the admittances of the AC interconnection lines. Besides, it is responsible for calculating the amount of active power flow on each transmission line in [MW]. The formation of this matrix is given as follows:

$$\text{Pij} = \begin{pmatrix} 10200 \\ 6580 \end{pmatrix} \quad (3.17)$$

$$\text{Diag(Pij)} = \begin{pmatrix} 10200 & 0 \\ 0 & 6580 \end{pmatrix} \quad (3.18)$$

Meanwhile, these two inputs make the **HVAC Regulation** block able to compute the outputs shown in figure 3-18 above with a green colour. The relevant outputs are being determined as follows:

- Find the **actual zonal angles** (X3) by integrating both inputs (X1 and X2):

$$\text{Zonal Delta Matrix} = \text{X3} = \begin{pmatrix} \delta_{NL} = X3_1 \\ \delta_{ESNL} = X3_2 \\ \delta_{SONL} = X3_3 \end{pmatrix} \quad (3.19)$$

- Obtain the angle difference across each AC line by multiplying the adjacency matrix with matrix (X3):

$$X4 = ADJ * X3 = \begin{pmatrix} -1 & 1 & 0 \\ -1 & 0 & 1 \end{pmatrix} * \begin{pmatrix} X3_1 \\ X3_2 \\ X3_3 \end{pmatrix} = \begin{pmatrix} -X3_1 + X3_2 \\ -X3_1 + X3_3 \end{pmatrix} = \begin{pmatrix} X4_1 \\ X4_2 \end{pmatrix} \quad (3.20)$$

- Apply the results of the previous step to a **Sin Function** that is introduced in the block diagram above in order to produce a dimensionalised output. The main task of this functions is to translate the input (X4) into a sinusoidal wave as an output (X5):

$$X5 = \begin{pmatrix} \sin[X4_1] \\ \sin[X4_2] \end{pmatrix} = \begin{pmatrix} X5_1 \\ X5_2 \end{pmatrix} \quad (3.21)$$

- Multiply matrix (X5) by the diagonal matrix:

$$X6 = Diag * X5 = \begin{pmatrix} 10200 & 0 \\ 0 & 6580 \end{pmatrix} * \begin{pmatrix} X5_1 \\ X5_2 \end{pmatrix} = \begin{pmatrix} 10200 * X5_1 \\ 6580 * X5_2 \end{pmatrix} = \begin{pmatrix} X6_1 \\ X6_2 \end{pmatrix} \quad (3.22)$$

  Next, check if there is a line trip by multiplying matrix (X6) with the Line Trips data (X7) stored in **Time-Series Part** in the form of a matrix file. This multiplication results in matrix the (X8) which consists of two elements that represent **the actual power flow through each AC transmission line in [MW]**.

- Determine the inverse of the adjacency matrix in equation 3.16 and multiply the result by matrix (X8). This process leads to a computation of **the actual export per each synchronous zone in [MW]:**

$$ADJ^{-1} = \begin{pmatrix} -1 & 1 & 0 \\ -1 & 0 & 1 \end{pmatrix}^{-1} = \begin{pmatrix} -1 & -1 \\ 1 & 0 \\ 0 & 1 \end{pmatrix} \quad (3.23)$$

$$X9 = ADJ^{-1} * X8 = \begin{pmatrix} -1 & -1 \\ 1 & 0 \\ 0 & 1 \end{pmatrix} * \begin{pmatrix} X8_1 \\ X8_2 \end{pmatrix} = \begin{pmatrix} -X8_1 - X8_2 \\ X8_1 + 0 \\ 0 + X8_2 \end{pmatrix} = \begin{pmatrix} X9_1 \\ X9_2 \\ X9_3 \end{pmatrix} \quad (3.24)$$

Finally, it is worth mentioning that the scheduled time-series data of AC lines are not needed at this stage because the determination of the power flow through these interconnections only depends on the model parameters and the zonal generation and load profiles.

3.3.3. Power Plants

The primary outputs of this part are the actual non-dispatchable generation for each zone, the set points of the synchronous dispatchable plants, and the actual dispatchable generation for each zone. Figure 3-19 illustrates the main block diagram of this part:

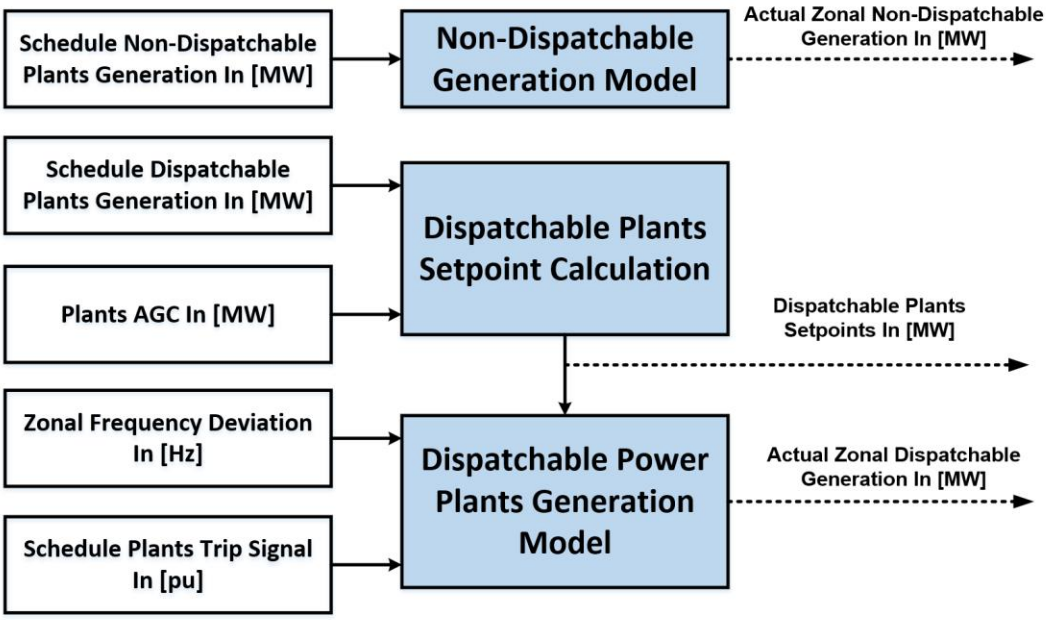

Figure 3-19:block Diagram of Power Plants Part

The three blocks together carry out the main function of the **Power Plants** part. Below follows a functional explanation of each block:

- **Non-Dispatchable Generation Model:** determines the actual renewable generation, i.e. wind and solar production, for each zone by translating the scheduled time-series data of non-dispatchable generation from plants map to zonal map using the matrix shown in figure 3-20:

ZonesandAreas

Legend
Bold values: user input on this sheet

Zone number in KERMIT	Zone name
1	NL
2	ESNL
3	SONL

Only Synchronous Areas

Area number in KERMIT	Area name
1	NL
2	ESNL
3	SONL

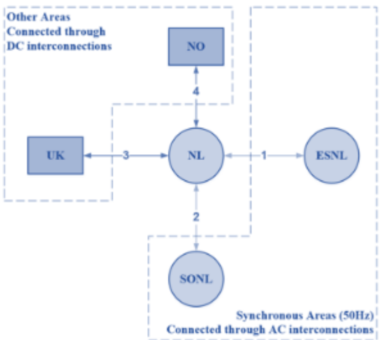

Zone to area mapping

	Area number	1	2	3
	Area name	NL	ESNL	SONL
Zone number	Zone name			
1	NL	1	0	0
2	ESNL	0	1	0
3	SONL	0	0	1

Figure 3-20: Zones Definition within the Control Panel of Kermit 'Excel'

Figure 3-21 illustrates the modelling of the plant to zone mapping within Simulink:

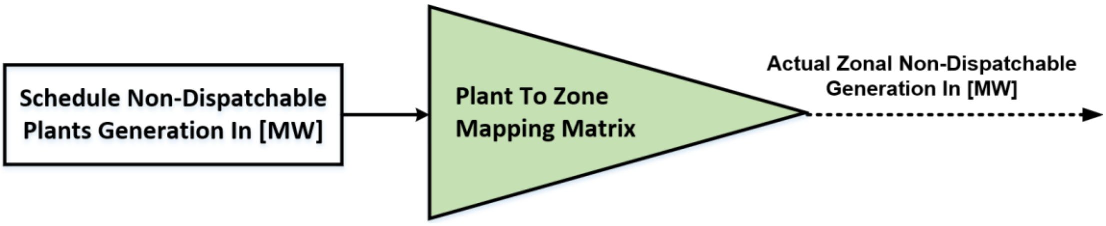

Figure 3-21: Non-Dispatchable Generation Conversion from Plant to Zonal Map

This conversion can be interpreted as follows:

$$\text{Plant to Zone Conversion} = \begin{pmatrix} 1 & 0 & 0 \\ 0 & 1 & 0 \\ 0 & 0 & 1 \end{pmatrix} * \begin{pmatrix} \text{Plant of NL} \\ \text{Plant of ESNL} \\ \text{Plant of SONL} \end{pmatrix} = \begin{pmatrix} \text{Zone NL} \\ \text{Zone ESNL} \\ \text{Zone SONL} \end{pmatrix} \qquad (3.25)$$

- **Setpoint Calculation of dispatchable plants:** determines the power setpoints of each dispatchable plant by considering the AGC signals at the instant of an incidence. In general, this block used in Kermit to ensure the generation to be within the defined capacity values of dispatchable plants. These capacity values are determined as follows:

  a. Find the maximum active power of each dispatchable plant over the entire simulated day.

  b. Set the generation margins (primary reserves) to **3000MW** as the same value of a reference incident defined in UTCE operation handbook [21].

  c. Define the capacity value of each dispatchable plant by adding the values of step (a) to the values of step (b). This step will result in the following capacity values:

     - NL Generating Capacity = 12.3GW
     - ESNL Generating Capacity = 108GW
     - SONL Generating Capacity = 142GW

  The block diagram in figure 3-22 below shows how the Kermit tool maintains these values:

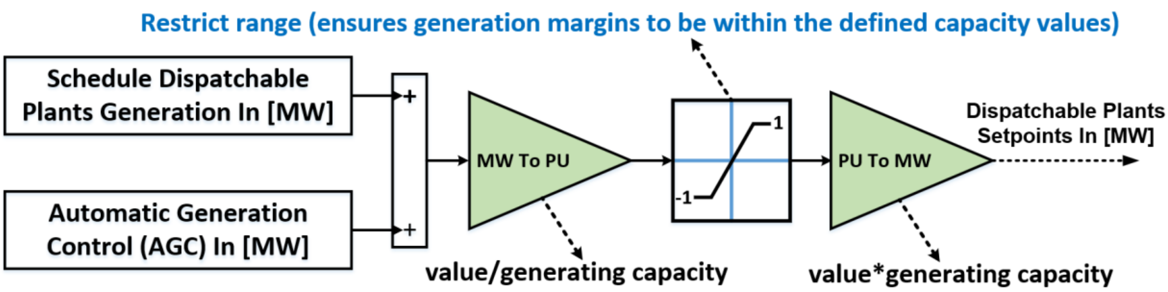

Figure 3-22: Ensuring Dispatchable Generating Capacity within Kermit

- **Dispatchable Power Plants Generation Model:** Kermit provides within this block different power plant models such as Coal, CCGT, Nuclear, and Generic power plant. These models give the possibility of representing the dynamics of synchronous power plants.

  Within this generation model, a generic power plant has been used to represent frequency performance and system dynamics of the dispatchable plants for each synchronous zone (NL, ESNL, and SONL). The use of such a generic power generation unit is due to:

  - A large number of countries within nodes ESNL and SONL, which makes difficult to create a specific power plant model.

  - The lack of technical and mechanical data for node NL that gives the possibility of forming specific models.

  The generic power plant model was straightforwardly developed by DNVGL using Simulink and the IEEE standards. Furthermore, this model has been fine-tuned based on real responses of power plants, which are gathered from the tests that DNVGL performs for power utilities in the Netherlands. However, these responses cannot be described in this document because they are confidentially.

  The overall objective of the generic power plant model is the ability to provide a primary control response upon frequency deviations at the instant of disturbances. This response is formed based on the requirement as given in the Netherlands, to be found on the site the Dutch TSO TenneT [15]. The block diagram given in figure 3-23 below illustrates the approach of the generic generation unit, in which a first order system with a time constant of (T_p) fed by the frequency deviation and droop function has been built. For the power setpoint changes, a rate of change limiter is present.

  The primary control response on frequency deviations is mainly formed within this block based on two inputs the dispatchable plant set points and frequency deviation. First of all, the zonal frequency deviations are translated into plant deviation using the mapping matrix explained earlier in this section. These deviations are further converted from Hz units to per unit values and applied to the frequency **deadband block**, which ensures that also small changes in system frequency will be controlled.

  Stated in [12] is that the effect of deadband on the governing system depends mainly on the magnitude of the steady-state frequency deviation. If the change in frequency is small, it would remain within the pre-defined deadband width. In general, the IEEE standards specify the deadband width to be in the range of (0.02%-0.06%) depending on the size of a power system. However, Kermit developers set the default value of the frequency response deadband to **0.1%**. This value means that primary control will start responding on frequency deviation (≤ ±50mHz).

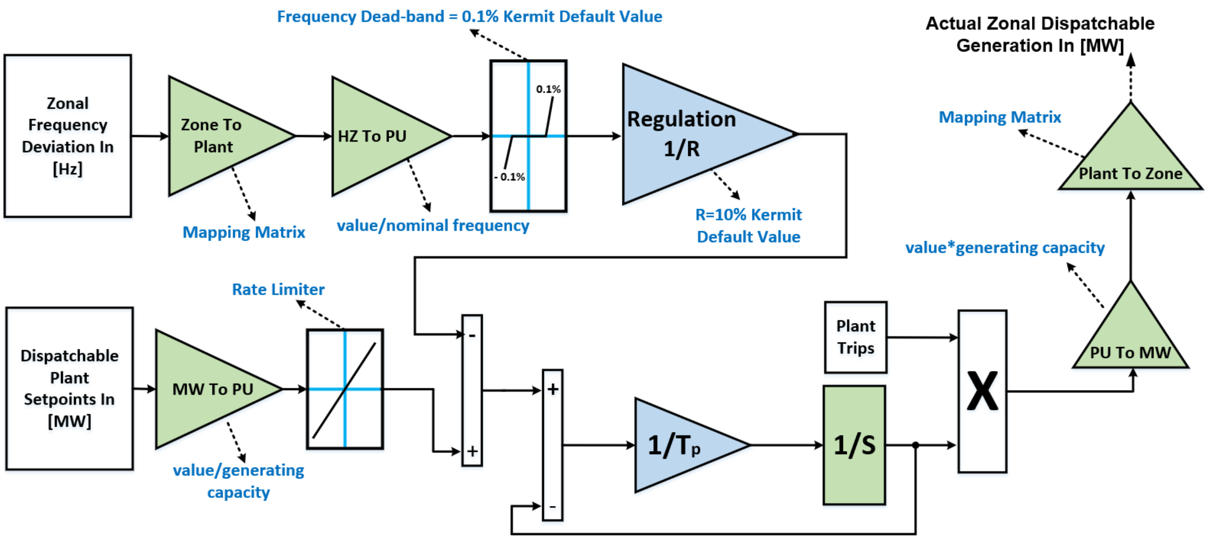

Figure 3-23: Generic Power Plant Model

Next, the outcome of the deadband block is applied to the **Regulation Droop Gain** that can be expressed in terms of Power-Frequency characteristic as illustrated in figure 3-24 below. For instance, a certain synchronous generator is supplying power (P_0) at a nominal frequency (f_0) highlighted by the equilibrium operating power (A). Due to some disturbances, the system frequency decreases to point (f), which in turn, moves the generator's operating point towards the point (B) as a result of the governor droop response. This response often called the primary response, will further cause an increase in the power generation as denoted by point (P).

Stated in [12] is that the actual Power-Frequency characteristic or the Regulation Gain (R) can vary between (2%-12%), depending on the power generation unit output. For example, the regulation gain of the **thermal** power plants is often in the range of (4%-5%), whereas that of the **hydropower** plants can be on the order of (2%-3%). For a 10% governor regulation associated with a 50Hz power system, a frequency change of 10% (5Hz) leads to a 100% change in power output.

Meanwhile, the power setpoints of the dispatchable plants are converted to the per unit values using the plants' capacity. These values are then applied to a so-called rate limiter, which provides stability to the power system by ramping output power up or down during load deviations. This increase or decrease in the outputs of dispatchable power plants is known as the ramp rate and is often given in the form of (MW/min). The ramp limiter sub-block shown in figure 3-23 reacts to power difference from minute-to-minute. A negative power change is defined as ramp-down, whereas a positive change is called a ramp-up.

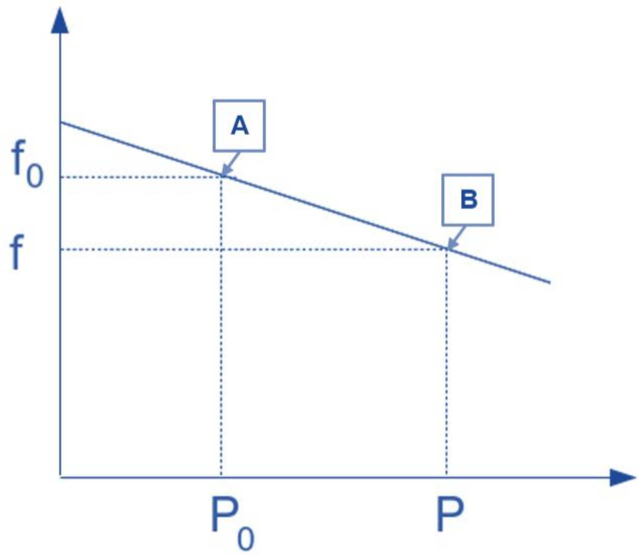

Figure 3-24: Power-Frequency Characteristic of Regulation Droop Gain [22]

Mentioned in [23] is that the production and demand variabilities are often met by a proper design of the control area's portfolio of conventional power generators. Such a matching design can be figured out by ensuring enough number of synchronous generators that are on a governor control with sufficient ramps to match the load and generation deviations. In general, the ramp rates of different types of power plants are expressed in terms of capacity percentage per minute such as:

- **Nuclear** (1%-5%)/min
- **CCGT** (4%-10%)/min
- **Steam turbine** (1%-5%)/min.

Next, the difference between the outcomes of both the Rate Limiter block and Regulation Gain are applied to a vectorized transfer function, which represents the governing control mechanism of the generic power plant model. The governing system has a closed control loop "feedback" that is introduced into this block to process power errors. The transfer function of the governing system can be expressed as follows:

$$\text{Governer Transfer Function} = \frac{1}{sT_p + 1} \quad (3.26)$$

Where (T_p) is the overall time constant of the governing system and the turbine prime-mover of the generic model. This constant form together with the regulation gain the main impacting factors that initiate the primary control response on system frequency deviation. Kermit developers set the default value of the governing time constant to the range of (6s-20s) depends on model parameters with a droop on the order of (8%-10%). In the next chapter, the most suitable parameters of the power plant model are elaborated through a set of simulations.

3.3.4. Automatic Generation Control

Stated in [12] that the full restoration process of system frequency to a specified value (50Hz) needs an additional control action alongside the primary action. Such a secondary control action is commonly referred as **Automatic Generation Control** (AGC) that maintains the system frequency at nominal value and regulates the power exchange between the control areas to the scheduled values by adjusting power outputs of the system generation units automatically. These primary objectives are often called the **Load-Frequency Control** (LFC).

For example, the basis of the LFC of two interconnected areas can be expressed using the relationship mentioned below. This relationship assumes that the power flow on the AC transmission line (or the so-called the tie-line) is from area 1 to area 2:

$$\Delta f * \beta_1 = -\Delta P_{12} - \Delta P_{L1} \text{ in [MW]} \quad (3.27)$$

$$\Delta f * \beta_2 = \Delta P_{12} \text{ in [MW]} \quad (3.28)$$

Solving equations 3.27 and 3.28 yields to the equations given below, which indicate that any increase in the load of area 1 will result in frequency decrease in both areas and the tie-line power flow. The negative sign of (ΔP_{12}) means that power flow through the AC transmission line connects both areas to each other.

$$\Delta f = \frac{-\Delta P_{L1}}{\beta_1 + \beta_2} \text{ in [Hz]} \quad (3.29)$$

And

$$\Delta P_{12} = \frac{-\Delta P_{L1}\, \beta_1}{\beta_1 + \beta_2} \text{ in [MW]} \quad (3.30)$$

Where:

- Δf = stead-state frequency deviation in [Hz]. This value is same for two interconnected areas.
- ΔP_{12} = the power transfer difference from area 1 to area 2 through the transmission line in [MW].
- ΔP_{L1} = represents the change in the load or generation in area 1 in [MW].
- β_1 = the power-frequency regulation factor of areas 1. This variable is often expressed using the Droop and Load Damping:

$$\beta = \frac{1}{R} + D \text{ in [MW/Hz]} \quad (3.31)$$

Mentioned further in [12] that the power flow deviation on the transmission line between these two areas reflects the contribution of the composite frequency response characteristic (regulation factor) of one area to another.

Examination of equations 3.29 and 3.30 shows that the control signal formed due to the change in power flow through the AC lines added to the change in system frequency is weighted by a so-called **bias factor** (B), which would achieve the desired objectives of the AGC. This control signal is commonly referred as the **Area Control Error** (ACE). A suitable value of the bias factor for a specific area can be predicted from equations 3.27 and 3.28 that is equal to the frequency regulation factor of that area as expressed below:

$$ACE = \Delta P_{tie} - B * \Delta f \quad \text{in [MW]} \tag{3.32}$$

And

$$B = -\beta \tag{3.33}$$

Where (ΔP_{tie}) is the difference between the actual and the scheduled power exchange across the AC transmission lines.

The area frequency regulation factor (or area frequency response characteristic) responsible for adjusting the bias factors might be estimated using the chart records following a sudden loss of a significant generation unit. However, such records are hard to be found due to the security and privacy concerns of TSO's.

A graceful way to find acceptable operating bands for the frequency regulation factor of a particular area is given in [21]. It is suggested that an interconnected system should operate in such a manner, depending on both the self-regulating effect and size of system load, that the power-frequency-response characteristic of the entire synchronous area fits within a narrow operating band.

Table 3-8 below gives the frequency-response characteristic that can be used to establish the frequency bias factor:

Table 3-8: Operating Range for Power- Frequency-Response Characteristic [21]

Self-Regulating-Effect [%/Hz]	Network Peak Load [GW]	Power-Frequency-Response-Characteristic [MW/Hz]
1	150	16500
1	300	18000
2	150	18000
2	300	21000

Considering the selected self-regulating effect and the load size (see paragraph 3.3.2), the frequency-response characteristic of each synchronous area was defined to fall within the following **operating bands** that establish the bias factor of the entire synchronous area:

- **NL:** Load = 20GW >>> $\beta_{NL} = 0 \rightarrow 16500 \text{MW/Hz}$
- **ENSL:** Load = 158GW >>> $\beta_{ESNL} = 0 \rightarrow 18000 \text{MW/Hz}$
- **SONL:** Load = 244GW >>> $\beta_{SONL} = 0 \rightarrow 18000 \text{MW/Hz}$

For example, a sudden loss of generation in area NL will cause a decline in system frequency. The first response to this drop is performed by the primary controllers of all controlled synchronous areas, i.e. NL and ESNL. This action will stop the decline of frequency and bring it up to a so-called steady-state value (Δf).

The AGC starts responding at the instant when the system frequency reaches this value:

$$\Delta f = \frac{-\Delta P_{L,NL}}{\beta_{NL} + \beta_{ESNL}} \quad \text{in [Hz]} \tag{3.34}$$

$$\Delta P_{NL \rightarrow ESNL} = \frac{-\Delta P_{L,NL}\, \beta_{NL}}{\beta_{NL} + \beta_{ESNL}} = \quad \text{in [MW]} \tag{3.35}$$

$$ACE_{NL} = \Delta P_{NL \rightarrow ESNL} - B_{NL} * \Delta f \quad \text{in [MW]} \tag{3.36}$$

Substituting equations 3.33, 3.34, and 3.35 into equation 3.36 will yield to the following results:

$$ACE_{NL} = \frac{-\Delta P_{L,NL}}{\beta_{NL} + \beta_{ESNL}} (\beta_{NL} + \beta_{ESNL}) = -\Delta P_{L,NL} \quad \text{in [MW]} \tag{3.37}$$

And

$$ACE_{ESNL} = -\Delta P_{NL\rightarrow ESNL} - B_{ESNL} * \Delta f = \frac{-\Delta P_{L,NL}}{\beta_{NL} + \beta_{ESNL}}(-\beta_{ESNL} + \beta_{ESNL}) = 0 \ \text{in [MW]} \qquad (3.38)$$

Both equations 3.37 and 3.38 highlight that the AGC of the Dutch power system, in this example, will only respond to the sudden generation loss in case that both the synchronous generating capacity and power reserves within the Netherlands are sufficient big. Such a response will, in turn, bring the signal error (ACE_{NL}) to zero.

The AGC scheme of the Netherlands has not been made available by the Dutch TSO “TenneT” due to privacy concerns. **Therefore, another scheme was developed during this thesis based on the theory provided by P. Kundur [12].** The figure below shows how the AGC scheme is implemented using Kermit to ensure that the synchronous areas of the studied interconnected power system will be fully controlled when it is subjected to severe disturbances:

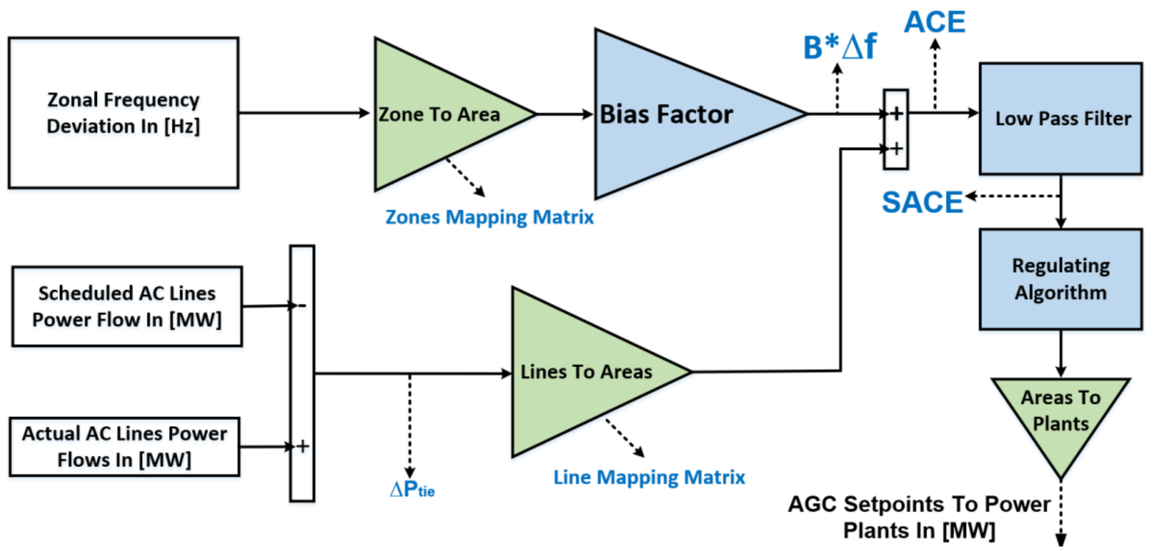

Figure 3-25: AGC Scheme Implemented Using Kermit Simulink

The difference between the **scheduled power flow through the transmission lines** and the **actual power flow** forms the variable **ΔP_{tie}**, which is further applied to the so-called **Line-To-Areas** gain. This gain ensures that flow through the AC lines between the controlled areas will be translated in terms of areas in such a manner that the AGC scheme will operate with three area elements instead of 2 lines elements. This conversion can be described as follows:

$$\text{Line} \rightarrow \text{Map (Matrix)} = [\,\text{Line} \rightarrow \text{Zone (Matrix)} * \text{Zone} \rightarrow \text{Area (Matrix)}]^{T} \qquad (3.39)$$

$$\text{Line} \rightarrow \text{Map (Matrix)} = \left[\begin{pmatrix} -1 & 1 & 0 \\ -1 & 0 & 1 \end{pmatrix} * \begin{pmatrix} 1 & 0 & 0 \\ 0 & 1 & 0 \\ 0 & 0 & 1 \end{pmatrix}\right]^{T} = \begin{pmatrix} -1 & -1 \\ 1 & 0 \\ 0 & 1 \end{pmatrix} \qquad (3.40)$$

Using equation 3.40, the three area elements can be formed as shown below:

$$\text{Lines} \rightarrow \text{Areas} = \begin{pmatrix} -1 & -1 \\ 1 & 0 \\ 0 & 1 \end{pmatrix} * \begin{pmatrix} \text{ENSL} \rightarrow \text{NL AC Line} \\ \text{SONL} \rightarrow \text{NL AC Line} \end{pmatrix} = \begin{pmatrix} -(\text{ESNL} \rightarrow \text{NL}) - (\text{SONL} \rightarrow \text{NL}) \\ (+\text{ESNL} \rightarrow \text{NL}) \\ (+\text{SONL} \rightarrow \text{NL}) \end{pmatrix} \qquad (3.41)$$

Meanwhile, the zonal frequency deviation is translated into the terms of frequency change per each area, followed by a multiplication with the **Bias Factor** gain. The values of this gain should fall within the pre-defined operating bands as described earlier in this paragraph. From control stability perspective, significantly larger values than the values of such bands are usually not desirable as the overall control actions of a specific area will become unstable.

Furthermore, the use of equations 3.32 and 3.33 forms the so-called **Area Control Error** (ACE) by applying the outcomes of both the Line Mapping Matrix and Bias Factor Gain to a main summation point. Often, this signal contains a large amount of oscillations caused by the load and generation variability to which the control actions response. Such actions do not reduce the error signal but actually, put more stress on the governing system. Therefore, the AGC scheme is usually provided with the **first-order filter** shown above to damp-out these oscillations.

This filtering process results in a so-called **Smoothed Area Error Signal** (SACE) that is further used as an input to the Regulating Algorithm block. The time constant of this filter depends mainly on the parameter of the AGC; therefore, calibration is required in order to find an appreciate value to run the AGC scheme on the right track.

The smoothed error signal indicates the instant at which the generation of dispatchable power plants should be increased or decrease in order to control the power system. This signal must thus be regulated to be zero depending on the size of disturbances. For this purpose, the SACE is connected to the input port of a so-called **Regulating Algorithm** block that contains the required logic for eliminating the steady-state frequency errors.

Mentioned in [24] that the current control systems of electric networks are designed with different strategies that provide a 'good' AGC operation. A suitable technique to implement the regulating algorithm of AGC is the tuning of PI parameters for an interconnected system with more than one power plant. The use of PI controller offers a simple way to achieve the primary objectives of the secondary control under different operation conditions.

The Proportional Integral (PI) regulating algorithm consists of two modes:

- Proportional Mode (PM): reduces the rise time of area control error, but never eliminates it.
- Integral Mode (IM): eliminates the area error but causes a worst transient response.

The figure below shows a simplified block diagram of a control system with the PI regulating algorithm as given in [25]. The output signal of this controller depends mainly upon two parameters:

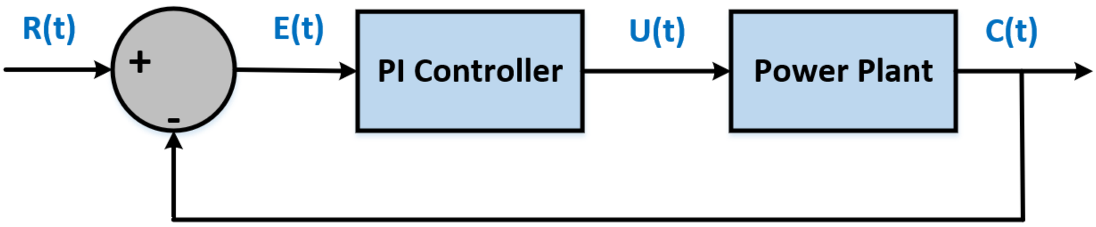

Figure 3-26: Simplified Control System with PI Controller

Where:

- R(t) = the setpoints of dispatchable power plants
- E(t) = the error signal, which is the difference between the setpoints and the feedback signal
- C(t) = the output signal of the power plants
- U(t) = the control signal provided by the standard PI controller with K_p and K_i are the proportional and integral gains. This signal can be expressed as follows:

$$u(t) = K_p\, e(t) + K_i \int_0^t e(t)\, dt = K_p \left[e(t) + \frac{1}{T_i} \int_0^t e(t) dt\right] \quad (3.42)$$

Simulink provides two structures of the PI controller: Ideal and Parallel. Each has its advantages and disadvantages. The main difference between them that the proportional gain of Ideal PI acts on the error signal as well as the integral mode whereas with the parallel algorithm it only acts on the error. In other words, the effect of gain constant (K_p) with Ideal PI controller is distributed among the two modes. Increasing this constant will make the (PM) and (IM) more aggressive to disturbances. In [25] simulation results have proven that the Ideal PI has the best performance in terms of settling time.

Figure 3-27 below shows how this controller is implemented within Kermit Simulink:

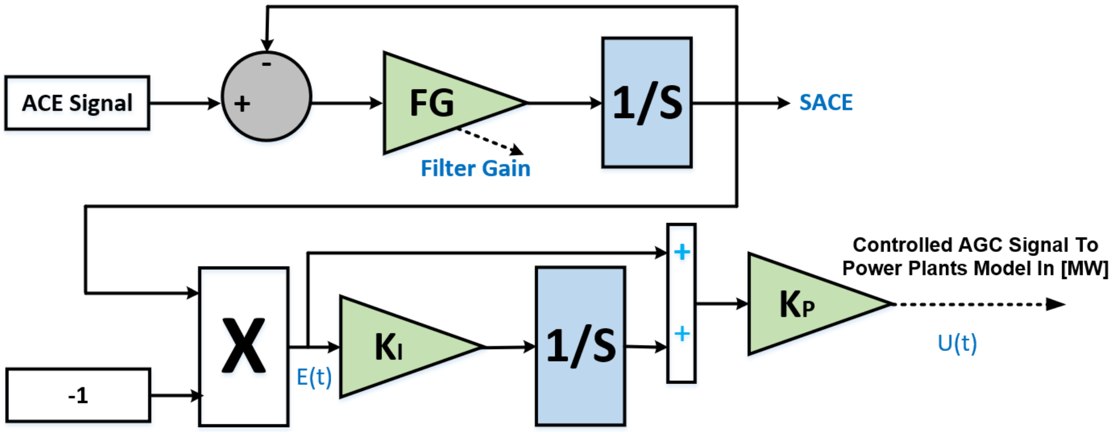

Figure 3-27: Implementation of PI Controller inside Kermit

This block diagram will achieve the desired behaviour of the AGC over time by considering the following transfer function of the PI algorithm, in which Kp and Ki gains should be calibrated with respect to the model parameters:

$$G_{PI}(s) = \frac{u(s)}{e(s)} = K_P \left[1 + \frac{K_I}{s} \right] \qquad (3.43)$$

3.4. Summary of Model Implementation

This chapter has described the proposed approaches for the dynamic power system model that can be used to assess the frequency performance of the Dutch system based on the Regional Groups (RG) as defined by ENTSO-e. Two approaches have been developed; the first approach is a detailed model that study the frequency stability concerns of all countries that covering the RG-Continental Europe and RG-Baltic, while the second approach is a more simplified model that examines the frequency performance of the Dutch system as part of the synchronous grid.

The modelling of the first approach using KERMIT has shown difficulties regarding the large number of input data, needed to run the simulations, compared to the second approach. For this reason, a decision has been made during the implementation phase to use the simplified (second) approach to achieve the overall objectives of this thesis.

The second approach consists of one primary node (NL) that represents the Dutch power system, connected to two aggregated synchronous nodes (ESNL & SONL) through AC transmission lines. Each of these two nodes contains the generation and load profiles of twelve countries. Besides these nodes, there are also two other nodes (the UK and NO) that are non-synchronously connected to the Netherlands through DC links. These latter nodes are needed for the cross-border power exchange between the (Dutch & British), and the (Dutch & Norwegian) power systems, respectively.

During the implementation of the second approach using DNVGL Kermit-Tool, several tasks have been performed to prepare the dynamic power system model for simulations purposes. These tasks are:

- Estimating the current amount of inertia constant for the involved countries based on non-renewable capacities data published by ENTSO-e
- Gathering the correct day-ahead data of production, demand, cross-border exchange, and system parameters
- Creating a detailed description of the Kermit power system model
- Modifying the Simulink blocks of the Kermit-Tool based on the selected approach
- Developing an AGC scheme for the secondary control action

4. SCENARIOS AND SIMULATION RESULTS

In this chapter, two scenarios have been created to answer the research questions of this thesis work. The first scenario, **pre-scenario**, was designed to verify the overall operation of the developed dynamic power system model using KERMIT as well to check the present frequency performance of the Dutch system with the estimated inertia values in chapter (3). The second scenario, **main-scenario**, has been developed to assess the frequency performance of the Dutch grid in a future situation by considering the high penetration of renewables in the total electricity production, followed by the possible inertia reduction.

4.1. Pre-Scenario

This scenario has been created to verify the operation of the second model shown in figures 3-3 and 3-4 to analyse the current frequency performance of the Dutch synchronous grid. For this purpose, different simulations were performed using Kermit-Simulink to find the most suitable values for the primary and secondary control actions.

In [21], it is mentioned that different disturbances, i.e. load and generation fluctuations, will lead to frequency deviation, to which the primary control action of dispatchable power plants will respond at any time to ensure that system frequency is kept at the acceptable operating ranges.

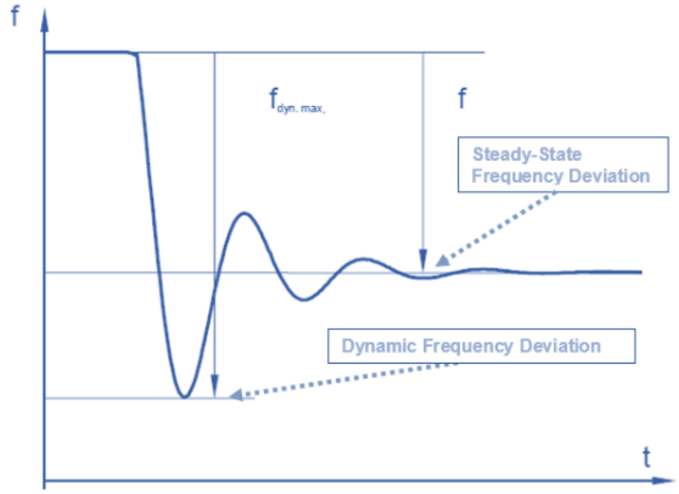

Figure 4-1: two deviations types of system frequency [21]

An example of specific frequency deviations is given in figure 4-1, in which the governing system of all synchronous generation units will subject to the primary control action to react within a few second typically (0s-30s). Such a reaction will sense the power produced by these generators until a balance between the supply and demand sides is reached. At the instant of the power balance between both sides, the system frequency is stabilized and kept at a steady-state value, which differs from the nominal system frequency (50Hz).

The consequence of this difference will cause an error between the actual and scheduled power cross-border exchange. At this instant, the secondary control associated with AGC will start responding to maintain the system frequency to the nominal value, and hence, the power exchange will be restored to the values agreed between TSOs of the synchronous zones within (5min-10min).

Stated further in [21] is that the magnitude of the dynamic frequency deviation is often governed by the disturbance's amplitude, the development over time of that disturbance, the inertial response of the dispatchable power plants, the number of synchronous generators and their dynamic characteristics within each plant, and the dynamic characteristic of system load, i.e. the self-regulating effect.

Whereas, the magnitude of the steady-state frequency deviation is mainly governed by the disturbance's amplitude and power-frequency characteristic of dispatchable power plants. The last characteristic is often influenced by the regulation droop characteristic of the synchronous generators and the sensitivity of load to variations (or the so-called load damping factor)

For the Dutch power system model described in chapter 3, the frequency performance including both the primary and secondary responses on deviations are carried out as illustrated in figure 4-2 below:

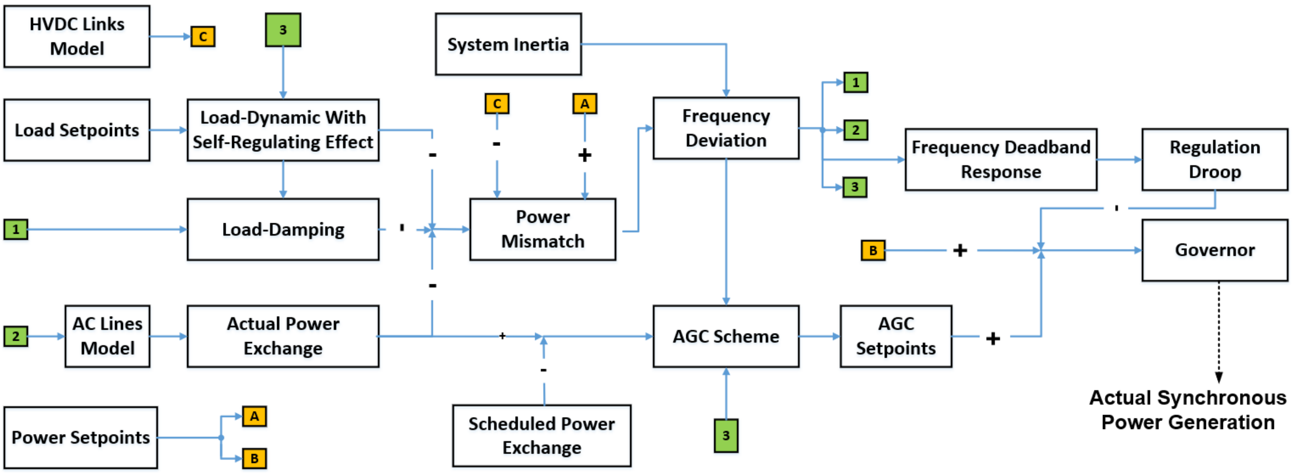

Figure 4-2: Overview of the Entire Frequency Control Response on Power Deviations

This section aims to examine the current level of inertia in the Dutch power system with 26% electricity produced by non-synchronous generation. It is well-known that the inertia parameter directly affects the dynamic behaviour of the power system. From a functional perspective, it can be summarised that the level of system inertia affects both the Rate of change of Frequency (=RoCoF) and frequency transients during contingencies as the RoCoF is inversely proportional to the overall system inertia (see equation 3.8).

Typically, system frequency starts oscillating from the nominal value due to an imbalance between both supply and demand sides. Within the synchronous grid of Continental Europe including that of the Netherlands, the frequency fluctuation is mainly stabilized by the primary control action. Such an action is designed in such a manner that the deviations are kept in a range of (49.8Hz-50.2Hz), which are the acceptable frequency operating ranges.

Meanwhile, UTCE Grid Codes state that the acceptable RoCoF operating ranges are on the order of (0.1Hz/s-1Hz/s). Higher RoCoF values mean large deviations in voltage angles within the synchronous grid that can lead in some specific situations to a trip of distance protective equipment. The **worst scenario** occurs when frequency transients triggered by 20% power imbalance, i.e. the loss of generation in a synchronous zone, are followed by a RoCoF higher than 1Hz/s. Such a conservative scenario can cause unpredictable states for the system and may lead to power outages as stated in [8].

The magnitude of a possible contingency depends mainly on the structure of the interconnected system. Different structures mean different amounts of power production that need to be maintained to the system load level, and also, different amounts of kinetic energy to stabilizes frequency gradients. Therefore, a so-called normative incident should be defined for stability studies. In [21], the normative contingencies (sometimes called also reference incidents) for the interconnected system of the synchronous grid of CE is defined as the tripping of the two largest power generation units connected to the same busbar. The value of such a trip is commonly set to 3000MW, which defines the required primary reserves.

ENTSO-E defines in [21] that a sudden loss of 3000MW generating capacity should be resolved by the primary control action of the dispatchable power plants, without the need for customer control actions, i.e. load-shedding. Figure 4-3 below shows how ENTSO-E defines the system frequency of the synchronous grid of CE for case A. This case has a hypothesis design, in which the requirements of the primary control action is fulfilled, and the maximum dynamic frequency deviation is 800mHz, which means that the customer control actions are required when frequency deviation exceeds this value.

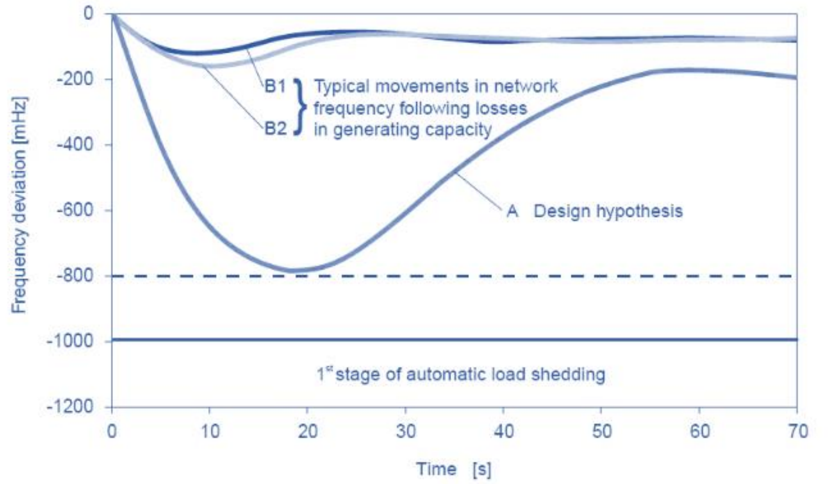

A Loss in generating capacity: P = 3000 MW, $P_{network}$ = 150 GW, self-regulating effect of load: 1% / Hz
B1 Loss in generating capacity: P = 1300 MW, $P_{network}$ = 200 GW, self-regulating effect of load: 2 % / Hz
B2 Loss in generating capacity: P = 1300 MW, $P_{network}$ = 200 GW, self-regulating effect of load: 1% / Hz

Figure 4-3:ENTSO-E Definition 'System Response Following Normative Incidents' [21]

Such a design was the main target of the pre-scenario in order to verify the operation of the created power system model in the previous chapter. Achieving this target means leading the system to operate in such a manner that the power frequency characteristic of the studied synchronous areas will fall within the defined operating bands in paragraph (**3.3.4**). For this purpose, a list of assumptions has been created that helps to find the suitable operating conditions of both the primary and secondary control. These assumptions are listed below as follows:

- Define the time constant of dispatchable power plants to be in the range of (6-20) seconds as it recommended in the Kermit tool for the generic power plant model
- Set the self-regulating effect to 1%
- Define the regulation droop characteristic of the generators to be on the order of (8-10) % as it is recommended in the Kermit tool for the generic power plant model
- Set the deadband response to 0.1% (=50mHz) as it is the default value of Kermit-Simulink
- Set the capacity values equal to the maximum dispatchable active power values mentioned in the paragraph (**3.3.3**)
- Define the peak load values to be equal to those values mentioned in the paragraph (**3.3.4**)
- Set the load damping constant (D) to value 1
- Design a normative reference contingency: set the sudden incident to 3000MW to create a power imbalance between the generation and load

The sudden incident has been applied to the power system model as indicated in figure **3-7**. Such a step fault will decrease the total generation within each zone by 3000MW, resulting in overall frequency deviations that must be offset by the primary control. Different simulations have been performed during this phase in order to find the most suitable values of both the generator time constant and regulation droop. Once these values are obtained, it would be a bit easier to predict the actual frequency performance of the Dutch power system with a focus on:

- The rate of change of frequency (RoCoF) with the actual level of system inertia
- The Frequency Nadir Point
- The deployment time of the primary control action

It is worth to be mentioned that suitable values of both the time constant and regulation droop mean that the dynamic frequency deviation should not exceed the ±800mHz with a steady-state deviation on the order of ±180mHz. Besides, the primary controller should be fully activated within a period between (15-30) seconds in response to a power change between (1500-3000) MW. In other words, the minimum power that the primary control provides for counteracting the frequency deviations is determined by the development time of the disturbance and the size of this disturbance.

Note that the instant of applying a disturbance to the studied model has been selected in such a manner that there is sufficient time before and after the disturbance, which do not contain small frequency fluctuations caused by cross-border power flow or the generation and load variability. Such a selection was made in order to show how the frequency control actions respond to the step fault without any other disruptions and to provide sufficient time for the action of AGG, which requires a period of [3min-10min]. Therefore, the 3000MW sudden generation loss has been applied at the instant (50700s=845min=14,083hour) of the 18th of January 2017.

In general, the main impact of disturbance size is on the initial rate of frequency drop (RoCoF), the maximum dynamic frequency deviation (Nadir point), and the steady-state frequency value after an incident. However, it can be observed that the size of a specific contingency has almost no influence on the time when frequency decline reaches the Nadir point.

Moreover, all measures of system frequency response following a disturbance, including the time required to reach the Nadir point are influenced by the value of system inertia. The higher values of system inertia are, the slower frequency decline, and hence, the slower frequency recovery. This slow process will limit the maximum frequency deviation as the governing system would need more time to response.

However, system inertia has no impact on the final steady-state values of frequency, which are mainly affected by both the regulation droop characteristic and load-damping effect. Both parameters have almost the same effects on the frequency recovery time and maximum frequency error *(error =difference between actual frequency value after the action of primary control and the nominal frequency value; sometimes called frequency offset).* Although both parameters have the same impact of the final steady-state values, the regulation droop (R) plays a more important role in the restoration process of system frequency than the load damping (D) as stated in [39]. For this purpose, the parameter (D) has been defined to be constant with value equals to (1), while the (R) was tuned.

On the other hand, the impact of the governor time constant (T_P) is significantly on time required to reach Nadir point. It does not affect the final values of the frequency offset. The smaller values (T_P), the faster response of governing system that is often suited for small frequency fluctuations.

To show the effect of the regulation droop and the governor time constant on the primary control action with a power imbalance of 3000 MW, the values of (R) and (T_P) have been varied between (8%-10%) and (6s-20s) in increments of 1% and 2s, respectively. Figures 4-4, 4-5, and 4-6 below show the simulation results of tuning these two parameters for the Dutch system frequency as the interest is to examine frequency performance of the Dutch system as part of CE. These simulations have been performed with a constant inertia value equals to (4.05) as estimated in chapter (3):

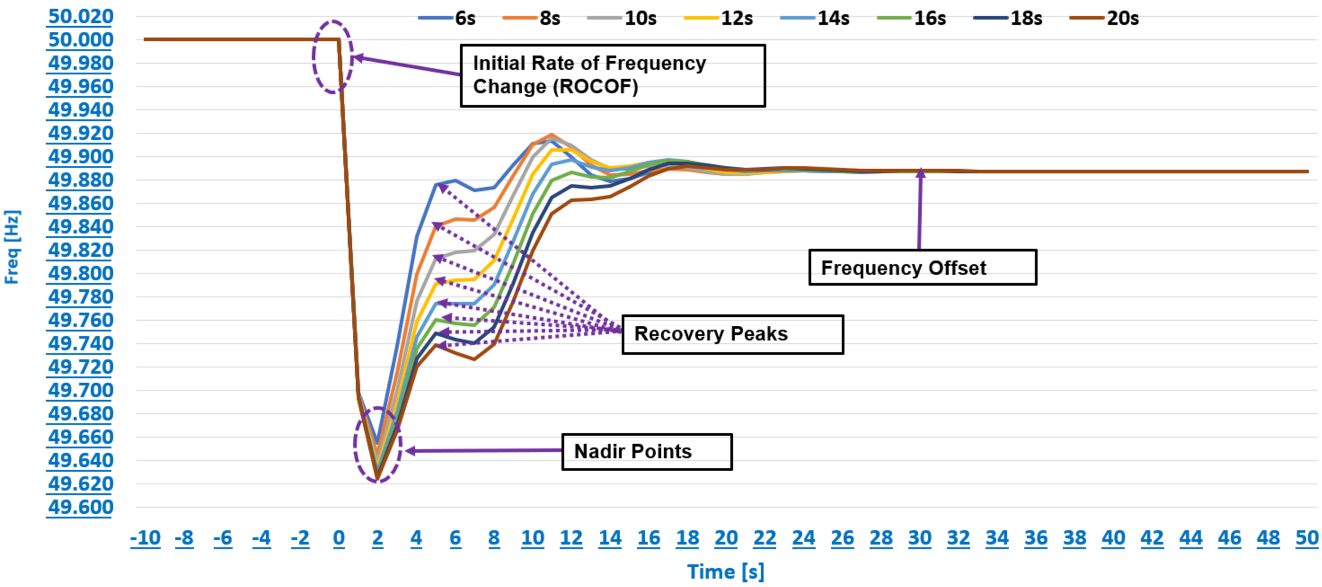

Figure 4-4: NL Frequency in [Hz], Droop 8%, Governor Time Constant between [6s-20] in increments of 2s

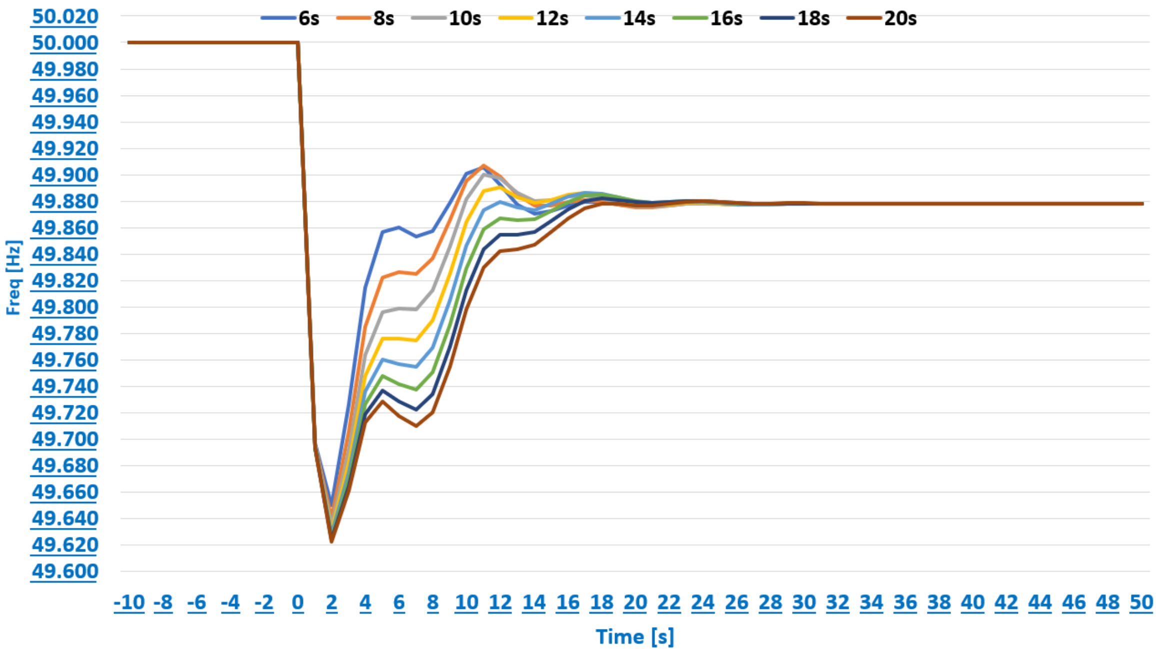

Figure 4-5: NL Frequency in [Hz], Droop 9%, Governor Time Constant between [6s-20] in increments of 2s

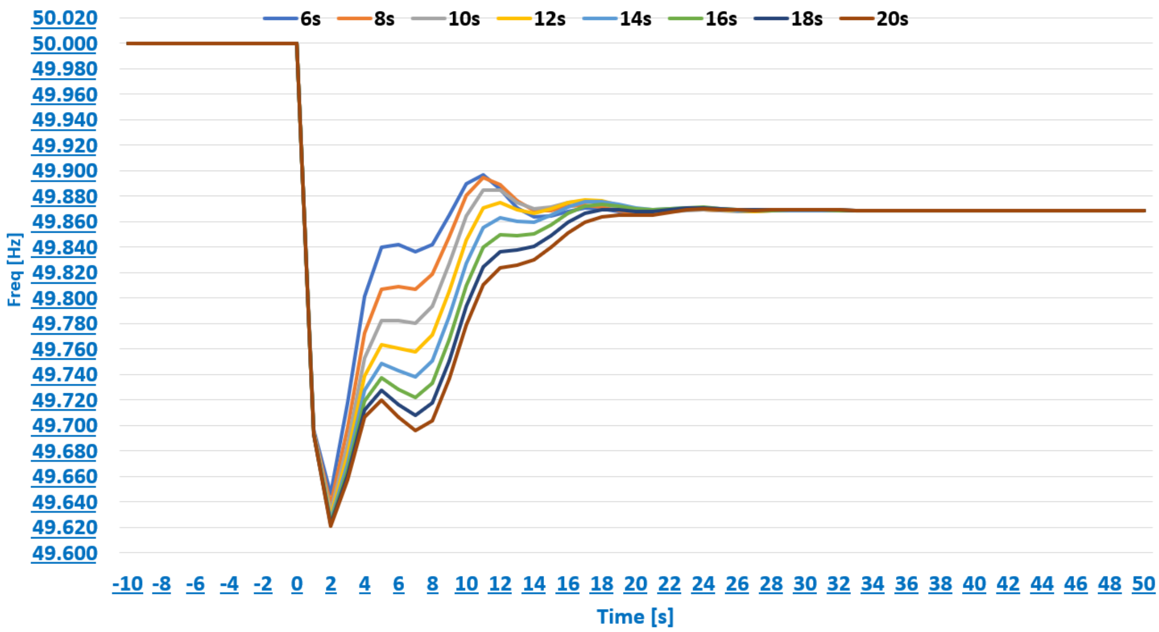

Figure 4-6: NL Frequency in [Hz], Droop 10%, Governor Time Constant between [6s-20] in increments of 2s

It is worth to be noted that the period of the simulation performed equals to one day (0-24h), which is equal to (0-86400s). At instant 50700s, the step-fault of 3000MW has been applied to the studied system. System frequency is analysed with a time resolution equals to 1s.

Within the primary control operating area, five impacting factors that should be considered during the evaluation of the simulation outcomes. These factors are the time required to reach both the maximum dynamic frequency deviation and final steady-state frequency value, the value of both the Nadir point and the frequency offset, the RoCoF value, and the value of recovery overshoot (=difference between Nadir point and the first recovery peak).

Let say, the time constant of the governing system is equal to 13s (=midway between 6s-20s). This assumption makes possible to create a comparison between the three regulation droop values of the governor in order to select the most suitable one. The outcomes of this comparison are depicted in figure 4-7 and table 4-1 below:

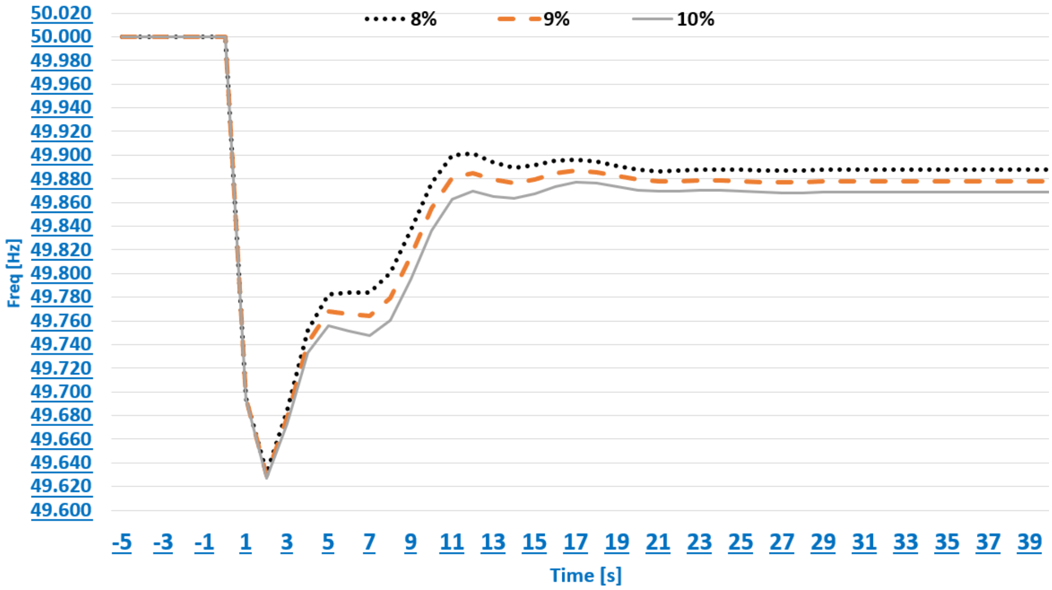

Figure 4-7: Simulations of Three Regulation Droop Values with a Fixed Governor Time Constant (13s)

Table 4-1: Comparison Between the Three Regulation Droop Values

Droop [%]	Nadir value [Hz]	Nadir time [s]	RoCoF [mHz/s]	Offset value [mHz]	Offset time [s]	Recovery Overshoot [mHz]
8	49.632	After 2s	306	112	After 25s	152
9	49.629	After 2s	307	122	After 25s	137
10	49.627	After 2s	308	132	After 25s	124

Below follows an elaboration on the method used to estimate the RoCoF values mentioned in table 4-1 above:

a. Compute the frequency centre of inertia (=f_{COI}) for each generator using equation 2.3 and then add these values up to get the overall centre of inertia for each synchronous area. However, there is no need for computation process as the number of synchronous generators within each area is assumed to be one, which results in a common (f_{COI}) value for the whole area that represents the Inertia Response (IR) of dispatchable power plant following disturbances.

b. Use the instants of both the event and Nadir, t_1 and t_2 respectively (see figure 2-9)

c. Find an appreciate index of an intermediate period to get the value of (f_{COI}) in such a manner that ($f_{COI} = f_{t3}$). Typically, this index is computed as the event time plus 500ms ($t_3 = t_1 +$ **0.5s**).

ENTSO-E defines in [40] the number of cycles required for frequency measurements to be in the range of few hundred milliseconds. For an accurate RoCoF estimation, it can be stated that a sliding window over five sequential measurements will result in reliable RoCoF values, which in the case of 100ms resolution leads to a **0.5s** time needed prior to an accurate RoCoF value would be available.

d. The initial rate of frequency decline (ROCOF) can then be estimated using the following equation:

$$\mathrm{RoCoF} = \frac{df(t)}{dt} = \frac{f_n - f_{COI}}{t_3 - t_1} = \frac{f_{t1} - f_{t3}}{0.5} \text{ in } \left[\frac{Hz}{s}\right] \tag{4.1}$$

Where: ($f_n = f_{t1}$), ($f_{COI} = f_{t3}$), and ($t_1 < t_3 < t_2$)

These outcomes highlight the minor difference between the characteristics of the three droop values. The only considerable difference is the value of the recovery shoot, which is smaller with the 10% droop than with 8% or 9%. Even though the 10% droop has this characteristic better than the 8%, but the latter has better characteristics such as the frequency Nadir, RoCoF, and frequency offset. As a trade-off between these values, it was decided to use the **9%** regulation droop as a fixed value for further simulations.

Furthermore, the simulation results of the 9% regulation droop (see figure 4-5) show that the different values of governor time constant affect mainly both the time and value of the Nadir-point, the RoCoF rate, and the recovery shoot. This parameter has further no impact on the final value of frequency offset. Table 4-2 below shows a comparison between these values:

Table 4-2: Characteristics of 9% Regulation Droop with a varied Governor Time Constant [6s-20s]

Droop [%]	Nadir value [Hz]	Nadir time [s]	RoCoF [mHz/s]	Recovery Overshoot [mHz]	Recovery Delay [s]
6	49.650	After 2s	303	210	After 3s
8	49.641	After 2s	304	186	After 3s
10	49.635	After 2s	305	164	After 3s
12	49.631	After 2s	306	145	After 3s
14	49.628	After 2s	306	129	After 3s
16	49.625	After 2s	307	116	After 3s
18	49.624	After 2s	307	105	After 3s
20	49.622	After 2s	308	95	After 3s

It can be concluded that smaller values of governor time constant mean lower Nadir values with higher RoCoF values. However, the contrast between the highest and lowest Nadir points or between the lowest and highest RoCoF values are small. Similar to the regulation droop characteristic, the notable contrast is the Recovery overshoot that is very large with the small-time constant values compared to those higher values. It is typically preferred to have a small transient overshoot during frequency restoration process in order to provide a sufficient delay *(delay = instant recovery peak – instant nadir)* for synchronous generation units to produce power that maintains the balance between the supply and demand sides to oppose the drop of system frequency and bring it up to the final steady-state value.

For this purpose, the decision was to select a time constant value that has a small recovery shoot, but not a too high RoCoF value or too low Nadir point. Following a trade-off between the values depicted in table 4-2, it can be stated that a **13s** governor time constant would be suitable for further simulations during this thesis project as it results in acceptable values of all those analysed properties.

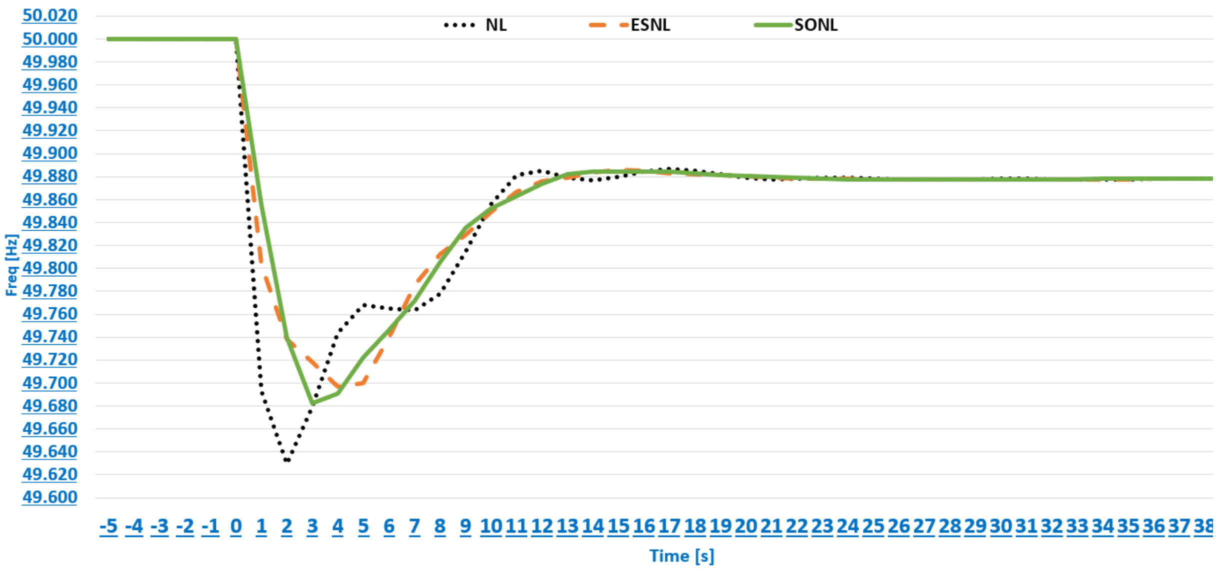

Figure 4-8: Frequency Deviation of NL, ESNL, and SONL following a Sudden Generation Loss of 3000MW

Figure 4-8 above depicts the final curve of the deviation of the Dutch frequency due to a sudden generation loss of 3000MW followed by a primary response action based on the selected value of both the regulation droop and governor time constant. Also, it gives the curves of both the ESNL and SONL areas that are synchronously connected to the Dutch power system.

Therefore, different primary control settings would result in different actions in the studied control areas, which in turn, leads to different values of frequency performances that are related to the primary action. Such a contrast is logic as it is related to the generating capacity value of each dispatchable plant. Also, it has to do with the load level within each synchronous area. Tables 4-3 and 4-4 below gives the final values of the primary controller and the final values of frequency performance related to this controller, respectively.

Table 4-3: Final Values of Primary Controller of Each Synchronous Area

Primary Control Properties	**NL**	**ESNL**	**SONL**
Synchronous Generating Capacity [GW]	12.3	108	142
Area Load [GW]	20	158	244
Regulation Droop Characteristics [%]	9	9	9
Frequency Deadband Response [mHz]	50	50	50
Governor Time Constant [s]	13	13	13
Self-Regulating Effect [%]	1	1	1
Load Damping Constant [-]	2	2	2
Rating up/down [GW/min]	1.3	11	14

Table 4-4: Final Values of Frequency Performance Under the Primary Action Due to a generation loss of 3000MW

Frequency Response Performance Related to Primary Control Action	**NL**	**ESNL**	**SONL**
Overall Response Time [s]	25	23	23
Nadir Instant [s]	2	4	3
Nadir Value [Hz]	49.629	49.697	49.683
RoCoF [mHz/s]	307	197	144
Frequency Offset Value [mHz]	122	122	122
Recovery Overshoot [mHz]	137	189	202
Delay [s] Delay = instant recovery peak – instant Nadir	3	11	11
Percentage of Generation Loss [%] equals to (Power Loss) divided by (Total Generation)	23.6	2.03	1.31

Up to now, this section has described the primary control action in response to a created step fault within each synchronous area of magnitude 3000MW. It shows how the selected values of the power plant can affect the frequency performance falls under the primary controller. Table 4-4 points out that the selected values result in acceptable frequency operating ranges as the RoCoF values are within the range of [100mHz/s-1Hz/s], the Nadir point does not exceed the threshold value (49.2Hz) depicted in figure 4-3, and the overall primary response time fits within the range of [0s-30s].

The next step is to elaborate on the performance of the developed secondary control scheme, which eliminates the frequency offset and brings up the system frequency to the nominal value. Alongside, it maintains the power exchange between the synchronous areas at the scheduled values as explained earlier in section (3.3). Finding the suitable values of the AGC parameters are quite hard as they are related to each other. In other words, any change in one parameter will require a change in another parameter in order to stabilise the operation of the AGC scheme.

As stated in the UTCE Operation Handbook [21], it is required to keep the proportional gain as small as possible in order to avoid any detrimental impact upon the stability of an interconnected power system. Similar to the P-gain, the integral parameter should be small to eliminate frequency oscillations. Table 4-5 below gives the values of the PI parameters and filter coefficient that are suitable for the simulations purposes of the Dutch power system. It is further assumed that these values are the same for the other synchronous area (ESNL and SONL) as the main interest is to examine the Dutch system as part of the synchronous grid of CE.

Furthermore, from the perspective of steady-state performance, the selection of the bias settings is not considered to be an impacting factor. Any combination area signal error (ACE) that contains components of power deviation across AC lines and frequency deviation will lead to a steady-state recovery of system frequency as the integral-mode of the Regulation Algorithm enforces the ACE to return to zero. However, from the dynamic performance consideration, the choice of the most suitable bias factor is crucial since the AGC should bring the frequency offset after a sudden loss to the nominal value (50Hz). Recommended in [12] is to set the bias factors of the controlled areas nearly equal to the power-frequency operating bands in order to avoid the unstable operation of the secondary control. From this point of view, it was decided to set the bias factors of the three-studied areas to the maximum power-frequency characteristic values, which are given in paragraph (3.3.4).

The table below gives the essential settings of the AGC scheme in accordance with the discussion held above. **These settings have been found after a long-term simulation and calibration process starting with some values (i.e. 1 for P-gain and 1 for I-gain) and then changing these values independently to get the most suitable values.**

Table 4-5: Automatic Generation Control Settings

Secondary Controller (AGC) Parameters	NL	ESNL	SONL
Proportional Gain [-]	0.1	0.1	0.1
Integral Gain [-]	0.1	0.1	0.1
Filter gain [-]	20	20	20
Bias Factor [MW/Hz]	-16500	-18000	-18000

These settings yield to the following frequency performance using both the primary and secondary settings:

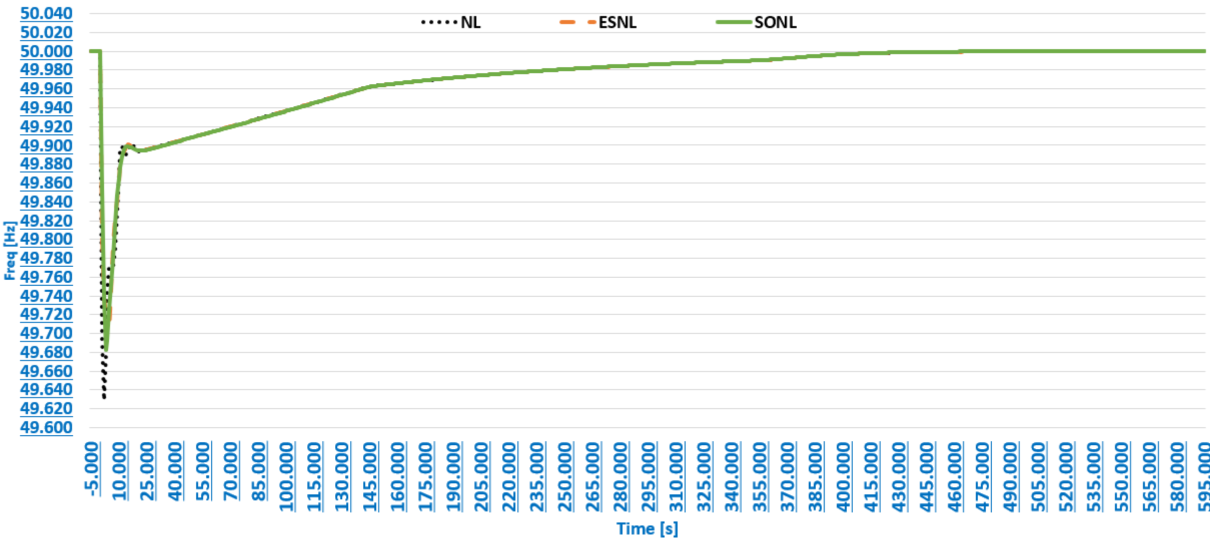

Figure 4-9: Secondary Control Action with the Selected AGC Settings

Figure **4-9** points out that the choice of the AGC settings has attained the main criteria, which states that the ACE, and hence, system frequency, must return to zero within **ten minutes** following the time instant of an event, i.e. a sudden loss of generation or increase/decrease of the load. As it can be noted that the actual frequency values of all three controlled areas are equal to (50Hz) after approximately 470s (~ 7.83min) from the incident instant.

Focusing on the created power imbalance event of magnitude 3000MW within each area, the corresponding ACE signals depicted in figure **4-11** below are the control area unbalance (ΔP_{tie}) **minus** its contribution to the activation of the primary control power ($B * \Delta f$) in case that the bias factors are equal to the power-frequency characteristics (β) of their relevant control areas (see equations **3.32** and **3.33**). The resulted ACE signal of area NL is negative as this area imports power from the other synchronous areas during the applied event.

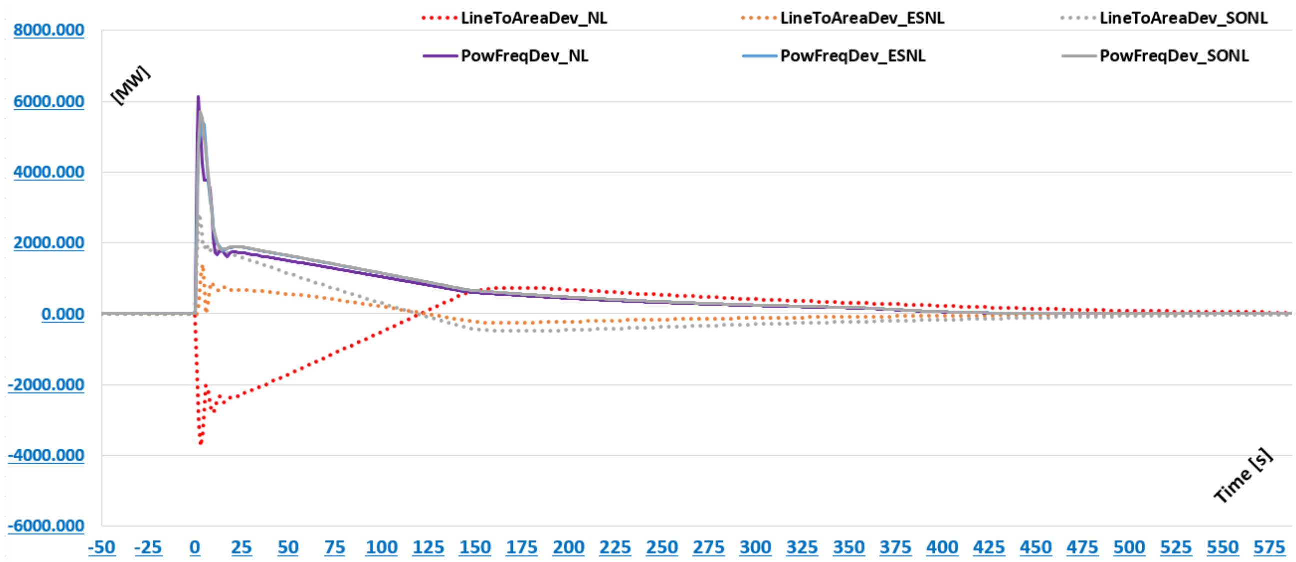

Figure 4-10: Areas Power Flow Unbalance Minus their Contribution to the Primary Control

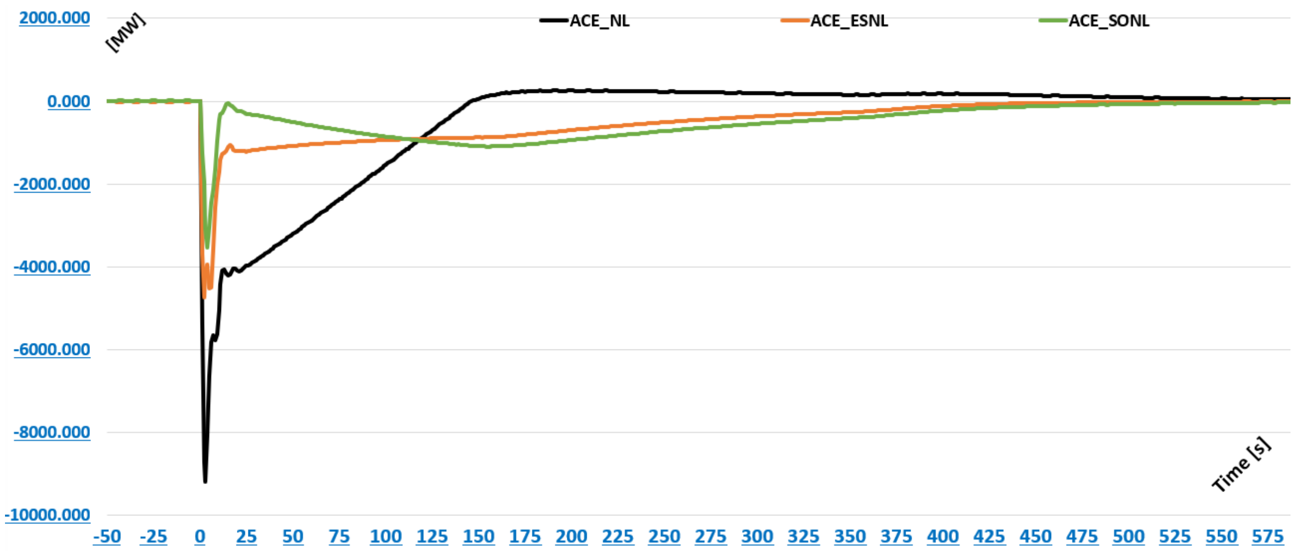

Figure 4-11: Areas Control Error Signal with a 3000MW Generation Loss in Each Area

As mentioned above, the negative Line-To-Area power flow error of area NL (highlighted by the red dotted curve in figure 4-10) means the Dutch power system imports about 4000MW from the other areas (ESNL and SONL) following the 3000MW event. The need for this amount of power is due to the lack of power (spinning) reserves on the secondary control in area NL and the limited synchronous generating capacity of this area compared with the capacity of the other control areas. In other words, the secondary control of the Dutch system is not able to control the ACE signal, which in turn, requires additional power from the other areas to cover this signal. The amount of power import from the synchronous control areas depends mainly on the final frequency offset value, the load-damping constant, the sensitivity of load to frequency, the amount of generation lost, and the value of power-frequency characteristic.

The ACE signals indicated in figure 4-11 are further applied to the PI-Regulating-Algorithm, which obtains the desired behaviour of the AGC over time. This logic eliminates the error signal in order to return the frequency to the nominal values and keep the power interchange between control areas at the scheduled values. This process is performed in accordance with the following expression:

$$\Delta P_{CI} = -[\, X_i * ACE_i + \frac{1}{T_i}\int ACE_i \,] \quad \text{in [MW]} \tag{4.2}$$

Where:

- ΔP_{CI} = the correcting variable of the AGC in a particular control area (i)
- X_i = the proportional factor of the AGC in area (i)
- T_i = integration time constant of the AGC in area (i)
- ACE_i = the area control error signal in area (i)

The outcomes of this expression are the AGC setpoints of dispatchable plants provide the required power to compensate the power lost due to the created event. It is worth of noting that the AGC setpoints of the control areas will be maintained around the value 3000MW after 7.83min from the incident instant due to the absence of supplementary power reserves within the developed scheme of the AGC. In other words, the need of power at the incident instant (t0) will be compensated by the power from the next instant (t1), resulting in a decrease in power production at (t1), which in turn, would require compensation from the following generation instant (t2). This process will continue until the end of the simulated day.

The following figures show the AGC setpoints and the lines flow errors. The transients in power flows are acceptable as they do not exceed the capacity (maximum power) given in table 3-7.

Figure 4-12: AGC Setpoints

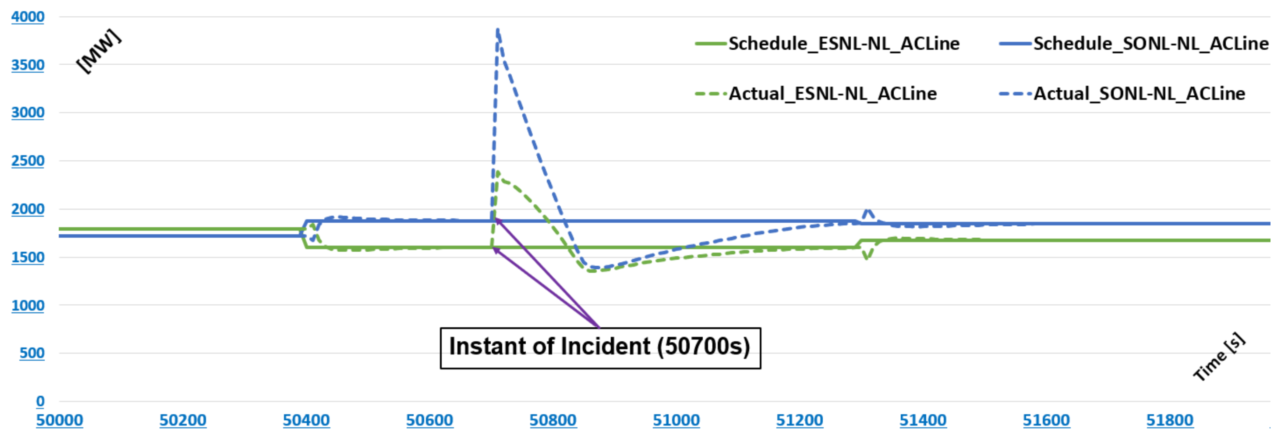

Figure 4-13: Line Flows both Actual and Scheduled Flow

Figure 4-14 below depicts the total power setpoints of control area NL in which the produced AGC setpoints are added up to the scheduled time-series power setpoints, while figure 4-15 shows the actual total generation, load, and AC/DC import of area NL.

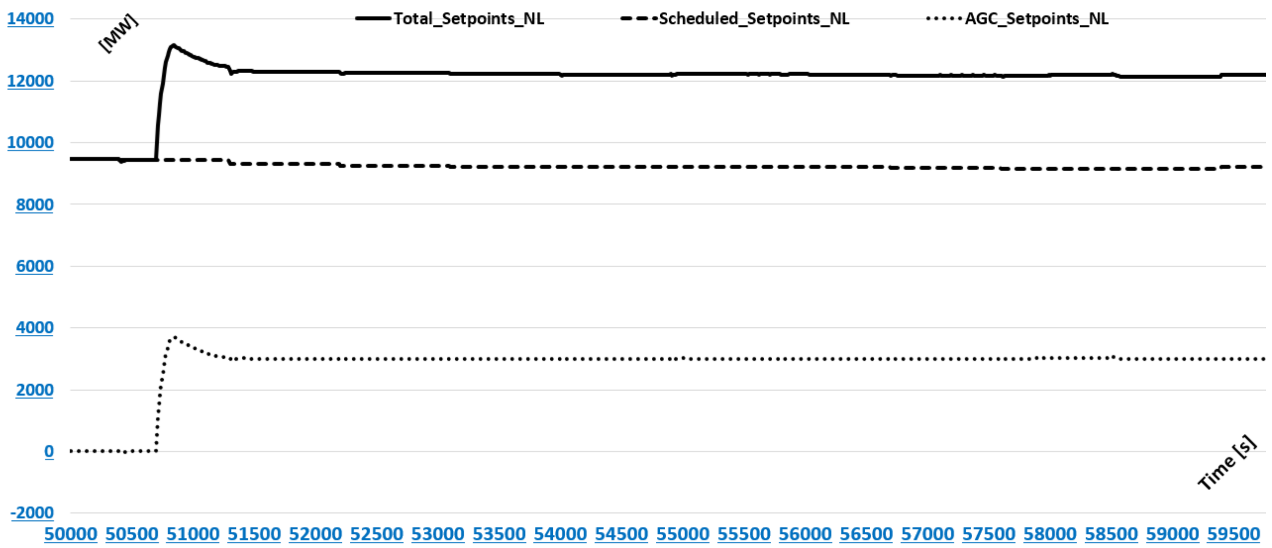

Figure 4-14: Total Setpoints of Area NL

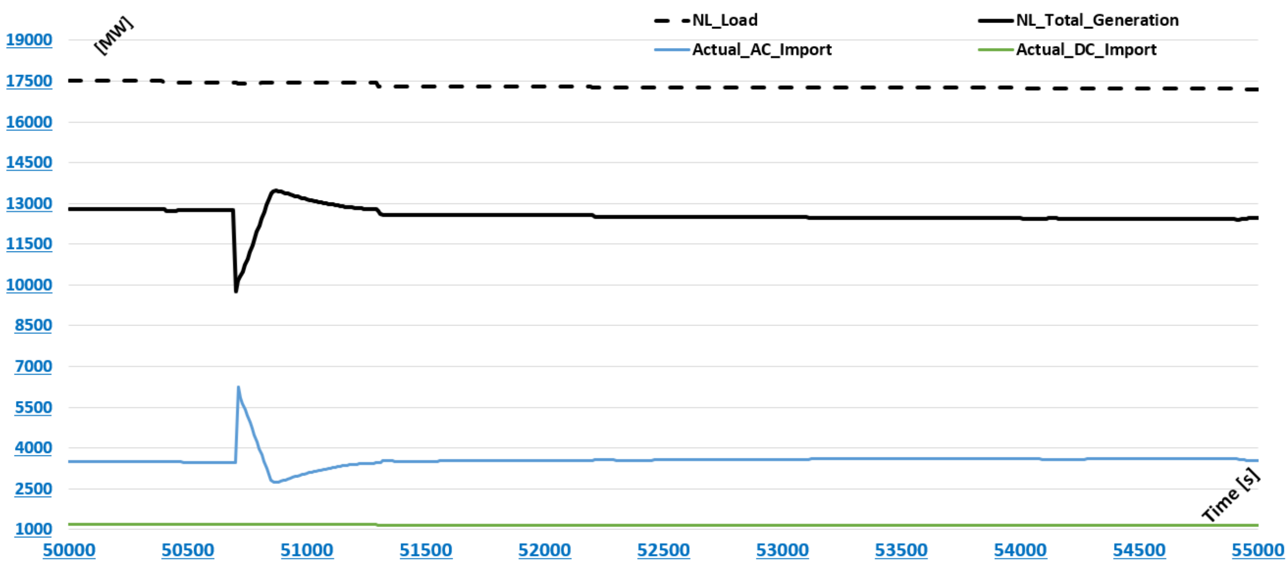

Figure 4-15: Actual Load, Generation, AC/DC Import within Area NL

In short, the developed AGC scheme cannot be considered as a real implementation of the secondary control in a particular power system as there is no power reverse provided within the AGC block and the selected parameters are not correlated to those of TSO's. However, this scheme would be suitable for the simulation purposes of this thesis due to its ability to estimate the time required to reach the 50Hz value after subjecting the Dutch power system to a disturbance. Such an estimation is useful for the frequency stability studies as it can indicate whether the increase of renewable power generation would affect the time required by AGC to achieve the nominal frequency value or not. Furthermore, the choice of the AGC settings, i.e. PI gains, Bias factors, and filter coefficient, has fulfilled the goal of eliminating the frequency offset error and bringing the frequency to value 50hz after 7.8minutes from the incident instant. Also, the actual power cross-border exchange has been maintained at the scheduled values as illustrated in the figures above.

Below flows a brief summarization of the work done throughout this section:

- **a.** Use the Kermit-Simulink model shown in chapter (3)

- **b.** Apply the created Dutch power approach as part of the synchronous grid to Simulink model. This approach represents the Dutch system as a primary area connected synchronously to two areas (ESNL and SONL) through AC cross-borders and non-synchronously to two areas (the UK and NO) through DC transmission links.

- **c.** Export the collected time-series data in Excel to MATLAB. This data contains the following essential factors that form the basis for the pre-scenario simulations:

Table 4-6: Basis Data settings for Pre-Scenario Simulations

Essential Data for Per-Scenario	NL	ESNL	SONL
Conventional Generation Share [%]	74	67	57
Renewable Generation Share [%]	26	33	43
Inertia Constant [s]	4.05	4.06	4.37
Maximum dispatchable active power generation on 18/01/2017 with 3000MW reserves [GW]	12.3	108	142

- **d.** Adjust the settings of the generic power plant model to get the best performance of the primary control action suited for the simulations of frequency stability studies. The main parameters that should be adjusted are the load damping constant, the load self-regulating effect, the frequency deadband response, the regulation droop, and the governor time constant.

- **e.** Check the operation of the developed AGC block and the selected settings, which are required to attain the secondary control targets. These settings are the bias factors, the proportional gain, the integral gain, and the filter coefficient.

- **f.** Assume, initially, that there is no imbalance between the load and generation within each of the control areas. For example, the collected data for area NL has shown that the load is higher than the generation during the simulated day (17-01-2017). This issue has been eliminated by increasing the power import from other areas (ESNL and SONL) in such a manner that the amount of both the generation and power import will be equal to the amount of load.

- **g.** Apply a step-fault to the total generation of the synchronous areas. The magnitude of this fault is equal to 3000MW similar to the design hypothesis of ENTSO-e as shown in figure 4-3. The main intention of applying such a disturbance is to check the frequency performance of the Dutch system.

  It is worth to be noted that the possibility of applying a sudden loss to only one area of the three synchronous areas is quite hard as the data transferred from MATLAB to Kermit-Simulink is in a matrix form. Such a form makes it challenging to create, for example, a specific disturbance in area NL. However, applying a 3000MW power imbalance event in each control area can provide the possibility of analysing the frequency performance with different shares of conventional and renewable power generation.

h. Run the Kermit-Simulink model and check the overall operation. The main interest falls within the simulation results of the generation and load data, the frequency primary and secondary responses, the overall frequency behaviour, the power imbalance, the AGC and total setpoints, and the actual import/export of the AC/DC transmission lines.

i. Store the simulation results of date (17 January 2017) in MATLAB using the Sink Store Block that incrementally writes the data into a variable in the specified MAT-File.

j. Export the data stored in MATLAB to Excel. This process requires more than one step:

- Load the data from the specified MAT-File
- Use the function Transpose of in MATLAB to convert the number of columns to rows. This step is required as the simulation outcomes of one day (86400s) result in a number of columns equals the number of seconds. However, Excel worksheet limits the total number of columns to 16384, which is much smaller than simulated time-series data. For this purpose, Transpose function allows to export the data to Excel in rows form instead of columns as the total limits of rows on an Excel worksheet is 1058576.
- Use the MATLAB function *'xlswrite(excelfilename.xlsx, mat-file-name, number of worksheet)'* to export the data to a specified worksheet in Excel.

k. Used the data exported to Excel in order to analyse the frequency performance of the overall interconnected system with a focus on the Dutch system using different indicators. Such indicators can be considered as high-level metrics that provide the ability to examine the impact of any change occurred within a particular power system, i.e. a sudden generation loss or an increase in renewable share, on the frequency performance of that system. The block diagram below shows the indicators used in this thesis:

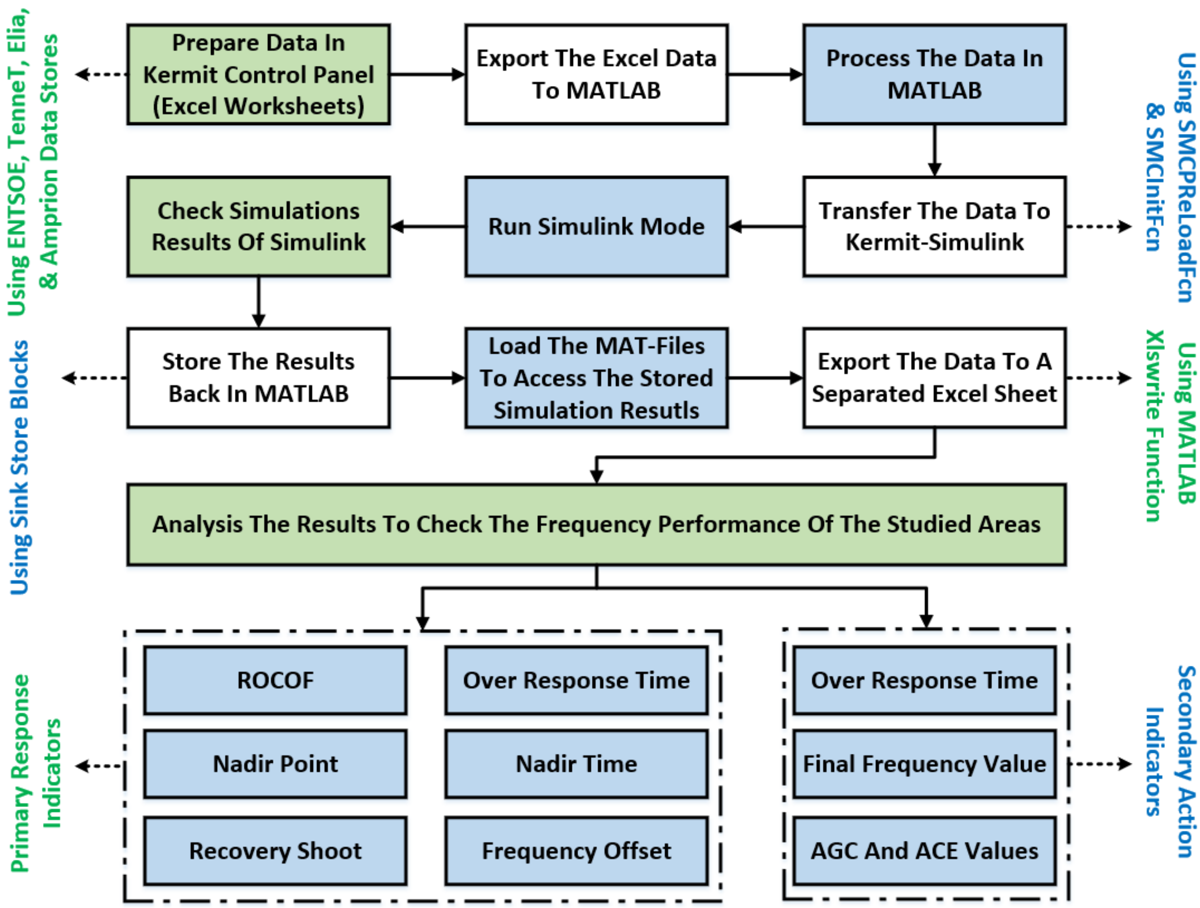

Figure 4-16: Process to Analyse the Simulation Results Using High-Level Metrics

Finally, in order to check the accuracy and reliability of the frequency control settings used in the case of 3000MW loss, a short sensitive analysis has been performed as shown in figure 4-17. In this analysis, case (B2) in figure 4-3 was considered by applying a 1300MW sudden generation loss in each control area. The outcomes of this analysis are given in table 4-7 below. It can be assumed that the studied model and the overall (selected) settings can be used for the simulations of the **main-scenario** as the results of ROCOF and Nadir Points lay within the limits of acceptable operating ranges defined by ENTSO-e.

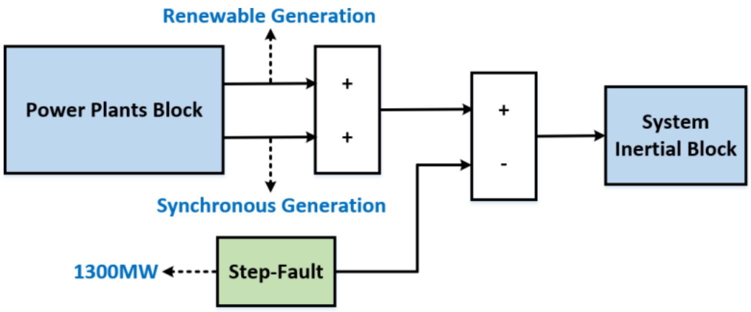

Figure 4-17: A Design of a 1300MW Sudden Generation Loss for a Short Sensitive Analysis

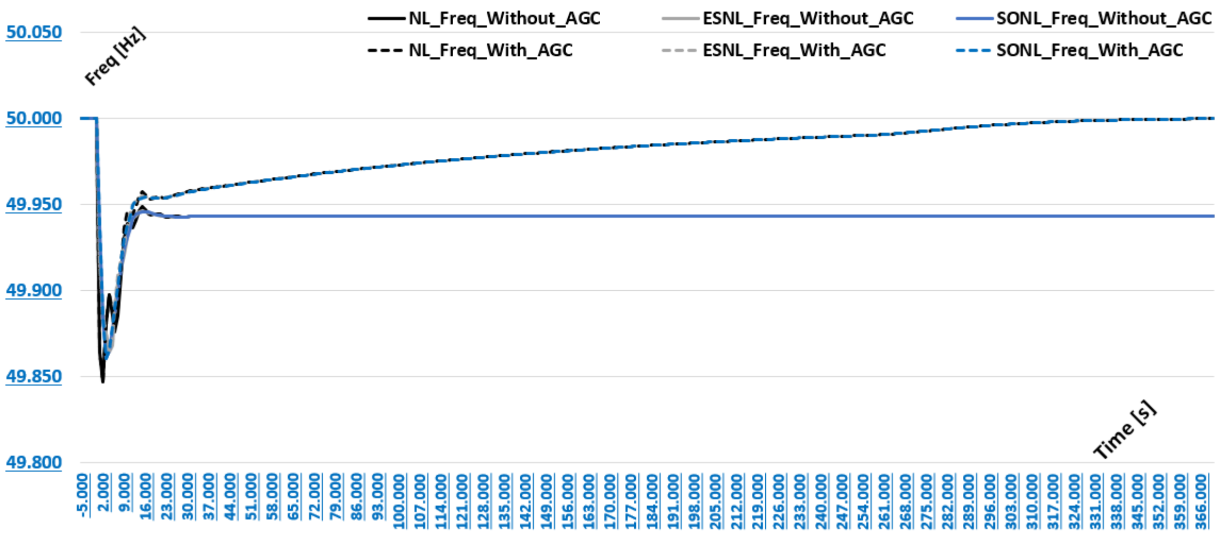

Figure 4-18: Frequency Performance following a 1300MW Sudden Loss

Table 4-7: Overall Frequency Response due to the 1300MW Generation Loss

Frequency Response Performance	**NL**	**ESNL**	**SONL**
Overall Primary Response Time [s]	22	22	22
Nadir Instant [s]	2	4	3
Nadir Value [Hz]	49.847	49.64	49.860
RoCoF [mHz/s]	136	85	63
Frequency Offset Value [mHz]	57	57	57
Recovery Overshoot[mHz]	50	92	84
Delay [s]	2	12	16
ACE Error	-1950	-895	-320
AGC setpoints [MW]	1300	1300	1300
Overall Secondary Response Time with AGC to reach the value 50Hz [min]	6	6	6

4.2. Main-Scenario

The primary purpose of this scenario is to assess the frequency performance of the Dutch power system as part of Continental Europe with respect to the high penetration of renewables in the total electricity production as forecasted in the Energy Transition Outlook (ETO) of both DNVGL and ENTOS-e.

In DNVGL ETO-model, it has been pointed out that the main aim of European countries, including the Netherlands, is to shift towards an electricity production dominated by renewable energy sources to be (nearly 70%) by mid-century. Due to this energy transition, it is expected that the capacities of both the renewables and non-renewables in Europe Continental will subject to radical changes by the end of the DNVGL ETO forecasting period (2050) as shown in figure 4-19 below:

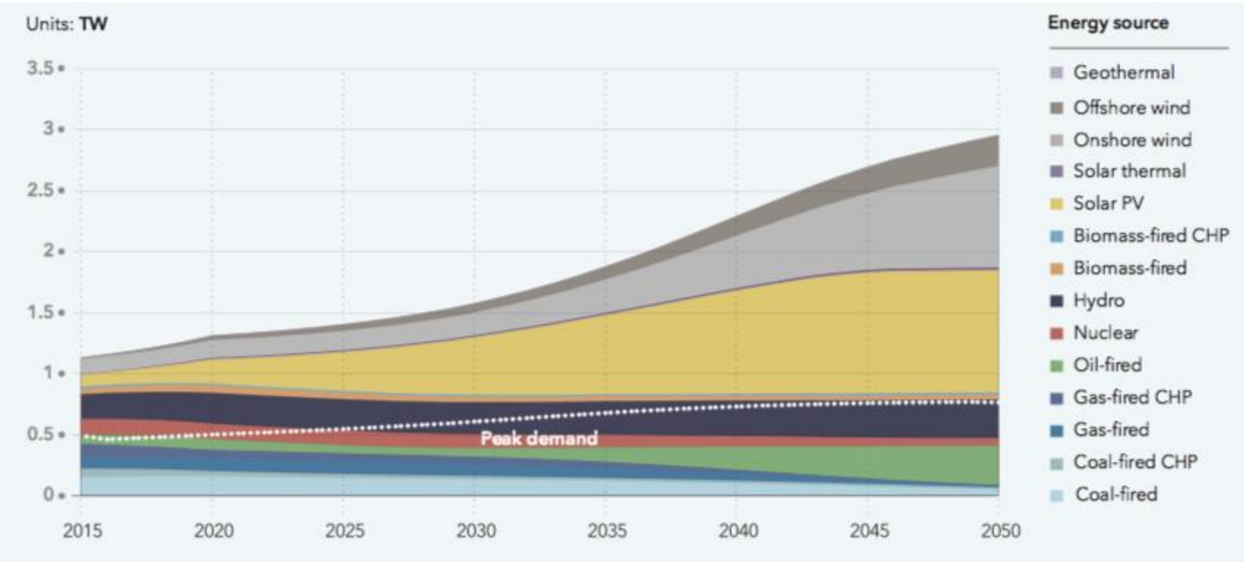

Figure 4-19: Electricity Capacity of Europe Continental as Forecasted in ETO-model [3]

It is worth mentioning that the increase and decrease in both the renewable and non-renewable capacities, respectively, are not linear as shown in figure 4-19 above. However, for simplicity, it has been decided to use a linear shift in the annual growth of both the production and demand. The outcomes of this assumption for Continental Europe are given in the table below:

Table 4-8: Shifts in Production and Load Based on the Outcomes of DNVGL ETO-Model for CE

Type of Change	In 2015	In 2050 Estimated by ETO	Annual Change
Load (peak demand)	0.50 TW	0.75 TW	1.43 % ↑
Total Capacity	1.16 TW	2.96 TW	4.43 % ↑
Renewable Capacity	0.35 TW	2.21 TW	2.40 % ↑
Non-Renewable Capacity	0.81 TW	0.75 TW	0.21 % ↓
Renewable Share in total capacity	30 %	75 %	1.29 % ↑
Non-Renewable Share in total Capacity	70 %	25 %	1.29 % ↓

Actually, these outcomes are intended to cover the whole region of Continental Europe, and it is not meant to represent the change of the generation and load profiles of a specific node within this region. Consequently, they are only useful for the frequency performance studies of ESNL and SONL control areas due to the aggregating properties of these areas. Such a feature gives the possibility of covering the generation and load profiles of twelve nodes (countries).

Furthermore, the main interesting factors for the simulations of main-scenario are highlighted with bold black colour in table 4-8 and explained below as follows:

- **Load (peak demand) annual change:** this factor is crucial for simulation purposes as it indicates the yearly increase of control areas' load starting from 2017 (=year of the simulated day in pre-scenario) towards the year 2050 (=end year of the ETO forecasting period).

- **Renewable and Non-renewable share in total capacity:** these two factors play an essential role in the assessment of frequency performance as both help to adjust the annual power production within each dispatchable and non-dispatchable plant to match the yearly change in system load.

It is worth mentioning that the analysis performed throughout this scenario assumes **the most conservative case** of load increase within each of the studied control areas. Thus, the outcomes indicated in table 4-8 will be applied to both ESNL and SONL areas, irrespective of the number of nodes that they represent.

Figure 4-20 below depicts the results of applying these factors to the actual generation and load profiles of both ESNL and SONL control areas. It is worth to be noted that the annual change in both renewable and non-renewable production should be optimised in order to meet the yearly demand change. Such optimisation has also been done in the figure below:

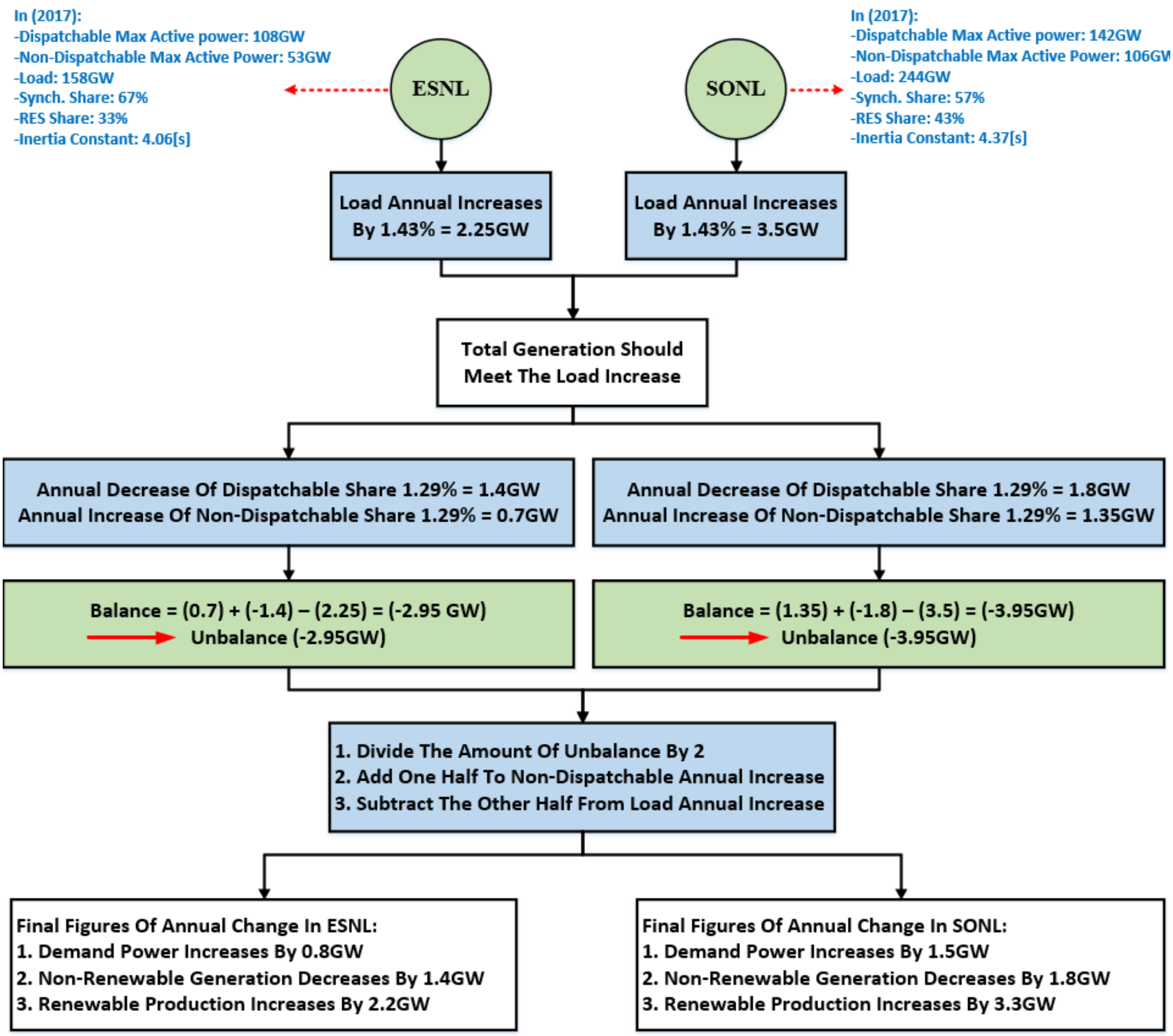

Figure 4-20: Annual Change in Both the Production and Demand Profiles for Areas ESNL and SONL

However, the results obtained in the figure above are not sufficient to perform the desired simulations of the main-scenario due to the inability of ETO to give an estimation of both the annual production and demand shifts for the Dutch system. Such shifts are essential as the main topic of this thesis is to assess the frequency performance of the Dutch system as part of the synchronous grid of CE.

For this reason, another reliable energy transition outlook provided by ENTSO-e in [41] has been used in order to predict the essential changes foreseen to occur within the Dutch grid. In this outlook, ENTSO-e aims to estimate the minimum and maximum values of load and generation changes of countries lay under ENTSO-e operating region. Actually, these extreme values have been obtained after examining three scenarios, which are listed below as follows:

- **Conservative Scenario:** indicates the required additional investments in power production that are needed to meet the extension of electricity demand in the future.
- **Best Estimate Scenario:** estimates the potential future developments expected to be performed within the European grid based on an essential requirement that the market signals should be optimistic to perform further investments
- **EU2020 Scenario:** gives an indication of future developments with a requirement that the targets of EU countries of expanding the renewable generating capacity in 2020 must be confirmed.

As the focus of this thesis lays on the analysis of the impacts of a massive renewable deployment on the Dutch system, the outcomes of EU2020 scenario will be considered in the simulations as it indicates an optimistic case for the expanding of renewable generating capacity in the Netherlands.

Based on the assessment of winter (January) and summer (July) demand peaks and the amount of power consumption as forecasted by the Dutch TSO (TenneT), this scenario gives an estimation of 0.9% annual growth of system load. Moreover, the outcomes of the EU2020 scenario depicted in figure 4-21 below show that the increase of renewable production capacity for the Dutch system in the total mix generation would be nearly 29% in 2020.

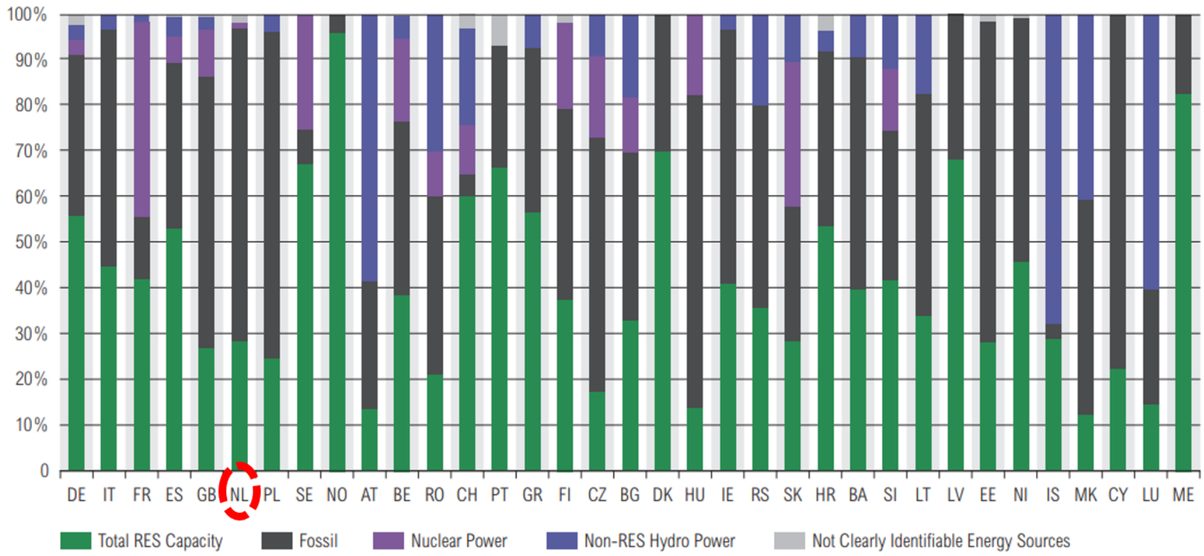

Figure 4-21: Scenario EU2020: Total Production Capacity per Country in January 2020 [41]

Furthermore, the EU2020 scenario anticipates that the Net Generating Capacity (NGC) in the Netherlands would be approximately 44.2GW due to the massive extension of both the onshore and offshore wind capacities. However, different factors, i.e. maintenance and outages, would cause a considerable amount of unavailable capacity. For this reason, the Reliable Available Capacity (RAC) is obtained in a very conservative manner by considering a 10GW unavailable capacity; resulting in an amount of RAC nearly 34.2GW in 2020.

Table 4-9 below summarizes the outcomes of the energy transition outlook of ENTSO-e that are foreseen to occur within the Dutch system in the year 2020. This year is further being considered as a bridge between the period (2017-2050) to estimate the annual change in both the production and demand, which will be used during the simulations of the main-scenario:

Table 4-9: Changes in Production and Load Based on the Outcomes of ENTSO-e Outlook for the NL

Type of Change	In 2017	In 2020	In 2050 (Estimation)	Annual Change
Load (peak demand)	20 GW	20.5 GW	26 GW	0.90 % ↑
Reliable Available Capacity	32 GW	34.2 GW	62.2 GW	2.85 % ↑
Renewable Capacity	8.45 GW	10 GW	36.9 GW	10.2 % ↑
Non-Renewable Capacity	23.55 GW	24.2 GW	25.3 GW	0.14 % ↑
Renewable Share in total capacity	26 %	29 %	59 %	1.00 % ↑
Non-Renewable Share in total Capacity	74 %	71 %	41 %	1.00 % ↓

Similar to the control areas (ESNL and SONL), figure 4-22 below shows the annual change in both the production and demand profiles of the control area NL based on the impacting factors mentioned earlier in this section.

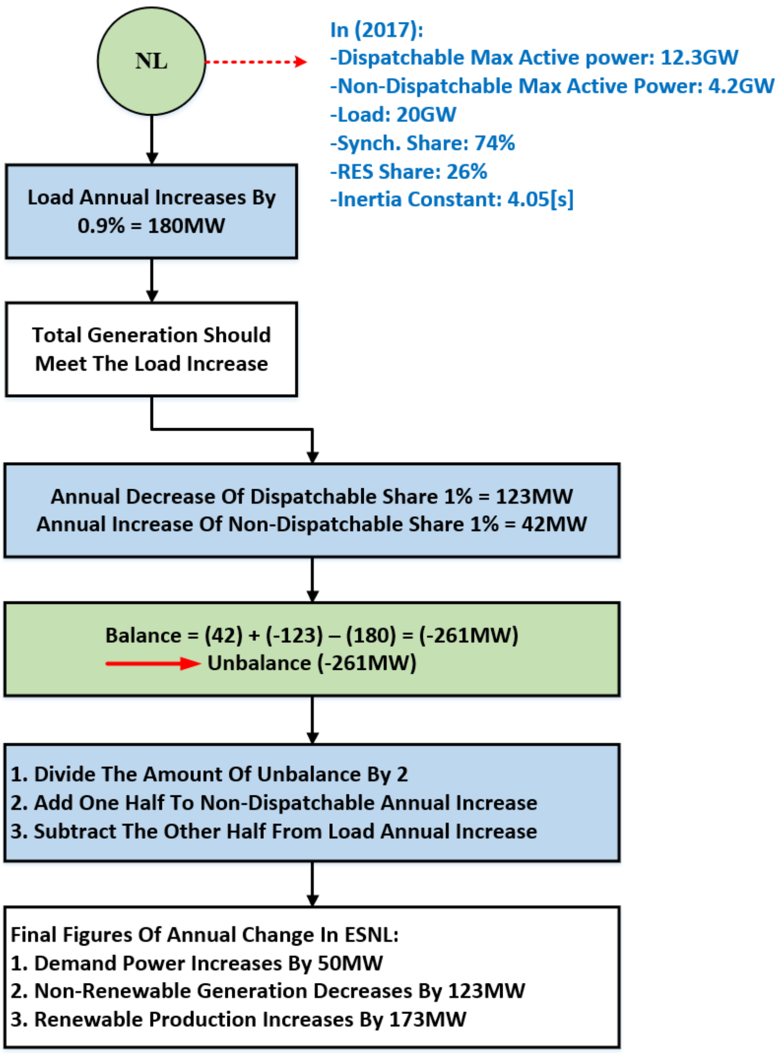

Figure 4-22: Annual Change in Both the Generation and Load Profiles of Control Area NL

The previous analysis results in different figures of the change foreseen to occur in the power production and demand for Continental Europe. Figures 4-20 and 4-22 assume that the share of dispatchable active power in the total production for a specific day (in this case the 18th of January) of each year (2017-2050) annually would become lower, followed by an annual increase of non-dispatchable active power. The annual decrease in synchronous generation per 18th of January of each year is approximately 1.26% and 1% for areas (ESNL & SONL) and (NL), respectively. This decrease points out that the level of system inertia annually would be lower due to the direct relation between dispatchable active power produced by synchronous generators and inertia.

The following figures depict the curves of the assumed shifts in both the production and demand of all control areas that are analysed in this thesis:

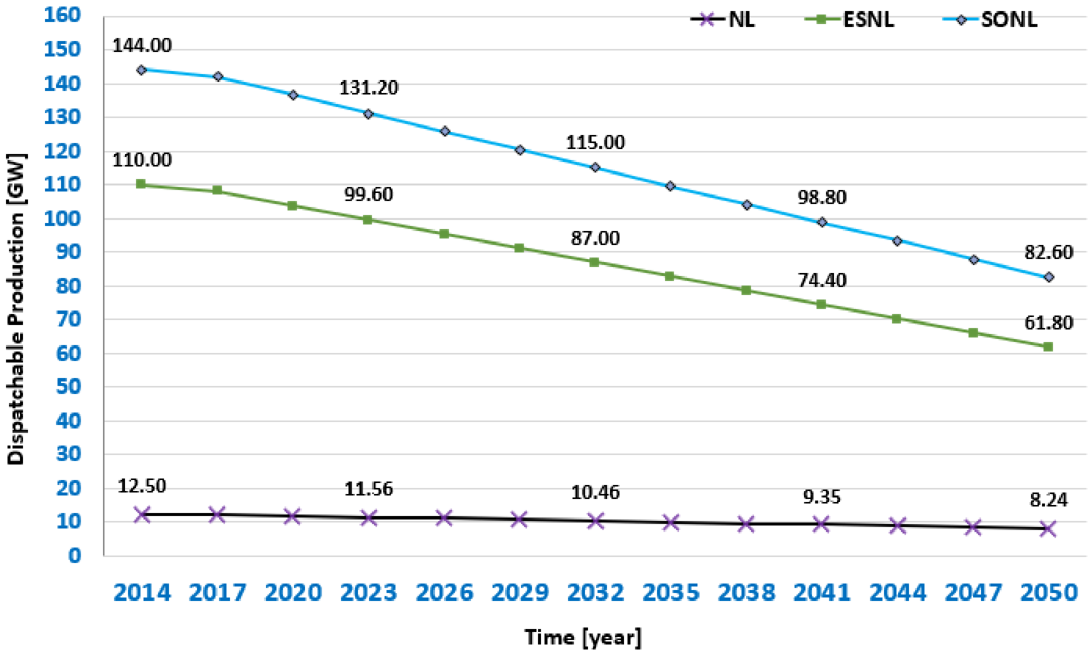

Figure 4-23: Dispatchable Active Power Share in the Total Power Production

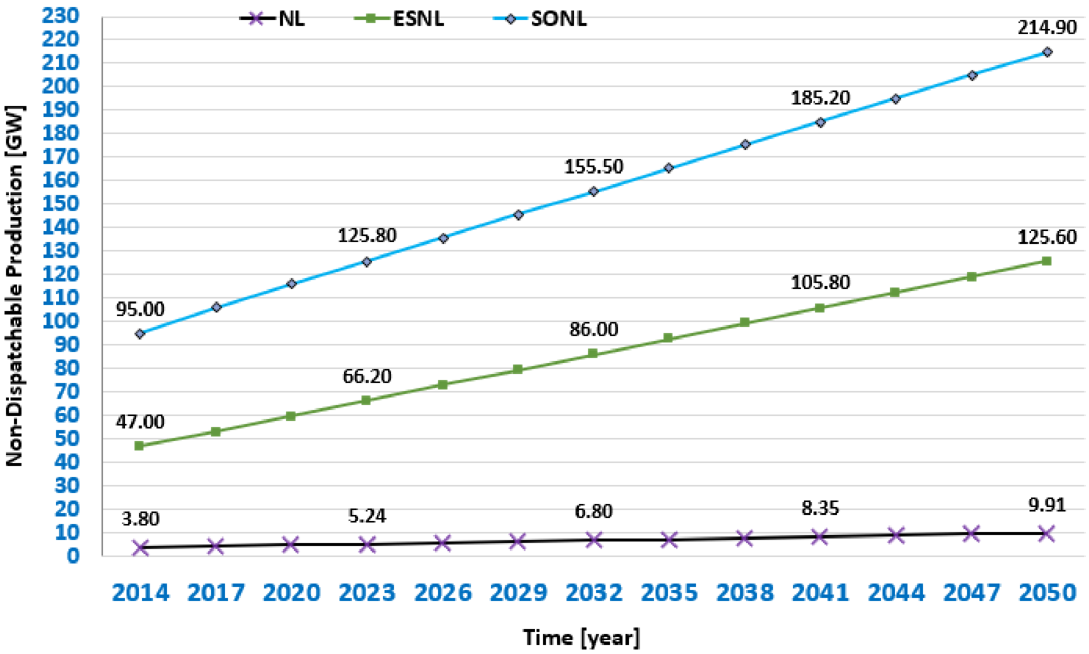

Figure 4-24: Non-Dispatchable Active Power Share in the Total Power Production

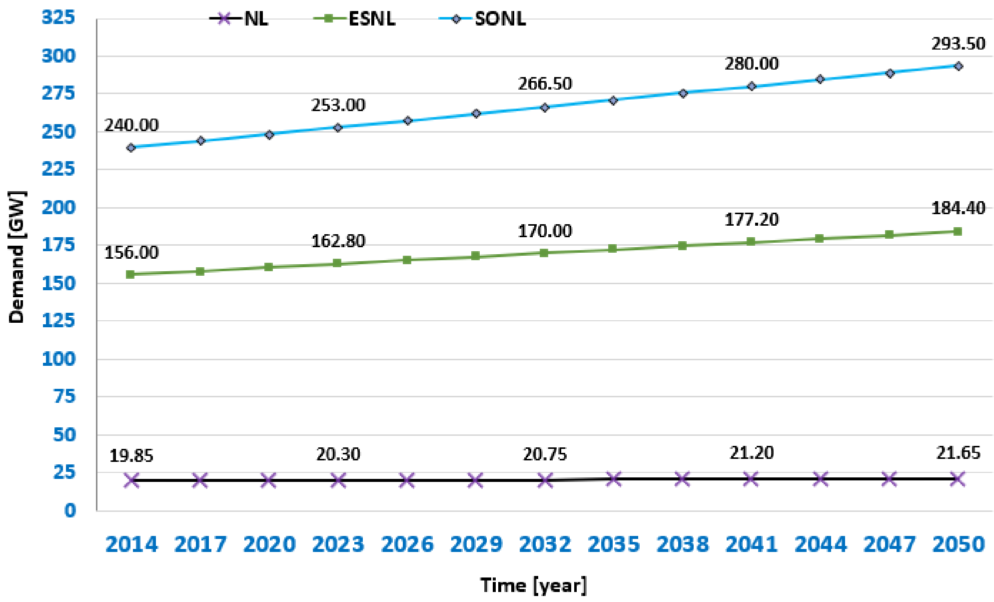

Figure 4-25: Demand Change over the Course of 33 years

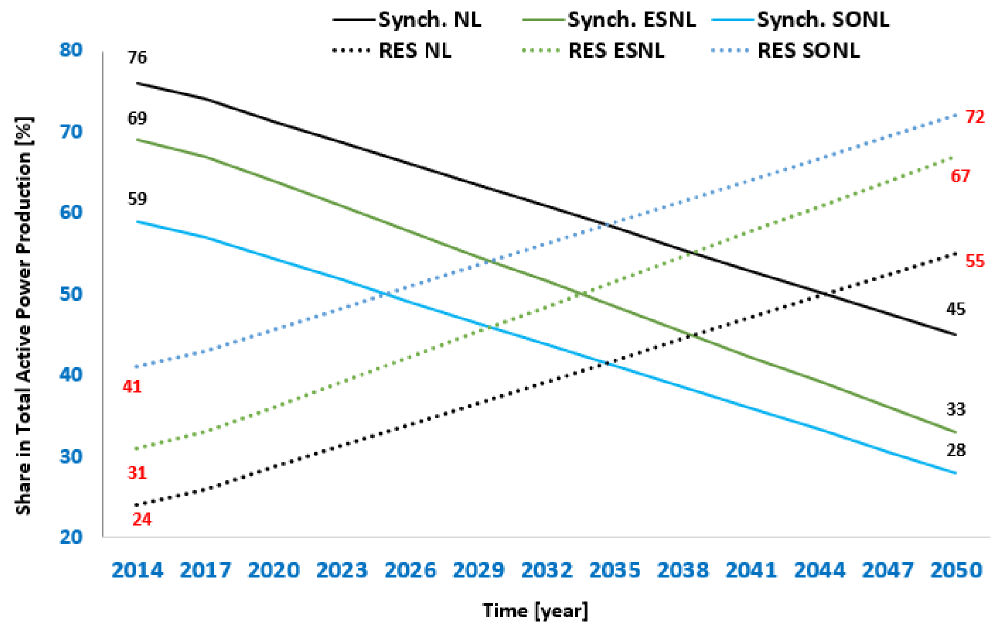

Figure 4-26: Percentage of Both the (Non-)Renewables Share in the Total Power Production

As it can be seen from the figures above 4-23 to 4-26, the shifts in both the active power production and the load are not similar to those values given in tables 4-8 and 4-9. This difference can be clarified using the values obtained in figures 4-20 and 4-22. For instance, the Energy transition Outlook of ENTSO-e presumed that the demand in the Netherlands would yearly increase by **0.9%** as outlined in table 4-9. However, this growth will cause a lack of power (=unbalance) between the total generation and load during the simulated days. Roughly speaks, the demand per every moment during the whole day should meet the total power production in order to avoid any power unbalance. For this purpose, an optimization process (=match the annual increase in production to the yearly demand growth) is required to prepare day-ahead time-series data for the simulated days without an initial power unbalance between the generation and load sides. As shown in figures 4-20 and 4-22, the results of such an optimization process assume that annual growth in the demand of the Dutch system turns out to be **0.25%** instead of 0.9% in order to meet the yearly shifts in the total production of both the renewables and non-renewables.

Due to the diversity in the shifts of future electricity production and demand, two cases have been developed that together form the basis of the simulation of the main-scenario. These cases give a suitable pathway to assess the changes expected to happen in the frequency performance of the Dutch system under different circumstances:

A. PRIMARY CASE:

In this case, the frequency performance of the Dutch system will be analysed for the period between (2017-2050) using the findings obtained earlier in this section. First of all, the system load of the 18th of January 2017 will be yearly increased in each of the control areas using the relevant annual (demand) change:

- NL day-ahead power consumption (demand) will be annually increased by an amount of 50MW as obtained in figure **4-22**.
- ESNL and SONL day-ahead demands will gain an annual raise of 0.8GW and 1.5GW, respectively, as predicted in figure **4-20**.

Next, the day-ahead power generation of both the dispatchable and non-dispatchable plants will be shifted in accordance with the relevant findings:

- NL day-ahead power generation of the dispatchable plant will be yearly decreased by 123MW as indicated in figure **4-22**, while the day-ahead power production of the non-dispatchable plant will be increased annually by 173GW as shown in the same figure.
- ESNL day-ahead dispatchable power production will have an annual decrease equal to 1.4GW, while that of the non-dispatchable plant will be increased by 2.2GW annually as shown in figure **4-20**.
- SONL production plants will have other power generation shifts than the ESNL. For the dispatchable plant, the day-ahead power production will be decreased annually by an amount equal to 1.8GW, while that of the non-dispatchable plant will have an annual raise equal to 3.3GW as indicated in figure **4-20**.

Although that both the production and demand profiles are shifted within the entitled studied period, the power import and export through the cross-border will be kept constant at those values of the 18th of January 2017 as the change in the production side is matched to the shift in the demand side. In other words, there will not be an unbalance between the generation and load that requires an additional import or export from the other areas to modify this unbalance. Alongside, the settings of both the primary and secondary controls will not be changed as the focus of this thesis is to assess the frequency stability with the current settings.

Finally, it has been earlier assumed in chapter (**3**) that the estimated inertia constants as a function of the synchronous Net Generation Capacity will be used in simulations as time-series data for the generic model of the dispatchable power plants to define the amount of inertia for each of the studied areas as required by Kermit model. Moreover, an assumption has been made (for simulation purposes of the main-scenario) that this inertia should be annually reduced since the dispatchable active power production is yearly decreased as shown of figures **4-20** and **4-22**. This assumption results in the following figures of system inertia:

- The estimated inertia in 2017 for the area NL inertia was 4.05s. As described above, this value has been used for the simulations of the 18th of January 2017 with dispatchable active power share in the total production equal to 74%. However, this share of dispatchable plants would be annually decreased by 0.88% as indicated in figure **4-26** to be around 45% in 2050. Following this outcome, it is possible to assume that the inertia of area NL will also be subjected to a yearly decrease equal to (~0.9%).
- Following the same method used above for the inertia of area NL and using the findings depicted in figures **4-26**, this will lead to a 1% and 0.9% annual decrease in inertia for areas ESNL and SONL, respectively.

Figure 4-27 below illustrates the change anticipated to occur in system inertia of the studied synchronous areas using the findings discussed earlier in this section:

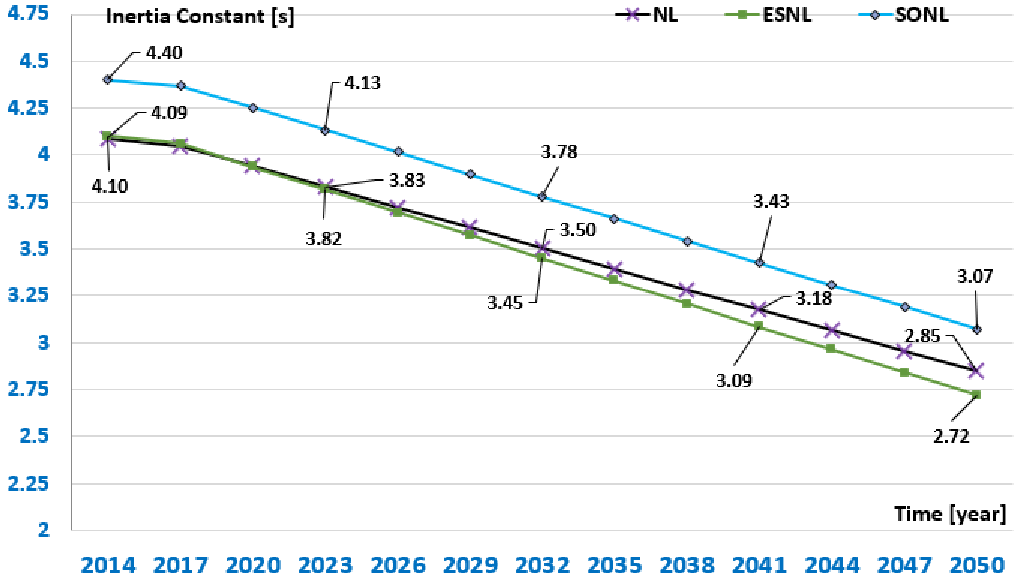

Figure 4-27: Change in Area's Inertia for the Simulations Purposes of Main-Scenario-Primary-Case

Figure 4-28 below indicates the method used to perform the simulations of the primary-case:

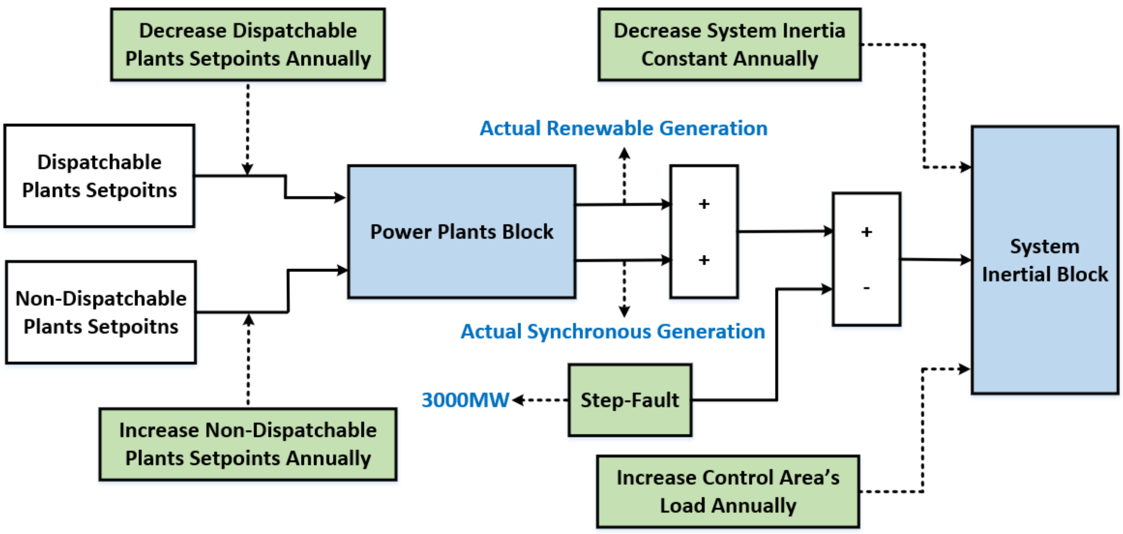

Figure 4-28: Method to Perform the Simulations of Primary Case (Main-Scenario)

B. SECONDARY CASE:

In this case, the same method described in the primary case will be used. The only difference that will be considered in the secondary case is that the initial values of the areas' inertia prior to the annual decrease obtained throughout the description of the primary case. In other words, the values of inertia estimated in chapter (3) for the year 2017 based on the synchronous Net Generation Capacity (NGC) data published by ENTOS-e in [14] will be changed.

Before listing a new assumption for the initial values of area's inertia, let's discuss some basic theory regarding both the kinetic energy and active power. It is well-known that the kinetic energy is the amount of work needed to move an object, and active power is the rate of delivering this work over time. Typically, the kinetic energy of a particular synchronous generator is expressed in terms of angular velocity and moment of inertia. From this relationship, it is possible to relate the inertia as a specific quantity in the system to the amount of active power in that system.

This basic theory points out that the estimated figures of areas' inertia in chapter (3) using the NGC values are much higher than the inertia needed at the instant of the 3000MW incident (step-fault) as the amount of active power at the same time instant is much lower than the NGC values. Such a difference between the NGC values and the actual dispatchable active power in each area gives the possibility of forming the following (conservative) assumption:

- **NL:** the estimation of area's inertia using a 23.55GW synchronous NGC has delivered a value equal to 4.05s. However, the amount of dispatchable active power at the incident time instant was nearly 9.5GW. This difference means that the required inertia constant at the incident time constant is much lower than the estimated value. The ratio of 9.5GW to 23.55GW is (~0.4), which results in an inertia constant equal to **1.62s** for the year 2017.

- **ESNL:** the estimation of area's inertia using a 238GW synchronous NGC has delivered a value equal to 4.06s. However, the amount of dispatchable active power at the incident time instant was nearly 99GW. This difference means that the required inertia constant at the incident time constant is much lower than the estimated value. The ratio of 99GW to 238GW is (~0.42), which results in an inertia constant equal to **1.71s** for the year 2017.

- **SONL:** the estimation of area's inertia using a 270GW synchronous NGC has delivered a value equal to 4.37s. However, the amount of dispatchable active power at the incident time instant was nearly 130GW. This difference means that the required inertia constant at the incident time constant is much lower than the estimated value. The ratio of 130GW to 270GW is (~0.48), which results in an inertia constant equal to **2.1s** for the year 2017.

Figure 4-29 below shows the change happing to system inertia throughout 33 years using initial inertia value obtained above, which are 1.62s, 1.71s, and 2.1s for the areas NL, ESNL, and SONL, respectively. The percentages of inertia reduction are similar to the values determined earlier in the description of primary-case (NL 0.9%, ESNL 1%, SONL 0.9%).

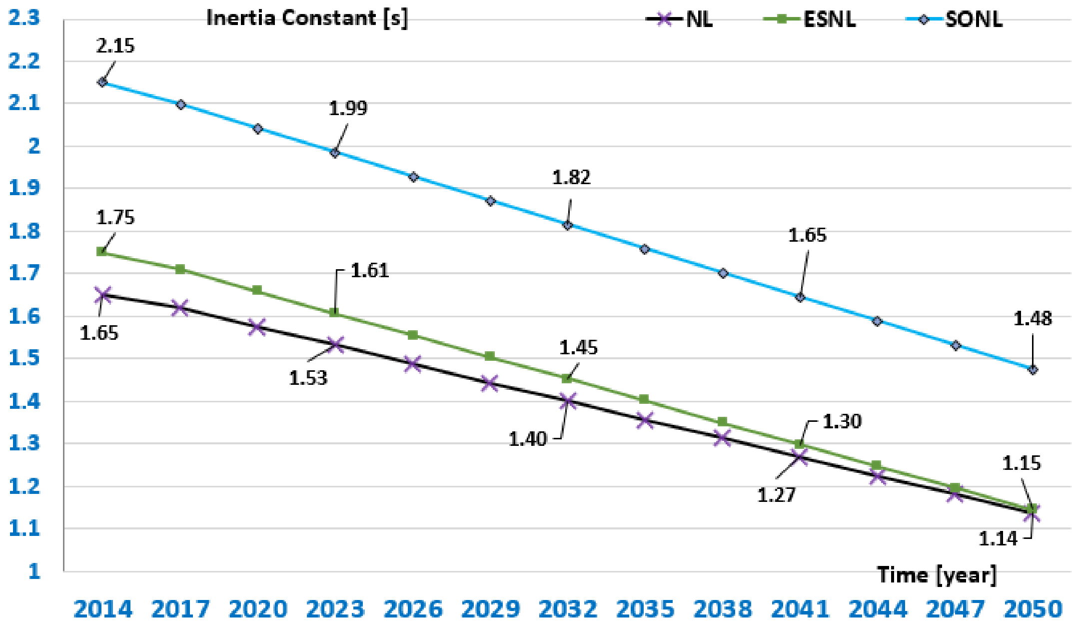

Figure 4-29: Change in Area's Inertia for the Simulations Purposes of Main-Scenario-Secondary-Case

4.2.1. Simulations Results of Primary-Case-Main-Scenario

This paragraph shows the simulation results of the primary-case based on the relevant findings, elaborated in section (4.2). The frequency of each area has been simulated following the method depicted in figure 4-28.

Moreover, five indicator graphs are used to present the outcomes of the simulation process to be able to assess the frequency performance of these areas under different circumstances. These indicator graphs are:

- Indicator (1) shown in figure 4-33: gives the changes foreseen to occur in RoCoF over 33 years. Such an indicator has a threshold value equals to (1Hz/s) due to the initial rate of change limitation following a specific disturbance as defined by the UTCE grid codes.
- Indicator (2) shown in figure 4-34: estimates the shift that would appear in the Nadir points as system inertia decreases throughout the simulated period. In according to figure 4-3, the threshold value of this indicator is (49.2Hz). This value must not be exceeded with a 3000MW power imbalance.
- Indicator (3) shown in figure 4-35: gives the maximum value of frequency deviation, which is frequency value at the instant of an event minus frequency minima (=maximum dynamic frequency deviation or Nadir Point)
- Indicator (4) shown in figure 4-36: predicts the value of frequency offset, which is the difference between the frequency nominal value minus the actual frequency value after a 30s from the time instant of an event.
- Indicator (5) shown in figure 4-37: illustrates the time instants of Nadir Points for the period between (2017-2050).

Figures 4-30 to 4-32 illustrates a couple of frequency samples as results of the simulation performed for areas (NL, ESNL, and SONL), respectively. These simulations have been performed for 30 years; starting from 2020 towards 2050 with an increment of 6 years. It can be seen from the curves depicted below that both the frequency performance of these areas changes over the years due to the shifts in both the non-renewable production and system inertia.

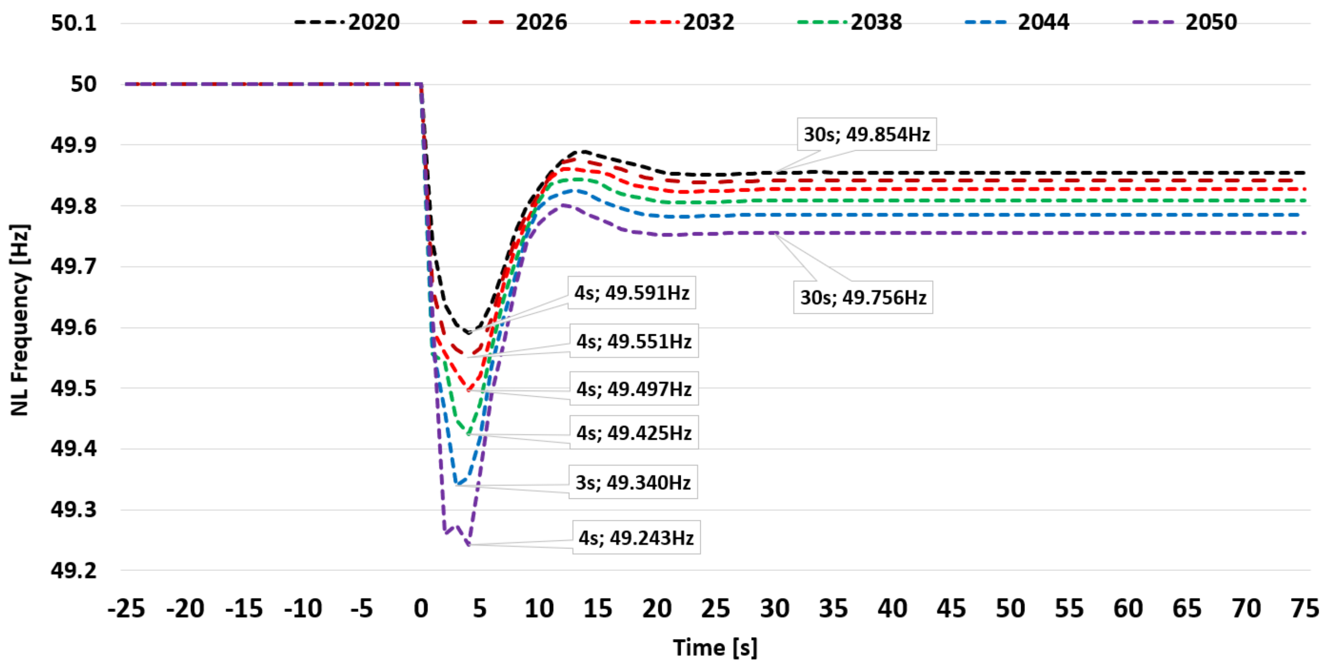

Figure 4-30: Samples of Simulated Frequency for Area NL throughout 30 Years (Main-Scenario-Primary-Case)

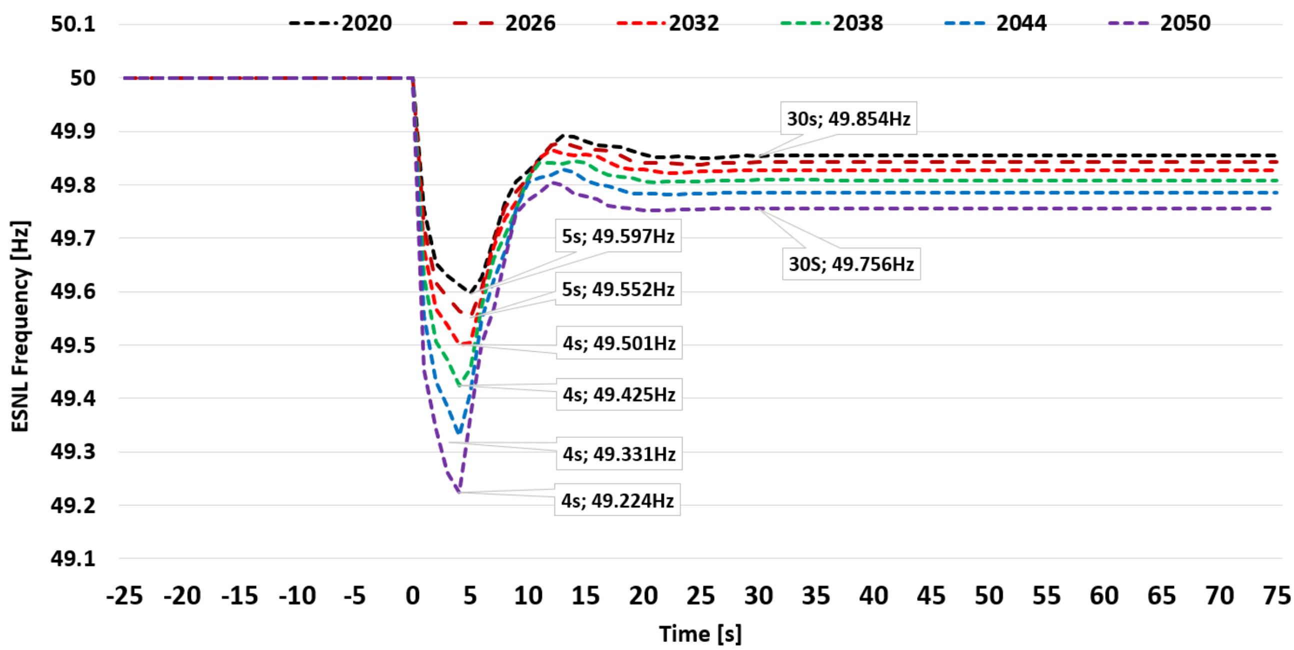

Figure 4-31: Samples of Simulated Frequency for Area ESNL throughout 30 Years (Main-Scenario-Primary-Case)

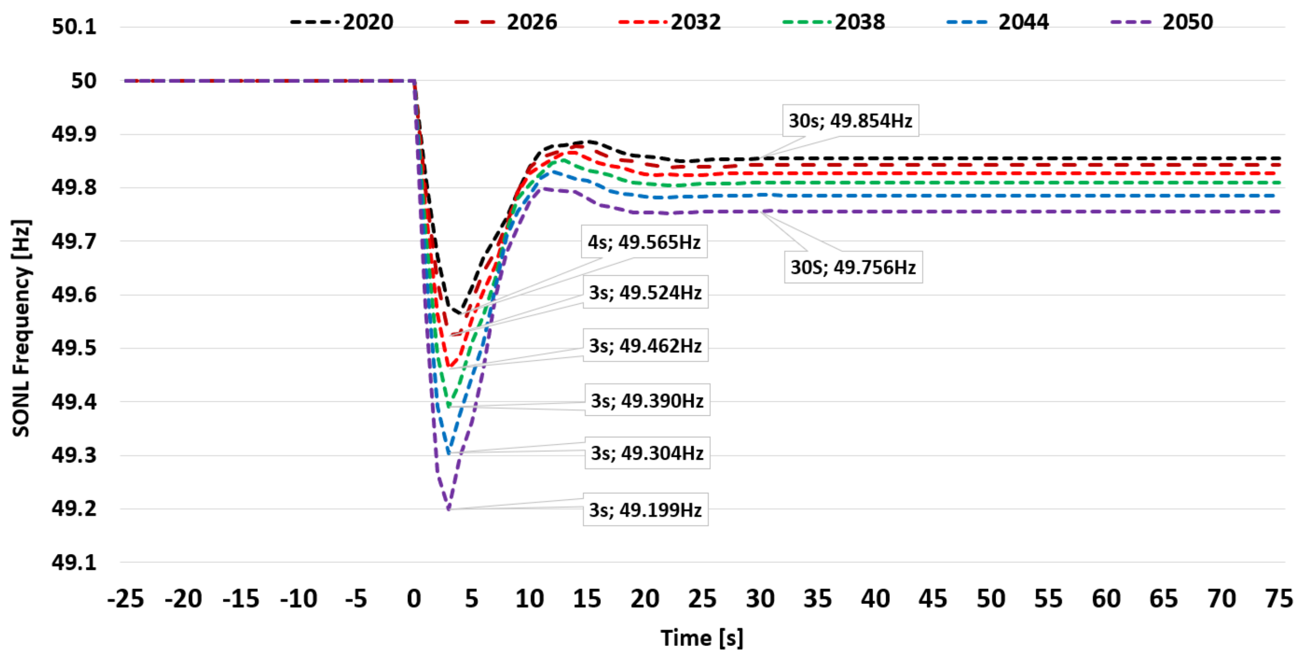

Figure 4-32: Samples of Simulated Frequency for Area SONL throughout 30 Years (Main-Scenario-Primary-Case)

Figures 4.33 and 4.34 below illustrates both the initial rate of change of frequency (RoCoF) and maximum dynamic frequency deviation (Nadir Point) for the studied areas. As it can be seen from these figures, the decrease in frequency minima over the 33 years is proportional to the reduction in system inertia and non-renewable production, while the RoCoF values get higher when inertia decreases because RoCoF is inversely related to inertia.

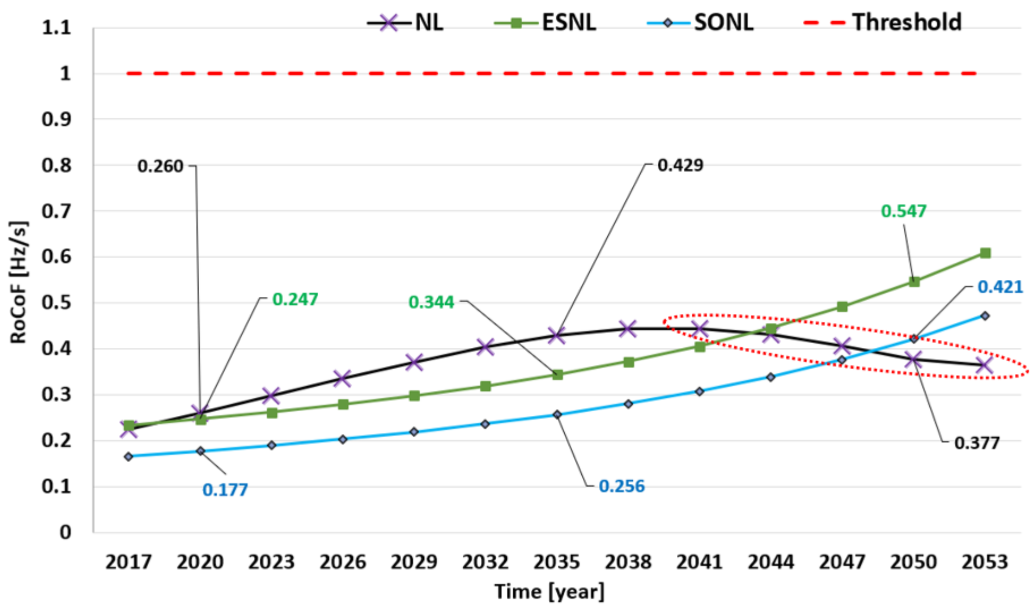

Figure 4-33: Graph Indicator (1); Rate of Change of Frequency (Main-Scenario-Primary-Case)

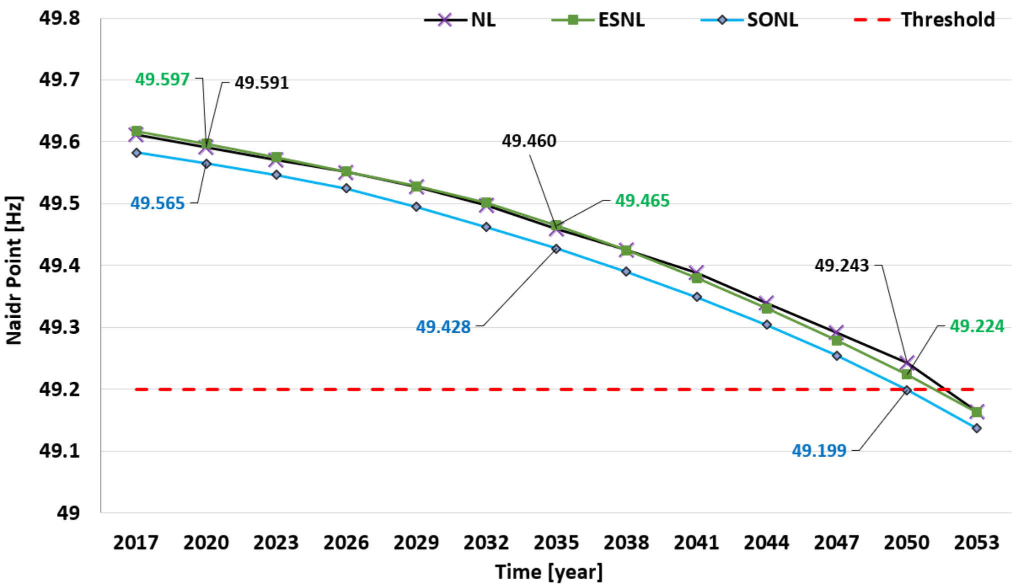

Figure 4-34: Graph Indicator (2); Maximum Dynamic Frequency Deviation (Main-Scenario-Primary-Case)

Figures 4-35 to 4-37 show the frequency deviation, the frequency offset, and the time instant of Nadir Points for each the studied areas. The curves depicted below makes possible to conclude that the studied areas will get an issue regarding the frequency performance with a 3000MW sudden loss as deviation of system frequency reaches the threshold value of 800mHz around 2050. this behaviour would cause a so-called under frequency issues that would require additional control systems such as Load Shedding technology. This measure is capable to prevent a power system from being unstable country-wide by decreasing the demand or increasing supply

Furthermore, a comparison between figure 4-33 and 4-37 results in a conclusion that the unexpected behaviour of RoCoF in the year 2044 as shown with dashed red circle can be related to the time instant of Nadir point. In this year, the Nadir time gets an increase of 1s to the value of 4s, while the RoCoF becomes lower compared with the year 2041. Equation (3.8) describes this behaviour as the amount of system inertia for area NL is much higher than what is required at the time instant of the created event. Such a high amount of inertia gives the power generic model of dispatchable power plant sufficient delay to react to the power imbalance event; resulting in a later frequency nadir point that, in turn, cause a lower RoCoF value.

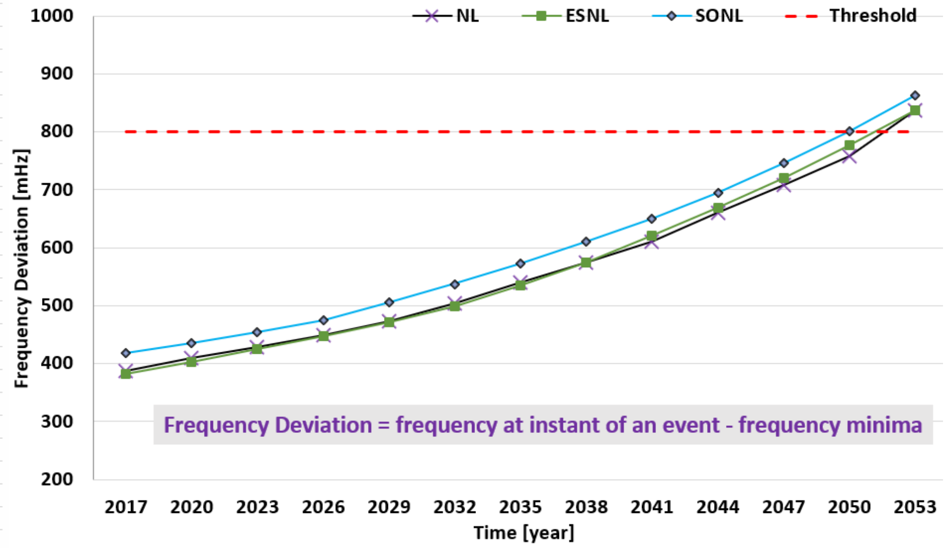

Figure 4-35: Graph Indicator (3); frequency Deviation (Main-Scenario-Primary-Case)

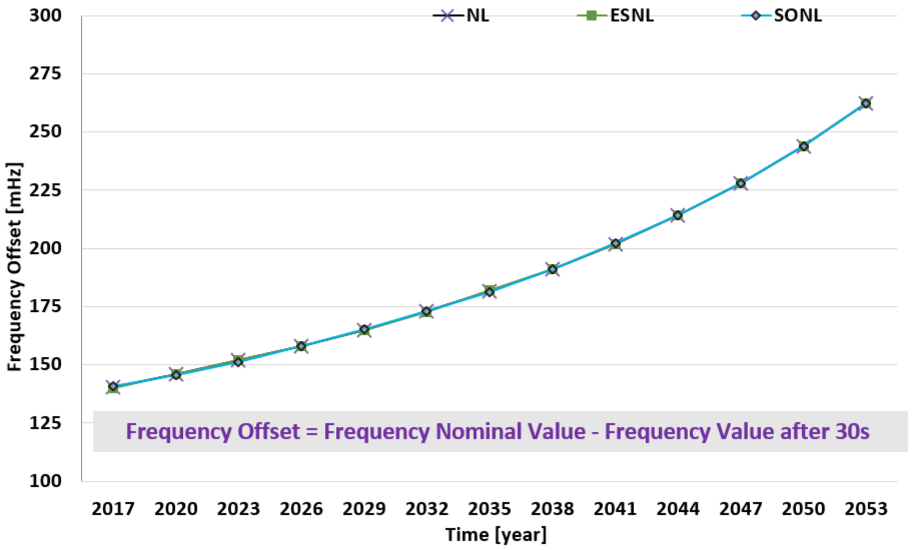

Figure 4-36: Graph Indicator (4); Frequency Offset (Main-Scenario-Primary-Case)

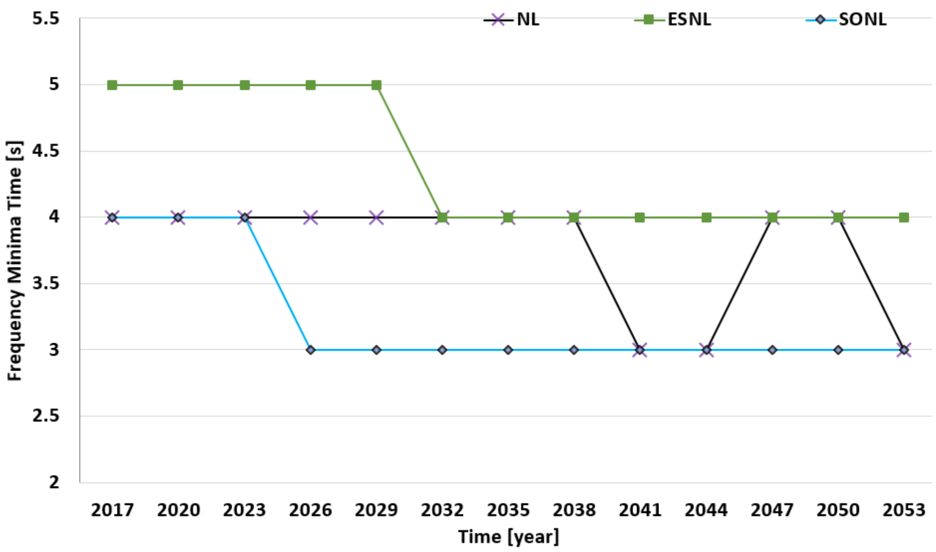

Figure 4-37: Graph Indicator (5); Nadir Point Time Instant (Main-Scenario-Primary-Case)

4.2.2. Simulations Results of Secondary-Case-Main-Scenario

This paragraph shows the simulation results of the secondary-case based on the relevant findings, elaborated in section (4.2). The simulated frequency of each control area is provided within this paragraph based on the method depicted in figure 4-28. Moreover, the same graph indicators used in the previous paragraph will also be applied here. Figures 4-38 to 4-40 shows the frequency performance of the studied areas as a function of system inertia that has been obtained using only the level of dispatchable active power at the time instant of an event (see secondary case description).

Furthermore, figures 4-41 to 4-45 illustrates the graph indicators applied to predict the deterioration foreseen to occur in the frequency performance of the synchronous grid of Continental Europe including that of the Netherlands. Graph indicator (2) shown in figure 4-42 indicates that frequency deviation would exceed the threshold of 800mHz earlier than in the primary-case as the values of system inertia are much lower. On the other hand, the problem of unexpected RoCoF behaviour has been eliminated here. This is shown using graph indicators (1) and (5). It can be seen that the time instant of Nadir Point of the NL area does not get any increase as in the primary case; resulting in continuous higher values of RoCoF. Although that the RoCoF values are still within the acceptable operating ranges, but they show a significant shift throughout 33 years.

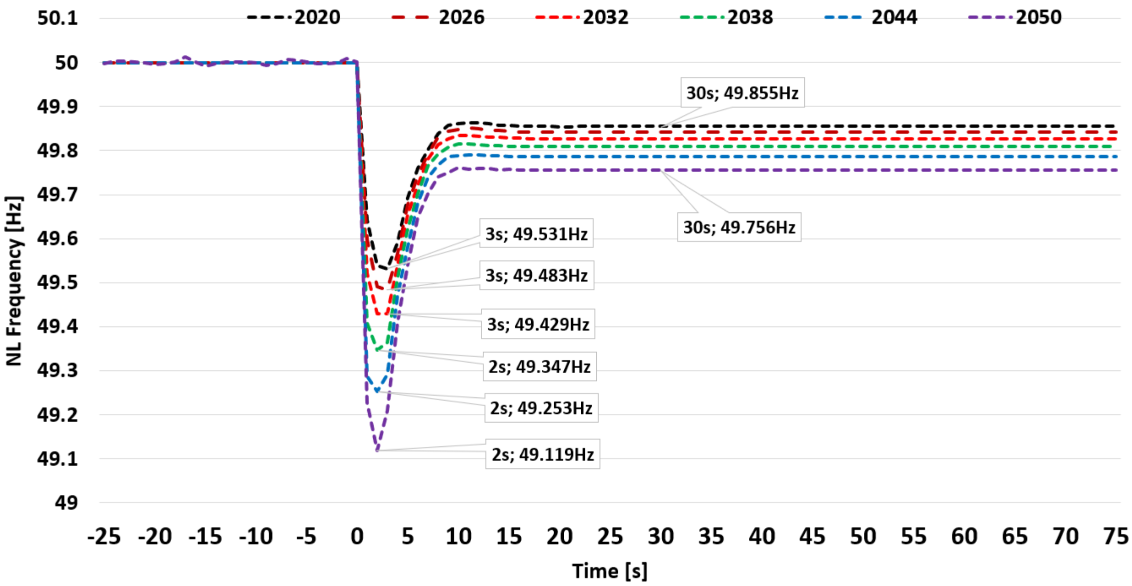

Figure 4-38: Samples of Simulated Frequency for Area NL throughout 30 Years (Main-Scenario-Secondary-Case)

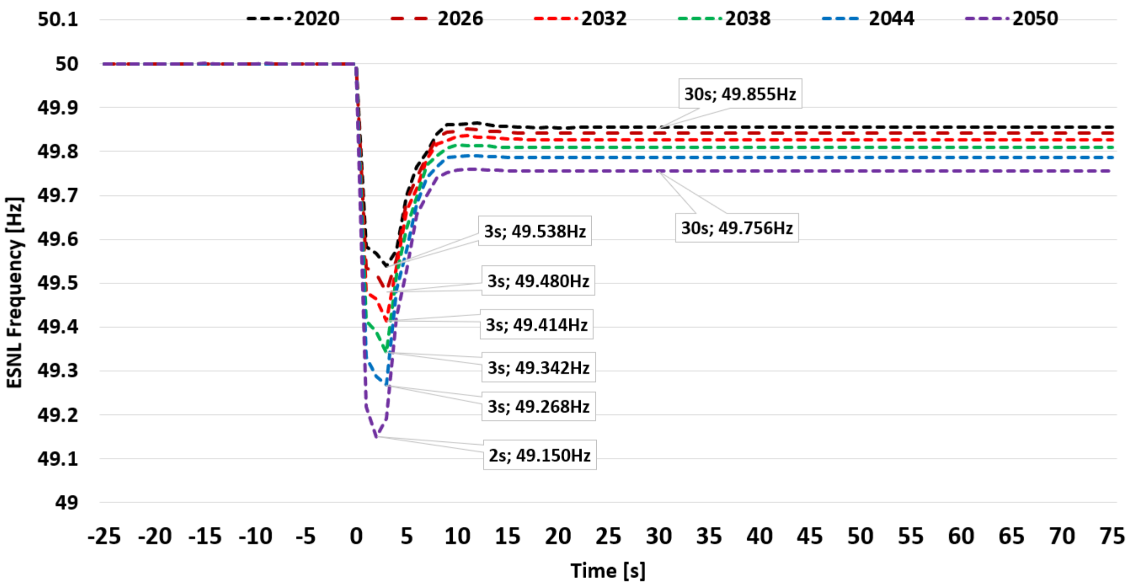

Figure 4-39: Samples of Simulated Frequency for Area ESNL throughout 30 Years (Main-Scenario-Secondary-Case)

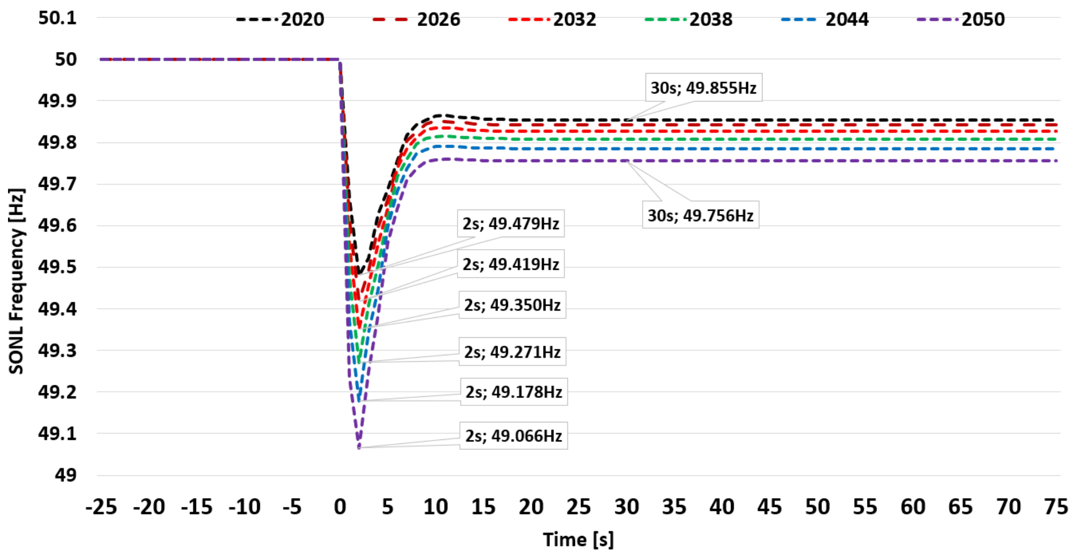

Figure 4-40: Samples of Simulated Frequency for Area SONL throughout 30 Years (Main-Scenario-Secondary-Case)

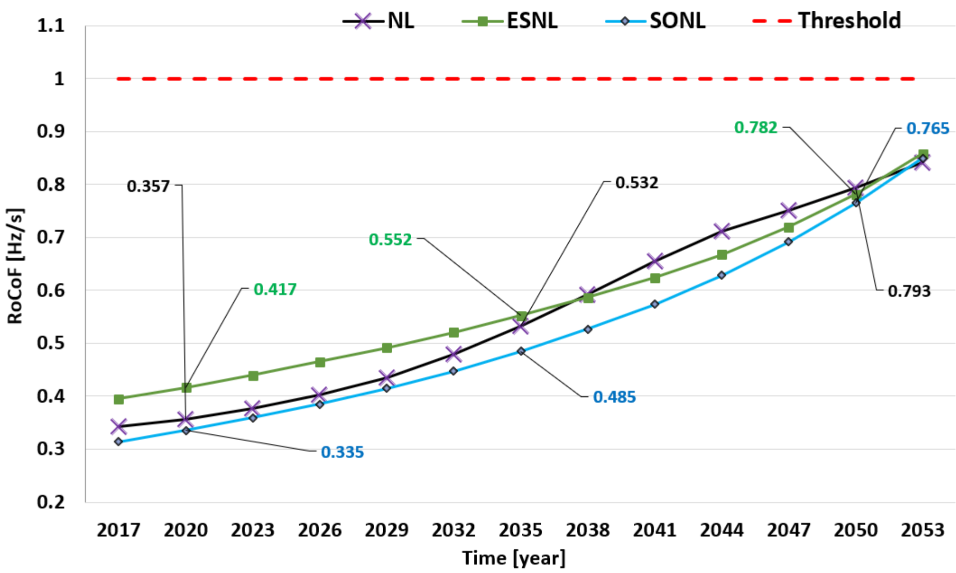

Figure 4-41: Graph Indicator (1); Rate of Change of Frequency (Main-Scenario-Secondary-Case)

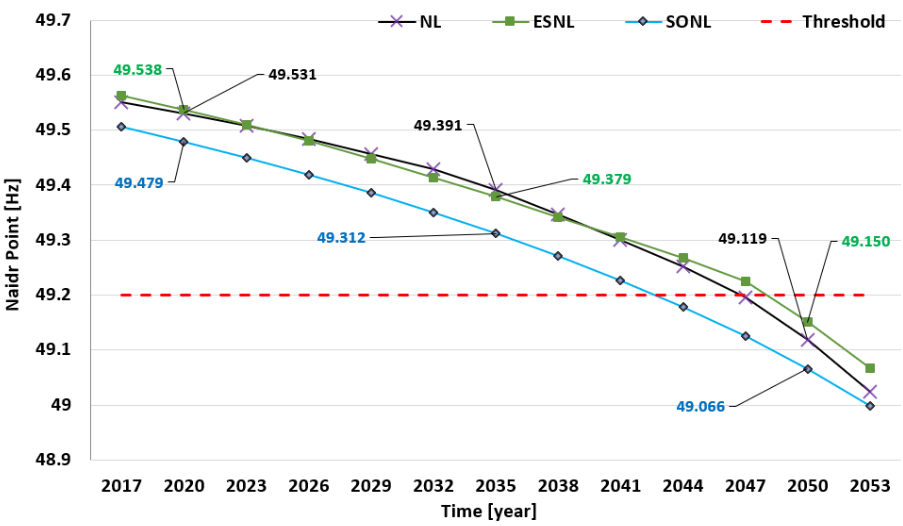

Figure 4-42: Graph Indicator (2); Maximum Dynamic Frequency Deviation (Main-Scenario-Secondary-Case)

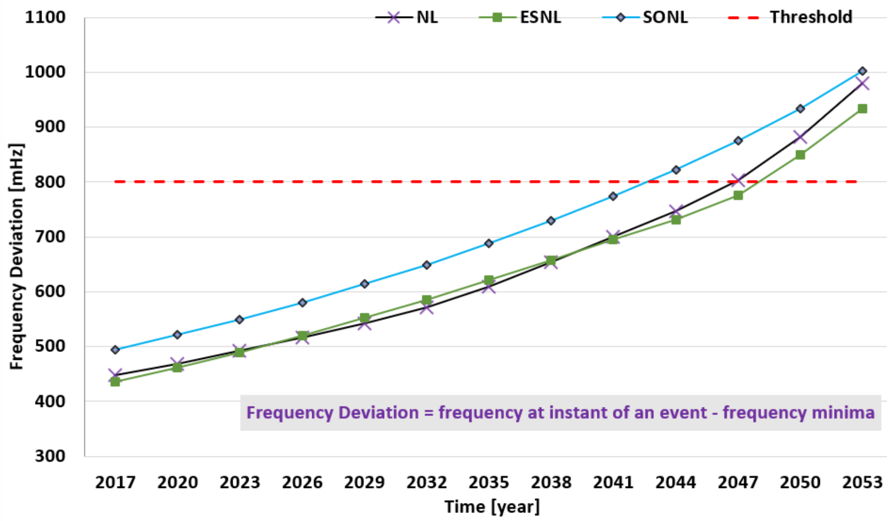

Figure 4-43: Graph Indicator (3); frequency Deviation (Main-Scenario-Secondary-Case)

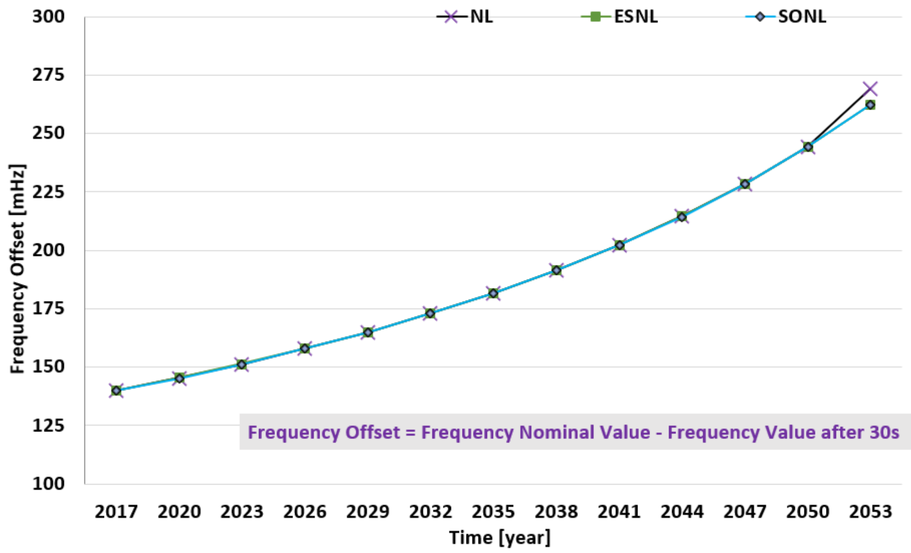

Figure 4-44: Graph Indicator (4); Frequency Offset (Main-Scenario-Secondary-Case)

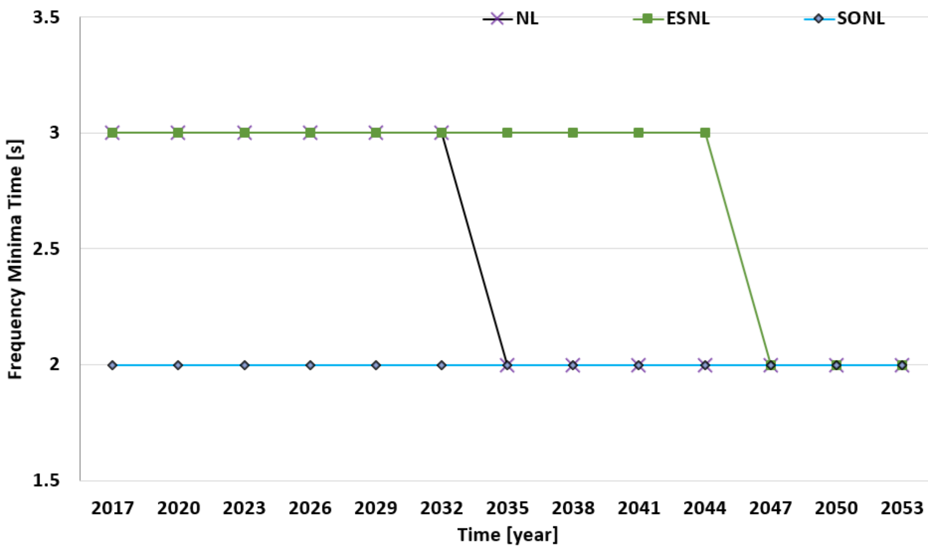

Figure 4-45: Graph Indicator (5); Nadir Point Time Instant (Main-Scenario-Secondary-Case)

4.3. Discussion and Results Analysis

This section discusses the work done throughout this report briefly with an analysis of the results obtained from the simulation scenarios.

Chapter (1) has described the current background and future conditions of the European grid regarding the possible problems of system inertia reduction. Moreover, the problem statement, the main goal, the research questions, and the overall objectives have been presented in this chapter.

In chapter (2), a literature study has been performed to study the existing control actions that are applied to keep the frequency within the acceptable operating ranges, the stability concerns that are foreseen to occur as a result of the massive integration of renewables, and the impacts of high renewable energy generation on system inertia in future situation.

The outcomes of this survey have shown the difficulties of estimating the minimum required inertia for the stable operation of a given power system. Furthermore, two figures have been found from published papers that gives an insight into the future level of grid inertia. Finally, a block diagram has been created at the end of this chapter that illustrates the consequences of a lower inertia level on the future frequency performance (figure 2-14).

Chapter (3) elaborates on the implementation phase of the dynamic power system model that can be used to assess the frequency performance of the Dutch system based on the Regional Groups (RG) under the operation of ENTSO-e. Two approaches have been proposed; the first approach is a detailed model that studies the frequency stability concerns of all countries covering under RG-Continental Europe and RG-Baltic, while the second approach is a more simplified model that examines the frequency performance of the Dutch system as part of the synchronous grid.

Although the first approach provides more accuracy and reliability to achieve the desired objectives of this thesis work, it has shown difficulties during the implementation phase compared to the simplified approach. The modelling of the first (detailed) approach using KERMIT is quite hard as it needs a large number of input data, i.e. day-ahead demand, production, and cross-border power exchange, to run simulations. For this reason, the choice was made to use the second model to assess the frequency performance of the Dutch grid in a European context.

In chapter (4), two scenarios have been created for simulations purposes; the first scenario (the so-called pre-scenario) was used to verify the overall performance of the developed dynamic model and to select the correct parameters of both the primary and secondary control actions. The hypothesis design of ENTSO-e with a 3000MW sudden generation loss was the basis of simulation throughout this phase. Moreover, the choice was made to use the generation and load data of the month January of each year for simulation purposes as it represents the winter peak load of the involved areas.

The selection of a generic dispatchable plant with a 1% frequency deadband response, 9% regulation droop, 1% load self-regulating effect, and 13s governor time has resulted in a suitable primary response as the simulated frequencies are within the acceptable operating ranges. Also, the selection of the AGC parameters has led to a satisfactory response of the secondary controller as the frequency returns to its nominal value within the pre-defined time range following the 3000MW power contingency. From these results, it could be assumed that the proposed second model with the selected values of both the primary and secondary control are suitable to perform the simulations of the main-scenario as the results do not exceed the operating limits of UTCE Grid Codes.

The second scenario (the so-called main-scenario) had been used to analyse the frequency performance of the studied area with a main focus on the Dutch grid for the period 2017-2050. The shifts in the annual growth of both the demand and electricity production were obtained based on the results of DNVGL and ENTSO-e Energy Transition Outlooks. Furthermore, two cases (primary and secondary) have been developed within this scenario, where both contain the same annual changes in load and generation data but have different values of inertia.

Simulation results of the main-scenario have shown that the diversity in inertia constants between the two cases has led to different figures for both the RoCoF and Nadir Points. Such figures are logical as any change in system inertia affects both values of the RoCoF and Nadir Point. However, figure 4-33 indicates an abnormal behaviour of RoCoF for the control area NL compared to figure 4-41. Such behaviour can be explained with help of the following example:

'you are required to spend more time and effort to move a heavy table from one place to another rather than moving a chair due to the difference in mass between these two objects'

This is precisely what happens in the first case since the values of inertia, estimated using the Net Generation Capacity, are much higher than those of the second case, obtained using the dispatchable active power values at the time instant of the created step-fault. In other words, the higher values of system inertia, and hence, the higher level of the stored kinetic energy and rotating mass would provide sufficient delay *(see the increase in NL curve depicted in figure 4-37)* for the generic model of a dispatchable plant to counteract the frequency decline caused by a 3000MW power contingency. This delay has resulted in lower RoCoF values.

Focusing on the (conservative) secondary case, figure 4-42 indicates that the frequency decline will exceed the maximum dynamic deviation limit of 800mHz around 2044 due, mostly, to the lower share of dispatchable active power, and hence, the lower inertia values in this year as shown in figures 4-26 and 4-29, respectively. This decline further shows that with a 3000MW generation loss in the Dutch grid, an under-frequency case can happen. Such a case would, in turn, cause real frequency stability issues that require additional control actions, i.e. Load Shedding technology, to arrest the significant dynamic frequency deviations. This measure is capable to prevent a power system from becoming unstable country-wide by decreasing the demand or increasing the supply

However, Different measures could be taken in the future to mitigate the impact of inertia reduction on the frequency stability performance of either the Dutch grid or any power system within a given region. An example of such measures is elaborated in section (2.5) that shows the possibility of maintaining system inertia at the desired level by modifying the existing synchronous compensation condensers. for instance, by connecting a flywheel to the flange of a rotor shaft.

Another example is discussed in Appendix (D) that provides a possible solution for the issues caused by inertia reduction through the introducing of a so-called virtual or synthetic inertia into the future power systems. Such a measure, e.g. grid-supporting power converters with energy reserves, would have the ability to operate in a short time. In general, the synthetic inertia will be provided using a system that combines control algorithms, renewable energy sources, energy storage systems, and power electronics. The main concept of virtual inertia is based on voltage-current signals, which are the outputs of inverters that connects renewables to the electric grid.

As the operation of the Kermit-Tool is only based on the active power in (MW) and frequency in (Hz) without considering the voltage and current signals, the possibility of developing a specific scheme for virtual inertia is limited. This, in turn, restricts the assessment of frequency performance using inertia produced by renewables. However, during this study, a generic model for non-dispatchable plants has been developed (see figure 4-46 below) to provide the ability to share the renewables active power in the primary response action. It is worth mentioning that no scenarios have been created for this case due to time considerations.

Focusing on the primary objective of this project of creating a Graph Indicator that predicts both the time it takes until inertia reduction will be a real issue for frequency stability as well the ability of inertia produced by renewables to mitigate this issue. Such a graph can now be created using the simulations results of the main-scenario-secondary-case.

As mentioned above, the inertia reduction issue would appear around the year 2044 corresponding to an inertia values equal to 1.23s. However, this value had been obtained using a multiplication factor of (~0.4) as pointed out in the description of the main-scenario-secondary-case. By using the same factor but now for the purpose of division, it is possible to return to the initial inertia values that have been estimated in chapter (3) based on the Net Generation Capacities. This means that maximum frequency deviation will exceed the limits (around 2044) with an inertia value equals to (3.07s), while RoCoF will reach the 1Hz/s (around 2060) with an inertia value of nearly 2.5s.

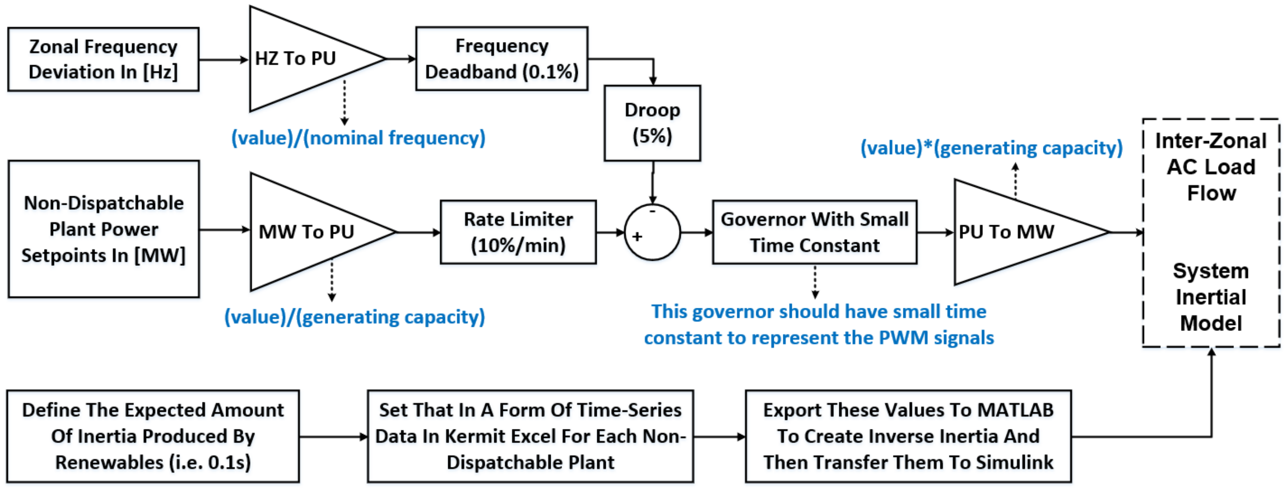

Figure 4-46: Renewable Plant Generic Model to Share Non-Dispatchable Active Power in Primary Response Action

From an engineering perspective, it is possible to argue that the rapid development of both power electronic switching devices and control system techniques would help researchers and TSO's to find suitable solutions to produce inertia from renewable sources soon. Assuming that the renewables and their control systems would be able to provide an amount of synthetic inertia equal to 0.05s every year; starting ten years from now (around 2028). This assumption will result in the following inertia values for the Dutch power system in a European context:

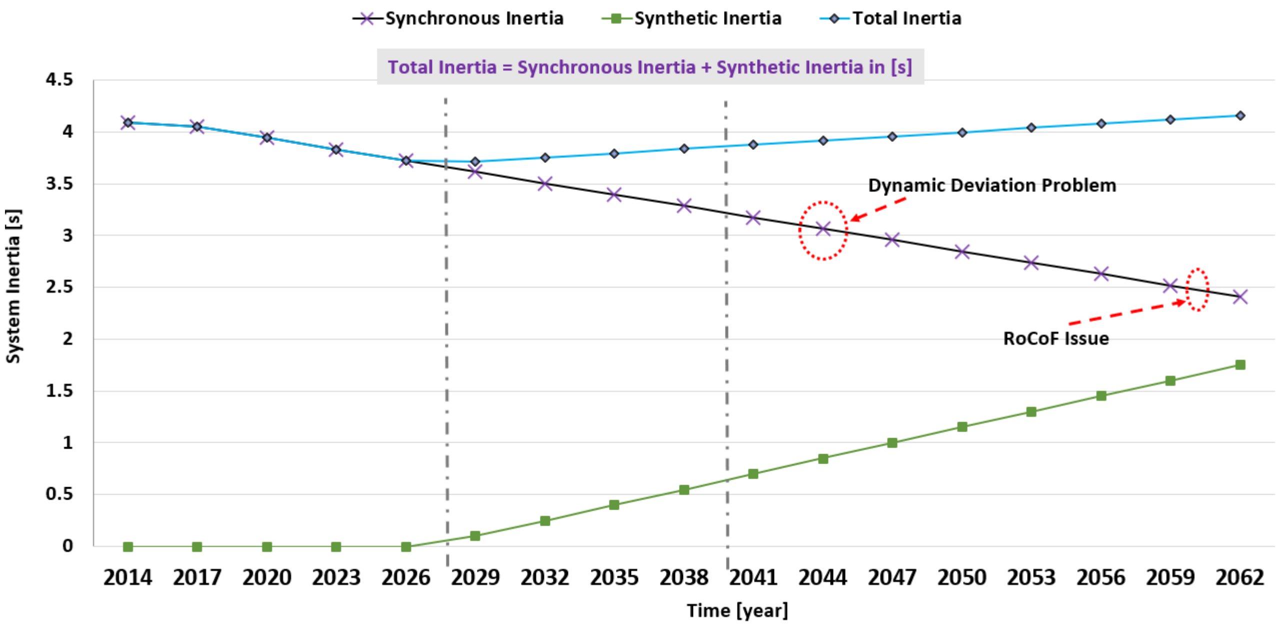

Figure 4-47: Main Graph Indicator; Possible Inertia Values in the Future Dutch power System

Figure 4-47 above indicates that the synthetic inertia, which is assumed to be provided to the Dutch power system by renewables will mitigate the stability issues of both the maximum frequency deviations and RoCoF values as highlighted with the red dashed circles. The first (grey colour) vertical line (from left) indicates the time when the synthetic inertia will be added to the synchronous inertia, while the second line points out that system inertia would be sufficiently high around the year 2040 with an approximate value of 3.9s.

It is worth to be noted that there was not enough time to simulate the performance of the secondary controller for the both cases of the main-scenario. However, it can be predicted from the impact of inertia reduction on the frequency performance of primary action that the performance of the secondary action would be subject to potential problems as well.

Finally, this discussion gives us the possibility of assuming that the developed dynamic model for the Dutch power system as part of the (50Hz) Synchronous Grid of Continental Europe is a working design that can be used to study the frequency performance of any region (including that of the Netherlands). The figure below shows the method of applying this study to other countries, areas, or even, regions:

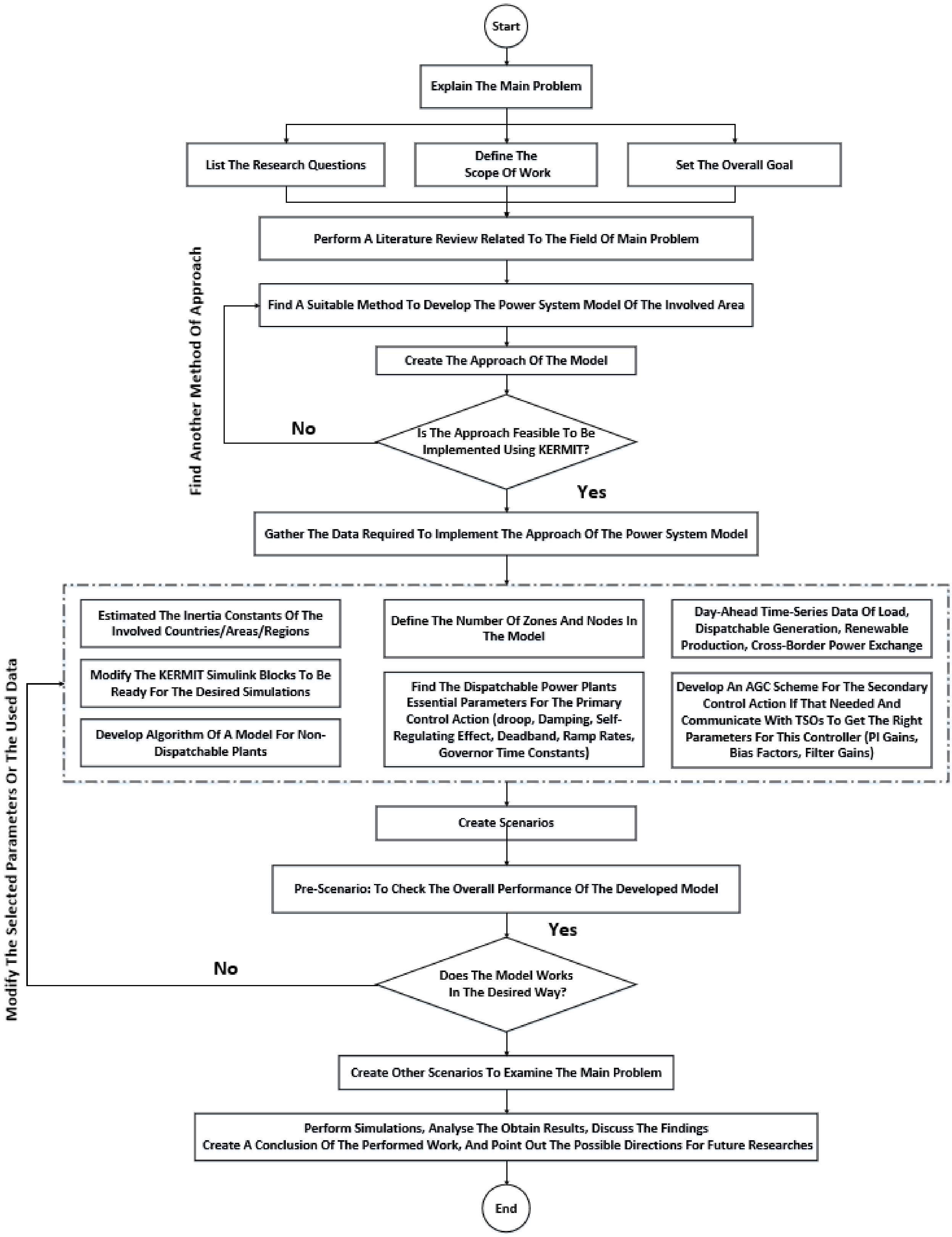

Figure 4-48: Flowchart of the Overall Study Method

5. CONCLUSION AND RECOMMENDATION

This chapter gives conclusions of the work performed within the period of this thesis, answers to the research questions, and points out possible directions for future research.

5.1. Conclusion

Nowadays, the primary target of the members of the European Union is to shift towards a more electrified world based on energy generated by renewable energy sources. By mid-century, it has been anticipated in the Energy Transition Outlook of DNVGL that inverter-connected generation units would provide nearly 70% of the total electricity production. Such an energy transition could cause stability concerns that require innovative solutions to tackle the possible consequences.

Traditionally, the synchronised operation of a power system assumes that the inertia in a given grid is sufficiently high to support the primary control actions of dispatchable plants to arrest the dynamic frequency deviation during power contingencies. Possibly, such an assumption would not be valid anymore in the future electric networks with renewables not contributing to system inertia; resulting in a compromised grid frequency performance.

Therefore, this study has been conducted to assess the frequency performance of the **Dutch power system as part of the Synchronous Grid of Continental Europe** by considering the decrease in system inertia caused by a massive deployment of renewable sources. Moreover, the so-called Kermit-tool developed by DNVGL has been used to model a dynamic power system model that can be used to achieve the overall objectives of this thesis work.

The conclusions of this assessment study are:

- Main Assumption: the developed simplified model in Kermit is sufficient to get an indication regarding the possible future stability issues as the simulation results of the pre-scenario has shown acceptable frequency performance compared to the operating limits of European Grid.

- Frequency stability problems are foreseen to occur in the Dutch grid after approximated 30 years from now as the maximum dynamic frequency deviation exceeds the operating limits, and also, RoCoF reaches considerable high values caused by the decrease in the traditional generation. These findings have been obtained from the simulations of the main-scenario-secondary-case with inertia values in the range of (4sec-2.5sec) using the winter-peak data. However, the stability issues mentioned above are very conservative as the 3000MW power contingency used in the analysis of the Dutch power system rarely happens.

- From an engineering perspective, it is possible to argue that with the rapid development of control system technologies will mitigate such frequency instabilities. The main focus of ENTSO-e and TSO’s nowadays is to produce synthetic inertia from renewables. This inertia can be added to the inertia generated by non-renewables units to support the overall frequency performance of the European grid (including that of the Netherlands).

- The high-level metrics RoCoF, Nadir Point value, and the time instant of Nadir Point are suitable to characterise the dynamic behaviour with inertia changes.

- The method used to model and analyse the future behaviour of the Dutch power system in a European context with a simplified approach using DNVGL tool Kermit can be applied to other countries, areas, or even, regions.

- A manual description of the Kermit power system model has been created during this thesis study, which has made it more usable and accessible for both the future academic and advisory projects.

- A detailed description of what is needed to run simulations using the Kermit-Tool is developed and laid down in a recipe manual:

    - Estimate the current amount of inertia constant for the involved countries based on non-renewable capacities data published by ENTSO-e
    - Gather the correct day-ahead data of production, demand, cross-border exchange, and system parameters
    - Modify the Simulink blocks of the Kermit-Tool based on the developed approach
    - Select the suitable parameters of the primary control action
    - Develop an AGC scheme for the secondary control action (in a case it is needed)
    - Use the following metrics to examine the frequency performance: RoCoF, Nadir Point value, Nadir Point time instant, recovery overshoot, frequency offset, and the deployment time of both the primary and secondary control actions

In short, this thesis work has achieved its main objectives of developing a dynamic power system model that can be used to examine the frequency performance of the Dutch power system as part of the (50Hz) Synchronous Grid of Continental Europe. Despite the limited accuracy of the obtained results, this project can be considered as a first step towards the development of a DNVGL position regarding the problems of system inertia reduction.

5.2. Answers to Research Questions

In this paragraph the answer to the research questions as formulated in section (**1.3**) are given:

- **Q1: How accurate can a model be implemented in Kermit to allow reliable assessment of` the frequency performance of the Dutch power system?**

  A dynamic power system has been developed and implemented using the Kermit-Tool. This model represents the Dutch power system as part of the Synchronous Grid of Continental Europe. The day-ahead time-series load, generation, and power exchange data provided to the Kermit control-panel can be considered as reliable data as it originates from ENTOS-e, TenneT, Amprion, and Elia. Furthermore, the first step towards finding the suitable parameter selection of both the primary and secondary control actions was based on data provided by DNVGL practical tests and ENTSO-e documents as mentioned in chapter (**3**). However, these parameters do not represent the actual values used by TSOs in real situations.

  In short, it is quite hard to create a statement regarding the accuracy of implementing a model using Kermit as the developed model contains two virtual nodes (ESNL and SONL). Each of these nodes aggregates the generation and load profiles of twelve countries. Such an aggregation puts obstacles towards the proper modelling of the simplified approach. However, the performed simulations of the pre-scenario have shown satisfactory frequency performances of the studied control areas (including that of the Netherlands). This means that the developed model can be used for frequency assessment studies.

- **Q2: Which metrics can be applied to indicate the impact of inertia reduction on system frequency deviation and frequency control actions during disturbances?**

  As the value of inertia has a direct impact on the initial rate of change of frequency (RoCoF), and the maximum dynamic deviation (Nadir Point) including its time instant (delay). These measures can be used as high-level metrics to predict the influence of inertia reduction on system frequency performance during power contingencies. Examples of such metrics are provided in the form of Graph Indicators in chapter (**4**).

- **Q3: Under which circumstances will the decrease in system inertia be a real issue for system frequency performance?**

  According to simulation results of the main-scenario-secondary-case, it can be stated that with a 50% share of renewable generation in the total production and a 3sec inertia constant, a 3000MW sudden generation loss can cause potential problems for the frequency performance of the Dutch power system. These problems could occur when the maximum dynamic deviation exceeds the acceptable operating limits of 800mHz.

  Also, these results have shown a considerable increase in RoCoF values from 340mHz/s to 800mHz/s in the Netherlands for the period between 2017-2050. Possibly, RoCoF can exceed the operating limits of 1Hz/s around the year 2060 as the inertia keeps decreasing to reach a value equal to 2.5sec as explained in section (**4.3**).

- **Q4: Which measures can be used to mitigate the influence of system inertia reduction regarding the massive deployment of renewable sources in the future power system?**

  This question is addressed by literature research. Measures that can be taken to mitigate the impact of a lower inertia level on the frequency stability performance of either the Dutch grid or any power system within a specific regional group are:

  - Modifying the mechanical parts of the existing synchronous compensation condensers, for instance, by connecting a flywheel to the flange of a rotor shaft. Such a modification will make the condensers capable to maintain the grid inertia at the desired level.

  - Introducing of a so-called virtual or synthetic inertia into the future power systems. Such a measure, i.e. grid-supporting power converters with energy reserves, would have the ability to operate in a short time. In general, the synthetic inertia will be provided using a specific system that combines control algorithms, renewable energy sources, energy storage systems, and power electronics. The main concept of virtual inertia is based on voltage-current signals that are the outputs of inverters that connects renewables to the electric grid.

  - Sharing the active power production of renewables in the primary control action is possible using the developed generic model of non-dispatchable plants depicted in figure **4-46**.

5.3. Recommendation for Future Work

This section points outs the possible directions for future researches regarding the problems of inertia reduction either in the Netherlands or other regions:

- Develop a KERMIT algorithm that provides the ability to produce synthetic inertia from renewable energy sources
- Find reliable ways to get the shifts in both the demand and production in a future situation
- Perform more sensitivity studies to become more confident about the results
- Consider the future possible expanding in both the cross-border power exchange and capacity
- Use specific dispatchable power plant models such as (Combined Cycle Gas Turbine, Non-Res Hydro Generator, and Coal Power Plants) to get more accurate results
- Adapt KERMIT is such a way that it accepts input data, e.g. for every 1sec
- Develop another interpolation method that performs frequency simulations for every 0.5sec instead of 1sec. Such an improvement would give better results regarding computation of RoCoF and Nadir Point value as well its time instants
- Find a way to gather the correct data of both the primary and secondary control actions from the responsible TSOs
- Consider the Frequency Containment Reserves for both the primary and secondary control
- Create simulation scenarios that cover the summer demand peaks
- Finally, follow the flowchart shown in figure **4-48** to use the method of this work in future research

BIBLIOGRAPHY

[1] G. Migliavacca, '**Advanced Technologies for Future Transmission Grids**,' in Power Systems, 1st ed., London: Springer-Verlag, 2013, pp. XII, 400.

[2] A. Ulbig, T. S. Borsche, and G. Andersson, '**Impact of Low Rotational Inertia on Power System Stability and Operation**,' arXiv:1312.6435 [math], Dec. 2013.

[3] 'Scenarios Energy Transition Outlook' (**ETO**) 2050, DNVGL (2017).

[4] P. Kundur et al., '**Definition and classification of power system stability IEEE/CIGRE joint task force on stability terms and definitions**,' IEEE Transactions on Power Systems, vol. 19, no. 3, pp. 1387–1401, Aug. 2004.

[5] J. Balke, '**Integration of Renewable Energy in Europe**,' Arnhem: KEMA Consulting GmbH, June 2014, Report No. 9011-700, pp. 236.

[6] P. Tielens, '**Operation and control of power systems with low synchronous inertia**,' Ph.D. dissertation, Dept. Elect. Eng., Leuven Univ., Leuven, Belgium, 2017.

[7] J. A. M. Jimenez, '**Evaluation of frequency and transient stability indicators in future power systems with high levels of wind power generation**,' M.S. thesis, Dept. Elect. Eng., Delft Univ., Delft, the Netherlands, 2017.

[8] RG-CE System Protection & Dynamics Sub Group, '**Frequency stability Evaluation Criteria for the Synchronous Zone of Continental Europe**,' Requirements and Impacting Factors, Belgium: ENTSO-E, March 2016, pp. 25.

[9] E. Ela, M. Milligan, and B. Kirby, '**Operating Reserves and Variable Generation**,' in Impact of Renewable Sources on Power System Stability, Colorado: NERL, Aug. 2011, pp.103.

[10] Rasing, '**Overzicht componenten 380 kV en 220 kV net inclusief technische gegevens**,' In Transmission Lines, Arnhem: TenneT, Feb. 2017, pp. 7.

[11] N. Modig et al., '**Future System Inertia**,' in the Estimation of Inertia in Nordic Area, Brussels: ENTSO-E, 2013, pp. 58.

[12] P. Kundur, '**Power System Stability and Control**,' in Power System Operation, Mcgraw-Hill Education, Jan. 1994, pp. 1176.

[13] "**Statistical Factsheet 2017**". [Online]. Available on: https://docstore.ENTSO-e.eu/Documents/Publications/Statistics/Factsheet/ENTSO-e_sfs_2017.pdf

[14] "**ENTSO-E Transparency Platform**". [Online]. Available: https://transparency.ENTSO-e.eu/.

[15] "**Data Dashboard Netherlands – TenneT**". [Online]. Available: https://www.tennet.eu/electricity-market/data-dashboard/data-dashboard-netherlands/.

[16] "**Grid Data – Amprion**". [Online]. Available: https://www.amprion.net/Grid-Data/.

[17] "**Data Download – Elia**". [Online]. Available: http://www.elia.be/en/grid-data/data-download.

[18] V. Sookha, '**Modelling and Investigation of the NorNed HVDC Link with RTDS**,' M.S. thesis, Dept. Elect. Eng., Delft Univ., Delft, the Netherlands, 2011.

[19] V. Satu, '**Nordic Synchronous Area Proposal for Ramping Restrictions for Active Power Output**,' in the establishing a guideline on electricity transmission system operation, pp. 7, Aug. 2017.

[20] De Haan, 'Cross-Border Balancing in Europe,' Ph.D. dissertation, Dept. Elect. Eng., Eindhoven Univ., Eindhoven, the Netherlands, March 2016.

[21] UTCE Ground Rules and Recommendations, 'A1-Appendix 1: Load-Frequency Control and Performance,' pp. 1–28, June. 2004.

[22] 'Droop Control - Open Electrical'. [Online]. Available: https://wiki.openelectrical.org/index.php?title=Droop_Control. [Accessed: 18-Nov-2018].

[23] J. McCalley, 'Wind Power Variability in the Grid: Regulation,' IOWA State University, Ames, Iowa, US, 2015.

[24] B. Mohanty, S. Panda, and P. K. Hota, 'Controller parameters tuning of differential evolution algorithm and its application to load frequency control of multi-source power system,' International Journal of Electrical Power & Energy Systems, vol. 54, pp. 77–85, Jan. 2014.

[25] A. S. Abd El-Hamid, A. H. Eissa, A. M. Abouel-Fotouh, and M. A. Abdel-Fatah, 'Comparison Study of Different Structures of PID Controllers,' Research Journal of Applied Sciences, Engineering and Technology, vol. 11, no. 6, pp. 645–652, Oct. 2015.

[26] L. Meegahapola and T. Littler, 'Characterisation of large disturbance rotor angle and voltage stability in interconnected power networks with distributed wind generation,' IET Renewable Power Generation, vol. 9, no. 3, pp. 272–283, 2015.

[27] J. C. M. Vieira, W. Freitas, Z. Huang, W. Xu, and A. Morelato, 'Formulas for predicting the dynamic performance of ROCOF relays for embedded generation applications,' Transmission and Distribution IEE Proceedings - Generation, vol. 153, no. 4, pp. 399–406, Jul. 2006.

[28] Y. Ma, S. Lv, X. Zhou, and Z. Gao, 'Review analysis of voltage stability in power system,' in 2017 IEEE International Conference on Mechatronics and Automation (ICMA), 2017, pp. 7–12.

[29] B. Reddy, 'Study of Voltage Stability Indices Suitable for Online Applications,' International Journal of Engineering and Applied Sciences (IJEAS) ISSN: 2394-3661, Volume-1, Issue-3, December 2014.

[30] Dong Joon Kim, Young Hwan Moon, Ho Yong Kim and Young Yoon, 'System and method for calculating real-time voltage stability risk index in power system using time series data,' United States Patent No. US 7236898 B2, Dt. June. 26, 2007.

[31] J. W. Simpson-Porco and F. Bullo, 'Distributed Monitoring of Voltage Collapse Sensitivity Indices,' IEEE Transactions on Smart Grid, vol. 7, no. 4, pp. 1979–1988, Jul. 2016.

[32] U. Tamrakar, D. Shrestha, M. Maharjan, B. P. Bhattarai, T. M. Hansen, and R. Tonkoski, 'Virtual Inertia: Current Trends and Future Directions,' Applied Sciences, vol. 7, no. 7, p. 654, Jun. 2017.

[33] H. Thiesen, C. Jauch, and A. Gloe, 'Design of a System Substituting Today's Inherent Inertia in the European Continental Synchronous Area,' Energies, vol. 9, p. 582, 2016.

[34] I. Signh, 'Effect of Reduced System Inertia Due to Increased Renewable Resource Penetration on Power System Stability,' M.S. thesis, Dept. Elect. Eng., ARIZONA STATE UNIVERSITY, August 2012.

[35] Nahid-Al-Masood, R. Yan, and T. K. Saha, 'Cascading contingencies in low inertia power systems: Frequency response challenges and a potential solution,' in 2017 IEEE Power Energy Society General Meeting, 2017, pp. 1–5.

[36] P. Tielens and D. Hertem, '**Grid Inertia and Frequency Control in Power System with High Penetration of Renewables**,'. Belgium: KU Leuven, ELECTA research group, Electrical Engineering Department, 2012.

[37] "**NERC Balancing and Frequency Control: A Technical Document Prepared by the NERC Resources Subcommittee**" [Online]. Available: https://www.nerc.com/docs/oc/rs/NERC%20Balancing%20and%20Frequency%20Control%20040520111.pdf. [Accessed: 11-Apr-2018].

[38] C.L. DeMarco et al. '**Primary and Secondary Control for High Penetration Renewables**,' Prepared for the Project "The Future Grid to Enable Sustainable Energy Systems" Funded by the U.S. Department of Energy, White Paper Team of University of Wisconsin-Madison, March 2012.

[39] I. Kuzle, T. Tomisa, and S. Tesnjak, '**A mathematical model for studying power system frequency changes**,' in 2004 IEEE Africon. 7th Africon Conference in Africa (IEEE Cat. No.04CH37590), Gaborone, Botswana, 2004, vol. ol.1, pp. 761–764.

[40] '**Frequency Measurement Requirements and Usage,**' Tech. Rep, RG-CE System Protection & Dynamics Sub Group, ENTSO-E, Brussels, Belgium, 2018.

[41] '**SCENARIO OUTLOOK AND ADEQUACY FORECAST 2013-2030**,' ENTSO-E, Brussels, Belgium, April 2013.

Appendix

A. Foundations of Power System Stability

This appendix describes the system theoretic foundations of power system stability, scenarios of stability analysis based on Lyapunov framework, and the historical definition of system stability.

1. System-Theoretic Foundations of Power System Stability

Power systems can, in general, be considered as an example of a constrained dynamical system due to the relationship between their state trajectories and a specific subset in the state space, which together form the feasible operating region. These trajectories can further cause an unsafe operation or may result in structural changes, for instance, breaker tripping in a power system.

The interaction with the environment makes power system non-autonomous (or time-varying) as explained in [4]. For instance, switching in substations causes load variations and changes in network topology. Moreover, any power system should be controlled with numerous feedback loops. Therefore, it is essential to introduce the effects of control input variables during the stability analysis, especially for long time horizons.

Next, consider the following system: **y = f(t,x)**

Where:

- x = the state vector
- y = the derivative of x
- f = differentiable, and its domain includes the origin
- t = time in [s]

System above is said to be:

- autonomous if **f(t,x)** is independent of time (t)
- non-autonomous if **f(t,x)** is dependent of time (t)

The outlined modelling problems of power system stability analysis can be listed as follows:

- Formulating a general stability definition for a non-autonomous system is quite challenging. One possible solution is to assume that such system is stable when both the input variables (from the environment) and the corresponding output variables are square-integrable, which can be constant or vary due to a specific response.

- The disturbances, which occur during the operation of a power system, can be categorised in two terms as given in [4]:

  - **event-type**: (incident-type) disturbance, which is characterized by a specific fault scenario, e.g. switching disturbances, or short circuit.
  - **norm-type**: (or signal intensity type) disturbance, which is described by its size, e.g. load variations.

- Designing suitable stabilising controllers for non-linear power systems is complicated because of the assumption that control actions are known concerning predictable system states.

In general, the stability study of power systems is influenced by various equilibrium sets. A typical power system stability study can be performed in the way mentioned below:

- Formulate a list of modelling assumptions

- Create a mathematical model that is suitable for time scales. In [4] it is indicated that the typical time scale is in a range from serval seconds to minutes.

- Select an appropriate stability definition
- Determine stability by analysing and simulating the created model
- Verify the results using the formulated list of assumptions.

2. Scenarios for Stability Analysis Based on Lyapunov Framework:

This section describes the analytical stability definition briefly based on the Lyapunov framework.

Given in [4] another stability framework, the so-called Input-to-Output stability, which describes the global properties of a system, so in its standard form. This framework is not suitable for the study of individual equilibrium sets. Often, the results of input-to-output stability are being used to establish the outcomes of a Lyapunov framework by using specific tools.

A typical scenario for power system stability analysis based on Lyapunov involves three different steps:

- Initially, the system is operating in a pre-disturbance equilibrium (**X**) set (e.g., an equilibrium point). Within this set, various driving forces, which influence the system in-output variables, are in balance.

  Mentioned in [3] that an equilibrium set, also often called an attractor, is a set of trajectories (or paths) in the phase space to which all neighbouring trajectories converge. These paths are usually used to describe the long-term behaviour of a dynamical system.

- Next, a disturbance acts on the system: **event-types** disturbances or **norm-type** disturbances.

  The essential problem in this stage is the determination of the maximum admissible duration of disturbances, e.g. the critical clearing time of a fault, for which the next response of system stays stable.

- After an event-type disturbance, the system dynamics is studied concerning a known post-disturbance equilibrium set (**Y**), which is different from the set (**X**).

  In the case of norm-type disturbances, set (**Y**) may be similar to set (**X**). Stability of system response means that set (Y) is stable, but a detected instability of system response requires new stability study with new sets, and possibly with new modelling assumptions.

The stability analysis of a power system is often non-local due to the contribution of different equilibrium sets; therefore, a proposed power system stability formulation from system theory has been created by [4] to provide prominent features of stability concepts:

“a given equilibrium set of a certain power system is stable if the system motion converges to that equilibrium set and the operating constraints are satisfied for all relevant variables along the entire trajectory, in case that the initial states of the power system are within the given starting set.”

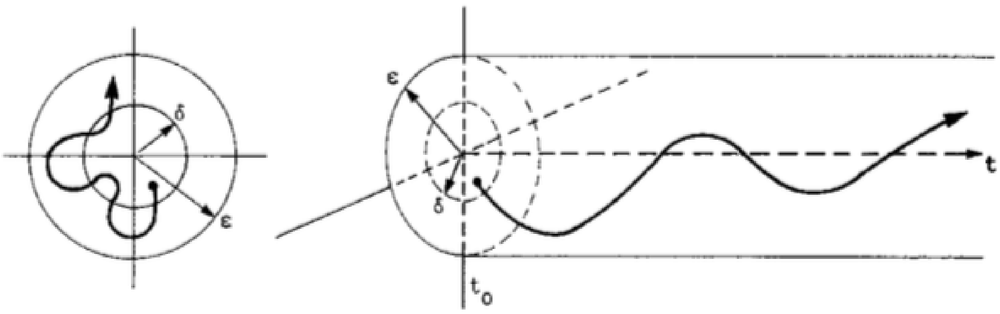

Figure A.1: definition of stability (behaviour of trajectories near a stable equilibrium) [4]

Within the Lyapunov framework stability analysis, it is assumed that control inputs are predictable over time (t) and states (x), and the equilibrium point (EP) is at the origin (i.e. x=0). Based on these assumptions and as illustrated in the figure above, it follows that:

- EP is stable, if for each (ε > 0), there exists a $\delta = \delta(\varepsilon, t0) > 0$. Thus, by choosing the initial conditions in a sufficiently small spherical neighbourhood of radius δ, it is possible to control the trajectory of the power system to lie inside a given cylinder of radius ε for all (t ≥ t0).

- EP is uniformly stable if, for each (ε > 0), $\delta = \delta(\varepsilon, t0) > 0$ independent of (t0).

- EP is unstable if not stable.

- EP is asymptotically stable if it is stable and there is η(t0)>0, for all (t) goes to infinity. This requirement is critical to enforce the system to return to its steady state as shown in figure A.2 below.

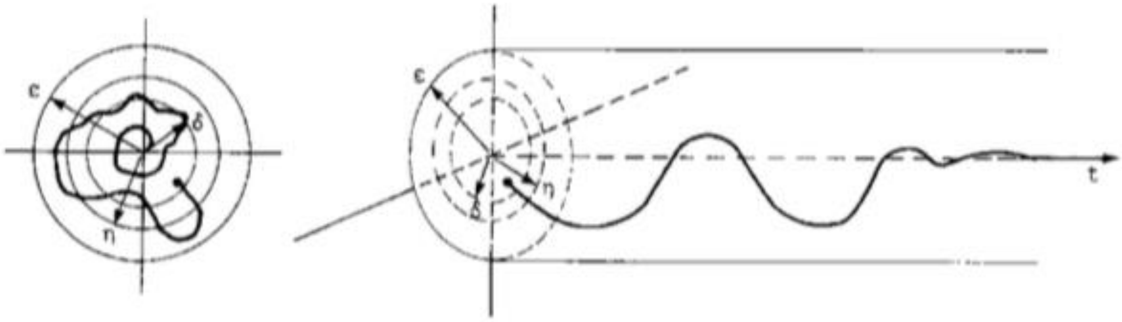

Figure A.2: definition of asymptotic stability [4]

- EP is uniformly asymptotically stable if it is uniformly stable and there is (δ 0 > 0), independent of (t0). Thus, by choosing the initial operating points in a sufficiently small spherical neighbourhood at (t=t0), it is possible to control the trajectory of the system to lie inside a given cylinder for all [t > t0+T(ε, δ 0)]. This illustration of this case is shown in the figure below:

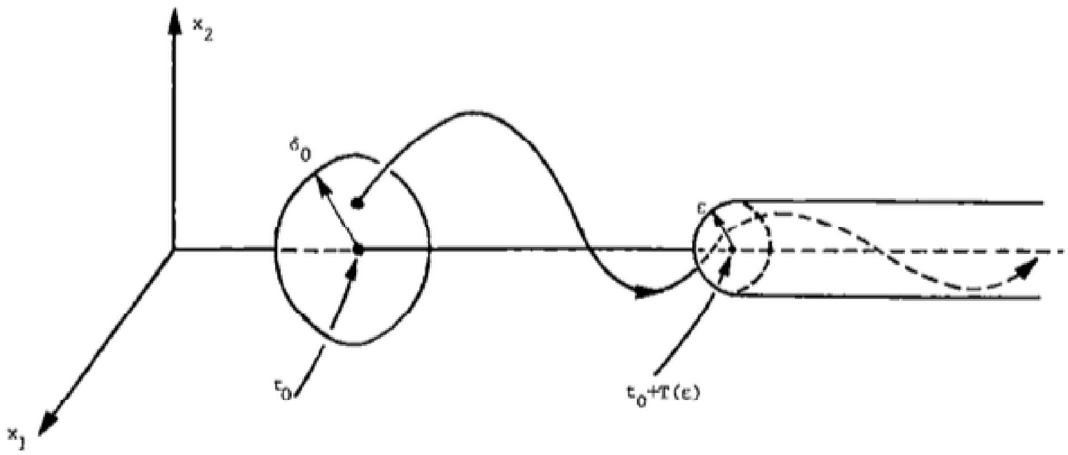

Figure A.3: definition of uniformly asymptotically stability [4]

- EP is exponentially stable if there are (ε > 0), (δ> 0), and (α>0), such that the system is in balance around its equilibrium point.

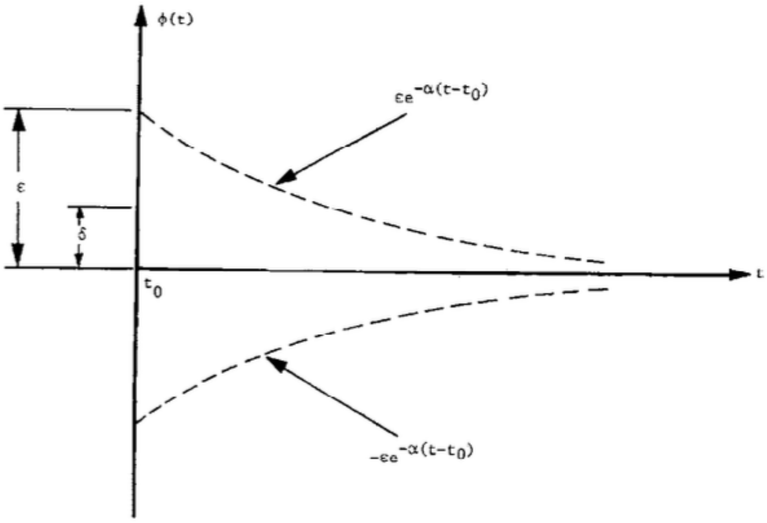

Figure A.4: definition of exponential stability [4]

All these definitions together form the foundation of the Lyapunov approach to system stability and can be most naturally checked for a specific system via so-called Lyapunov functions.

Mentioned in [4] that the stability of a power system can be determined from the hierarchical (two-level) approach since any power system is often modelled as an interconnection of lower-order subsystems.

First, the stability of each subsystem should be individually analysed by ignoring the interconnections. Next, a combination of the results of the previous step with information about the interconnections should be carried out to investigate the stability of the whole system.

In a Lyapunov framework, this will result in the study of composite Lyapunov functions. A significant result is that if the isolated subsystems are sufficiently stable, compared to the strength of the interconnections, then the overall system is uniformly asymptotically stable at the origin.

3. Historical Definition of Power System Stability

As mentioned in [4], the proposed definition of power system stability that applies to any interconnected system can be expressed as follows:

Power system stability is the ability of a power system, for a given initial operating condition, to maintain a steady state after being subjected to disturbances, with most system variables bounded in such way that the entire system remains intact.

In general, the operation of a power system is non-linear due to the changing of an environment; therefore, the stability of a specific power system is a property of system motion around a detailed equilibrium set, i.e. the initial operating conditions.

As stated in [4], within a given equilibrium set, a power system may be stable for a given physical disturbance, and unstable for another. Due to economic and practical considerations, it is impossible to design a power system that may be stable for every perturbation.

For this propose, a stable equilibrium set should have a limited region of attraction, which is a region with a set of points in the state space where all initiated trajectories at these points will converge to the given equilibrium set. In other words, the larger the attraction region is, the more reliable and secure the system is concerning large disturbances.

B. Measurement of Stability Criteria

This appendix elaborates on the indicators that are used to verify the performance of the stability criteria.

1. Rotor Angle Stability

Mentioned in [25] that the rotor angles of synchronous generators are typically measured against the local bus voltages of the relevant generators. which gives the possibility to analyse the transient stability locally by using conventional methods.

In general, the variation of voltage phase angels of a power system is high when the network is subjected to (large) disturbances in response to the transient currents, which flow in that network. Therefore, the current methods of rotor angle using the local reference frames may give inaccurate results.

As given in [25], the typical rotor angle measurement can be illustrated using vector diagram as shown in figure B.1 below:

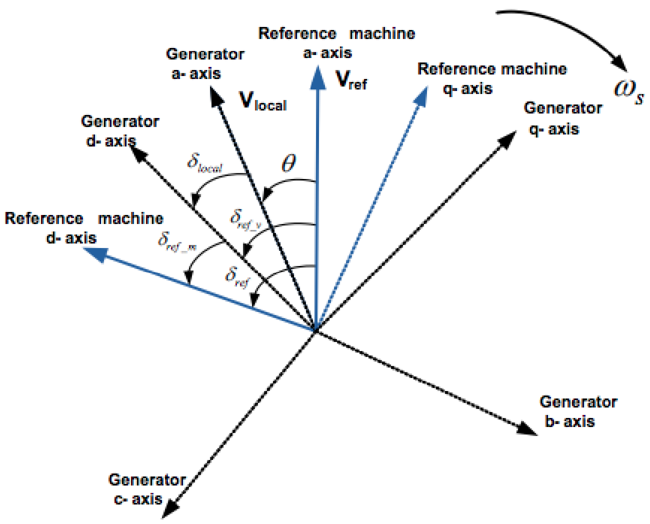

Figure B.1: rotor angle measurement reference frames [25]

Where:

- δ_{local} = Rotor angle with reference to a local bus voltage
- $\delta_{\mathrm{ref\_v}}$ = Rotor angle with reference to a bus voltage angle of reference machine
- $\delta_{\mathrm{ref\_m}}$= Rotor angle with reference to a bus rotor angle of reference machine
- δ_{ref} = Rotor angle of the reference machine
- θ = The generator bus voltage angle (a-axis) with reference to the reference machine voltage angle (a-axis)

To provide a better stability indicator, specifying the relative rotor angle in terms of reference machine angle makes possible to combine both the local voltage angle and rotor angle of any machine in the network. This can be represented as follows:

$$\delta_{\mathrm{ref\_v}} = \delta_{\mathrm{ref\_v}} + \theta \qquad \text{in [degree]} \tag{B.1}$$

$$\delta_{\mathrm{ref\_m}} = \delta_{\mathrm{local}} + \theta - \delta_{\mathrm{ref}} \qquad \text{in [degree]} \tag{B.2}$$

Next, the maximum rotor angle difference over time can be realized in terms of the measured rotor angles with reference to the angle of reference machine following a (large) disturbance:

$$\delta_{\mathrm{max\_d}}\,(t) = \max[\,\delta_{\mathrm{ref\_m}_1}(t) + \cdots + \delta_{\mathrm{ref m}_n}(t)] - \min[\,\delta_{\mathrm{ref m}_1}(t) + \cdots + \delta_{\mathrm{ref m}_n}(t)] \quad \text{in [degree]} \tag{B.3}$$

From the perspective of a synchronous electric network, the variation of the rotor angle difference is in a range between [0 to 360] degree depends on the severity of the disturbances and the power system strength.

Moreover, a specific index was proposed in [25] to examine the severity of the angular separation between synchronous. This index measures the rotor angle separation of a network following a transient disturbance (e.g. fault):

$$\mathrm{TRASI} = \frac{360° - \max(\delta^{\mathrm{pst}}_{\mathrm{max\_d}})}{360° - \delta^{\mathrm{pre}}_{\mathrm{max\_d}}} \qquad \text{in } [\%] \qquad (\mathbf{A.4})$$

Where:

- $\delta^{\mathrm{pst}}_{\mathrm{max\_d}}$ = post-disturbances maximum rotor angle difference
- $\delta^{\mathrm{pre}}_{\mathrm{max\_d}}$ = pre-disturbances maximum rotor angle difference

The output of this index is a real value in a range from 0 to 1. Closer values to one mean that the system is more stable due to a reduction of the angular separation between synchronous generators compared to the case of pre-fault values.

Mentioned further in [25] that the DSA Power Tech tools provide a similar index to TRASI, the so-called Transient Stability Index (TSI). However, in TSI the rotor angles are measured regarding local bus voltage angle, whereas in TRASI, they are measured concerning reference machine rotor angle.

Moreover, in [7] three rotor angles stability indicators have been elaborated. These indicators are:

➢ Power Angle-Based Stability Margin

This indicator gives the percentage value of the maximum rotor angular deviation between two synchronous generators in a certain power system. It is further defined by TSOs using the following equation:

$$\mathrm{Margin} = \frac{360° - \delta_{\mathrm{max}}}{360° + \delta_{\mathrm{max}}} * 100\% \qquad \text{in}[\%] \qquad (\mathbf{B.5})$$

Where (δ_{max}) is maximum angular separation of any two synchronous generators at the same instants when the system is subjected to a post-fault disturbance. This maximum can be computed using the following procedure.

- Use a time domain simulator with a short circuit at instant t_1.
- Export to the simulator, the signals of rotor angle of every online synchronous generator.
- Calculate the possible combinations of angular difference:

$$\delta_{1,2} = \delta_1 - \delta_2\,, \qquad \delta_{1,3} = \delta_1 - \delta_3\,, \ldots\ldots\ \delta_{n-1,n} = \delta_{n-1} - \delta_n \qquad (\mathbf{B.6})$$

- Choose the most significant possible value after performing the previous step.

The importance of this metric lays on the information about the possible islanding due to its ability to manage the rotor angles in a power system. The occurrences of disturbances and the subsequent loss of synchronism, both result in the activation of out-of-step relays that represents the low values of this indicator.

Traditionally, the range of angular separation is between [-180°, +180°], for which the margin value is approximated at 33.3%. This percentage reflects a total separation between synchronous zones of 180°.

➢ Power Angle-Based Stability Margin

The objective of this metric is based on the equivalent inertia values in the system, which represents the total inertia in each synchronous zone and for the entire power system. This indicator has almost the same principle as Margin indicator in terms of angular separation.

However, the main difference is the difficulties of collecting the required data to compute this metric because the input data for the calculation process is not taken from a single synchronous machine, but from the value of COI of each area, and then, this value is compared with the COI value of the entire power system.

➢ Critical Clearing Time

CCT is the most prolonged duration of any fault occurred within an area, without resulting in a loss of synchronism or transient stability. Mentioned in [7] that this time can be considered as the best method to measure how to serve a disturbance (contingency) is. This indicator is in general able to provide TSOs with the required data about protection and planning, such as the analysing of wind power generation expansion.

An example of this time is given in figure B.2, which is performed using a series of constant (repetitive) time domain simulations. The main objective of this example was to find the precise instant where the studied power system becomes unstable by moving the Fault Clearing Time (FCT).

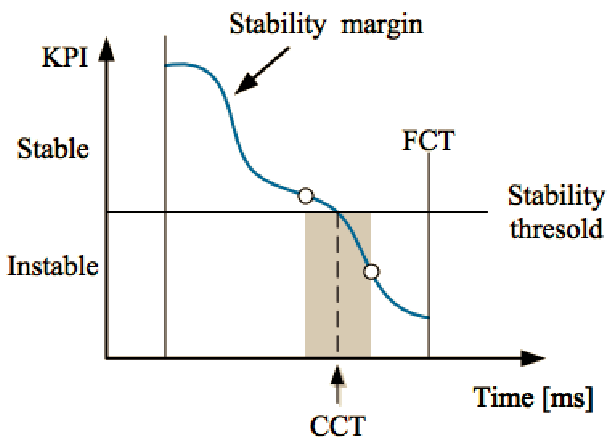

Figure B.2: an example of a visual representation of CCT [7]

2. Frequency Stability

The operation of a power system is traditionally based on the assumption that synchronous generators maintain the grid frequency due to the possibility of electro-mechanical coupling. Such coupling allows the rotating mass of these generators to supply the grid with the required kinetic energy during frequency deviation, which in turns, provides the so-called moment of inertia or rotational inertia. This energy is proportional to the rate of change of frequency (ROCOF).

In [27], the moment of inertia is defined as the resistance to any change occurs in the power system and it is directly proportional to the amount of rotating mass of the synchronous generators in the system. This quantity prevents sudden deviation in the grid frequency, and thus, determines the ROCOF after subjecting to any load event that results in a mismatch between supply and demand in the system. In other words, the higher amount of inertia, the less ROCOF is following a power imbalance event. The frequency of the power grid is directly coupled to the rotational speed of the synchronous generators, and hence, also directly coupled to the balance relation of the active power.

When any deviation in grid frequency occurs, the inertia constant provides the possibility of minimising these oscillations, which makes the frequency dynamics of the system more robust, and thus, increasing the reaction response time to an existing fault. Such response is often called the inertia response or frequency response of a power system.

Following a perturbation, the system frequency deviation must be restored to the acceptable operating ranges to attain a stable operation. Such restoration process can usually be achieved by maintaining the power flow in balance, which means that the total generated power minus the sum of consumed power plus power losses should be kept nearly zero.
In [27], the rate of change of frequency is derived as follows:

At steady-state condition, there is an equilibrium between the mechanical power of the synchronous generator (P_M), the electrical power (P_L) consumed by the load, and the grid power injected/provided into/by the grid (P_{sys}). In this case, both the rotor speed (ω) and the rotor angle (ϑ) of a synchronous generator are constant.

When a power system is subjected to disturbances, a power imbalance event occurs due to the loss of (P_{sys}), resulting in generator transients. The dynamic behaviour of these transients can further be described by the swing equation, which is typically given as follows:

$$\frac{2H}{\omega_0}\frac{d\omega}{dt} = P_M - P_L = -P_{sys} = \Delta P \qquad \text{in [MW]} \tag{B.7}$$

$$\frac{d\vartheta}{dt} = \omega - \omega_0 \qquad \text{in } [\frac{rad}{s}] \tag{B.8}$$

Equations (B.7) and (B.8) gives further the possibility of formulating the main expression of ROCOF:

$$\text{ROFOC} = \frac{df}{dt} = \frac{1}{2\pi}\frac{d\omega}{dt} = \frac{\Delta P\, f}{2H} \qquad \text{in } [\frac{Hz}{s}] \tag{B.9}$$

Where:

- H = per unit inertia constant of the system in [s]
- J = moment of inertia of rotating mass of synchronous generator in [Kg*m^2]
- $\omega_0 = 2\pi f_0$, is the synchronous speed of generator in [rad/s]
- f = system nominal frequency in [Hz]
- S = nominal generator apparent power rating in [MVA]
- ΔP= generation/load lost power, power imbalance, or contingency size in [MW]

3. Voltage Stability

In general, voltage instability can be described concerning a static mechanism based on power flow calculations, as the voltage level in a network is typically influenced by the system reactive power. From the study carried out by [28], it can be concluded that static mechanism is mainly indented to obtain the limitations of grid operation state and to guide power generation scheduling.

However, this mechanism cannot be applied to a system with large interconnections because of the influences of both angle and voltage instabilities on each other in addition to the interaction of load. One possible way to apply this mechanism is by using Q-U and P-U curves to analysis the voltage stability issues.

The current studies on voltage instability have shown that variation of voltage level may also be considered as a dynamic problem based on differential equations. Within this mechanism, the dynamic effects of generation units, load and other components are considered to improve the accuracy of voltage stability. However, the mechanisms mentioned above are not able to provide a full interpretation of the nature of system collapses. Therefore, new studies on the voltage collapse mechanisms are required to develop better ways of assessing the system voltage collapses.

Mentioned further in [28] that a more difficult situation of voltage instability can occur in the form of cascading outages that causes major blackouts, significant low voltage profiles in some parts of a power system, abnormally loaded systems, and intense reactive power flows.

Recently, the study analysis of voltage stability issues is rapidly increased due to the following factors:

- Larger power generation plants are being more decentralised, which means fewer voltage-controlled busses, and longer electrical distances
- Integration of large-scale RES units
- The more and more use of shunt capacitors for compensation purposes
- The increased numbers of blackouts throughout the world

In general, loads are considered as the driving force for voltage stability issues, thus, when the system is subjected to disturbances, the consumption of power by the loads will be maintained by distribution voltage regulators, tap changing transformers, and motor slip adjustment. This power restoration process usually increases the reactive power consumption, resulting in a reduction of the voltage level. A worst case may also occur when the system load dynamics try to maintain the power consumption above the power limits of both generation units and transmission system.

In [28] it is stated that one of the most known factors related to voltage instability is the voltage drop caused by the flow of active and reactive power through the inductive reactance of a transmission network. This flow has further effects on the capability of transmission network, e.g. the limitation of both voltage support and power transfer.

Moreover, the capacitive behaviour of power system components and high-voltage transmission lines have recently increased the risk of over-voltage instability, which is related to the inability of both transmission system and generation units to operate below the specified load level.

To have a stable system voltage at all busses, it essential to know how close an individual operating point to the boundary point of being stable or unstable to prevent the power system from going towards the final instability voltage state. In most cases, voltage collapses occur after a couple of minutes of the time instant of a disturbance. Thus, studies take often the voltage stability as a static phenomenon into account.

In [29], several voltage stability indices are mentioned. These indices can be used to assess the voltage stability and predict the collapse voltage blackouts:

a. Examine voltage stability using PV and QV curves
b. Investigate stability margins using power flow method.

Note that load margin is the distance from the current operating point to the theoretical or assumed unstable position and can further be defined as the total increment of a load in a specific pattern, which may lead to voltage collapse at a certain instant.

Methods (a) and (b) assume of load change in a linear direction. However, the real results are different than the theoretical because the direction of load change in practice does not follow the assumed paths. Also, it is too complicated to take all possible routes of load change into account.

c. Predicting voltage collapses using load flow solutions and Y-bus system indices
d. Predicting voltage collapses using load flow Jacobian indices

Both methods of (c) and (d) require solutions of load flow at any instant of a load change, and, advanced data topology to update Y-bus system to combine all possible changes in the configuration of the system.
Note that all four methods mentioned above are complicated to be used for online applications because their developments are based on the measurements from SCADA systems, which have slow data refresh rate.

The current developments based on Synchronized Phasor Measurement units have proven the possibility of obtaining fast data refresh rate, e.g. 50 times per second in 50Hz systems. Therefore, it is possible to build Wide Area Monitoring and Wide Area Control systems for the assessment purposes of voltage (in)stability.

Furthermore, the phasor measurement methods can be categorized into:

e. Local Phasor Measurement-based methods: uses Thevenin equivalent concept.

f. Global Phasor Measurement-based methods: uses algorithms based on extensive measurements.

Next, two voltage stability indices that are suitable to be used for real-time applications, are described:

g. Real-Time Voltage Stability Risk Index [30]: this method is performed using three calculation levels:

- Calculating the RMS voltage value of a measured bus voltage
- Estimating several moving average voltages for the calculated RMS values.
- Computing a percentage diversity between the average number of moving voltages and the measured voltage buses.

In general, Risk Index can be obtained by dividing the area obtained from the percentage diversity by several sections, resulting in transferring this index from real-time phasor measurement to an upper monitoring index. The final index output, which indicates the voltage stability, is further obtained by sequencing the upper monitoring index.

h. A System-Wide Improved Voltage Instability Monitoring Index [31]: this index is suitable for online applications, since, it needs less computational efforts than other methods. The primary objective of such index is to detect the relative long-term voltage stability based on measurements of voltage phasors and magnitudes at all system buses.

C. Rotational Inertia in Power System

From the perspective of stability, any power system develops, in general, restoring forces that are equal or greater than the disturbing forces, to return the system to its steady-state following disturbances. The steady-state stability is typically studied using the swing equation mentioned earlier in this document, which describes the transients in the rotor angle of a synchronous generator. During disturbances, the change in this angle leads to change in real power, resulting in frequency oscillations.

Stated in [6] that the position of both the rotor axis and the corresponding magnetic field is fixed at steady-state conditions. The angle between these axes is often called the torque angle or the power angle. During this state, both torques; mechanical (T_m) and electromagnetic (T_e), are equal by neglecting any losses.

When a power system is subjected to perturbations, a relative motion is developed due to acceleration/deceleration of generator rotor concerning the rotating air gap. This motion is usually described by the swing equation. Following a power flow imbalance event, the rotor may change its state in response to the new power-angle position.

By using the second law of Newton, it is possible to express the torque equation of the mechanical dynamics of synchronous generators:

$$J\frac{d^2\theta_m}{dt^2} = T_m - T_e = T_a \qquad \text{in } [kg \cdot m^2 \cdot s^{-2}] \tag{C.1}$$

Where:

- T_m = mechanical torque in $[kg \cdot m^2 \cdot s^{-2}]$
- T_e = electromagnetic torque in $[kg \cdot m^2 \cdot s^{-2}]$
- T_a = acceleration torque as results of disturbances in $[kg \cdot m^2 \cdot s^{-2}]$
- θ_m = rotor angular displacement concerning a stationary reference axis on the stator in [degree]
- ω_m= rotational speed with reference to a stationary frame in [rad/s]
- J = total equivalent inertia of the drive train within power plants that resists any change occurs in the system in case of an imbalance between both torques in $[kg \cdot m^2]$

Due to the importance of rotor speed, the angular reference is often chosen in such way that the rotating reference frame will synchronously move with constant angular velocity (ω_{sm}), resulting in:

$$\theta_m = \omega_{sm}\, t + \varphi_m \qquad \text{in [degree]} \tag{C.2}$$

Where (φ_m) is the rotor position before subjecting the system to disturbances. By taking the derivative of the previous equation, it is possible to express the equation of rotor angular velocity:

$$\omega_m = \frac{d\theta_m}{dt} = \omega_{sm} + \frac{d\varphi_m}{dt} \text{ in } \left[\frac{rad}{s}\right] \tag{C.3}$$

With rotor acceleration in the form of:

$$\frac{d^2\theta_m}{dt^2} = \frac{d^2\varphi_m}{dt^2} \tag{C.4}$$

Substituting equation (C.4) into equation (C.1):

$$J\frac{d^2\varphi_m}{dt^2} = T_m - T_e \tag{C.5}$$

Multiplying both sides of (C.5) by (ω_m), gives:

$$J\omega_m\frac{d^2\varphi_m}{dt^2} = \omega_m T_m - \omega_m T_e = P_m - P_e \quad \text{in [MW]} \tag{C.6}$$

In general, the relation between rotational motion to linear motion is given by:

$$Rotation\ Energy = 0.5 * moment\ of\ inertia * angular\ velocity^2$$

$$Kinetic\ Engery = 0.5 * mass * \ velocity^2$$

Now, it is possible to express the general form swing equation that can be used during the stability analysing of rotor dynamics:

$$\frac{2\ \mathrm{E_{kinetic}}}{\omega_\mathrm{m}} \frac{\mathrm{d}^2\varphi_\mathrm{m}}{\mathrm{dt}^2} = \mathrm{M}\frac{\mathrm{d}^2\varphi_\mathrm{m}}{\mathrm{dt}^2} = \ \mathrm{P_m} - \ \mathrm{P_e} \quad \text{in [MW]} \qquad (\mathrm{C.7})$$

From the perspective of electrical system, it is more convenient to express equation (7) in terms of the electrical power angle (φ_e):

$$\mathrm{M}\frac{2}{\mathrm{p}}\frac{\mathrm{d}^2\varphi_\mathrm{e}}{\mathrm{dt}^2} = \frac{\mathrm{p}\ \ \mathrm{E_{kinetic}}}{\omega_\mathrm{e}}\frac{2}{\mathrm{p}}\frac{\mathrm{d}^2\varphi_\mathrm{e}}{\mathrm{dt}^2} = \frac{2\ \mathrm{E_{kinetic}}}{\omega_\mathrm{e}}\frac{\mathrm{d}^2\varphi_\mathrm{e}}{\mathrm{dt}^2} = \ \mathrm{P_m} - \ \mathrm{P_e} \text{ in [MW]} \qquad (\mathrm{C.8})$$

Where:

- $\varphi_\mathrm{e} = \frac{p}{2}\ \varphi_\mathrm{m}$ = electrical power angle
- $\omega_\mathrm{e} = \frac{p}{2}\ \omega_\mathrm{m}$ = rated electrical angular frequency
- p = number of poles of the synchronous generator
- $\mathrm{P_m}$ = the input mechanical power to the shaft of the synchronous generator
- $\mathrm{P_e}$ = the electrical output power

Usually, the study analysis of power systems is performed using per unit system; therefore, equation (C.8) can further be written in per unit terms as follows:

$$\frac{2}{\omega_\mathrm{e}}\frac{\mathrm{E_{kinetic}}}{\mathrm{S_B}}\frac{\mathrm{d}^2\varphi_\mathrm{e}}{\mathrm{dt}^2} = \frac{\mathrm{P_m} - \ \mathrm{P_e}}{\mathrm{S_B}} \quad \text{in} \left[\frac{\mathrm{MW}}{\mathrm{mVA}}\right] \qquad (\mathrm{C.9})$$

The left side of the equation (C.9) is the time derivative of the stored kinetic energy in the drive train of the system at rated speed. This energy is directly proportional to the rating power of the synchronous generator. The per unit inertia constant is thus equal to:

$$\mathrm{H} = \frac{\mathrm{E_{kinetic}}}{\mathrm{S_B}} = \frac{\mathrm{J}\omega_\mathrm{m}^2}{2\mathrm{S_B}} \quad \text{in [s]} \qquad (\mathrm{C.9})$$

Where ($\mathrm{S_B}$) is the base power. The primary function of machine inertia is to resist any change occurred in the rotational speed that is further translated into a deviation in the frequency of the generator EMF induced by the rotating magnetic flux of the field windings.

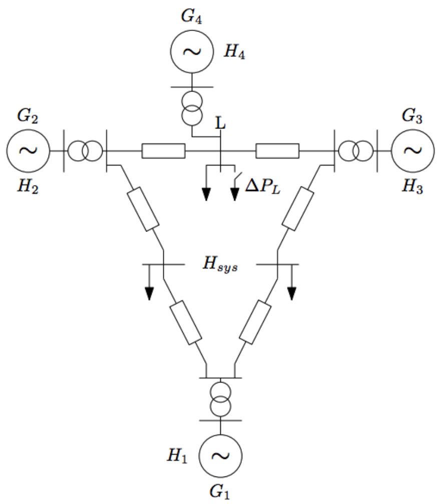

Figure C.1: test system for demonstrating the concept of synchronization mechanism with (H1 =6s, H2 = 3s, H3 = 9s, and H4 = 3s) [6]

Explained further in [6] that the change in the load in any power system influences the rotational speed of the interconnected generators, which results in an initiating of synchronizing forces between these generators. The change of a load followed by a deviation in rotational speed and a change in active power demand can be analysed using classical machine modelling and a test network as shown in figure C.1 above. Within this test network, all synchronous generators are in equilibrium condition, and they are rotating at rated (synchronous) speed = 50Hz.

At the instance (t_L = 0.1s), the demand for active power (ΔP) is increased at the load bus (L). By using the machine modelling approach, the power grid in the figure above can further be simplified to only the internal generators nodes and the load bus node (L). Moreover, using a specific tool, i.e. DIGSILENT Power Factory software, gives the possibility of analysing the rotational speed variation following a load change event of load change as illustrated in figure C.2 below:

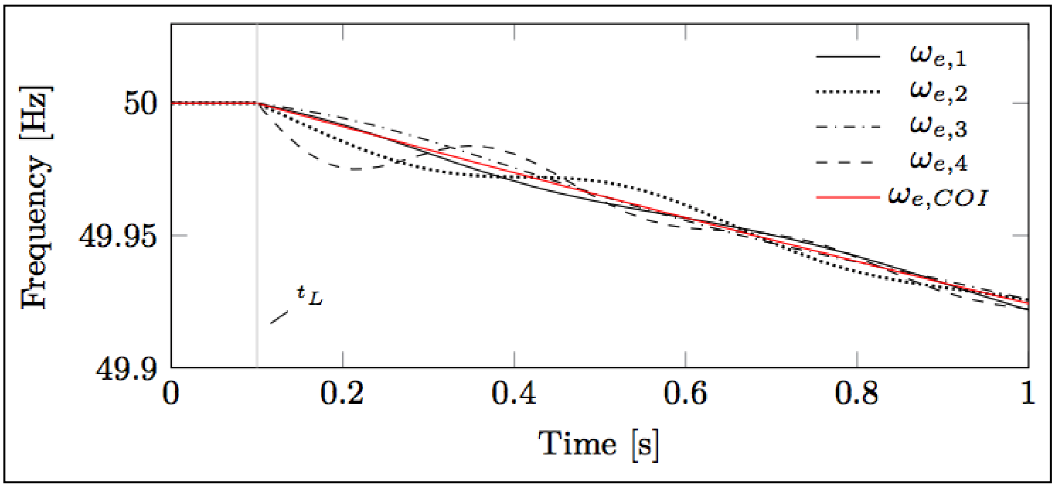

Figure C.2: rotational speeds variation of a synchronous generator [6]

According to the concept of rotational machine inertia, the generators rotor angles are kept constant although after applying load change steps. The required kinetic energy to maintain the supply-load balance is provided by the magnetic fields and not from the rotating mass, which in turns, results in distributing the effects of load change between all generators depending on the so-called the synchronising power coefficient of each generator.

In this way, all generators in the above test network will start decelerating at different speeds due to the various electrical distances from the load bus (L) and different inertia constants (H) values. The overall deceleration of all generators in the given network occurs that can be observed from the reduction of the total frequency of the system at so-called the inertial centre ($\omega_{e,COI}$).

Around the inertial centre, each generator will further follow some various motion oscillations, which results in the tendency of the synchronizing forces between the generators to pull the individual oscillatory motion of each machine together, leading to that all generators will decelerate at the same rotational speed.

Moreover, it is possible to consider the individual generators of the given network as a single unit because of the synchronising mechanism within the transmission system. The mechanical behaviour of this unit can be expressed using a single swing equation, resulting in the possibility of formulating the overall response of all generators in terms of the total system inertia constant:

$$2H_{system}\frac{d\omega_{e,COI}}{dt} = P_G - P_L = -\Delta P_L \text{ in [MW]} \qquad (C.10)$$

With:

$$H_{system} = \frac{\text{sum of } (H_i * S_i)}{S_{system}} = \frac{\text{sum of } (E_{kin,i})}{S_{system}}, \qquad i = 1, 2, 3, 4 \quad \text{in [s]} \qquad (C.11)$$

Where:

- H_i= per unit inertia constant of individual generator
- S_i = individual synchronous generation capacity connected to a generator
- S_{system}= common system base equals to the total synchronous generation capacity
- H_{system}= equivalent per unit inertia constant of the overall system
- P_G = sum of all mechanical output powers of individual generator turbines
- P_L = total load in the power system

The swing equation mentioned above gives the possibility of interpreting the total inertia of a power system as the resistance due to the exchange of kinetic energy between all generators in the system to resist the deviation in frequency around the inertial centre occurred due to any change in the power balance between supply and load. Therefore, the system inertia concept cannot be considered as a constant value because of the variation of both the number and the type of synchronous machines at generation and load sides over time as explained in [6].

D. Virtual Inertia Response

Recent studies have proven that the future energy transition towards a power system with more renewable sources integration and less fuel fossil generation units will have significant impacts on the system stability criteria, primarily, on frequency stability criterion due to the lack of inertial response from renewable sources as mentioned earlier in this document.

Mentioned in [32] that the European Network of Transmission System Operators for Electricity, ENTSO-E, has shown that the massive deployment of RES units in the Nordic grid will increase frequency deviations. Therefore, the need of virtual inertia from wind turbines and PV-solar plants is now mandatory to provide the required inertial response for the future power systems. Also, many research papers have shown the possibility of implementing virtual inertia as an ancillary service to reduce frequency deviation in large power grids.

According to this issue, different control actions have been developed over multiple time frames to reduce the deviation in system frequency as shown in figure D.1 below. Typically, the restoration process of system frequency is performed using three controls (primary control, secondary control, and tertiary control). When the system is subjected to disturbances or power imbalance events, synchronous generators are not able to react instantaneously to restore the steady-state of the power system. The kinetic energy, which is stored in the rotating mass of these generators, provides the possibility of opposing frequency deviations through inertial response until the primary (govern) has been activated, as indicated in [32].

In the future power system with significant RES penetration, the inertial response is expected to be low, resulting in an increase in ROCOF and a low minimum frequency point (frequency nadir) in a small period. The primary (governing) control may not be able to react within a short time (e.g. less than 10s) to counteract the frequency oscillations (see section AB in the figure below).

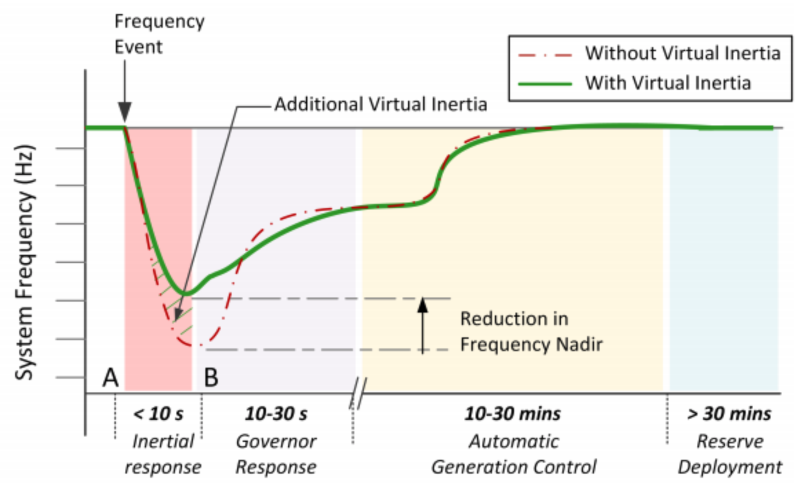

Figure D.1: Multiple time-frame frequency response during frequency deviations [32]

The relation between the change in power and frequency deviation can be expressed as follows:

$$\frac{2H}{f}\frac{df}{dt} = \Delta P = \frac{P_m - P_e}{S_B} \quad \text{in} \left[\frac{MW}{MVA}\right] \qquad (D.1)$$

Where $\left(\frac{df}{dt}\right)$ is the rate of change of frequency (ROCOF). The expected reduction in system inertia (H) will cause an increase in ROCOF, lower frequency nadir, and less inertial response, resulting in more significant frequency oscillations in tight time.

A significant low inertial response may lead to tripping of frequency relays or other protective equipment, resulting in cascaded outages. A possible solution for this issue is to introduce virtual inertia to the future power systems with the fundamental requirement of the ability to operate in a short period and an autonomous form.

Stated in [32] that virtual inertia systems are in general a combination of control algorithms, renewable energy sources (RES), energy storage systems (ESS), and power electronics. The development of virtual inertia systems (VIS) differs from one power system to another, for instance, some VIS topologies tend to imitative the exact behaviour of conventional SGs using detailed mathematical models to replicate the dynamic behaviour of these generators, while other concepts use the traditional swing equation to determine the response of SG. Figure D.2 shows a list of the different VIS approaches:

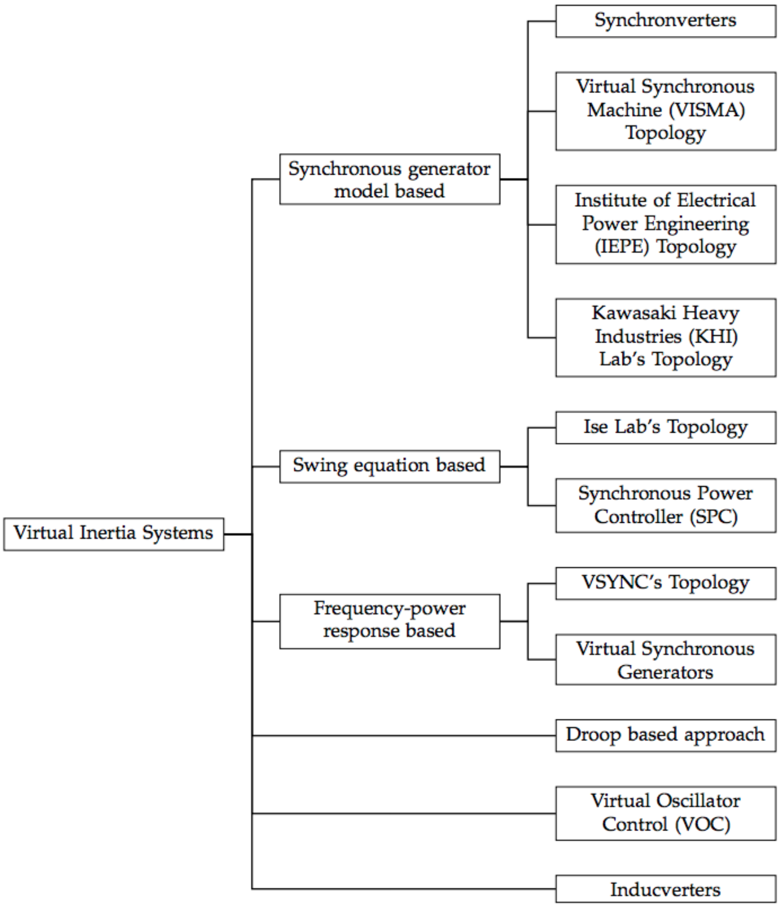

Figure D.2: a list of different VIS approaches [32]

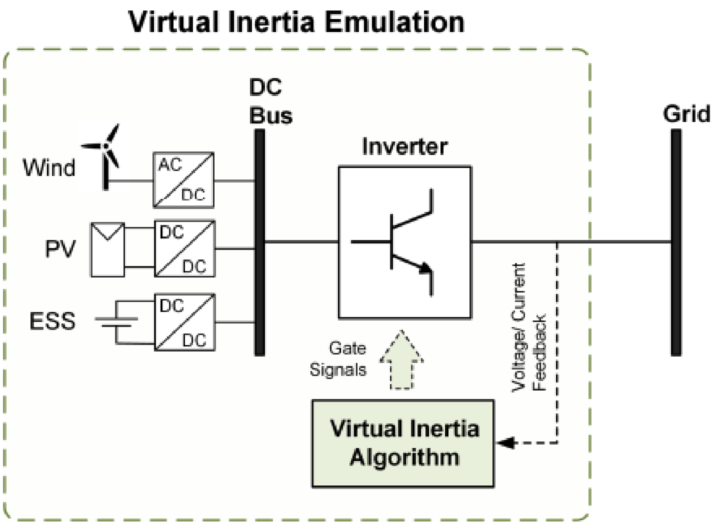

Figure D.3: virtual inertia main concept [32]

The main concept of virtual inertia is shown in figure D.3 above. Its operation based on voltage-current signals from the inverter output. These signals created so-called gating commands to enforce RES and EES units to behave as synchronous generators (SG) from the grid perspective.

The primary advantages and disadvantages of the various VIS topologies are highlighted in table D.1 below as given in [32]:

Table D.1: Pros and Cons of different VIS approaches [32]

Control Approach	Pros	Cons
SG based model	Accurate representation of SG dynamic behaviour	Issues of numerical instability
	No need for frequency derivative	
	Synchronization is implemented using Phase Locked Loop (PPL)	No over-current protection due to the implementation of voltage-source
Swing Equation based model	Less complex compared to SG based model	Deviation in frequency and power
	No need for frequency derivative	No over-current protection due to the implementation of voltage-source
	Synchronization is implemented using (PPL)	
Frequency-power response-based model	Simple to be implemented using current-source; comprises over-current protection	PLL stability issues
		Need for frequency derivative, resulting in noise
Droop-based approach	The same approach used in typical droop control of conventional SG	Slow transient response
	Less need for communication	

In [32] different simulations have been performed to study the behaviour of the topologies as mentioned earlier. It can be concluded that by an efficient method of parameter selection for these different topologies, an accepted inertial response level can be attained regarding power exchange from the front-end inverter and frequency deviation reduction. The choice of a suitable topology depends mainly upon the desired level of SG dynamic behaviour representation and the application of a power system.

One of the obstacles in the way of introducing more virtual inertia systems to power grids is the system inertia estimation issue. Estimation of inertia is expected to be critical in the future power system with a massive deployment of RES units. The available system inertia will be dependent on the state of RES units (online or offline), and on the availability of different resources, e.g. irradiance of PV-solar, wind speed of wind turbines, and the charge of EES.

Mentioned in [32] that the current market structure for virtual inertia systems and inertia from SGs is insufficient. Power system operation is typically based on the assumption that both SGs and specific loads in the power systems provide a sufficient inertial response to counteract frequency deviations. In case of inverter-dominated (future) power system, the inertial response will become strong enough to be a concern, and RES units will seek more financial compensation.

A possible cost-effective solution is a market-based concept that is the ability to guarantee sufficient inertial services. System inertia response in future power girds can be provided, for instance, by PV-solar systems with suitable energy storage devices to operate PV-solar systems below the Maximum Power Point (MPP) with a reserve for the inertial response.

Stated in [33] that the future system inertia should be traded concerning inertia metric and not in power/energy terms. In other words, the assumption of charge-free inertia services would not be valid, since the supplying of virtual inertia will demand additional costs. An appropriate trading method is the use of inertia unit $[\mathrm{kg} \cdot \mathrm{m}^2]$, which represents, in general, the behaviour of synchronous generators concerning system inertia. Classification of inertia cost (€/kg.m2) could be a satisfactory comparison parameter for the supplying of virtual inertia by various sources.

Further in [32] a method has been proposed to recognise system inertia as power quality service (PQS) metric as in the case of a micro-grid operator. Within this grid, the possibility of inertial services provision is based on specific criteria, for instance, the maximum admissible ROCOF rate or the maximum allowable frequency deviation range. The power quality of this grid could then be assessed through the response time after subjecting the micro-grid to frequency deviation event.

Moreover, energy storages systems, i.e. ultra-capacitor, are typically intended to control the dynamic frequency behaviour of the hybrid power system through power electronics converters. The life-time of these systems could be affected by the virtual inertia that is introduced to the power system to eliminate fast-frequency events. In [32] a solution for this issue has been proposed based on a parallel combination of ultra-capacitors and batteries.

The combination mentioned above provides the possibility of virtual inertia provision and reducing the influences of fast-frequency dynamics on the batteries since ultra-capacitors can supply high-frequency components. Other solutions to offer virtual inertia and reducing fast frequency dynamics are, for instance, energy storage system based on the flywheel and PV-solar panels with the capabilities of built-in energy storage system.

Nowadays, the focus is on finding alternate energy resources, which can provide virtual inertia. A possible inertia area that deserves to be more explored is the thermal inertia coming from heating, ventilation, and air conditioning (HVAC) systems of buildings and data centres. As explained in [15], the amount of power consumed by these systems, which are developed using power electronics devices, may be controlled to provide the required virtual inertia.

Usually, the synchronous generators of large power systems have inertia constant in the range of (2s-9s) as mentioned in [34], while the inertia of wind-turbine is in order of (2s-6s). This inertia is often stored as kinetic energy in the rotating blades of the turbine and decamped from the power system. Theoretical, it is possible to use this isolated inertia and support the system by developing new control techniques.

Finally, the indicated topics in this section, e.g. system inertia estimation, virtual inertia market structure, energy storage system for the provision of virtual inertia, and improvement of control strategies could be appropriate research directions. Such investigations can be used for further work on the possible ways of eliminating frequency deviation in future hybrid power system with dominated-inverter generation units and less inertial response.

E. Inertia Reduction and Cascading Contingencies

Large system frequency deviations often occur due to tripping of large generation units and high voltage DC links, resulting in an imbalance between supply and demand sides. Such tripping can lead to frequency declining below the desired operating range, which in turn, disconnects the generation units and loads from the rest of network, causing cascades power outages, especially for a low inertia system.

A low inertia system is defined in [35] as the dependency of a hybrid power system with dominated-inverter generation units on a few synchronous generators to maintain the frequency stability of the system after the tripping of some AC interconnections. Within such system, undesired deviation in system frequency can occur with high ROCOF.

During rare situation, tripping of a certain number of interconnections can lead to ultimately network separation, resulting in operation of some areas as islands, for instance, network separation in South Australia due to lightning, thunderstorm, and bus fire. Following a network termination, the tripped interconnection should be restored to re-connect the network of South Australia with the rest of Australian power system.

In [35] a 14-generator (50Hz) equivalent system of South-East Australian network has been studied by applying a specific case of cascading contingency, the so-called network separation event which represents the tripping of AC interconnections during power import of 450MW. The studied system is shown in figure E.1 below.

Area (5) of this system represents the South-Australian power network, which includes the power generation of both wind-turbines and PV-solar systems. Moreover, three conventional generators are introduced to the studied system with a total installed capacity around (2300MW). To examine the dynamic behaviour of the system, these generators are modified with standard primary (governs) controls, exciters, and stabilisers.

During this study, the number of online generators has been varied between (4-6) at different periods. Such variety makes possible to analysis the system operation with different low inertia levels, the number of online synchronous generators has been varied between 4-6. The ratings of these conventional generators are:

- PPS-5 with 6 units and for each unit: 150MW installed capacity, 166MVA power rating, and 7.5s inertia constant (H).
- TPS-5 with 4 units and for each unit: 200MW installed capacity, 250MVA power rating, and 4s inertia constant.
- NPS-5 with 2 units and for each unit: 300MW installed capacity, 333MVA power rating, and 3.5s inertia constant.

Moreover, two load scenarios have been investigated for each of the cases mentioned above (day-time and night-time scenarios). The simulations of these scenarios are based on a high penetration of renewable sources with a limited amount of power generation coming from conventional generators, resulting in low system inertia

Table E.1 below gives the operating conditions for network separation case:

Table E.1: operating conditions for network separation case [35]

Load Condition	No. of online generators	Total available inertia (MWs)	Synchronous Generation (MW)	Wind Generation (MW)	PV Generation (MW)
Day-time (2200MW)	6	6820	600	800	0
	5	5575	570	830	0
	4	4575	430	970	0
Night-time (1200MW)	6	6820	600	190	400
	5	5575	570	220	400
	4	4575	430	360	400

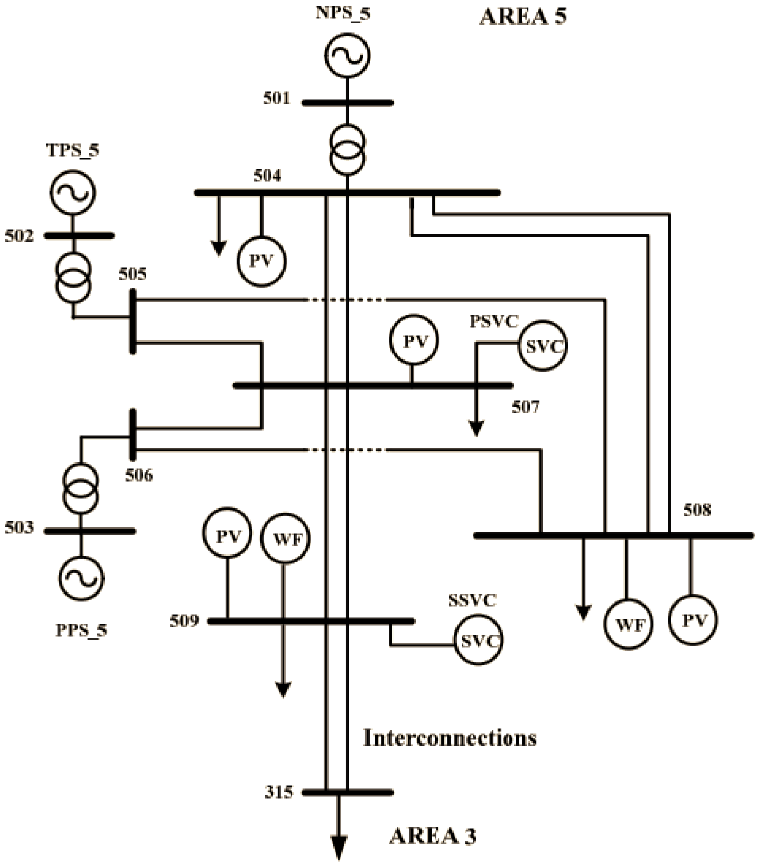

Figure E.1: South-East Australian equivalent power system [35]

At night-time load condition with six online generators, system frequency drops from (50Hz) to (48.61Hz) after the tripping of some AC interconnections. Simulation results showed a further declining of frequency nadir when the number of online generators was changed from 6 to 4. This frequency decline results in the activation of Under Frequency Load Shedding (UFLS) system, since the acceptable frequency operating ranges, is between (49-50Hz) as stated in Australian Grid Code. A worst case is when the system frequency further drops below the UFLS threshold, leading to system load shedding that causes a system collapse. This case is illustrated in figure E.2 below:

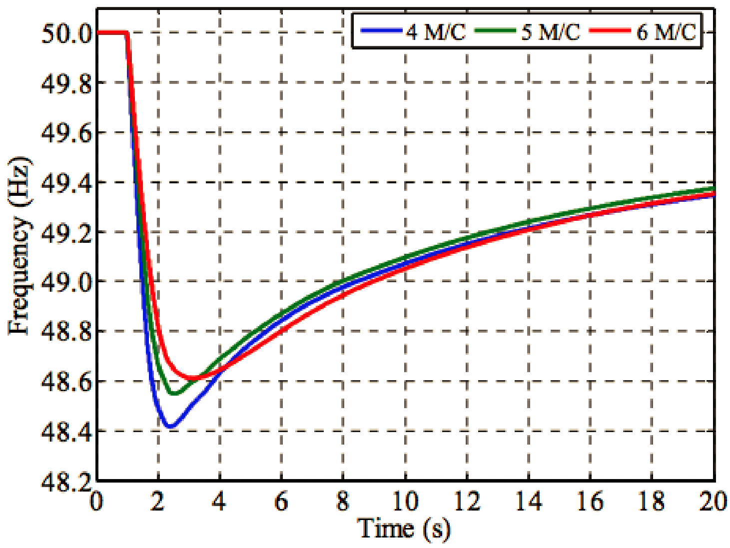

Figure E.2: Frequency response after tripping of AC interconnection at night-time load condition [35]

Typically, it is assumed that the value of ROCOF following a contingency must be (1Hz/s) for (1s) to prevent further tripping of AC interconnections. Simulation results have also shown higher values of ROCOF after (1s); the highest value was around (1.51Hz/s) in case of 4 online generators. These higher values may cause a triggering of generators protective equipment, resulting in secondary tripping of AC interconnections.

Figure E.3 below gives an example of the impact of higher ROCOF values on the operation of the studied power system. In this example, one generation unit out of 6 online generators has been tripped by its protective equipment when ROCOF exceeded the acceptable margin of (1Hz/s). This secondary (or subsequent) trip causes, in turn, a further decrease of system frequency nadir; from (48.61Hz) to (48.1Hz).

Therefore, the possibility of frequency response deterioration due to secondary trip is very high that often increases system load shedding quantity to restore the system frequency stability, especially for systems with low inertia level.

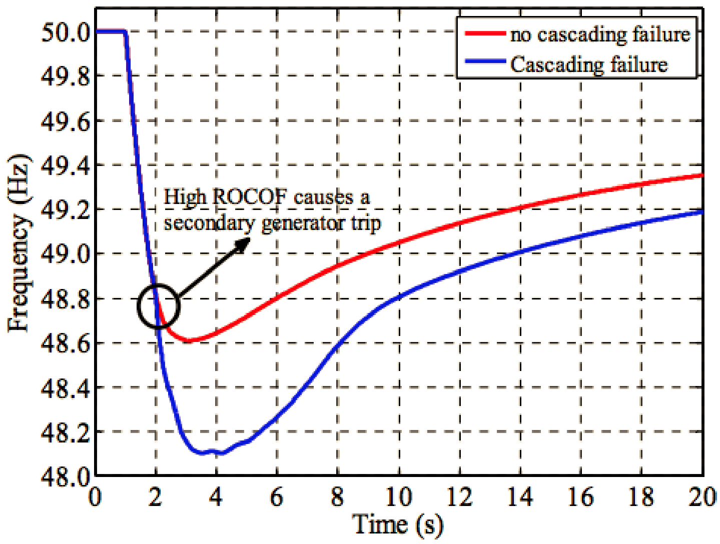

Figure E.3: Frequency response due to secondary trip [35]

Moreover, frequency decline below the acceptable margin has occurred during day-time condition. In case of 6 online generators and AC interconnection tripping, for instance, the frequency nadir dropped until (48.77Hz), and ROCOF was around (1.1Hz/s) after (1s), resulting in a secondary trip of one of the generation units. Figure E.4 shows the simulation results of AC interconnection tripping at day-time load scenario:

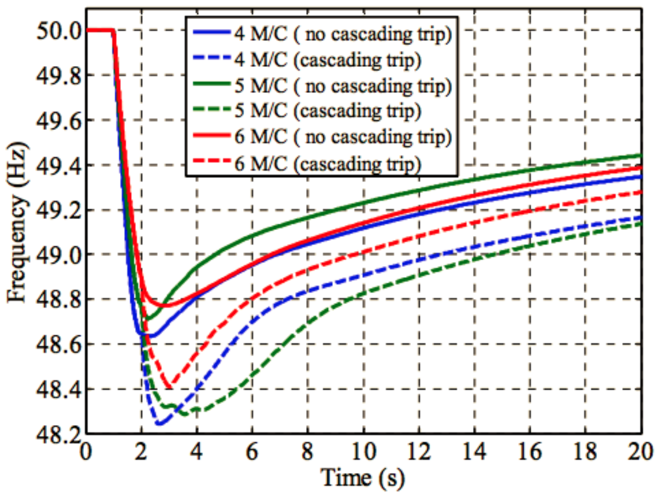

Figure E.4: Frequency response after tripping of AC interconnection at day-time load condition [35]

A comparison between figures E.2 and E.4 gives an indication of a more notable frequency decline at the night-time condition than at the day-time condition. The reason for this difference is related to the contribution of PV-solar to the total amount of power generation. Typically, there is no PV generation at night-time, while the PV generation during day-time is assumed to be around 66% of the total capacity for the above-studied system.

Following a serve, ROCOF depends mainly on the total inertia amount in the system, and, on the size of contingency. To limit ROCOF to (1Hz/s) after (1s) following a (450MW) synchronous generation trip, the amount of total inertia in the system should be around (11250MWs), whereas the highest inertia of the above-studied system was around (6820MWs) in case of 6 online generators.

Mentioned further in [18] that several mitigation measures are therefore required, e.g. introducing additional inertia to the system, to prevent cascading failures caused by subsequent trips of AC interconnections. Such measures can be achieved, for instance, by using a certain number of retired conventional generators as synchronous condensers.

These condensers may have the possibility of providing additional inertia to the system, which in turn, improves the system frequency response during the periods of high penetration of renewable energy sources, resulting in better power grid performances and customer services. However, a significant issue related to the development of such action is the high costs that are needed to convert the retired generators to be used as condensers.

The two figures below show the results of introducing such mitigation measures to the above-studied system:

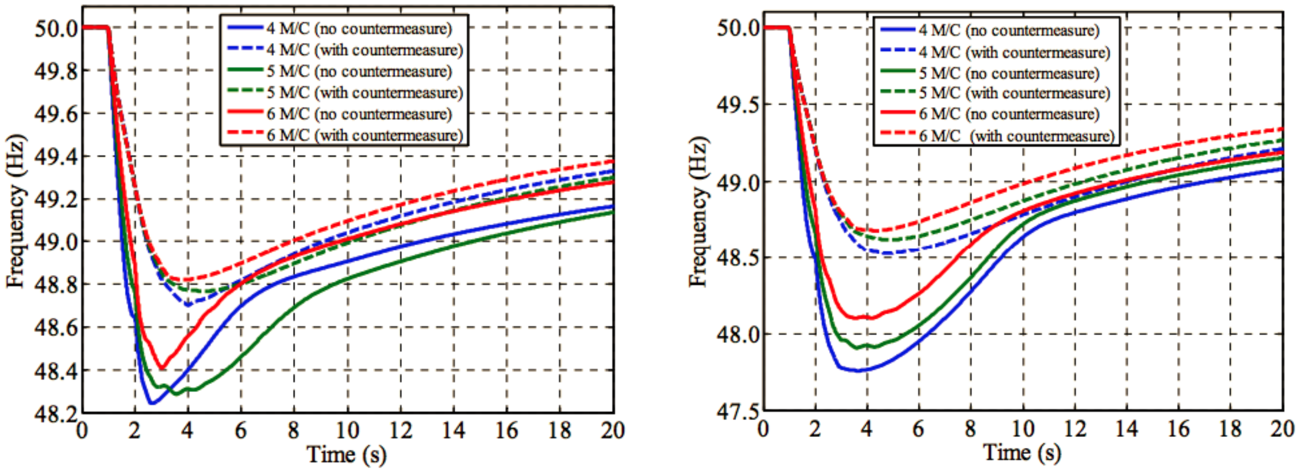

Figure E.5: Frequency response after tripping of AC interconnection with introducing countermeasures at the night-time and day-time load condition, respectively [35]

Finally, it can be concluded from paper [7] that any loss of interconnections will not cause a trigger of load shedding system in the first instance. Such failures can lead to tripping of PV-generation, for example, resulting in frequency deviations from the acceptable operating range. As consequences, an unusual amount of load shedding should be spent to retain frequency at the desired margins.

In future power system with less amount of inertia due to increased penetration of RES, a deterioration of frequency response is highly expected; therefore, the amount of load shedding can be further increased, which in turn, may cause cascading outages.

A possible solution proposed in [7] is to use wind-turbine generators to support system frequency using specific control systems that may prevent the subsequent PV trip. However, such solutions are still academic work and require more investment/efforts to be implemented in a real electric power system.

F. Frequency-Load-Control and Performance

This appendix describes the importance of the **Load-Frequency-Control** (LFC) for a secure and stable operation of power system briefly. This mechanism is often used by TSOs to carry out their operational tasks as mentioned in [21], [36], [37], and [38].

1. Traditional System Frequency Control

Typically, the frequency control actions in a power system can be categorised into two phases as given in [36]. The first phase is often called inertia response, in which the responsible frequency control scheme is not triggered yet. Frequency deviations within this phase are arrested using kinetic energy stored in the rotating mass of generators because the inertia damps out the frequency oscillations.

In general, system inertia plays within this stage a key role in keeping the frequency of power system at its regular scheduled value. Frequency restoration is often carried out by dedicating the extensiveness of frequency oscillations, and then, adjusting the eigenvalues and eigenvectors of stability matrix, which in turn, computes the mode and stability shape of transient response.

The larger the inertia, the smaller the rate of change in generator's rotor speed following serve disturbances. This type of response of the conventional synchronous is often determined using the following equation:

$$P_g - P_l = \frac{d\left(\frac{1}{2} J_{sysm}\ \omega_{el}^2\right)}{dt} \quad \text{in [MW]} \tag{F.1}$$

Where:
- P_g = generated power
- P_l = power demand
- ω_{el} = electrical angular frequency
- J_{sysm} = inertia of the system

The right hand of equation (F.1) is the derivative of the stored kinetic energy in the rotating mass of single generator, and it is directly related to the power rating of that generator. This energy often called the inertia constant of a generator:

$$H_{gen} = \frac{\left(\frac{J_{sysm}}{p^2}\ \omega_{el,0}^2\right)}{2\ S_{gen}} \quad \text{in [s]} \tag{F.2}$$

Where:
- S_{gen} = nominal apparent rating power of a generator
- $\omega_{el,0}$ = nominal system frequency
- p = number of pole pairs

In general, this constant is expressed in seconds, and it is typically on the order of (2-9s) for large electrical power systems. Equation (F.1) can be further written in per unit form, resulting in the expression of ROCOF.

This rate is typically computed using the magnitude of the power imbalance and the system inertia:

$$\frac{d\omega'_{el}}{dt} = \frac{P'_g - P'_l}{2\ H_{system}} \quad \text{in} \left[\frac{MW}{s}\right] \tag{F.3}$$

In the second phase, the frequency deviation is stabilised and then restored to the standard value by the different control actions shown in figure F.1 below. These control actions are typically executed using different stages; each stage has with different characteristics and depends on other stages as given in [21]:

- Primary Control (PC): initiates within seconds
- Secondary Control (SC): replaces PC over minutes and is being activated only by TSOs.
- Tertiary Control (TC): partially complements and finally replaces SC by re-scheduling generation plans and being activated only by (responsible) TSOs.
- Time Control (TiC): corrects the global time deviations of all performed actions.

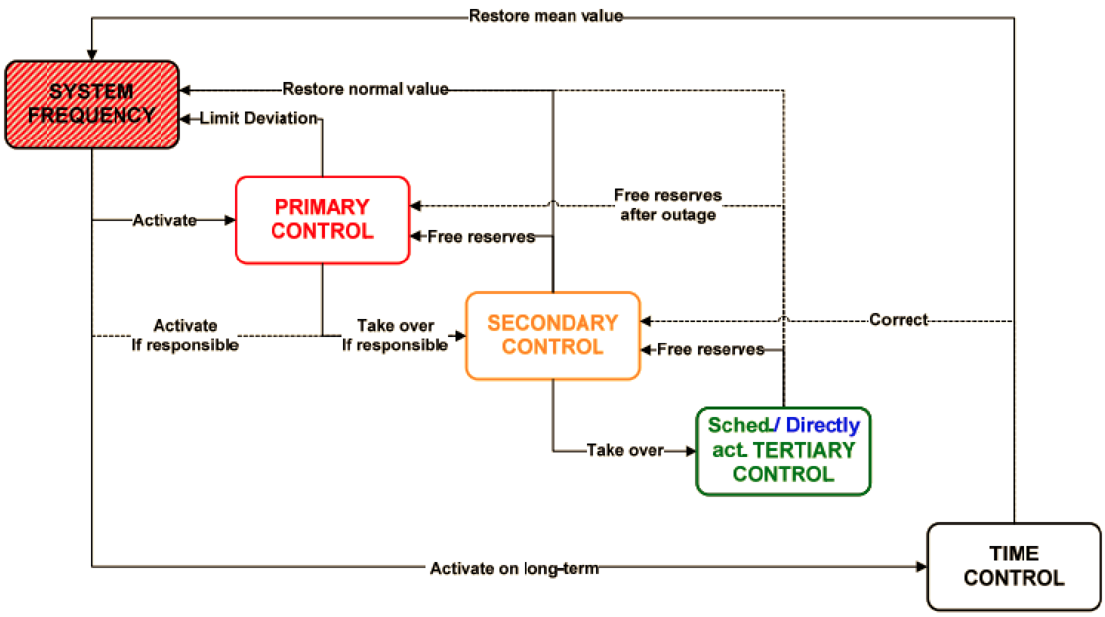

Figure F.1: control strategy and actions during system frequency deviations [21]

The primary function of this control scheme is to keep a balance between both supply and demand sides within the synchronous area of a power system to provide reliable operation and stable system frequency.

Stated in [21] that the normal system frequency (NSF) value is standardized for European Continent at (50Hz). When the frequency deviation exceeds this value, a power flow imbalance occurs, resulting in undesired operation of power system and activation of the above-shown scheme. In general, the size of frequency deviation (FD) is defined using different criteria.

The balancing and control of system frequency can be performed over a continuous-time using various resources as given in the figure below:

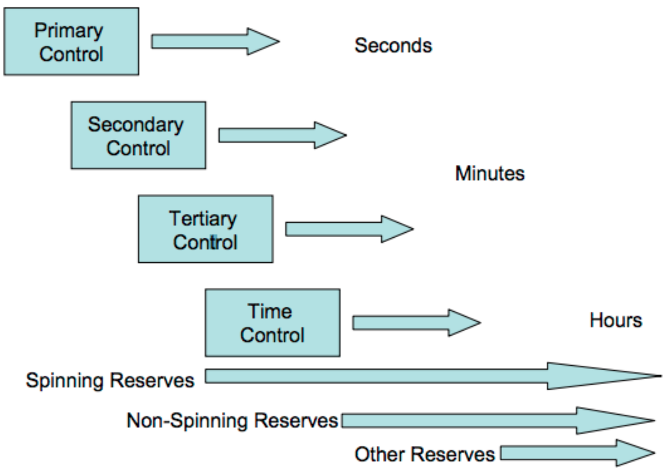

Figure F.2: power-frequency capability of wind turbines in some countries [37]

Primary Control

PC is often known as the Frequency Response (FR) of the system that is executed within the first few seconds after subjecting the system to (serve) disturbances to stabilise the different interconnected components of a power network, but not restoring the standard value of system frequency. This response is typically provided by:

a. **Governor Action:** Governors usually detect any change in the speed of their relevant generator and adjust the kinetic energy input into the prime mover of that generator.

b. **Load:** The change in speed of motors in an interconnection area is directly related to the change of system frequency. For instance, when the system frequency declines, engines will turn slower and draw less energy, resulting in rapid reduction of system load. Such decrease can further be provided in the form of secure resources, e.g. ancillary services. For safety network operation, a part of the load may thus be dropped by under-frequency load-shedding programs to provide a stable system following perturbations.

One of the most known types of serve disturbances in an interconnected network is the loss of a generator that often results in frequency drop. The amount of spinning reserve is directly determined from the amount of available FR.

Thus, the term of primary control is typically reserved for local control actions that manage the amount of active power generation in response to frequency deviation. PC design must comply with the standard regulation objectives, i.e. quasi-steady state and dynamic objectives, in a stable mode following large disturbances.

From the perspective of dynamic behaviour, the rotational acceleration of synchronous generator is always driven by the difference between the input shaft power from the prime mover and the output electrical power supplied from generator terminals to the electrical network. When this difference is zero, generator will then operate in its steady-state at a constant speed as mentioned in [38].

The operation of PC governor is directly related to the direct "droop" feedback, which modifies the mechanical shaft power "negative sign" proportion to the speed error of generator's rotor. The primary objective of this droop is to ensure that the mechanical power is matched to the electrical power.

Secondary Control

The primary function of SC is to maintain the minute-to-minute balance throughout the whole day and to return the system frequency to the standard scheduled value, which is typically 50 or 60Hz, following a disturbance. SC is often provided by both spinning and non-spinning reserves as shown in figure F.2.

A conventional method to implement SC is through the Automatic Generation Control (AGC), which usually operates together with Supervisory Control and Data Acquisition (SCADA) systems. SCADA collects information about the electrical power network, e.g. system frequency, the output of generators, and the net actual power exchange between interconnected systems. These details provide the possibility of determining the energy balance between the interconnected systems in near-real-time.

AGC determines further the so-called Area Control Error (ACE) from power exchange and frequency data that provides information about the actual state of the system, e.g., if the system needs to be balanced or not, to adjust the amount of power generation. ACE tools have thus the ability to compute the most suitable economic output for generating resources while observing energy balance and frequency control, which is often executed using sending set-points to synchronous generators.

In [38], it is given that SC operates from a perspective of more centralised power system. By employing a suitable design and operational agreement as defined "Balancing Authorities", SC will have the ability to maintain the load and generation balance within an area with a power flow imbalance.

From the engineering perspective, SC provides the possibility to update the desired set-points that are usually used to feed the control loops of individual generators' PC, resulting in a better adjusting of power generation among the relevant areas. Therefore, the relative size of the change in the output power of different generators is often set by direct droop feedback gains in the PC. Moreover, PC is often realised as a closed loop feedback with automatic actions, while, the slower time scales (several minutes) of SC, allows operators to automate and adjust the operation of this control.

Mentioned further in [38] that the maintenance of balance between generation and load is typically ensured within an adjacent electrical region as defined by Balancing Authority. Such region, which consists of voltage buses and measurement devices, is responsible for maintaining the power exchange with the adjacent areas, and, regulating system frequency. These objectives are typically combined in a single measure "ACE" as mentioned before. This measure is often used for multi-area interconnected systems; it is the weighted sum of power flow deviation from the target set-point with a term that is proportional to system frequency deviation. This sum provides the ability to check whether a generating area is well controlled or not.

- **Tertiary Control**

TR covers actions taken to get resources in place to manage actual and future contingencies. Common types of this control are the reserve deployment and restoration that are used after subjecting the system to perturbations.

- **Time Control**

The operation of frequency control scheme is not always perfect because of several errors, i.e. problems with SCADA hardware/software, or communications errors. These errors in addition to the existed variations of load and generation profiles sometimes lead to the inability of keeping the net ACE value between interconnected systems at zero, resulting in frequency fluctuation around the standard value. For this purpose, each interconnection is provided with a so-called Time Control (TC) process to maintain the long-term average frequency at the scheduled value. In short, the stability of system frequency represents the ability of the system to keep a balance between supply and demand side, by ensuring that the resources mentioned above are available at any time to react on power imbalance events.

2. Frequency Control in Future Power System

Stated in [36] that system inertia depends in traditional power system with synchronous generators on two factors: the inertia of each of the synchronous generators in a power plants, and on the number of operating generators.

On the other hand, converter-connected wind turbines and PV-solar units provide in general no inertial response because they are electrically decoupled from the grid frequency. Therefore, replacing conventional generation by RES units can lead to a lower inertia system, resulting in high ROCOF values in case of frequency deviation.

The higher increase in ROCOF values can cause cascading outages of generation units. Due to these outages, a part of power system becomes sometimes electrically isolated from the rest of the power system, resulting in a so-called islanding operation, which can often be detected by ROCOF or vector shift relays.

Following an islanding operation, a power flow imbalance occurs between generation and load sides, resulting in a rapid change of system frequency, which depends mainly on the amount of imbalance power and the inertia level in the islanded network.

If the protective system of a low inertia system is equipped with many of these relays, the relays can also affect the frequency control scheme, see figure F.1. In case of serve disturbances, the ROCOF relays may cause a disconnection of the power generation units. Typically, these relays are set in a range of (0.1-1 Hz/s), depending on the available system inertia of the grid.

Further explained in [36] that RES units are also not able to provide primary or secondary control. Therefore, a future power system with dominated converter-connected units will have a low-frequency response, because not only the ROCOF values are increased, but also, the standard frequency operating ranges will be change. With more and more RES penetration, a further decrease in frequency nadir can also result in load shedding and major black-out.

In some countries with high RES penetration, TSOs require sometimes wind power plants to operate their turbines near to the behaviour of conventional power plants, e.g., by setting the wind turbines at standard frequency value and request a frequency response as illustrated in figure F.3.

When system frequency drops below point B, the coupled frequency response system to wind-turbine will try to increase the generation of active power, following the droop characteristic indicated by line B-A.

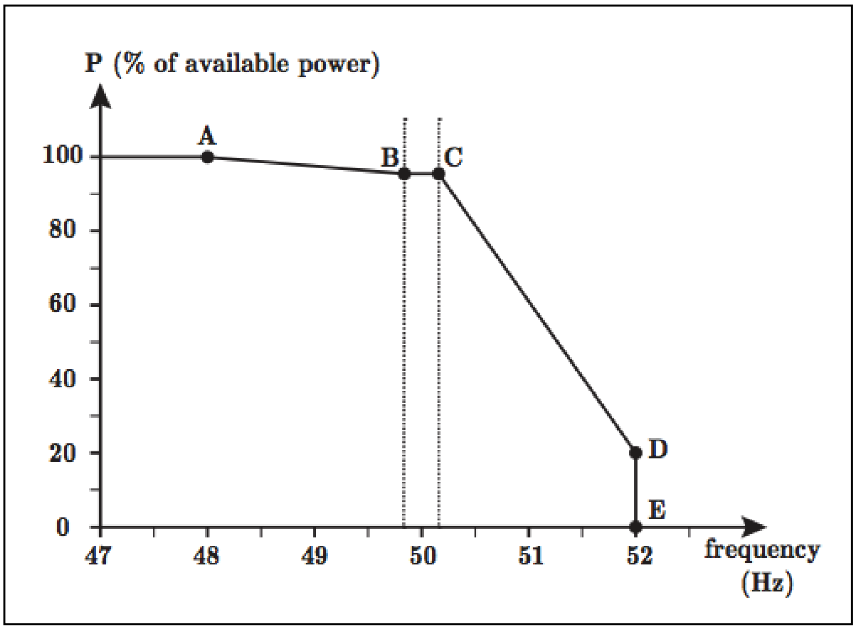

Figure F.3: power-frequency capability of wind turbines in some countries [36]

In general, PV-solar systems do not store any kinetic energy, but only a specific amount of energy in their coupled EES. In the future power system, a combination of PV-solar with specific batteries will give the possibility of controlling this energy to support system frequency.

On the other hand, wind farms without unique control systems are not able to provide inertia to the power system. However, both the gearbox and the blades of wind-turbines often contribute to the stored energy that can also be used to support the frequency stability of an electric power system.

Typically, the speed of wind turbine is (80-100) times faster than blades, therefore, in case that a gearbox is present, the blades with high inertia characteristics may be the main source of the stored kinetic energy. This inertia can be expressed as an inertia constant (H), varies in a range of (2-5s).

This inertia can be compared with the inertial constants of conventional synchronous generators. However, there are several differences, which should be mentioned when distinguishing between these two types of inertias:

- The kinetic energy stored in a wind turbine varies with time. For example, an increase of wind velocity leads to an increase in rotor speed, resulting in operation at maximum efficiency, which in turn, increases the total amount of stored kinetic energy. In a conventional power plant, the stored kinetic energy is virtually constant, since the synchronous generator speed is directly coupled with the frequency of a power system.

- The strong coupling between the rotor speed and the system frequency has another consequence. For instance, a frequency decline leads to a release of the stored kinetic energy, which is directly related to ROCO. Therefore, it is expected that this release can be controlled independently from ROCOF, resulting in a more substantial amount of inertial response supplied to the power system to counteract frequency deviation events.

G. Methods of Available System Inertia Estimation

In this appendix, two approaches of estimating the exact amount of available system inertia are elaborated.

1. Retroactive Approach:

This approach is based on the concept shown below:

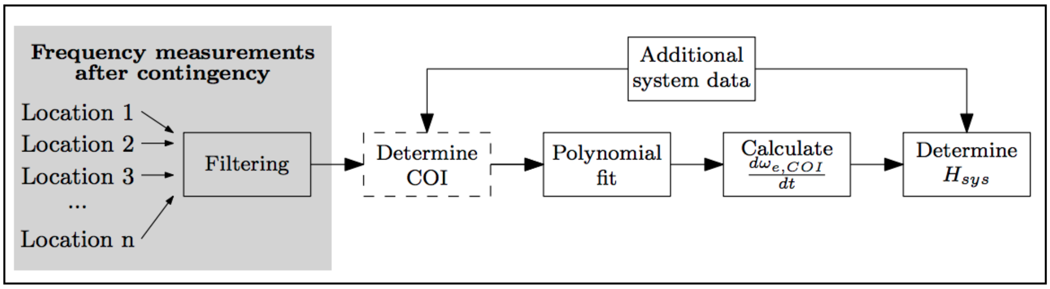

Figure G.1: different stages to determine system inertia based on retroactive method [6]

First, the deviation of system frequency following disturbances are determined at different locations in a power system, followed by filtering the determined to remove any noise.

Next, the mean frequency around the centre of inertia (COI) is computed in the case of variations of system frequency due to different locations. Further on, using a so-called polynomial fitting tool, the obtained frequency trajectory can be fitted to determine the rate of change of frequency (ROCOF) utilizing the time-derivative.

Finally, the available system inertia can be estimated by introducing information of the contingency and load voltage behaviour.

2. Real-Time Approach:

This approach is based on the Control and Data Acquisition, often simplified to SCADA, measurements. It analyses the system inertia based on the present operational data coming from the generation units.

In [6], it is stated that the future usage of real-time tools to estimate the available inertia may offer significant advantages concerning the development of power system control and operation.

Although, that these tools can measure the inertia of system in real-time, a couple of improvements are required to increase the accuracy of such measurements, e.g., considering the load contribution during these measurements, increasing the number of generation units, and improving the inertia data quality.